Complementary aerosol mass spectrometry elucidates sources of wintertime sub-micron particle pollution in Fairbanks, Alaska, during ALPACA 2022

Amna Ijaz[1,2], Brice Temime-Roussel[1], Benjamin Chazeau[1], Sarah Albertin[3], Stephen R. Arnold[4], Brice Barret[5], Slimane Bekki[6], Natalie Brett[6], Meeta Cesler-Maloney[7], Elsa Dieudonne[8], Kayane K. Dingilian[9], Javier Fochesatto[10], Jingqiu Mao[7], Allison Moon[11], Joel Savarino[3], William Simpson[7], Rodney J. Weber[9], Kathy S. Law[6], Barbara D'Anna[1]

[1]Aix-Marseille Université, CNRS, LCE, Marseille, France
[2]Present Address: Atmospheric, Climate, & Earth Sciences Division, Pacific Northwest National Laboratory, Richland, Washington 99354, United States
[3]University of Grenoble Alpes, CNRS, IRD, Grenoble INP, INRAE, IGE, F-38000 Grenoble, France
[4]School of Earth and Environment, University of Leeds, Leeds, LS2 9JT, United Kingdom
[5]Laboratoire d'Aérologie, Université Toulouse III-Paul Sabatier, CNRS, Toulouse, France
[6]Sorbonne Université, UVSQ, CNRS, LATMOS-IPSL, Paris, France
[7]Department of Chemistry and Biochemistry and Geophysical Institute, University of Alaska, Fairbanks, AK, United States
[8]Laboratory of Physics and Chemistry of the Atmosphere, University of Littoral and Opal Coast, Dunkerque, France
[9]School of Earth and Atmospheric Sciences, Georgia Institute of Technology, Atlanta, Georgia 30332, United States
[10]Department of Atmospheric Sciences, University of Alaska, Fairbanks, AK, United States
[11]Department of Atmospheric Sciences, University of Washington, Seattle, Washington 98195, United States

Correspondence to: Barbara D'Anna (barbara.danna@univ-amu.fr) and Amna Ijaz (amna.ijaz@pnnl.gov)

Fairbanks, Alaska, is a sub-arctic city that frequently suffers from non-attainment of national air quality standards in the wintertime due to the coincidence of weak atmospheric dispersion and increased local

emissions. As part of the Alaskan Layered Pollution and Chemical Analysis (ALPACA) campaign, we deployed a Chemical Analysis of Aerosol Online (CHARON) inlet coupled with a proton transfer reaction - time of flight mass spectrometer (PTR-ToF MS) and an Aerodyne high-resolution aerosol mass spectrometer (AMS) to measure organic aerosol (OA) and NR-PM_1, respectively. We deployed Positive Matrix Factorisation (PMF) analysis for source identification of the NR-PM_1. The AMS analysis identified three primary factors: biomass burning, hydrocarbon-like and cooking factors which together accounted for 28, 38 and 11 % of the total OA, respectively. Additionally, a combined organic and inorganic PMF analysis revealed two further factors: one enriched in nitrates and another rich in sulphates of organic and inorganic origin. The PTR_{CHARON} factorization could identify four primary sources from residential heating - one from oil combustion and three wood combustion, categorised as low temperature, softwood, and hardwood. Collectively, all residential heating factors accounted for 79% of the total OA. Cooking and road transport were also recognised as primary contributors to overall emission profile provided by PTR_{CHARON}. All PMF could apportion a single secondary organic fraction. These results evidence the complementarity of the two instruments and their ability in describing the complex chemical composition of PM_1 and the related sources. This work further demonstrates the capability of PTR_{CHARON} to provide both qualitative and quantitative information offering a comprehensive understanding of the organic aerosol sources. Such insights into the sources of sub-micron aerosol can assist environmental regulators and citizen efforts to improve air quality in Fairbanks and the fast-urbanising regional sub-Arctic areas.

Keywords PM_1, mass spectrometry, source apportionment, organic and inorganic aerosol, Fairbanks, Arctic cities, air quality, CHARON PTR-ToF MS, HR-ToF AMS, residential heating, wood combustion

1 Introduction

Extremely cold urban regions of the Earth, such as in the Arctic, experience poor dispersion of atmospheric pollution, especially during the wintertime, when the unique meteorological characteristics, such as extremely low solar radiation and strong radiative cooling at the surface, are coupled with enhanced local anthropogenic emissions from heating, industry, and transport. A good example is the sub-arctic city of Fairbanks, Alaska, where air quality standards are frequently violated during the winters with concentrations of fine particulate matter (i.e., with aerodynamic diameters smaller than 2.5 μm; $PM_{2.5}$) exceeding the 24-h limit of 35 $\mu g/m^3$ defined by EPA's National Ambient Air Quality Standards (Dunleavy and Brune, 2020; Epa, n.d.). Not only is Fairbanks one of the cities with the most polluted wintertime air in the US, but it has also been declared a 'moderate non-attainment area' since 2009, and due to the persistence of the problem, it was reclassified as a 'severe non-

attainment area' in 2017. Increased local anthropogenic emissions and poor atmospheric dispersion due to strong surface-based temperature inversions (> 0.5°C/m in the lowest 10 m above the ground) are major causes of wintertime pollution in the region (Tran and Mölders, 2011; Mayfield and Fochesatto, 2013). Many research studies have recognised biomass combustion as the major source of aerosol in Fairbanks (Ward et al., 2012; Wang and Hopke, 2014; Kotchenruther, 2016; Ye and Wang, 2020; Haque et al., 2021) that drives overall $PM_{2.5}$ concentrations across the city during strong temperature inversion conditions (Robinson et al., 2023). A comprehensive study covering three winters from 2008–2011 apportioned 60–80% of $PM_{2.5}$ mass at four locations in Fairbanks to emissions from residential wood stoves, open burning of biomass, outdoor boilers, and other solid-fuel combustion. (Ward et al., 2012). Source apportionment of year-round $PM_{2.5}$ in the past two decades [2008–2009 (Haque et al., 2021), 2005–2012 (Wang and Hopke, 2014), 2009–2014 (Kotchenruther, 2016), and 2013–2019 (Ye and Wang, 2020)] also revealed woodsmoke as a major contributor to $PM_{2.5}$ loads [47.5% (Haque et al., 2021), 40.5% (Wang and Hopke, 2014), ~52% (Kotchenruther, 2016), and ~19% (Ye and Wang, 2020)]. Wildfire activity and residential wood combustion are the major sources in summer and winter, respectively. The persistent role of wood-burning emissions in shaping the air quality of Fairbanks during winters triggered the implementation of a two-stage burn restriction in 2015 by the Alaska Department of Environmental Conservation (ADEC). The ADEC advisories restricted the operation of solid-fuel heating devices and required alternative heat sources to be used on days with weak atmospheric dispersion and $PM_{2.5} > 25$ μg/m^3 are observed or forecasted (Fye et al., 2009; Czarnecki, 2017; Jentgen, 2022). Sulphate has been observed to be the second largest component of $PM_{2.5}$ mass in Fairbanks (Ward et al., 2012; Wang and Hopke, 2014), forming ~33% of the annual average $PM_{2.5}$ mass (Ye and Wang, 2020). Isotope analyses have revealed 62% of this $PM_{2.5}$ sulphate to be primary (e.g., from residential heating oil combustion) during the winters (Moon et al., 2023).

The aforementioned studies on air quality in Fairbanks have focused on $PM_{2.5}$ even though PM_1 has been recognised as the major cause of negative health effects (Wang et al., 2015; Mainka and Zajusz-Zubek, 2019) due to its capability to spread deeper into the respiratory or cardiovascular systems (Meng et al., 2013; Liu et al., 2013; Chen et al., 2017). Currently, efforts to monitor PM_1 are surprisingly scarce, even in 'non-attaining' cities, such as Fairbanks, underscoring the need for a better characterisation of sub-micron aerosols to understand local sources, , chemical composition and ultimately to inform public health and support policy decisions.

Mass spectrometric techniques have advanced over the years, featuring greater mass accurancy, resolving power, and sensitivity. For instance, the Aerodyne high-resolution time-of-flight aerosol mass spectrometer (HR-ToF AMS; called AMS from hereon) is a well-established method for quantification of non-refractory NR-PM_1. Aerosol vapourisation at high temperatures and electron ionisation result in substantive molecular decomposition, facilitating quantification with high time resolution (Decarlo et

al., 2006), but at the cost of molecular-level information. This limitation has encouraged the rise of complementary techniques. For instance, extractive electrospray ionisation (EESI)-ToF MS has been successfully deployed in Beijing (Tong et al., 2021) and in Zurich to resolve multiple OA sources (Stefenelli et al., 2019a; Qi et al., 2019). Although the instrument provides molecular-level information, its quantitative response is variable and selective for polar species, preventing its independent application for ambient measurements. Other measurement methods, such as thermal desorption aerosol GC/MS flame ionisation detector (TAG)(Williams et al., 2006) and filter inlet for gases and aerosols chemical ionisation (FIGAERO-CIMS)-ToF MS (Lopez-Hilfiker et al., 2014), similarly offer better chemical resolution than the AMS, but a lower temporal resolution. Semi-continuous measurements, such as those from TAG and FIGAERO-CIMS, may not capture the rapid variation in sources.

To improve the analysis of sub-micron OA in ambient air, a novel inlet system called the chemical analysis for aerosol online (CHARON) was developed to collect real-time measurements (Eichler et al., 2015). This inlet minimises thermal and ionisation-induced fragmentation of sampled OA by employing a low-temperature vapourisation system (150°C ≤) and coupling with a relatively softer ionisation method, such as the proton-transfer reaction (PTR). The CHARON PTR-ToF MS (called PTR_{CHARON} from hereon) was successfully used for the characterisation of OA from ship exhaust (Eichler et al., 2017), ambient OA in Lyon, France, and Valencia, Spain, and OA source apportionment in Innsbruck, Austria (Müller et al., 2017). Recently, the inlet was used to quantify individual compounds in laboratory-generated secondary organic aerosol (Lannuque et al., 2023) and complex mixtures, such as vehicular gasoline emissions and atmospheric organic matter (Piel et al., 2019; Kostenidou et al., 2024). The system can measure gas-phase species as well, creating the opportunity to explore VOC precursor emissions or phase partitioning (Peng et al., 2023; Gkatzelis et al., 2018). Overall, PTR_{CHARON} and AMS are complementary techniques; the former features molecular level information of the OA faction but has limited ability to detect particles below 150 nm (Eichler et al., 2015); the latter covers smaller particle size range (i.e., > 60 nm) and detects inorganic components too (Decarlo et al., 2006). Together they provide an excellent combination of real-time and quantitative data on atmospheric ambient aerosol.

The detailed composition of sub-micron aerosol in Fairbanks and other anthropogenically influenced sub-Arctic regions – is still not well-understood. To address this issue, we deployed a PTR_{CHARON} and an AMS in the urban centre of Fairbanks during the ALPACA (Alaskan Layered Pollution and Chemical Analysis) campaign as part of the French CASPA (Climate-Relevant Aerosol Sources and Processes in the Arctic) project in January–February 2022 (Simpson et al. 2024). We aimed to determine the composition, concentrations, and sources of atmospheric NR-PM_1. In this paper, we present: (i) an intercomparison of the performance of the two instruments focusing on OA quantitation, (ii) the identification of major OA sources in Fairbanks, and (iii) the source apportionment of organic and

inorganic aerosol (e.g., ammonium, nitrate, and sulphate). These findings highlight the synergistic benefits of combining multiple analytical techniques and emphasise how soft ionisation mass spectroscopic methods enhance molecular-level insights into particulate organic carbon. This integrated approach advances our understanding of the complex composition of particulate matter, offering valuable contributions to environmental characterisation and source apportionment studies.

2 Methodology

2.1 Field campaign

The data presented in this study were collected during the ALPACA campaign in Fairbanks, Alaska, US from January 20 to February 26, 2022. ALPACA is an international collaborative field experiment to understand sources of outdoor and indoor air pollution in the cold and dark conditions of Fairbanks' winter. The scientific objectives and broad preliminary findings of the experiment were recently reviewed (Simpson et al. 2024). All instruments used for this study were housed in a trailer parked at the Community and Technical College (CTC) of the University of Alaska, Fairbanks (64.84064°N, 147.72677°W; 136 m above sea level). The CTC is in the urban core of Fairbanks, close (within 40 m) to a major downtown road and parking area (Simpson et al. 2024); the west of this locality is dominated by residential activities, while the north and east have commercial activity.

The trailer was equipped with a suite of particle counters and mass spectrometers with high temporal resolutions (varying from 10 seconds to 2 minutes). A scanning mobility particle sizer (SMPS) and a multi-angle absorption photometer (MAAP) were utilised to measure the distribution of particles sized 15.1 to 661.2 nm and black carbon concentrations, respectively. A separate inlet was used for PM_1/$PM_{2.5}$/PM_{10} measurements conducted with a commercial optical particle counter (model OPC 1.109, Grimm Aerosol Technik) at a time resolution of 1 min. Two mass spectrometers, PTR_{CHARON} (150-1000 nm) and AMS (60-700 nm), were connected to the same inlet that sampled air at 3.5 meters above ground level through a short (≈ 1 m) stainless tube with a 1/2" outer diameter extending through the trailer roof. A HEPA filter was placed upstream of the inlet for an hour at regular intervals (twice a week) to measure the instrumental background. Additionally, meteorological data, including ambient temperatures at 3 and 23 m; wind speed and direction; and trace gases, namely CO, SO_2, O_3, NO and NO_2, were recorded as described in a previous study associated with the campaign (Cesler-Maloney et al., 2022).

2.2 Instrumentation

2.2.1 PTR-ToF MS: operation and data processing

The OA was quantified with a PTR-ToF MS (PTR-TOF 6000 X2, Ionicon Analytik GmbH, Austria) coupled to a CHARON inlet in near real-time at 20-s temporal resolution, i.e., the PTR_{CHARON}. The CHARON inlet has been described in detail by Eichler et al (Eichler et al., 2015) and its applications were further evaluated and improved in subsequent studies (Müller et al., 2017; Leglise et al., 2019; Müller et al., 2019; Piel et al., 2019; Peng et al., 2023). Here, the PTR-ToF MS was configured to alternate between sampling of ambient air to measure VOCs for 15 minutes (not included in the current study) and sampling of particulate matter through the CHARON inlet for 45 minutes. The instrument was operated at a low E/N of 65 Td (i.e., drift voltage/pressure; pressure, temperature, and voltage of the drift tube were set at 2.6 mbar, 120°C, and 265 V) and in RF mode for optimal sensitivity. The thermodesorber was operated at 150°C and 8 mbar; this combination of moderate temperature with low pressure expands the range of detection to include ELVOCs as well (Piel et al. 2021). Raw data was obtained as described in **Section S1** and pre-processed with the Ionicon Data Analyzer (IDA, version 1.0.0.2), followed by post-processing (i.e., background subtraction, conversion of raw signal to mixing ratios, temporal averaging, PMF input generation) with an in-house data processing tool, PeTeR Toolkit (version 6.0; Igor 6.37). The error matrix was also calculated by PeTeR using uncertainties in ion counts and background signals. Among the resolved 1118 ions spanning the range of *m/z* 50–425, only 336 were retained above the S/N, and 318 ions could be given a molecular formula based on the criteria described in **Section S2**. PTR ToF MS records raw signals in counts per second (cps) that were converted to mixing ratios according to the molecular identity determined for the detected ions and their protonation efficiencies (further details in **Section S1**). For comparison with the AMS, mixing ratios were converted to mass concentrations, i.e., $\mu g/m^3$, using **Equation S2**. Mass concentrations calculated for the PTR_{CHARON} require a critical correction for the enrichment of sampled OA in the aerodynamic lens of the CHARON inlet (Eichler et al., 2015; Müller et al., 2017); further details are provided in **Section S3**. Total (or bulk) OA at a given point in time was the sum of mass concentrations of all ions, which was corrected for fragmentation using a previously reported method (Leglise et al., 2019), which increased the total OA mass concentrations by 17%.

Species with $m/z > 50$ were retained for PMF of OA, as molecules between *m/z* 18–50 were presented in low concentrations and are expected to be too volatile to be present in OA and were likely detected by PTR_{CHARON} as artefacts from the denuder. Time series were averaged to 2 minutes (from 20 seconds) and two matrices (*m/z* × time points) were extracted: (i) ion concentrations and (ii) their measurement

uncertainties, using PeTeR. The final matrices had the following dimensions 336 × 17,986. Where required, ion intensities (in either ppb or $\mu g/m^3$) were normalised to the sum of all measured intensities.

2.2.2 HR-ToF-AMS: operation and data processing

$NR\text{-}PM_1$ wasmonitored with 1-minute time resolution by a high-resolution time-of-flight mass spectrometer (AMS) (Aerodyne Research Inc., Billerica, USA), extensively described by Decarlo et al., (2006) and Canagaratna et al.(2007). Briefly, ambient particles are sampled through a critical orifice, focused into a narrow beam by an aerodynamic lens, accelerated toward a standard vapouriser heated at 600°C, and then ionised by electron impact (70 eV at 10^{-7} torr). Finally, the ions are analysed by a time-of-flight mass spectrometer. Standard calibrations were performed using 300 nm size-selected dried ammonium nitrate and ammonium sulphate particles at the beginning and the end of the campaign. Nitrate-equivalent values of sample mass concentrations were converted by applying relative ionisation efficiencies (RIEs) for organics, nitrates, ammonium, sulphate, and chloride (1.4, 1.1, 3.15, 1.93, and 1.3, respectively). Collection efficiency (CE) has been calculated in PIKA using the composition-dependent CE (CDCE) following Middlebrook et al., (2012) method. The calculated CE values ranged from 1.00 to 0.35.

Data was averaged to 2 minutes and extracted as concentration and measurement uncertainty matrices (*m/z* × time points) using SQUIRREL version 1.65 and PIKA version 1.25 in Igor 8.04. Separate matrices (and subsequently PMF) were prepared for organic only (abbreviated AMS_{org}) and by combining organic and inorganic species (abbreviated $AMS_{org+inorg}$). The inorganic species included in the analyses were nitrate (*m/z* 30, NO^+ and 46, NO_2^+), sulphate (*m/z* 48, SO^+; 64, SO_2^+; 80, SO_3^+; 81, HSO_3^+; and 98, $H_2SO_4^+$), ammonium (*m/z* 15, NH^+; 16, NH_2^+; and 17, NH_3^+), and chloride (*m/z* 35, Cl^+ and 36, HCl^+). Error matrices were calculated by PIKA based on uncertainty in ion counts, background signal, air beam correction, and electronic noise (Sueper, 2014). Atomic O/C and H/C ratios were calculated based on established methods (Aiken et al., 2007; Aiken et al., 2008; Canagaratna et al., 2015). Where needed for comparison with the PTR_{CHARON}, mass concentrations of PAHs were estimated from fragments as described previously (Herring et al., 2015), and levoglucosan was estimated as detailed in **Section S4**.

Species with *m/z* 12–120 were retained for PMF in this study, excluding important PAHs detected up to *m/z* 252; such PAHs were used as external tracers for factor identification. All PAHs were included in total OA quantification and associated comparisons. This exclusion is expected to cause underestimation below the 2% of the mass of some factors, particularly HOA (hydrocarbon-like organic

aerosol) and BBOA (biomass-burning organic aerosol). Final matrices from AMS_{org} and $AMS_{org+inorg}$ analyses had the following dimensions: 193 × 24,762 and 205 × 24,762, respectively.

2.3 Source apportionment: Positive matrix factorisation

Source apportionment was performed using a PMF implemented in the multilinear engine (ME-2) (Paatero, 1997a, 1999). The PMF was configured and analysed using the SoFi (Source Finder) Pro interface (Canonaco et al., 2013) (version 8.4.1.9.1; Igor 8.04). PMF is a descriptive mathematical algorithm that describes the input data, i.e. measurements of several variables collected over time (here, *m/z* × sampling time points), as a linear combination of factors that have constant mass spectra associated with temporally varying concentrations of the spectral constituents (Paatero, 1997b; Paatero and Tapper, 1994). The mathematical expressions and functions of the PMF algorithm have been exhaustively detailed in previous studies (e.g., refs. (Tong et al., 2021; Stefenelli et al., 2019a; Chen et al., 2022; Chazeau et al., 2022), etc.). Below we summarise the user-defined configurations applied in SoFi Pro to optimise the PMF of our datasets, PTR_{CHARON}, AMS_{org}, and $AMS_{org+inorg}$.

2.3.1. General methodology for PMF analysis

Preliminary PMF was performed without using *a priori* information to explore factor variability, source contributions, and guide the selection of an optimal solution before applying constraints. We considered solutions ranging from 3 to 13 factors, applying a step-wise, cell-wise down-weighting approach: variables with S/N < 0.2 ("bad" variables) were down-weighted by a factor of 10, while those with 0.2 < S/N < 2 ("weak" variables) were down-weighted by a factor of 2 (Paatero and Hopke, 2003; Ulbrich et al., 2009). Upon establishing some primary factors, such as cooking and biomass burning, which were successfully identified in unconstrained trials, we narrowed the range of possible solutions by applying the a-value approach, which allows for improve factorisation by constraining the PMF with external data when available (Canonaco et al., 2013; Paatero, 1999). For instance, a factor profile from a PMF trial in the same experiment, a time series from an external tracer, or a well-established factor profile for a source from another experiment may be provided to the PMF as an 'anchor/vector' around which it can build a factor in its overall solution. The extent to which each PMF factor can diverge from the anchor is defined by the value of *a* (Tong et al., 2021), which varies from 0 to 1. This anchor can be provided for one or multiple factors and has been proven to improve the quality of PMF solutions compared to unconstrained trials (Tong et al., 2021; Stefenelli et al., 2019a; Chen et al., 2022).

Currently, there are no fully objective criteria for choosing the best number of factors, but some criteria have been suggested in the literature to make an appropriate selection (Chen et al., 2022; Zhang et al., 2011; Ulbrich et al., 2009; Crippa et al., 2014). The PMF solutions reported here were primarily selected

based on their physical meaning, which was determined by the presence of known tracer compounds in the factors, temporal correlation with co-located measurements of external tracers (e.g., NO_x, SO_2).. We selected an eight, four, and six factors solution from PTR_{CHARON}, AMS_{org}, and $AMS_{org+inorg}$, respectively. The justification for these solutions is presented in **Table S2**. Once the most suitable solution, i.e., the base-case, was established, bootstrap analyses were performed to assess its stability, evaluate uncertainties, and conduct a sensitivity analysis on the range of *a*-values used. In an unblocked bootstrapping approach, the original matrices (both data and error) are perturbed by random resampling of the rows to create a new input of the same dimensions, resulting in some duplications and deletions throughout the input (Paatero et al., 2014). The need and application of this approach differed between the PTR_{CHARON} and the two AMS datasets as discussed in **Sections S5** and **S6**, respectively. Ancillary data on particle size distribution have been associated to mass spectrometry data in an additional PMF analysis (**Section S7**). Finally, the quality of solutions was gauged by the Q/Q_{exp} values and from key diagnostic plots of residuals and the statistical stability across multiple runs (**Figure S5–S7**).

3 Results and Discussion

3.1 Campaign overview

Figure 1 summarises meteorological conditions, chemical composition and particle size distribution of NR-PM_1 observed from January 20 to February 26, 2022. High aerosol loads coincided with poor atmospheric dispersion, due to low wind speeds (<2 m/s), low temperature (below - 10°C) associated with strong surface temperature inversions, as temperature differences between 23 and 3 m above sea level ranging from 3°C to 10°C. The average values of BC and NR-PM_1 measured with the MAAP and AMS were **1.4 ± 1.4 µg/m^3** and **8.3 ± 9.3 µg/m^3**, respectively. During intense pollution events daily average concentrations of NR-PM_1 were **24–27 µg/m^3**. During the same sampling period at NCore site (Fairbanks) $PM_{2.5}$ value of ~25 and ~29 µg/m^3 were reported (Robinson et al., 2023). Ancillary OPC measurements at the CTC site showed that the hourly PM_1 mass comprised up to 99% of the $PM_{2.5}$.Organics were the predominant component of NR-PM_1 throughout the campaign, constituting **~66 ± 11**% of its total mass, while chloride, ammonium, nitrate, and sulphate- contributed **2 ± 3, 3 ± 3**, **6 ± 4**, and **22 ± 10**%. This is in line with previous studies in Fairbanks, where OA was the largest component of $PM_{2.5}$ mass (Ward et al., 2012; Ye and Wang, 2020; Robinson et al., 2024). Specifically, according to a recent study from 2020 to 2021, ACSM analysis during the wintertime demonstrated inorganics to form less than 25% of the $PM_{2.5}$ mass only, with sulphate (~10%) and nitrate (~8%) being the predominant components (Robinson et al., 2024). Despite the different average concentrations, the fractional contributions of these non-refractory components remained almost invariable throughout the campaign (**Figure 1D**). Detailed molecular-level composition of organics with the PTR_{CHARON} reveals

a large majority of organics to comprise only C, H, and/or O atoms, while only **~9 ± 4%** of the OA_{CHARON} mass measured with this instrument was attributable to heteroatomic molecules, including organonitrates and organosulphates (**Figure 4 and S8**). Generally, heteroatomic species cannot be distinguished at a resolving power of 5000 FWHM in complex environmental mixtures, such as atmospheric aerosol (Reemtsma, 2009). In this study, based on the low formula error and lack of an appropriate alternate, we gave 53 low-concentration ions (< 2% of the total signal) CHOS or CHNO identities, but due to the low confidence in their formula assignments, they were not considered for factor identification. Prominent peaks include *m/z* 217.09 ($C_{12}H_{12}N_2O_2$), 219.09 ($C_{15}H_{10}N_2$), 123.05 ($C_4H_{10}O_2S$), and 151.08 ($C_6H_{14}O_2S$).

On average, the OA mass loading recovered by PTR_{CHARON} (i.e., OA_{CHARON}) accounted for approximately 85% of the OA mass measured by the AMS (i.e., OA_{AMS}). While the two instruments showed a good temporal agreement (R^2 = 0.60) as depicted in **Figures 2A–B**, measurements were biased either toward the AMS_{org} or the PTR_{CHARON} (i.e., distributed away from the 1:1 line in the scatter plot of **Figure 2C**) during different periods of the campaign. These trends could be explained by the variation in relative contributions of two major emission sources identified by both instruments in this study: on-road transport and biomass burning. OA_{CHARON} was comparable to OA_{AMS}, when the relative contribution of $BBOA_{AMS,org}$ was more than 50% of total OA_{AMS} and $HOA_{AMS,org}$ (i.e., $transport_{CHARON}$) was less than 10% (**Figure 2D–E**). Similar trends were observed for some major constituents of BBOA, e.g., levoglucosan and a PAH ($C_{20}H_{12}$) as shown in **Figure S9**. Part of such discrepancy can be traced back to the size transmission of particles, where sub-100 nm urban vehicular emissions are underestimated by the PTR_{CHARON} (Guo et al., 2020; Pikridas et al., 2015; Louis et al., 2017; Kostenidou et al., 2020), and larger than 100 nm biomass burning emissions (Reid et al., 2005) are estimated well (Janhäll et al., 2010). Another part of the quantitative difference can be explained by the PTR limitation in ionisation and the induced fragmentation of analyte ions. Tests conducted in our laboratory with five C_{16}–C_{26} alkanes as markers of vehicle emissions revealed that they undergo extensive fragmentation, resulting in 2–4 times underestimation of their actual concentrations. In line with this, the ineffective ionisation of saturated alkanes by PTR (Ellis and Mayhew, 2014) and their tendency to undergo dissociative ionisation (Gueneron et al., 2015) have also been reported.

3.2 Source apportionment

3.2.1. Overview of source apportionment

A four-factor solution was selected for the AMS_{org} measurements with three primary factors (i.e., HOA, COA, and BBOA) and an oxygenated or aged OA factor (i.e., OOA). The mass spectra and time series are presented in the supplement (**Figure S10**). Counterparts of these four factors were diagnosed in

$AMS_{org+inorg}$ based on a high temporal correlation ($R^2 > 0.9$; Table S4), along with two additional factors: a sulphur-rich factor (labelled sulph-OA) and a nitrate-rich factor (labelled AmNi) (**Figure 3**). An eight-factor solution was selected for PTR_{CHARON} and is summarised in **Figures 4 and 5**. To differentiate between corresponding factors retrieved from the different datasets, they have been given unique subscripts, e.g. $COA_{AMS,org}$, $COA_{AMS,org+inorg}$, COA_{AMS} (i.e., referring to both AMS datasets), or COA_{CHARON}. Amongst the three datasets COA, HOA (labelled 'transport' in PTR_{CHARON} analyses), and OOA were common. A single BBOA factor was observed in AMS_{org} and $AMS_{org+inorg}$, while four chemically distinct, but closely co-varying counterparts were detected by PTR_{CHARON}. 3.2.2. Organic aerosol from residential heating.

Both AMS analyses indicate that biomass burning is among the major sources of PM_1 during the ALPACA campaign. On average, BBOA contributed **1.5 ± 1.9 µg/m³** (**28 ± 18%** of total OA_{AMS}) and **1.6 ± 2.2 µg/m³** NR-PM_1 (**19 ± 14%** of total NR-PM_1 mass). The mass spectra of $BBOA_{AMS}$ featured a strong peak at *m/z* 60 ($C_2H_4O_2^+$) and 73 ($C_3H_5O_2^+$) (**Figure S10A–B**). These fragments are markers of anhydrosugars in wood-forming polymers, such as cellulose. Wood combustion has previously been estimated to be the largest emitter of aerosols in Fairbanks and surrounding areas, where it may produce as much as 80% of the aerosol load. Wood burning emissions are also the major driver of the spatial variability of $PM_{2.5}$ and BC in Fairbanks during strong atmospheric temperature inversions. Other typical residential heating sources of emissions in Fairbanks include coal, gas, and fuel oil.

The $BBOA_{AMS}$ factor was strongly correlated with PAHs ($R^2 \geq 0.7$) while a moderate correlation was observed with SO_2 ($R^2 = 0.4$) (**Table 1**). While PAHs are a major component of biomass combustion emissions, the emission of SO_2 is largely associated with coal and oil combustion (Smith et al., 2011; Dunleavy and Brune, 2019). However, the AMS was unable to distinguish between multiple combustion-related sources. As shown in the diurnal plots in **Figure 3**, the concentration of the $BBOA_{AMS}$ factor enhanced at ~1800 AKST, stayed stable through the night and then decreased in the early morning. Its lowest mass concentrations occurred during the afternoon (1300–1500 AKST). Therefore, $BBOA_{AMS}$ was associated with residential heating, i.e., the combustion of a variety of fuels by residents within their homes (non-commercially), such as in wood-burning stoves, furnaces, boilers, etc. for heating living space. We did not find evidence of OA or NR-PM_1 from commercial heat providers, such as power plants, likely due to their small contribution to surface-level aerosol due to smokestacks lying above the inversion layer.

PTR_{CHARON} apportioned **2.6 ± 3.4** µg/m³ of OA_{CHARON}, on average, to four distinct residential heating-related sources expressed as ResH1–4 (**62 ± 26%** of total OA_{CHARON}). These factors closely co-varied in time and were correlated reasonably well ($R^2 = 0.5–0.7$; **Table S5**) with the $BBOA_{AMS}$ factor. In

addition, combining all four residential heating-related factors in PTR_{CHARON} into a composite factor increased the correlation (R^2) with AMS_{org} and $AMS_{org+inorg}$ to 0.79 and 0.82, respectively, suggesting that PMF was not able to effectively separate these closely co-varying residential heating factors in AMS dataset.

The four factors from PTR_{CHARON} were identified as different sources based on the distribution of key marker species and correlation with external (e.g., trace gases, etc.) and internal (e.g., PAHs). . Levoglucosan is used here as an internal tracer of biomass burning being relatively stable under atmospheric conditions (Fraser and Lakshmanan, 2000). Protonated levoglucosan (*m/z* 163) and its fragments (at *m/z* 85, 127, and 145) were found in ResH1, ResH4, and ResH2 with **30, 26, 14%** of the total signal respectively **(Figure S11**), suggesting that they originate from biomass wood-burning (**Figure 4 and S11**). These three factors collectively accounted for **2.1 ± 2.5 µg/m^3** (**47 ± 20%)** of total factorised OA_{CHARON}.

ResH1 includes low temperature combustion markers: this factor is small as it contributes to only an average of **0.5 ± 0.5 µg/m^3** (**14%**) of the total OA_{CHARON}, but it contains the highest fraction of levoglucosan (~30%). Approximately 65% of the total signal of ResH1 is due to compounds with six or fewer carbon atoms, compared to heavier species present in the other factors (**Figure S13**). The most abundant species are at *m/z* 69.03 (C_4H_4O; furan) (Palm et al., 2020; Jiang et al., 2019), m/z 87.04 ($C_4H_6O_2$; oxobutanal) (Brégonzio-Rozier et al., 2015), *m/z* 97.03 ($C_5H_4O_2$; furfural), *m/z* 109.0286 ($C_6H_4O_2$; benzoquinone) (Stefenelli et al., 2019b) and *m/z* 115.04 ($C_5H_6O_3$; methyl-dihydrofuran) (Koss et al., 2018). Consistent with these molecular formulae, the concentration-weighted average O/C of ResH1 was relatively higher (i.e., 0.42) compared to other residential heating factors (O/C = 0.2–0.3). The most abundant species observed in ResH1 can be related to depolymerisation reactions occurring during low temperature and early stages of the combustion process (Collard and Blin, 2014; Sekimoto et al., 2018).

ResH2 and ResH4 include OA from hardwood and pinewood combustion, respectively: Two more factors associated with wood-burning were ResH2 and ResH4. Their average concentrations were **1.1 ± 1.9** and **0.8 ± 0.9 µg/m^3**, respectively, corresponding to **28** and **20%** of the OA_{CHARON} (**Figure 6**). The ResH2 was dominant factor in the PMF and could reach **~37 µg/m^3** during the most severe pollution episodes. Both factors were associated to particles greater than 300 nm (**Figure S12**), typical of woodsmoke (Glasius et al., 2006), and presented unique molecular signatures of different wood types (**Figure S11)**. Generally, the specific nature of wood cannot be inferred unambiguously because the emissions of known marker species, such as levoglucosan or methoxy phenols, vary not just with fuel used and its quality, but also with the type of heating appliance, operational conditions, appliance

efficiency, and stage in the combustion cycle (Fine et al., 2002; Alves et al., 2017). Regardless, several studies (Fine et al., 2002; Schauer and Cass, 2000; Kawamoto, 2017) have distinguished between softwood from hardwood by investigating the presence of marker compounds that were observed in our study as well, such as substituted phenols and resin acids **(Figure S11).**

ResH2 featured an abundance of methoxy phenols, including $C_7H_8O_2$ (guaiacol), $C_8H_{10}O_3$ (syringol), $C_{10}H_{10}O_3$ (coniferaldehyde), $C_6H_6O_2$ (benzenediol or methylfurfural), and $C_8H_{10}O_2$ (creosol), that collectively accounted for ~9% of the total signal, compared to 1, 2, and 2% in ResH1, ResH3, and ResH4, respectively. These compounds are important products of lignin pyrolysis in birch, aspen, and spruce and are usually detected in the gas phase at mild ambient temperatures (Kong et al., 2021). Guaiacol and syringol are depolymerisation products of guaiacyl and syringyl units of lignin at 200–400°C, and they rapidly transition to catechols, cresols, and phenols during secondary pyrolysis reactions at 400–450°C (Kawamoto, 2017). While guaiacols are emitted by both hardwood and softwood, semi- or low-volatility substituted syringols are emitted in higher amounts by hardwood combustion (Kawamoto, 2017; Fine et al., 2002, 2001; Schauer and Cass, 2000). In this study, derivatives of guaiacols, including $C_{10}H_{12}O_2$ (eugenol), $C_{10}H_{14}O_2$ (4-propyl guaiacol), and $C_{10}H_{10}O_3$ (coniferaldehyde) presented higher "relative concentration" (**Equation S4**) of 0.56–1.41 for ResH2 and ResH4 compared to ResH1 (<0). Other compounds, such as $C_8H_8O_3$ (vanillin), $C_9H_{10}O_3$ (acetovanillone), $C_{10}H_{12}O_3$ (propiovanillone), and $C_{10}H_{12}O_4$ (methyl homovanillate) were predominantly found in ResH2. Similarly, substituted syringols, i.e., $C_{11}H_{14}O_3$ (methoxy eugenol), $C_{10}H_{12}O_4$ (acetosyringone), and $C_{11}H_{14}O_4$ (syringyl acetone, propionyl syringol, or sinapyl alcohol) were almost entirely associated with ResH2 as well. These compounds have been reported as markers of hardwood burning (Fine et al., 2001), implying a greater contribution of hardwood emissions to the ResH2 factor. In Alaska, relevant hardwood species include deciduous leafy trees, i.e., paper birch, balsam poplar, quaking aspen, etc (Adec, 2023).

The ResH4presented a unique fingerprint characterised by oxygenated molecules bearing more than 13 carbon atoms (**Figure S13**), such as $C_{16}H_{30}O_6$ (*m/z* 319.21), $C_{20}H_{28}O_2$ (*m/z* 301.21), $C_{20}H_{18}O_4$ (*m/z* 323.12), $C_{20}H_{30}O_2$ (*m/z* 303.24) and $C_{22}H_{18}O$ (*m/z* 299.14), in addition to the levoglucosan marker ions (26% of the total signal). The intense signals from *m/z* 301 ($C_{20}H_{28}O_2$) and *m/z* 303 ($C_{20}H_{30}O_2$) (**Figure S11**) are likely related to resin acids, dehydroabietic acid and abietic acid, respectively, which are almost exclusively emitted from the thermal alteration of resins in coniferous species, and thus, are indicative of softwood burning (Simoneit, 2002, 1999). Due to the presence of these compounds, ResH4 was interpreted as an OA factor influenced by softwood combustion. Softwood species in Alaska include trees with needles and cones, e.g. hemlock, cedar, and spruce (Adec, 2023).

ResH3 includes OA from heating oil combustion: this factor contributed to **16 ± 9%** of the total OA_{CHARON} (**0.6 ± 0.6 µg/m^3**) and showed the characteristic diurnal pattern of residential heating as it correlated quite well (R^2 = 0.56) with $BBOA_{AMS,org.}$ However, its chemical composition was different from the other residential heating factors. Notably, levoglucosan contributed to a smaller fraction of the total signal of ResH3 (i.e., 9%) compared to other residential heating factors (14–30%; **Figure S11**), while PAHs represented a much larger fraction of its total signal (for instance, 30, 31, and 29% of $C_{16}H_{10}$ (*m/z* 203.09), $C_{18}H_{12}$ (*m/z* 229.10), and $C_{20}H_{12}$ (*m/z* 253.10); **Figure S13**). These PAHs could be fluoranthene (or pyrene), naphthacene (or benzo[*x*]anthracene, chrysene), and benzo(*x*)pyrene (or benzo(*x*)fluoranthene)), which have been reported in emissions of light oil combustion (Bari et al., 2009). Additionally, ResH3 was strongly correlated with SO_2 (R_2 = 0.61), compared to a lower correlation ($R^2 \leq 0.47$) with the other residential heating factors. Residential combustion of heating oil is an important source of SO_2 in Fairbanks, compared to wood and coal, due to ~2/3rd of the households using oil-fired space heaters and the high sulphur content of > 1600 ppm in fuel oils commonly consumed here (e.g., #1 and #2 fuel oil and waste motor oil are relevant in Fairbanks)(Dunleavy and Brune, 2019). Consistent with the possibility of the ResH3 factor being associated with fuel oil emissions, the factor is characterised by particles smaller than 100 nm (**Figure S12**) and due to the CHARON inlet's cut-off, its mass concentration was possibly underestimated.

3.2.3. Hydrocarbon-like organic aerosol

The HOA_{AMS} factors were characterised by notable peaks at *m/z* 43 ($C_3H_7^+$), 57 ($C_4H_9^+$), 71 ($C_5H_{11}^+$), 85 ($C_6H_{13}^+$), and 99 ($C_7H_{15}^+$), belonging to $[C_nH_{2n+1}]^+$ series, typical of *n*- and branched alkanes. Additional peaks at *m/z* 55 ($C_4H_7^+$), 69 ($C_5H_9^+$), 81 ($C_6H_9^+$), 83 ($C_6H_{11}^+$), 95 ($C_7H_{11}^+$), 97 ($C_7H_{13}^+$), 107 ($C_8H_{11}^+$), 109 ($C_8H_{13}^+$), and 111 ($C_8H_{15}^+$) represented $[C_nH_{2n-1}]^+$ and $[C_nH_{2n-3}]^+$ series, related to cycloalkanes (McLafferty et al. 1993). These ions are associated with engine-lubricating oils, vehicular exhaust, and diesel fuel (Canagaratna et al., 2004). The HOA_{AMS} factors contributed **38 ± 20%** and **21 ± 14%** of the OA_{AMS} and NR-PM_1 mass, respectively (**Figures 6 and S14**).

The unconstrained PTR_{CHARON} analysis was not able to apportion a road transport-related factor, however, by constraining the factorisation with the time series of a mobile gasoline factor, identified in the gas-phase PTR-ToF MS analyses of ALPACA campaign (Temime Roussel et al., 2022), a small road transport-associated factor was identified. For instance, this latter was strongly correlated with black carbon and NO_x (R^2 of 0.58 and 0.66; **Table 1**) and featured high contributions of C_8H_{10} (xylene; ethylbenzene), C_7H_8 (toluene), and C_6H_6 (benzene) (**Figures 4 and S11**). Despite exhibiting some reasonable diurnal trend peaking at the morning (0900 AKST) and evening (1700–1600 AKST) rush hours (**Figure 5**), the factor accounted for negligible concentrations (< 1 µg/m^3) and presented some unlikely species, such as *m/z* 315.22 ($C_{21}H_{30}O_2$; possibly cannabidiol) absent in the unconstrained PMF.

For instance, on average, **2.1 ± 3.0 µg/m^3** of OA was associated with $HOA_{AMS,org}$, compared to only **0.1 ± 0.1 µg/m^3** for the road $transport_{CHARON}$ factor (**Figure 6**). These discrepancies are largely instrumental, partly due to the poor transmission of the small particles (<100 nm) by the CHARON inlet and the limited sensitivity towards hydrocarbons by PTR, but other possible biases can be due to heating oil OA signal interfering with the HOA_{AMS}, as discussed in **S8**.

3.2.4. Cooking organic aerosol

Another primary factor identified in Fairbanks was cooking, likely arising from residential or commercial activities around the CTC. The COA_{AMS} factor featured a high abundance of $C_xH_y^+$ ions, along with prominent O_1 fragments at *m/z* 55 ($C_3H_3O^+$), 84 ($C_5H_8O^+$), and 98 ($C_6H_{10}O^+$) originating from organic acids (Mohr et al., 2009) and used as diagnostic markers of COA in urban settings (Sun et al., 2011). The *f*55/*f*57 value (i.e., the ratio of fractions of $C_4H_7^+$ to $C_4H_9^+$) was ~3.00 for COA_{AMS}, compared to ~1.04 for HOA_{AMS} (**Figure S10D**). As a reliable tracer for COA remains unidentified in the AMS spectrum, a *f*55/*f*57 ratio >1 is considered a characteristic feature (Katz et al., 2021; Sun et al., 2011). The PMF analysis of PTR_{CHARON} also revealed a distinct COA factor dominated by long-chain fatty acids, $C_{18}H_{32}O_2$, $C_{18}H_{34}O_2$, and $C_{18}H_{36}O_2$, identified as linoleic, oleic, and stearic acids contributing to11, 16, and 4% to the total COA_{CHARON} mass (**Figure 4 and S11**). These fatty acids are commonly found in OA from cooking oil and meat (Katz et al., 2021; Mohr et al., 2009). The COA_{CHARON} contributed to a maximum of ~9% of the total OA_{CHARON} mass and exhibited a unique diurnal pattern visualised in **Figure 5** with a minor maximum in the afternoon (lunchtime) and a second maximum in the evening (dinnertime). The average absolute concentrations of COA were **0.6 ± 0.8** for the AMS and **0.1 ± 0.2 µg/m^3** for the CHARON, such a discrepancy can be explained by the same reason discussed above and detailed in the section **S9**.

3.2.5. Oxygenated organic aerosol

Past source apportionment studies have reported multiple OOA factors differing in volatilities or oxygenation levels (e.g., Stefenelli et al., 2019a; Kumar et al., 2022; Cash et al., 2020). Here, we diagnosed only a single OOA factor in either AMS or PTR_{CHARON} measurements. Specifically, the OOA_{AMS} factors were identified based on a prominent peak at *m/z* 43 ($C_2H_3O^+$) and *m/z* 29 (CHO^+; **Figure S10A**) and showed a strong correlation (R^2 0.74) with OOA_{CHARON}. The average absolute concentrations of OOA_{CHARON} and $OOA_{AMS,org}$ were **0.4 ± 0.6** and **1.0 ± 2.1 µg/m^3**, respectively. Notably, the most intense ions in the mass spectrum of OOA_{CHARON} have been tentatively assigned to *m/z* 73.03 ($C_3H_5O_2$, e.g., methylglyoxal), *m/z* 99.04 ($C_5H_6O_2$, e.g., oxo-pentanal), *m/z* 113.06 ($C_6H_8O_2$, e.g.,methyl-oxo-pentanal), *m/z* 127.08 ($C_7H_{10}O_2$; e.g., heptadienoic acid), *m/z* 137.06 ($C_8H_8O_2$; e.g.,

methoxy-benzaldehyde), *m/z* 167.10 ($C_{10}H_{14}O_2$), *m/z* 171.07 ($C_8H_{10}O_4$) and *m/z* 185.10 ($C_{13}H_{12}O$; e.g., benzyl phenol). Among these compounds some have previously been associated with atmospheric oxidation or photolysis of BBOA (Montoya-Aguilera et al., 2017; Lignell et al., 2013; Smith et al., 2020), other could be due to oxidation aromatic VOCs detected originating from road transport (Temime-Roussel et al., 2022). Few other species overlapped with the residential heating tracers, notably *m/z* 163.06 ($C_6H_{10}O_5$; e.g., levoglucosan), *m/z* 179.08 ($C_{10}H_{10}O_3$; e.g., coniferaldehyde), and *m/z* 301.21 ($C_{20}H_{28}O_2$; e.g., dehydroabietic acid). But given the prominence of wood-burning as a major primary emissions, the OOA is likely linked to BBOA. A recent study in Fairbanks identified wintertime OOA as a mixture of BBOA and SOA formed from non-photochemical processing using an ACSM (Robinson et al., 2024). The examination of *f*44 versus *f*60 in the AMS_{org} dataset plot (**Figure S10C)** is consistence with aged OOA derived by biomass burning, as previously demonstrated by Xu et al., (2023). Another recent source apportionment study with the HR-ToF AMS at a site close to the CTC did not identified an OOA factor, while BBOA, HOA, and a mixed primary factor (HOA, COA, etc.) comprised 45, 25, and 31% of total OA(Yang et al., 2024). A limited OOA formation is plausible due to reduced solar light exposure in this period of the year (Cesler-Maloney et al., 2024), however, the absence of OOA is more likely a result of an unresolved organic fraction.

Sulphate and OOA. An intriguing insight about the OOA factor emerged from the $AMS_{org+inorg}$ measurements, indicating a significant content of sulphur containing compounds (**Figure S15**). The AMS does not distinguish among the different sulphur-containing species, but following guidelines from previous works (Chen et al., 2019; Schueneman et al., 2021) we could explored the ratio of sulphur fragments to investigate the presence of different species such as hydroxymethane sulphonate (HMS; $CH_2(OH)SO^{-3}$), HSO_4^- (bisulphite), SO_4^{2-} (sulphate) and (H2SO4) sulphuric acid. An organosulphate content of ~ **0.8 ± 1.3 µg/m³** (**~20 ± 16%**) was then derived using the ratios of SO^+ and SO_2^+ ions against SO_3^+, HSO_3^+, and $H_2SO_4^+$ ions as detailed by Song et al., (2019). This value is in good agreement with previous reports from the same field campaign (Campbell et al., 2022; Robinson et al., 2024). Additionally, to mimic potential matrix effects of wood burning OA on sulphate fragmentation patterns, AMS spectra from a solution of $(NH_4)_2SO_4$ mixed with various amounts of levoglucosan (i.e., 0–80% in mass) were compared to ambient data and PMF factors as shown in **Figure S16A**. Among the sulphate-rich factors the $OOA_{AMS,org+inorg}$ exhibited lower HSO_3^+ to $H_2SO_4^+$ intensities suggesting an higher fraction of organosulphate compounds, as it is also evidenced in **Figure S16D–E** by the strong correlation between derived organosulphur fraction and sulphate-ions in the $OOA_{AMS,org+inorg}$ factor (R^2 = 0.85, slope = 0.57).

Further information on chemical composition was gathered by comparing AMS results with IC measurements from $PM_{0.7}$ filters sampled as part of another ALPACA study (Dingilian et al., 2024).

Despite the good correlations between the two datasets, shown in **Figure 7A,** the AMS results underestimated by 30%, 26%, and 35% sulphate, ammonium, and nitrate, respectively (see **Section 2.2.2**). Both the total estimated organosulphur fraction and the $OOA_{AMS,org+inorg}$ factor presented robust correlations ($R^2 > 0.90$) with the $S_{(IV)}$ and HMS ions from filter analysis and a somewhat weaker correlation ($R^2 > 0.61–0.68$) with the SO_4^{2-} ion (**Figures 7 and S16F–I**). The $OOA_{AMS,org+inorg}$ factor was also strongly correlated with ammonium (AMS data $R^2 = 0.86$, **Table 1**; filter IC $R^2 = 0.77$, **Figure 7B**), potentially promoting the formation of $S_{(IV)}$ species (Campbell et al., 2024). This author also reported that $S_{(IV)}$ species, including HMS, represented the major secondary organosulphur component of $PM_{2.5}$ in Fairbanks during wintertime, contributing to 26–41% of total sulphate (Campbell et al., 2022). Overall, the molecular level composition of OOA from PTR_{CHARON} and the inorganic chemical information from $AMS_{org+inorg}$, as well as diurnal patters with enhanced concentrations in the afternoon (**Figure 3**), are indicative of chemical daytime processing underscoring the need for further exploration of the atmospheric processing pathways involved.

3.2.6. Additional insights from combined analysis of organic and inorganic AMS data

Two additional factors, sulph-OA (i.e., sulphur-rich OA) and AmNi (i.e., ammonium nitrate), were observed from the PMF of $AMS_{org+inorg}$ (**Figure 3**). Approximately 40–60% of these factors' masses comprised sulphur and nitrogen species (**Figure S15**).

Sulphur-rich organic aerosol: Sulph-OA is composed by sulphate 60%, organics 30%, ammonium 6% and nitrate 4%. The chemical composition was further explored via the $f HSO_3/f H_2SO_4$ analysis detailed in **Section 3.2.4** and as shown in **Figure S16A**, the factor is positioned between H_2SO_4 and $(NH_4)_2SO_4$. The measured $[NH_4]/[SO_4]$ ratio was 0.07, considerably lower than the theoretical mass ratio of 0.38 and 0.18 of $(NH_4)_2SO_4$ and NH_4HSO_4, respectively, indicating an acidic nature of Sulph-OA (Chen et al. 2019). The factor was well correlated with SO_2 ($R^2 = 0.6$) and moderately correlated with the ResH3 factor (R^2 of 0.33). The factor was also associated with ultrafine particles in the 50–80 nm range (**Figure S12D**). Regardless of the low correlation, we speculate that ResH3 and sulph-OA originated from the same source, i.e., residential heating oil combustion, and their temporal disagreement may result from instrumental biases of the CHARON inlet in quantifying particles smaller than 100 nm (**Figures S12B and D**). For instance, as shown in **Figures S12E–F**, the organic ResH3 supersedes sulph-OA concentrations when larger particles are abundant, and it has lower concentrations for smaller particles.

This factor contained **0.6 ± 0.5 µg/m^3 (~58 ± 26%)** of total sulphate measured with the AMS and it dominated during the low-pollution periods, which were more frequent and lasted longer than the high-pollution events (**Figure 1**). Other primary factors, $HOA_{AMS,org+inorg}$, $COA_{AMS,org+inorg}$, and

BBOA$_{AMS,org+inorg}$, contained an additional 11 ± 9% of the sulphate (**0.2 ± 0.2 µg/m^3**), so collectively, primary factors made up **69 ± 24%** (**0.7 ± 0.6 µg/m^3**) of total sulphate. This value is in close agreement with a previous ALPACA study that reported ~62 ± 12% of total SO_4^{2-} mass to be of primary origin (Moon et al., 2023).

AmNi factor. The second inorganic factor was composed of 35% nitrate, 14% ammonium, and 43% organics accounting for 71 ± 23% of the total nitrate measured by the AMS (R^2 = 0.98). The average concentration of this factor and the nitrate species in it were **1.1 ± 1.6** µg/m^3 and **0.4 ± 0.5** µg/m^3. The factor was more abundant when NOx concentrations were high (above 130 ppbv)(**Figure S17B**), its diurnal trend peaked around 1400 **AKST** (Figure 3), roughly 3-4 hours after the morning peak of HOA$_{AMS}$ and was associated with relatively small particles of 110 nm (**Figure S12D**). A high contribution of aliphatic moieties characterised the organic fraction, and according to the difference in mass concentrations of HOA$_{AMS,org}$ and HOA$_{AMS,org+inorg}$ of 13% (**Figure S17A**), we speculate that some organic components of HOA$_{AMS,org}$ were transferred to the AmNi factor (**Figure 6**). All these elements suggest a probable contribution from the vehicular emissions to this factor. The presence of inorganic compounds provided more variables to the PMF, and thus, improved the resolution of factors into distinct AmNi and HOA$_{AMS,org+inorg}$ factors.

4. Local environmental implications

During the period of the campaign, 12–48-hour-long ADEC advisories for wood-burning restrictions were implemented seven times. Variation in the relative contributions of ResH1–4 during these advisories is depicted in **Figures 8** and **S18–21**. For all advisory events, ResH2 and ResH4, i.e., woodsmoke, were the predominant contributors *before* and *after* the advisories were in place. A notable increase was observed in ResH3 contribution, i.e., heating oil, *during* the 2nd (Stage 1), 5th (Stage 1), 6th (Stage 1), and 7th advisory events. While ResH2 (i.e., hardwood-related fuels) remained a prominent contributor to OA$_{CHARON}$ *during* the 3rd (Stage 2), 4th (Stage 1), and 5th (Stage 1) advisories. Most households in Fairbanks use heating oil (~72% of residents), followed by wood (~22% of residents) (Dunleavy and Brune, 2019), which was not reflected in the relative contributions apportioned to ResH3. This can be linked to a higher PM_1 release from wood combustion per given volume of fuel compared to heating oil and/or an underestimation of ResH3 by PTR$_{CHARON}$ being associated with smaller than 100 nm (**Figure S12**).

As expected, the absolute average concentrations of all factors were inversely related to ambient temperature, but the percent change differed considerably across factors. Specifically, as temperatures

decreased from -10°C to below -25°C, the average absolute concentrations for $transport_{CHARON}$, COA_{CHARON}, OOA_{CHARON}, ResH1–4 increased 0.25×, 0.75×, 9.0×, 1.4×, 25.1×, 3.0×, and 2.9×, respectively (**Figure S22**). The steep increase in the relative contribution of ResH2,associated with hardwood-tracers, contrasts with previous reports, based on surveys (Dunleavy and Brune, 2019) and organic tracers (Haque et al., 2021), indicating birch and spruce as the most popular firewood in Fairbanks. Laboratory studies have shown that the burning of softwood pellets of Douglas Fir or eastern white pine emits less PM than hardwood pellets of the same volume, and this response varies based on the moisture content of the wood and the heating appliance used (Morin et al., 2022). Also ResH2 comprises a broader spectrum of volatile and semi-volatile substituted phenolic species, and thus, it is likely to undergo efficient gas-to-particle partitioning at low temperatures toward increasing OA loads (Ijaz et al., 2025).

5. Conclusion

A CHARON inlet coupled with PTR-ToF MS and HE-ToF-AMS were deployed during the Alaskan Layered Pollution and Chemical Analysis (ALPACA) campaign. The PMF analysis of AMS data revealed three primary factors: biomass burning, hydrocarbon-like and cooking factors accounting for 28, 38 and 11 % of the total OA, respectively. A combined organic and inorganic PMF analysis provided additional insights and revealed the presence of an organo-sulphate compounds mostly associated to the OOA factor and of another sulphate-rich factor of acidic nature. A nitrate factor, associated with hydrocarbon-like OA and high NOx levels, was interpreted as aged road transport emissions. The PTR_{CHARON} PMF analysis could differentiate four residential heating sources—one oil combustion and three wood combustion types, associated with low temperature, softwood, and hardwood combustion. Such factorisation was achieved with the support of specific tracers that CHARON could successfully identify, as furans, aromatic alcohols (resorcinol, guaiacol, eugenol, syringiol), aldehydes (furfural, coniferaldehyde), acids (benzoic, dehydroabietic, abietic, linoleic, oleic, and stearic) and various PAHs. Collectively all residential heating factors accounting for 79% of the total OA_{CHARON}. Cooking and road transport were also recognised as primary sources by PTR_{CHARON}. All PMF analyses could apportion a single secondary organic fraction accounting for 11-19% of the total OA. This work evidence the complementarity of the two instruments and their ability in describing the complex chemical composition of PM_1 and the related sources. The enhanced deconvolution of closely co-varying sources of ambient pollution epitomises the novelty of our study and demonstrates the capability of PTR_{CHARON} to deliver detailed qualitative and quantitative insights, thus enabling a comprehensive understanding of organic aerosol sources. These advances can assist environmental regulators and citizen efforts to improve air quality in Fairbanks and the fast-urbanising regional sub-Arctic areas.

Data availability

Supporting text, figures, and tables are available in the Supplementary Material.

Author contributions

The manuscript was written with the contributions of all authors. BT-R and BDA set up, ran, and maintained the instrumentation during the campaign in Fairbanks. SA, NB, and ED aided during the campaign. MC-S collected and contributed meteorological and trace gas data. BA, RJW, KD, and AM provided data on ion chromatography analysis of offline filter samples. BT-R and AI processed and analysed the data with help from BC. WS and KS coordinated the ALPACA and CASPA projects. KL, BDA, BB, SB, JF, JM, and JS contributed to funding acquisition for the CASPA project. BDA supervised the project reported here.

Competing interests

The authors declare that they have no conflict of interest.

Acknowledgements

We thank the ALPACA team of researchers and all others involved in designing the project and providing the necessary logistical support to carry it out. We thank Dr Anna Tobler (Datalystica Ltd, Switzerland) for providing technical support for SoFi analysis. This work was funded by the CASPA (Climate-relevant Aerosol Sources and Processes in the Arctic) project of the Agence Nationale de la Recherche (grant no. ANR-21-CE01-0017) and the IPEV (French Polar Institute Paul-Émile Victor). KD and RJW were supported by the National Science Foundation's (NSF) Atmospheric Geoscience Program (grant no. AGS-2029730) and the NSF Navigating the New Arctic Program (grant no. NNA-1927778). SRA acknowledges support from the UK Natural Environment Research Council (grant ref: NE/W00609X/1). We thank the MASSALYA instrumental platform (Aix-Marseille Université, Laboratory of Chemistry and Environment, lce.univ-amu.fr) for the measurements used in this publication. AI is grateful to Subuktageen Qitta, Nastaran Mahmud, Laal Boo'on-Wali, and Minuit Mahmud for the many useful discussions that helped compile this report.

References

Aiken, A. C., DeCarlo, P. F., and Jimenez, J. L.: Elemental analysis of organic species with electron ionization high-resolution mass spectrometry, Analytical chemistry, 79, 8350-8358, 2007.

Aiken, A. C., Decarlo, P. F., Kroll, J. H., Worsnop, D. R., Huffman, J. A., Docherty, K. S., Ulbrich, I. M., Mohr, C., Kimmel, J. R., and Sueper, D.: O/C and OM/OC ratios of primary, secondary, and ambient organic aerosols with high-resolution time-of-flight aerosol mass spectrometry, Environmental science & technology, 42, 4478-4485, 2008.

Alaska Department of Environmental Conservation, Know Your Wood: https://dec.alaska.gov/air/burnwise/know-your-wood

Alves, C. A., Vicente, E. D., Rocha, S., and Vicente, A. M.: Organic tracers in aerosols from the residential combustion of pellets and agro-fuels, Air Quality, Atmosphere & Health, 10, 37-45, 2017.

Bari, M. A., Baumbach, G., Kuch, B., and Scheffknecht, G.: Wood smoke as a source of particle-phase organic compounds in residential areas, Atmospheric Environment, 43, 4722–4732, 2009.

Brégonzio-Rozier, L., Siekmann, F., Giorio, C., Pangui, E., Morales, S., Temime-Roussel, B., Gratien, A., Michoud, V., Ravier, S., and Cazaunau, M.: Gaseous products and secondary organic aerosol formation during long term oxidation of isoprene and methacrolein, Atmospheric Chemistry and Physics, 15, 2953-2968, 2015.

Campbell, J. R., Battaglia Jr, M., Dingilian, K., Cesler-Maloney, M., St Clair, J. M., Hanisco, T. F., Robinson, E., DeCarlo, P., Simpson, W., and Nenes, A.: Source and Chemistry of Hydroxymethanesulfonate (HMS) in Fairbanks, Alaska, Environmental Science & Technology, 2022.

Campbell, J. R., Battaglia Jr, M., Dingilian, K. K., Cesler-Maloney, M., Simpson, W. R., Robinson, E. S., DeCarlo, P. F., Temime-Roussel, B., D'Anna, B., and Holen, A. L.: Enhanced aqueous formation and neutralization of fine atmospheric particles driven by extreme cold, Science Advances, 10, eado4373, 2024.

Canagaratna, M., Jayne, J., Jimenez, J., Allan, J., Alfarra, M., Zhang, Q., Onasch, T., Drewnick, F., Coe, H., and Middlebrook, A.: Chemical and microphysical characterization of ambient aerosols with the aerodyne aerosol mass spectrometer, Mass spectrometry reviews, 26, 185-222, 2007.

Canagaratna, M., Jimenez, J., Kroll, J., Chen, Q., Kessler, S., Massoli, P., Hildebrandt Ruiz, L., Fortner, E., Williams, L., and Wilson, K.: Elemental ratio measurements of organic compounds using aerosol mass spectrometry: characterization, improved calibration, and implications, Atmospheric Chemistry and Physics, 15, 253-272, 2015.

Canagaratna, M. R., Jayne, J. T., Ghertner, D. A., Herndon, S., Shi, Q., Jimenez, J. L., Silva, P. J., Williams, P., Lanni, T., and Drewnick, F.: Chase studies of particulate emissions from in-use New York City vehicles, Aerosol Science and Technology, 38, 555-573, 2004.

Canonaco, F., Crippa, M., Slowik, J. G., Baltensperger, U., and Prévôt, A. S.: SoFi, an IGOR-based interface for the efficient use of the generalized multilinear engine (ME-2) for the source apportionment: ME-2 application to aerosol mass spectrometer data, Atmospheric Measurement Techniques, 6, 3649-3661, 2013.

Cash, J. M., Langford, B., Di Marco, C., Mullinger, N., Allan, J., Reyes-Villegas, E., Joshi, R., Heal, M. R., Acton, W. J. F., and Hewitt, N.: Seasonal analysis of submicron aerosol in Old Delhi using high resolution aerosol mass spectrometry: Chemical characterisation, source apportionment and new marker identification, Atmospheric Chemistry and Physics Discussions, 2020, 1-42, 2020.

Cesler-Maloney, M., Simpson, W., Kuhn, J., Stutz, J., Thomas, J., Roberts, T., Huff, D., and Cooperdock, S.: Shallow boundary layer heights controlled by the surface-based temperature inversion strength are responsible for trapping home heating emissions near the ground level in Fairbanks, Alaska, EGUsphere, 2024, 1-51, 2024.

Cesler-Maloney, M., Simpson, W. R., Miles, T., Mao, J., Law, K. S., and Roberts, T. J.: Differences in Ozone and Particulate Matter Between Ground Level and 20 m Aloft are Frequent During Wintertime Surface-Based Temperature Inversions in Fairbanks, Alaska, Journal of Geophysical Research: Atmospheres, 127, e2021JD036215, 2022.

Chazeau, B., El Haddad, I., Canonaco, F., Temime-Roussel, B., d'Anna, B., Gille, G., Mesbah, B., Prévôt, A. S., Wortham, H., and Marchand, N.: Organic aerosol source apportionment by using rolling positive matrix factorization: Application to a Mediterranean coastal city, Atmospheric environment: X, 14, 100176, 2022.

Chen, G., Canonaco, F., Tobler, A., Aas, W., Alastuey, A., Allan, J., Atabakhsh, S., Aurela, M., Baltensperger, U., and Bougiatioti, A.: European aerosol phenomenology− 8: Harmonised source apportionment of organic aerosol using 22 Year-long ACSM/AMS datasets, Environment international, 166, 107325, 2022.

Chen, G., Li, S., Zhang, Y., Zhang, W., Li, D., Wei, X., He, Y., Bell, M. L., Williams, G., and Marks, G. B.: Effects of ambient PM1 air pollution on daily emergency hospital visits in China: an epidemiological study, The Lancet Planetary Health, 1, e221-e229, 2017.

Chen, Y., Xu, L., Humphry, T., Hettiyadura, A. P., Ovadnevaite, J., Huang, S., Poulain, L., Schroder, J. C., Campuzano-Jost, P., and Jimenez, J. L.: Response of the aerodyne aerosol mass spectrometer to inorganic sulfates and organosulfur compounds: Applications in field and laboratory measurements, Environmental science & technology, 53, 5176-5186, 2019.

Collard, F.-X. and Blin, J.: A review on pyrolysis of biomass constituents: Mechanisms and composition of the products obtained from the conversion of cellulose, hemicelluloses and lignin, Renew. Sustain. Energy Rev., 38, 594–608, https://doi.org/10.1016/j.rser.2014.06.013, 2014.

Crippa, M., Canonaco, F., Lanz, V., Äijälä, M., Allan, J., Carbone, S., Capes, G., Ceburnis, D., Dall'Osto, M., and Day, D.: Organic aerosol components derived from 25 AMS data sets across Europe using a consistent ME-2 based source apportionment approach, Atmospheric chemistry and physics, 14, 6159-6176, 2014.

Cubison, M., Ortega, A., Hayes, P., Farmer, D., Day, D., Lechner, M., Brune, W., Apel, E., Diskin, G., and Fisher, J.: Effects of aging on organic aerosol from open biomass burning smoke in aircraft and laboratory studies, Atmospheric Chemistry and Physics, 11, 12049-12064, 2011.

Czarnecki, N.: Local Air Quality Regulations: How to Participate and Comply, Clear the Air Home Heating Forum and Expo,

DeCarlo, P. F., Kimmel, J. R., Trimborn, A., Northway, M. J., Jayne, J. T., Aiken, A. C., Gonin, M., Fuhrer, K., Horvath, T., and Docherty, K. S.: Field-deployable, high-resolution, time-of-flight aerosol mass spectrometer, Analytical chemistry, 78, 8281-8289, 2006.

Dingilian, K., Hebert, E., Battaglia Jr, M., Campbell, J. R., Cesler-Maloney, M., Simpson, W., St. Clair, J. M., Dibb, J., Temime-Roussel, B., and D'anna, B.: Hydroxymethanesulfonate and Sulfur (IV) in Fairbanks Winter During the ALPACA Study, ACS ES&T Air, 2024.

Dunleavy, M. and Brune, J. W.: Amendments to: State Air Quality Control Plan. Vol. III: Appendix III.D.7.06, 2019.

Dunleavy, M. J. and Brune, J. W.: Amendments to State Air Quality Control Plan: Vol. III: Appendix III.D.7.7, Alaska Department of Environmental Conservation, 2020.

Eichler, P., Müller, M., D'anna, B., and Wisthaler, A.: A novel inlet system for online chemical analysis of semi-volatile submicron particulate matter, Atmospheric Measurement Techniques, 8, 1353-1360, 2015.

Eichler, P., Müller, M., Rohmann, C., Stengel, B., Orasche, J. r., Zimmermann, R., and Wisthaler, A.: Lubricating oil as a major constituent of ship exhaust particles, Environmental Science & Technology Letters, 4, 54-58, 2017.

Ellis, A. and Mayhew, C.: Chemical Ionization: Chemistry, Thermodynamics and Kinetics, Proton Transfer Reaction Mass Spectrometry, 25-48, 2014.

Fairbanks Air Quality Plan: https://www.epa.gov/ak/fairbanks-air-quality-plan, last access: May 07, 2024.

Fine, P. M., Cass, G. R., and Simoneit, B. R.: Chemical characterization of fine particle emissions from fireplace combustion of woods grown in the northeastern United States, Environmental Science & Technology, 35, 2665-2675, 2001.

Fine, P. M., Cass, G. R., and Simoneit, B. R.: Organic compounds in biomass smoke from residential wood combustion: Emissions characterization at a continental scale, Journal of Geophysical Research: Atmospheres, 107, ICC 11-11-ICC 11-19, 2002.

Fraser, M. P. and Lakshmanan, K.: Using levoglucosan as a molecular marker for the long-range transport of biomass combustion aerosols, Environmental Science & Technology, 34, 4560-4564, 2000.

Fye, M., Havel, B., Havel, H., and Putnam, J.: Opportunities for Air Quality Improvement in the Fairbanks North Star Borough, 2009.

Gkatzelis, G. I., Hohaus, T., Tillmann, R., Gensch, I., Müller, M., Eichler, P., Xu, K.-M., Schlag, P., Schmitt, S. H., and Yu, Z.: Gas-to-particle partitioning of major biogenic oxidation products: a study on freshly formed and aged biogenic SOA, Atmospheric chemistry and physics, 18, 12969-12989, 2018.

Glasius, M., Ketzel, M., Wåhlin, P., Jensen, B., Mønster, J., Berkowicz, R., and Palmgren, F.: Impact of wood combustion on particle levels in a residential area in Denmark, Atmospheric Environment, 40, 7115-7124, 2006.

Gueneron, M., Erickson, M. H., VanderSchelden, G. S., and Jobson, B. T.: PTR-MS fragmentation patterns of gasoline hydrocarbons, International Journal of Mass Spectrometry, 379, 97-109, 2015.

Guo, S., Hu, M., Peng, J., Wu, Z., Zamora, M. L., Shang, D., Du, Z., Zheng, J., Fang, X., and Tang, R.: Remarkable nucleation and growth of ultrafine particles from vehicular exhaust, Proceedings of the National Academy of Sciences, 117, 3427-3432, 2020.

Haque, M. M., Kawamura, K., Deshmukh, D. K., Kunwar, B., and Kim, Y.: Biomass burning is an important source of organic aerosols in interior Alaska, Journal of Geophysical Research: Atmospheres, 126, e2021JD034586, 2021.

Herring, C. L., Faiola, C. L., Massoli, P., Sueper, D., Erickson, M. H., McDonald, J. D., Simpson, C. D., Yost, M. G., Jobson, B. T., and VanReken, T. M.: New methodology for quantifying polycyclic aromatic hydrocarbons (PAHs) using high-resolution aerosol mass spectrometry, Aerosol Science and Technology, 49, 1131-1148, 2015.

Ijaz, A., Temime Roussel, B., Kammer, J., Mao, J., Simpson, W., Law, K., and D'Anna, B.: In situ measurements of gas-particle partitioning of organic compounds in Fairbanks, Faraday Discussions - In Prep, 2025.

Janhäll, S., Andreae, M. O., and Pöschl, U.: Biomass burning aerosol emissions from vegetation fires: particle number and mass emission factors and size distributions, Atmospheric chemistry and physics, 10, 1427-1439, 2010.

Jentgen, M.: Technical support document for Alaska Department of Environmental Conservation's (ADEC) control measure analysis, under 40 CFR 1010(a) and (c), US EPA, Region 10, Air and Radiation Division, 2022.

Jiang, X., Tsona, N. T., Jia, L., Liu, S., Zhang, H., Xu, Y., and Du, L.: Secondary organic aerosol formation from photooxidation of furan: effects of NO x and humidity, Atmospheric chemistry and physics, 19, 13591-13609, 2019.

Joyce, P., Von Glasow, R., and Simpson, W.: The fate of NO x emissions due to nocturnal oxidation at high latitudes: 1-D simulations and sensitivity experiments, Atmospheric Chemistry and Physics, 14, 7601-7616, 2014.

Katz, E. F., Guo, H., Campuzano-Jost, P., Day, D. A., Brown, W. L., Boedicker, E., Pothier, M., Lunderberg, D. M., Patel, S., and Patel, K.: Quantification of cooking organic aerosol in the indoor environment using aerodyne aerosol mass spectrometers, Aerosol Science and Technology, 55, 1099-1114, 2021.

Kawamoto, H.: Lignin pyrolysis reactions, Journal of Wood Science, 63, 117-132, 2017.

Kong, X., Salvador, C. M., Carlsson, S., Pathak, R., Davidsson, K. O., Le Breton, M., Gaita, S. M., Mitra, K., Hallquist, Å. M., and Hallquist, M.: Molecular characterization and optical properties of primary emissions from a residential wood burning boiler, Science of the Total Environment, 754, 142143, 2021.

Koss, A. R., Sekimoto, K., Gilman, J. B., Selimovic, V., Coggon, M. M., Zarzana, K. J., Yuan, B., Lerner, B. M., Brown, S. S., Jimenez, J. L., Krechmer, J., Roberts, J. M., Warneke, C., Yokelson, R. J., and De Gouw, J.: Non-methane organic gas emissions from biomass burning: identification, quantification, and emission factors from PTR-ToF during the FIREX 2016 laboratory experiment, Atmospheric Chem. Phys., 18, 3299–3319, https://doi.org/10.5194/acp-18-3299-2018, 2018.

Kostenidou, E., Marques, B., Temime-Roussel, B., Liu, Y., Vansevenant, B., Sartelet, K., and D'Anna, B.: Secondary organic aerosol formed by Euro 5 gasoline vehicle emissions: chemical composition and gas-to-particle phase partitioning, Atmospheric Chemistry and Physics, 24, 2705-2729, 2024.

Kostenidou, E., Martinez-Valiente, A., R'Mili, B., Marques, B., Temime-Roussel, B., André, M., Liu, Y., Louis, C., Vansevenant, B., and Ferry, D.: Emission factors, chemical composition and morphology of particles emitted from Euro 5 diesel and gasoline light duty vehicles during transient cycles, Atmospheric Chemistry and Physics Discussions, 2020, 1-33, 2020.

Kotchenruther, R. A.: Source apportionment of PM2. 5 at multiple Northwest US sites: Assessing regional winter wood smoke impacts from residential wood combustion, Atmospheric Environment, 142, 210-219, 2016.

Kumar, V., Giannoukos, S., Haslett, S. L., Tong, Y., Singh, A., Bertrand, A., Lee, C. P., Wang, D. S., Bhattu, D., and Stefenelli, G.: Highly time-resolved chemical speciation and source apportionment of organic aerosol components in Delhi, India, using extractive electrospray ionization mass spectrometry, Atmospheric Chemistry and Physics, 22, 7739-7761, 2022.

Lannuque, V., d'Anna, B., Kostenidou, E., Couvidat, F., Martinez-Valiente, A., Eichler, P., Wisthaler, A., Müller, M., Temime-Roussel, B., and Valorso, R.: Gas–particle partitioning of toluene oxidation products: an experimental and modeling study, Atmospheric Chemistry and Physics, 23, 15537-15560, 2023.

Leglise, J., Müller, M., Piel, F., Otto, T., and Wisthaler, A.: Bulk Organic Aerosol Analysis by Proton-Transfer-Reaction Mass Spectrometry: An Improved Methodology for the Determination of Total Organic Mass, O: C and H: C Elemental Ratios, and the Average Molecular Formula, Analytical chemistry, 91, 12619-12624, 2019.

Lignell, H., Epstein, S. A., Marvin, M. R., Shemesh, D., Gerber, B., and Nizkorodov, S.: Experimental and theoretical study of aqueous cis-pinonic acid photolysis, The Journal of Physical Chemistry A, 117, 12930-12945, 2013.

Liu, L., Breitner, S., Schneider, A., Cyrys, J., Brüske, I., Franck, U., Schlink, U., Leitte, A. M., Herbarth, O., and Wiedensohler, A.: Size-fractioned particulate air pollution and cardiovascular emergency room visits in Beijing, China, Environmental research, 121, 52-63, 2013.

Lopez-Hilfiker, F., Mohr, C., Ehn, M., Rubach, F., Kleist, E., Wildt, J., Mentel, T. F., Lutz, A., Hallquist, M., and Worsnop, D.: A novel method for online analysis of gas and particle composition: description and evaluation of a Filter Inlet for Gases and AEROsols (FIGAERO), Atmospheric Measurement Techniques, 7, 983-1001, 2014.

Louis, C., Liu, Y., Martinet, S., D'Anna, B., Valiente, A. M., Boreave, A., R'Mili, B., Tassel, P., Perret, P., and Andre, M.: Dilution effects on ultrafine particle emissions from Euro 5 and Euro 6 diesel and gasoline vehicles, Atmospheric environment, 169, 80-88, 2017.

Mainka, A. and Zajusz-Zubek, E.: PM1 in ambient and indoor air—urban and rural areas in the Upper Silesian Region, Poland, Atmosphere, 10, 662, 2019.

Mayfield, J. A. and Fochesatto, G. J.: The layered structure of the winter atmospheric boundary layer in the interior of Alaska, Journal of Applied Meteorology and Climatology, 52, 953-973, 2013.

McLafferty, F. W. and Tureˇcek, F.: Interpretation of mass spectra, Mill Valley (Calif.) : University Science Books, 4th ed. edn., ISBN 0935702253, 1993.

Meng, X., Ma, Y., Chen, R., Zhou, Z., Chen, B., and Kan, H.: Size-fractionated particle number concentrations and daily mortality in a Chinese city, Environmental health perspectives, 121, 1174-1178, 2013.

Middlebrook, A. M., Bahreini, R., Jimenez, J. L., and Canagaratna, M. R.: Evaluation of composition-dependent collection efficiencies for the aerodyne aerosol mass spectrometer using field data, Aerosol Science and Technology, 46, 258-271, 2012.

Mohr, C., Huffman, J. A., Cubison, M. J., Aiken, A. C., Docherty, K. S., Kimmel, J. R., Ulbrich, I. M., Hannigan, M., and Jimenez, J. L.: Characterization of primary organic aerosol emissions from meat cooking, trash burning, and motor vehicles with high-resolution aerosol mass spectrometry and comparison with ambient and chamber observations, Environmental Science & Technology, 43, 2443-2449, 2009.

Montoya-Aguilera, J., Horne, J. R., Hinks, M. L., Fleming, L. T., Perraud, V., Lin, P., Laskin, A., Laskin, J., Dabdub, D., and Nizkorodov, S. A.: Secondary organic aerosol from atmospheric photooxidation of indole, Atmospheric Chemistry and Physics, 17, 11605-11621, 2017.

Moon, A., Jongebloed, U., Dingilian, K. K., Schauer, A. J., Chan, Y.-C., Cesler-Maloney, M., Simpson, W. R., Weber, R. J., Tsiang, L., and Yazbeck, F.: Primary Sulfate Is the Dominant Source of Particulate Sulfate during Winter in Fairbanks, Alaska, ACS ES&T Air, 2023.

Morin, B., Allen, G., Marin, A., Rector, L., and Ahmadi, M.: Impacts of wood species and moisture content on emissions from residential wood heaters, Journal of the Air & Waste Management Association, 72, 647-661, 2022.

Müller, M., Leglise, J., Piel, F., and Wisthaler, A.: A CHARON PTR-ToF-MS study on the volatility of freshly formed biogenic SOA, Geophysical Research Abstracts,

Müller, M., Eichler, P., D'Anna, B., Tan, W., and Wisthaler, A.: Direct sampling and analysis of atmospheric particulate organic matter by proton-transfer-reaction mass spectrometry, Analytical chemistry, 89, 10889-10897, 2017.

Paatero, P.: Least squares formulation of robust non-negative factor analysis, Chemometrics and intelligent laboratory systems, 37, 23-35, 1997a.

Paatero, P.: A weighted non-negative least squares algorithm for three-way 'PARAFAC'factor analysis, Chemometrics and Intelligent Laboratory Systems, 38, 223-242, 1997b.

Paatero, P.: The multilinear engine—a table-driven, least squares program for solving multilinear problems, including the n-way parallel factor analysis model, Journal of Computational and Graphical Statistics, 8, 854-888, 1999.

Paatero, P. and Hopke, P. K.: Discarding or downweighting high-noise variables in factor analytic models, Analytica Chimica Acta, 490, 277-289, 2003.

Paatero, P. and Tapper, U.: Positive matrix factorization: A non-negative factor model with optimal utilization of error estimates of data values, Environmetrics, 5, 111-126, 1994.

Paatero, P., Eberly, S., Brown, S., and Norris, G.: Methods for estimating uncertainty in factor analytic solutions, Atmospheric Measurement Techniques, 7, 781-797, 2014.

Palm, B. B., Peng, Q., Fredrickson, C. D., Lee, B. H., Garofalo, L. A., Pothier, M. A., Kreidenweis, S. M., Farmer, D. K., Pokhrel, R. P., and Shen, Y.: Quantification of organic aerosol and brown carbon evolution in fresh wildfire plumes, Proceedings of the National Academy of Sciences, 117, 29469-29477, 2020.

Peng, Y., Wang, H., Gao, Y., Jing, S., Zhu, S., Huang, D., Hao, P., Lou, S., Cheng, T., and Huang, C.: Real-time measurement of phase partitioning of organic compounds using a proton-transfer-reaction time-of-flight mass spectrometer coupled to a CHARON inlet, Atmospheric Measurement Techniques, 16, 15-28, 2023.

Piel, F., Müller, M., Mikoviny, T., Pusede, S. E., and Wisthaler, A.: Airborne measurements of particulate organic matter by proton-transfer-reaction mass spectrometry (PTR-MS): a pilot study, Atmospheric Measurement Techniques, 12, 5947-5958, 2019.

Piel, F., Müller, M., Winkler, K., Skytte af Sätra, J., and Wisthaler, A.: Introducing the extended volatility range proton-transfer-reaction mass spectrometer (EVR PTR-MS), Atmospheric Meas. Tech., 14, 1355–1363, 2021.

Pikridas, M., Sciare, J., Freutel, F., Crumeyrolle, S., Von Der Weiden-Reinmüller, S., Borbon, A., Schwarzenboeck, A., Merkel, M., Crippa, M., and Kostenidou, E.: In situ formation and spatial variability of particle number concentration in a European megacity, Atmospheric Chemistry and Physics, 15, 10219-10237, 2015.

Qi, L., Chen, M., Stefenelli, G., Pospisilova, V., Tong, Y., Bertrand, A., Hueglin, C., Ge, X., Baltensperger, U., and Prévôt, A. S.: Organic aerosol source apportionment in Zurich using an extractive electrospray ionization time-of-flight mass spectrometer (EESI-TOF-MS)–Part 2: Biomass burning influences in winter, Atmospheric Chemistry and Physics, 19, 8037-8062, 2019.

Reemtsma, T.: Determination of molecular formulas of natural organic matter molecules by (ultra-) high-resolution mass spectrometry: status and needs, Journal of chromatography A, 1216, 3687-3701, 2009.

Reid, J., Koppmann, R., Eck, T., and Eleuterio, D.: A review of biomass burning emissions part II: intensive physical properties of biomass burning particles, Atmospheric chemistry and physics, 5, 799-825, 2005.

Robinson, E. S., Cesler-Maloney, M., Tan, X., Mao, J., Simpson, W., and DeCarlo, P. F.: Wintertime spatial patterns of particulate matter in Fairbanks, AK during ALPACA 2022, Environmental Science: Atmospheres, 3, 568-580, 2023.

Robinson, E. S., Battaglia Jr, M., Campbell, J. R., Cesler-Maloney, M., Simpson, W., Mao, J., Weber, R. J., and DeCarlo, P. F.: Multi-year, high-time resolution aerosol chemical composition and mass measurements from Fairbanks, Alaska, Environmental Science: Atmospheres, 2024.

Schauer, J. J. and Cass, G. R.: Source apportionment of wintertime gas-phase and particle-phase air pollutants using organic compounds as tracers, Environmental science & technology, 34, 1821-1832, 2000.

Schueneman, M. K., Nault, B. A., Campuzano-Jost, P., Jo, D. S., Day, D. A., Schroder, J. C., Palm, B. B., Hodzic, A., Dibb, J. E., and Jimenez, J. L.: Aerosol pH indicator and organosulfate detectability from aerosol mass spectrometry measurements, Atmospheric Measurement Techniques, 14, 2237-2260, 2021.

Simoneit, B. R.: A review of biomarker compounds as source indicators and tracers for air pollution, Environmental Science and Pollution Research, 6, 159-169, 1999.

Simoneit, B. R.: Biomass burning—a review of organic tracers for smoke from incomplete combustion, Applied Geochemistry, 17, 129-162, 2002.

Simpson, W., Law, K., Schmale, J., Pratt, K., Arnold, S., Mao, J., Alexander, B., Anenberg, S., Baklanov, A., Bell, D., Brown, S., Creamean, J., Boer, G. d., DeCarlo, P., Descari, S., Elleman, R., Flynn, J., and al, e.: Alaskan Layered Pollution And Chemical Analysis (ALPACA) White Paper, 2019.

Simpson, W. R., Mao, J., Fochesatto, G. J., Law, K. S., DeCarlo, P. F., Schmale, J., Pratt, K. A., Arnold, S. R., Stutz, J., Dibb, J. E., Creamean, J. M., Weber, R. J., Williams, B. J., Alexander, B., Hu, L., Yokelson, R. J., Shiraiwa, M., Decesari, S., Anastasio, C., D'Anna, B., Gilliam, R. C., Nenes, A., St. Clair, J. M., Trost, B., Flynn, J. H., Savarino, J., Conner, L. D., Kettle, N., Heeringa, K. M., Albertin, S., Baccarini, A., Barret, B., Battaglia, M. A., Bekki, S., Brado, T. J., Brett, N., Brus, D., Campbell, J. R., Cesler-Maloney, M., Cooperdock, S., Cysneiros De Carvalho, K., Delbarre, H., DeMott, P. J., Dennehy, C. J. S., Dieudonné, E., Dingilian, K. K., Donateo, A., Doulgeris, K. M., Edwards, K. C., Fahey, K., Fang, T., Guo, F., Heinlein, L. M. D., Holen, A. L., Huff, D., Ijaz, A., Johnson, S., Kapur, S., Ketcherside, D. T., Levin, E., Lill, E., Moon, A. R., Onishi, T., Pappaccogli, G., Perkins, R., Pohorsky, R., Raut, J.-C., Ravetta, F., Roberts, T., Robinson, E. S., Scoto, F., Selimovic, V., Sunday, M. O., Temime-Roussel, B., Tian, X., Wu, J., and Yang, Y.: Overview of the Alaskan Layered Pollution and Chemical Analysis (ALPACA) Field Experiment, ACS EST Air, 1, 200–222, https://doi.org/10.1021/acsestair.3c00076, 2024.

Smith, D. M., Cui, T., Fiddler, M. N., Pokhrel, R. P., Surratt, J. D., and Bililign, S.: Laboratory studies of fresh and aged biomass burning aerosol emitted from east African biomass fuels–Part 2: Chemical properties and characterization, Atmospheric Chemistry and Physics, 20, 10169-10191, 2020.

Smith, S. J., van Aardenne, J., Klimont, Z., Andres, R. J., Volke, A., and Delgado Arias, S.: Anthropogenic sulfur dioxide emissions: 1850–2005, Atmospheric Chemistry and Physics, 11, 1101-1116, 2011.

Song, S., Gao, M., Xu, W., Sun, Y., Worsnop, D. R., Jayne, J. T., Zhang, Y., Zhu, L., Li, M., Zhou, Z., Cheng, C., Lv, Y., Wang, Y., Peng, W., Xu, X., Lin, N., Wang, Y., Wang, S., Munger, J. W., Jacob, D. J., and McElroy, M. B.: Possible heterogeneous chemistry of hydroxymethanesulfonate (HMS) in northern China winter haze, Atmos. Chem. Phys., 19, 1357-1371, 10.5194/acp-19-1357-2019, 2019.

Stefenelli, G., Pospisilova, V., Lopez-Hilfiker, F. D., Daellenbach, K. R., Hüglin, C., Tong, Y., Baltensperger, U., Prévôt, A. S., and Slowik, J. G.: Organic aerosol source apportionment in Zurich using an extractive electrospray ionization time-of-flight mass spectrometer (EESI-TOF-MS)–Part 1: Biogenic influences and day–night chemistry in summer, Atmospheric Chemistry and Physics, 19, 14825-14848, 2019a.

Stefenelli, G., Jiang, J., Bertrand, A., Bruns, E. A., Pieber, S. M., Baltensperger, U., Marchand, N., Aksoyoglu, S., Prévôt, A. S., and Slowik, J. G.: Secondary organic aerosol formation from smoldering and flaming combustion of biomass: a box model parametrization based on volatility basis set, Atmospheric Chemistry and Physics, 19, 11461-11484, 2019b.

Sueper, D.: Squirrel and Pika Error Estimates, 2014.
Sun, Y.-L., Zhang, Q., Schwab, J., Demerjian, K., Chen, W.-N., Bae, M.-S., Hung, H.-M., Hogrefe, O., Frank, B., and Rattigan, O.: Characterization of the sources and processes of organic and inorganic aerosols in New York city with a high-resolution time-of-flight aerosol mass apectrometer, Atmospheric Chemistry and Physics, 11, 1581-1602, 2011.
Temime Roussel, B., Cesler-Maloney, M., Chazeau, B., Ijaz, A., Brett, N., Law, K., Bekki, S., Mao, J., Ketcherside, D., Selimovic, V., Hu, L., Simpson, W. R., and D'Anna, B.: Concentrations and Sources of VOCs during wintertime urban pollution at Fairbanks, Alaska, December 01, 20222022: https://agu.confex.com/agu/fm22/meetingapp.cgi/Paper/1072876
Tobler, A. K., Skiba, A., Canonaco, F., Močnik, G., Rai, P., Chen, G., Bartyzel, J., Zimnoch, M., Styszko, K., and Nęcki, J.: Characterization of non-refractory (NR) PM 1 and source apportionment of organic aerosol in Kraków, Poland, Atmospheric chemistry and physics, 21, 14893-14906, 2021.
Tong, Y., Pospisilova, V., Qi, L., Duan, J., Gu, Y., Kumar, V., Rai, P., Stefenelli, G., Wang, L., and Wang, Y.: Quantification of solid fuel combustion and aqueous chemistry contributions to secondary organic aerosol during wintertime haze events in Beijing, Atmospheric Chemistry and Physics, 21, 9859-9886, 2021.
Tran, H. N. and Mölders, N.: Investigations on meteorological conditions for elevated PM2. 5 in Fairbanks, Alaska, Atmospheric Research, 99, 39-49, 2011.
Ulbrich, I., Canagaratna, M., Zhang, Q., Worsnop, D., and Jimenez, J.: Interpretation of organic components from Positive Matrix Factorization of aerosol mass spectrometric data, Atmospheric Chemistry and Physics, 9, 2891-2918, 2009.
Wang, Y. and Hopke, P. K.: Is Alaska truly the great escape from air pollution?-long term source apportionment of fine particulate matter in Fairbanks, Alaska, Aerosol and Air Quality Research, 14, 1875-1882, 2014.
Wang, Y., Zhang, X., Sun, J., Zhang, X., Che, H., and Li, Y.: Spatial and temporal variations of the concentrations of PM 10, PM 2.5 and PM 1 in China, Atmospheric Chemistry and Physics, 15, 13585-13598, 2015.
Ward, T., Trost, B., Conner, J., Flanagan, J., and Jayanty, R.: Source apportionment of PM2. 5 in a subarctic airshed-fairbanks, Alaska, Aerosol and Air Quality Research, 12, 536-543, 2012.
Williams, B. J., Goldstein, A. H., Kreisberg, N. M., and Hering, S. V.: An in-situ instrument for speciated organic composition of atmospheric aerosols: T hermal desorption a erosol GC/MS-FID (TAG), Aerosol Science and Technology, 40, 627-638, 2006.
Xu, W., Li, Z., Zhang, Z., Li, J., Karnezi, E., Lambe, A. T., Zhou, W., Sun, J., Du, A., and Li, Y.: Changes in physicochemical properties of organic aerosol during photochemical aging of cooking and burning emissions, Journal of Geophysical Research: Atmospheres, 128, e2022JD037911, 2023.
Yang, Y., Battaglia, M. A., Mohan, M. K., Robinson, E. S., DeCarlo, P. F., Edwards, K. C., Fang, T., Kapur, S., Shiraiwa, M., and Cesler-Maloney, M.: Assessing the Oxidative Potential of Outdoor PM2. 5 in Wintertime Fairbanks, Alaska, ACS ES&T Air, 2024.
Ye, L. and Wang, Y.: Long-term air quality study in Fairbanks, Alaska: Air pollutant temporal variations, correlations, and PM2. 5 source apportionment, Atmosphere, 11, 1203, 2020.
Zhang, Q., Jimenez, J. L., Canagaratna, M. R., Ulbrich, I. M., Ng, N. L., Worsnop, D. R., and Sun, Y.: Understanding atmospheric organic aerosols via factor analysis of aerosol mass spectrometry: a review, Analytical and bioanalytical chemistry, 401, 3045-3067, 2011.

Complementary aerosol mass spectrometry elucidates sources of wintertime sub-micron particle pollution in Fairbanks, Alaska, during ALPACA 2022

Amna Ijaz[1,2], Brice Temime-Roussel[1], Benjamin Chazeau[1], Sarah Albertin[3], Stephen R. Arnold[4], Brice Barret[5], Slimane Bekki[6], Natalie Brett[6], Meeta Cesler-Maloney[7], Elsa Dieudonne[8], Kayane K. Dingilian[9], Javier Fochesatto[10], Jingqiu Mao[7], Allison Moon[11], Joel Savarino[3], William Simpson[7], Rodney J. Weber[9], Kathy S. Law[6], Barbara D'Anna[1]

[1]Aix-Marseille Université, CNRS, LCE, Marseille, France
[2]Present Address: Atmospheric, Climate, & Earth Sciences Division, Pacific Northwest National Laboratory, Richland, Washington 99354, United States
[3]University of Grenoble Alpes, CNRS, IRD, Grenoble INP, INRAE, IGE, F-38000 Grenoble, France
[4]School of Earth and Environment, University of Leeds, Leeds, LS2 9JT, United Kingdom
[5]Laboratoire d'Aérologie, Université Toulouse III-Paul Sabatier, CNRS, Toulouse, France
[6]Sorbonne Université, UVSQ, CNRS, LATMOS-IPSL, Paris, France
[7]Department of Chemistry and Biochemistry and Geophysical Institute, University of Alaska, Fairbanks, AK, United States
[8]Laboratory of Physics and Chemistry of the Atmosphere, University of Littoral and Opal Coast, Dunkerque, France
[9]School of Earth and Atmospheric Sciences, Georgia Institute of Technology, Atlanta, Georgia 30332, United States
[10]Department of Atmospheric Sciences, University of Alaska, Fairbanks, AK, United States
[11]Department of Atmospheric Sciences, University of Washington, Seattle, Washington 98195, United States

Correspondence to: Barbara D'Anna (barbara.danna@univ-amu.fr) and Amna Ijaz (amna.ijaz@pnnl.gov)

Fairbanks, Alaska, is a sub-arctic city that frequently suffers from non-attainment of national air quality standards in the wintertime due to the coincidence of weak atmospheric dispersion and increased local

emissions. ~~However, significant uncertainties exist about aerosol sources, formation, and chemical processes during cold winter periods. We identified and quantified~~ various local sources ~~using source apportionment approach and could determine the~~ their chemical ~~composition, size distribution, and concentrations of atmospheric sub-micron non-refractory particulate matter (NR-PM_1)~~ emitted from ~~them and quantify their sources in the urban centre of Fairbanks.~~ As part of the Alaskan Layered Pollution and Chemical Analysis (ALPACA) campaign, we deployed a Chemical Analysis of Aerosol Online (CHARON) inlet coupled with a proton transfer reaction - time of flight mass spectrometer (PTR-ToF MS) and an Aerodyne high-resolution aerosol mass spectrometer (AMS) to measure organic aerosol (OA) and NR-PM_1, respectively. We deployed Positive Matrix Factorisation (PMF) analysis for source identification of the NR-PM_1. ~~The PTR_{CHARON} factorisation identified four residential heating sources, with oil combustion accounting for 16 ± 9% and wood combustion contributing to 47 ± 20% of the OA. The analysis could further differentiate between hardwood and softwood combustion. In contrast,~~ The AMS analysis identified three primary factors: ~~a single~~ biomass burning, ~~a~~ hydrocarbon-like and cooking factors which together accounted for 28, 38 and 11 % of the total OA, respectively. Additionally, a combined organic and inorganic PMF analysis revealed two further factors: one enriched in nitrates and another rich in sulphates of organic and inorganic origin. The PTR_{CHARON} factorization could identify four primary sources from residential heating - one from oil combustion and three wood combustion, categorised as ~~types (~~low temperature, softwood, and hardwood~~)~~. Collectively, all residential heating factors accounted for 79% of the total OA. ~~c~~Cooking and road transport were also recognised as primary contributors to overall emission profile provided by PTR_{CHARON}. All PMF could apportion a single secondary organic fraction. These results evidence the complementarity of the two instruments and their ability in describing the complex chemical composition of PM_1 and the related sources. ~~These results demonstrate that~~ This work further demonstrates the capability of PTR_{CHARON} to provide both ~~generates~~ qualitative and quantitative information offering ~~with enhanced~~a comprehensive understanding of the organic aerosol sources. ~~resolution of organic aerosol sources.~~ Such ~~When combined with suitable complementary instruments like the AMS, such evidence based~~ insights into the sources of sub-micron aerosol ~~pollution~~ can assist environmental regulators and citizen efforts to improve ~~for the improvement in~~ air quality in Fairbanks and ~~in~~ the ~~wider~~ fast-urbanising regional sub-Arctic areas.

Keywords PM_1, mass spectrometry, source apportionment, organic and inorganic aerosol, Fairbanks, Arctic cities, air quality, CHARON PTR-ToF MS, HR-ToF AMS, ~~proton transfer reaction~~residential heating, wood combustion

1 Introduction

Extremely cold urban regions of the Earth, such as in the Arctic, experience poor dispersion of atmospheric pollution, especially during the wintertime, when the unique meteorological characteristics, such as extremely low solar radiation and strong radiative cooling at the surface, are coupled with enhanced local anthropogenic emissions from heating, industry, and transport. A good example is the sub-arctic city of Fairbanks, Alaska, where air quality standards are frequently violated during the winters with concentrations of fine particulate matter (i.e., with aerodynamic diameters smaller than 2.5 μm; $PM_{2.5}$) exceeding the 24-h limit of 35 μg/m^3 defined by EPA's National Ambient Air Quality Standards (Dunleavy and Brune, 2020; Epa, n.d.). Not only is Fairbanks one of the cities with the most polluted wintertime air in the US, but it has also been declared a 'moderate non-attainment area' since 2009, and due to the persistence of the problem, it was reclassified as a 'severe non-attainment area' in 2017. Increased local anthropogenic emissions and poor atmospheric dispersion due to strong surface-based temperature inversions (> 0.5°C/m in the lowest 10 m above the ground) are major causes of wintertime pollution in the region (Tran and Mölders, 2011; Mayfield and Fochesatto, 2013). Many research studies have recognised biomass combustion as the major source of aerosol in Fairbanks (Ward et al., 2012; Wang and Hopke, 2014; Kotchenruther, 2016; Ye and Wang, 2020; Haque et al., 2021) that drives overall $PM_{2.5}$ concentrations across the city during strong temperature inversion conditions (Robinson et al., 2023). A comprehensive study covering three winters from 2008–2011 apportioned 60–80% of $PM_{2.5}$ mass at four locations in Fairbanks to emissions from residential wood stoves, open burning of biomass, outdoor boilers, and other solid-fuel combustion. (Ward et al., 2012). Source apportionment of year-round $PM_{2.5}$ in the past two decades [2008–2009 (Haque et al., 2021), 2005–2012 (Wang and Hopke, 2014), 2009–2014 (Kotchenruther, 2016), and 2013–2019 (Ye and Wang, 2020)] also revealed woodsmoke as a major contributor to $PM_{2.5}$ loads [47.5% (Haque et al., 2021), 40.5% (Wang and Hopke, 2014), ~52% (Kotchenruther, 2016), and ~19% (Ye and Wang, 2020)]. Wildfire activity and residential wood combustion are the major sources in summer and winter, respectively. The persistent role of wood-burning emissions in shaping the air quality of Fairbanks during winters triggered the implementation of a two-stage burn restriction in 2015 by the Alaska Department of Environmental Conservation (ADEC). The ADEC advisories restricted the operation of solid-fuel heating devices and required alternative heat sources to be used on days with weak atmospheric dispersion and $PM_{2.5}$ > 25 μg/m^3 are observed or forecasted (Fye et al., 2009; Czarnecki, 2017; Jentgen, 2022). Sulphate has been observed to be the second largest component of $PM_{2.5}$ mass in Fairbanks (Ward et al., 2012; Wang and Hopke, 2014), forming ~33% of the annual average $PM_{2.5}$ mass (Ye and Wang, 2020). Isotope analyses have revealed 62% of this $PM_{2.5}$ sulphate to be primary (e.g., from residential heating oil combustion) during the winters (Moon et al., 2023).

The aforementioned studies on air quality in Fairbanks have focused on $PM_{2.5}$ even though PM_1 has been recognised as the major cause of negative health effects (Wang et al., 2015; Mainka and Zajusz-Zubek, 2019) due to its capability to spread deeper into the respiratory or cardiovascular systems (Meng et al., 2013; Liu et al., 2013; Chen et al., 2017). Currently, ~~PM_1 concentrations are not regulated globally, but its strong contribution to atmospheric $PM_{2.5}$ loads and impacts has implications for the attainment of the latter's regulatory limits.~~ efforts to monitor PM_1 are surprisingly scarce, even in ~~a~~ 'non-attaining' ~~city~~cities, such as Fairbanks, underscoring the need for a better characterisation of sub-micron aerosols to understand local sources~~emissions~~, ~~atmospheric processes~~, chemical composition and ultimately to inform public health and support policy decisions. ~~even though characterising the chemical composition of sub-micron atmospheric aerosol and capturing the variation in their mass concentrations is key to unravelling the complexities of local emissions and their transformation in Fairbanks and, most importantly, to underscore the health and policy implications of atmospheric emissions.~~

Mass spectrometric techniques have advanced over the years, featuring greater mass accurancy, resolving power, and sensitivity. For instance, the Aerodyne high-resolution time-of-flight aerosol mass spectrometer (HR-ToF AMS; called AMS from hereon) is a well-established method for quantification of non-refractory NR-PM_1. Aerosol vapourisation at high temperatures and electron ionisation result in substantive molecular decomposition, facilitating quantification with high time resolution (Decarlo et al., 2006), but at the cost of molecular-level information~~resolution~~. ~~The lack of molecular-level information provided by AMS~~ This limitation has encourage~~d~~s the rise of complementary techniques ~~to better understand both primary aerosol sources and secondary aerosol formation~~. For instance, extractive electrospray ionisation (EESI)-ToF MS has been successfully deployed in Beijing (Tong et al., 2021) and in Zurich to resolve multiple OA sources (Stefenelli et al., 2019a; Qi et al., 2019). Although the instrument ~~the EESI-ToF-MS~~ provides molecular-level information, its quantitative response is variable and selective for polar species, preventing its independent application for ambient measurements. Other measurement methods, such as thermal desorption aerosol GC/MS flame ionisation detector (TAG)(Williams et al., 2006) and filter inlet for gases and aerosols chemical ionisation (FIGAERO-CIMS)-ToF MS (Lopez-Hilfiker et al., 2014), similarly offer better chemical resolution than the AMS, but a lower temporal resolution. Semi-continuous measurements, such as those from TAG and FIGAERO-CIMS, may not capture the rapid variation in sources.

To improve the analysis of sub-micron OA in ambient air, a novel inlet system called the chemical analysis for aerosol online (CHARON) was developed to collect real-time measurements (Eichler et al., 2015). This inlet minimises thermal and ionisation-induced fragmentation of sampled OA by employing a low-temperature vapourisation system (150°C ≤) and coupling with a relatively softer ~~and less selective~~ ionisation method, such as the proton-transfer reaction (PTR). The CHARON PTR-ToF MS (called PTR_{CHARON} from hereon) was ~~first~~ successfully used for the characterisation of OA from ship

exhaust (Eichler et al., 2017), ambient OA in Lyon, France, and Valencia, Spain, and OA source apportionment in Innsbruck, Austria (Mü~~L~~ller et al., 2017). Recently, the inlet was used to quantify individual compounds in laboratory-generated secondary organic aerosol (Lannuque et al., 2023) and complex mixtures, such as vehicular gasoline emissions and atmospheric organic matter (Piel et al., 2019; Kostenidou et al., 2024). ~~Additionally, the analyser (commonly a PTR-ToF-MS) coupled to the CHARON inlet~~ The system can measure gas-phase species as well, creating the opportunity to explore VOC precursor emissions or phase partitioning (Peng et al., 2023; Gkatzelis et al., 2018). Overall, PTR_{CHARON} and AMS are complementary techniques; ~~that provide robust qualitative and quantitative info. T~~the former features molecular level information of the OA faction ~~in contrast to the AMS,~~ but has limited ability to ~~analyse~~ detect particles ~~smaller than~~below 150 nm (Eichler et al., 2015); the latter ~~instrument~~ covers smaller particle size range (i.e., > 60 nm) and detects inorganic components too (Decarlo et al., 2006). Together they provide an excellent combination of real-time and quantitative data on atmospheric ambient aerosol.

The detailed composition of sub-micron aerosol ~~pollution in the deterioration of air quality~~ in Fairbanks ~~–~~and other anthropogenically influenced ~~regions of the~~ sub-~~wider~~ Arctic regions – is still not well-understood. To address this issue, we deployed a PTR_{CHARON} and an AMS in the urban centre of Fairbanks during the ALPACA (Alaskan Layered Pollution and Chemical Analysis) campaign as part of the French CASPA (Climate-Relevant Aerosol Sources and Processes in the Arctic) project in January–February 2022 (Simpson et al. 2024). We aimed to determine the composition, concentrations, and sources of atmospheric NR-PM_1. In this paper, we present: (i) an intercomparison of the performance of the two instruments focusing on OA quantitation, (ii) the identification of major OA sources in Fairbanks ~~and their variation during the field campaign~~, and (iii) the source apportionment of organic and inorganic aerosol (e.g., ammonium, nitrate, and ~~sulphur~~sulphate). These findings highlight the synergistic benefits of combining multiple analytical techniques and emphasise how soft ionisation mass spectroscopic methods enhance molecular-level insights into particulate organic carbon. This integrated approach advances our understanding of the complex composition of particulate matter, offering valuable contributions to environmental characterisation and source apportionment studies. ~~The results obtained here demonstrates the capability of technique a *m*/Δ*m* of ~5000good mass resolution, combined with the soft ionisation of the PTR_{CHARON},provide significant to capabilities for both molecular-level qualitative and quantitative data, and allowings a better better ultimately contributing to a better understanding of the complex composition of particulate organic carbonand its related sources.~~

2 Methodology

2.1 Field campaign

The data presented in this study were collected during the ALPACA campaign in Fairbanks, Alaska, US from January 20 to February 26, 2022. ALPACA is an international collaborative field experiment to understand sources of outdoor and indoor air pollution in the cold and dark conditions of Fairbanks' winter. The scientific objectives and broad preliminary findings of the experiment were recently reviewed (Simpson et al. 2024). All instruments used for this study were housed in a trailer parked at the Community and Technical College (CTC) of the University of Alaska, Fairbanks (64.84064°N, 147.72677°W; 136 m above sea level). The CTC is in the urban core of Fairbanks, close (within 40 m) to a major downtown road and parking area (Simpson et al. 2024); the west of this locality is dominated by residential activities, while the north and east have commercial activity.

The trailer was equipped with a suite of particle counters and mass spectrometers with high temporal resolutions (varying from 10 seconds to 2 minutes). A scanning mobility particle sizer (SMPS) and a multi-angle absorption photometer (MAAP) were utilised to measure the distribution of particles sized 15.1 to 661.2 nm and black carbon concentrations, respectively. A separate inlet was used for PM_1/$PM_{2.5}$/PM_{10} measurements conducted with a commercial optical particle counter (model OPC 1.109, Grimm Aerosol Technik) at a time resolution of 1 min. Two mass spectrometers, PTR_{CHARON} (150-~~1000 nm) and AMS (60-700~~1000 nm), were connected to the same inlet that sampled air at 3.5 meters above ground level through a short (≈ 1 m) stainless tube with a 1/2" outer diameter extending through the trailer roof. A HEPA filter was placed upstream of the inlet for an hour at regular intervals (twice a week) to measure the instrumental background. Additionally, meteorological data, including ambient temperatures at 3 and 23 m; wind speed and direction; and trace gases, namely CO, SO_2, O_3, NO and NO_2, were recorded as described in a previous study associated with the campaign (Cesler-Maloney et al., 2022).

2.2 Instrumentation

2.2.1 PTR-ToF MS: ~~Operation~~ operation and data processing

The OA was quantified with a PTR-ToF MS (PTR-TOF 6000 X2, Ionicon Analytik GmbH, Austria) coupled to a CHARON inlet in near real-time at 20-s~~ec~~ temporal resolution, i.e., the PTR_{CHARON}. The CHARON inlet has been described in detail by Eichler et al (Eichler et al., 2015) and its applications were further evaluated and improved in subsequent studies (Mül~~l~~ler et al., 2017; Leglise et al., 2019; Müller et al., 2019; Piel et al., 2019; Peng et al., 2023). Here, the PTR-ToF MS was configured to

alternate between ~~direct~~ sampling of ambient~~of~~ air to measure VOCs for 15 minutes (not included in the current study) and sampling of particulate matter through the CHARON inlet for 45 minutes. The instrument was operated at a low E/N of 65 Td (i.e., drift voltage/pressure; pressure, temperature, and voltage of the drift tube were set at 2.6 mbar, 120°C, and 265 V) and in RF mode for optimal sensitivity. The thermodesorber ~~in the CHARON inlet~~ was operated at 150°C and 8 mbar; this combination of moderate temperature with low pressure expands the range of detection to include ELVOCs as well (Piel et al. 2021). Raw data was obtained as described in **Section S1** and pre-processed with the Ionicon Data Analyzer (IDA, version 1.0.0.2), followed by post-processing (i.e., background subtraction, conversion of raw signal to mixing ratios, temporal averaging, PMF input generation) with an in-house data processing tool, PeTeR Toolkit (version 6.0; Igor 6.37). The error matrix was also calculated by PeTeR using uncertainties in ion counts and background signals. Among the resolved 1118 ions ~~resolved~~spanning the range of *m/z* 50–425, only 336 were retained above the S/N ~~with *m/z* 50–425~~, and 318 ions could be given a molecular formula based on the criteria described in **Section S2**. PTR ToF MS records raw signals in counts per second (cps) that were converted to mixing ratios according to the molecular identity determined for the detected ions and their protonation efficiencies (further details in **Section S1**). For comparison with the AMS, mixing ratios were converted to mass concentrations, i.e., µg/m^3, using **Equation S2**. Mass concentrations calculated for the PTR$_{CHARON}$ require a critical correction for the enrichment of sampled OA in the aerodynamic lens of the CHARON inlet (Eichler et al., 2015; ~~MüLler~~ Müller et al., 2017); further details are provided in **Section S3**. Total (or bulk) OA at a given point in time was the sum of mass concentrations of all ions, which was corrected for fragmentation using a previously reported method (Leglise et al., 2019), which increased the total OA mass concentrations by 17%.

Species with *m/z* > 50 ~~(the largest *m/z* detected above the S/N was 425)~~ were retained for PMF of OA. ~~Smaller~~ as molecules ~~of~~ between *m/z* 18–50 were present~~ed~~ in low concentrations and~~; they~~ are expected to be too volatile to be present in OA and were likely detected by PTR$_{CHARON}$ as artefacts from the denuder ~~function~~. Time series were averaged to 2 minutes (from 20 seconds) and two matrices (*m/z* × time points) were extracted: (i) ion concentrations and (ii) their measurement uncertainties, using PeTeR ~~version 6.0 in Igor 6.37~~. The final matrices ~~after removing empty rows and columns~~ had the following dimensions 336 × 17,986. Where required, ion intensities (in either ppb or µg/m^3) were normalised to the sum of all measured intensities.

2.2.2 HR-ToF-AMS: o~~O~~peration and data processing ~~of the AMS~~

NR-PM$_1$ was~~were~~ monitored with 1-minute time resolution by a high-resolution time-of-flight mass spectrometer (AMS) (Aerodyne Research Inc., Billerica, USA), extensively ~~with spectral acquisition~~

~~at 1-minute intervals. The instrument has been~~ described ~~by previously (~~Decarlo et al., ~~(~~2006~~)~~ and ~~;~~ Canagaratna et al~~.~~.(2007). Briefly, ambient particles are sampled through a critical orifice, focused into a narrow~~ed~~ beam by an aerodynamic lens, accelerated toward a standard vapouriser heated ~~element~~ at ~~(~~600°C~~) for flash vapourisation~~, and then ionised by electron impact (70 eV at 10^{-7} torr). Finally, the ions are analysed by a time-of-flight mass spectrometer. Standard calibrations were performed using 300 nm size-selected dried ammonium nitrate and ammonium sulphate particles at the beginning and the end of the campaign. Nitrate-equivalent values of sample mass concentrations were converted by applying relative ionisation efficiencies (RIEs) for organics, nitrates, ammonium, ~~sulphur~~sulphate, and chloride~~s~~ (1.4, 1.1, 3.15, 1.93, and 1.3, respectively). ~~For quantitative purposes, the c~~Collection efficiency (CE) ~~of particles must be considered as strongly viscous particles in the sampled air are prone to bouncing off the vapouriser~~has been calculated in PIKA using ~~, thereby suffering from reduced detection. We used the time series of~~the composition-dependent CE (CDCE) ~~generated by PIKA~~following ~~using a previously reported algorithm (~~Middlebrook et al., ~~(~~2012~~)~~ method. The calculated CE values ~~, which~~ ranged from 1.00 to 0.35.

Data was averaged to 2 minutes and extracted as concentration and measurement uncertainty matrices (*m/z* × time points) using SQUIRREL version 1.65 and PIKA version 1.25 in Igor 8.04. Separate matrices (and subsequently PMF) were prepared for organic only (abbreviated AMS_{org}) and by combining organic and inorganic species (abbreviated $AMS_{org+inorg}$). The inorganic species included in the analyses were nitrate~~s~~ (*m/z* 30, NO^+ and 46, NO_2^+), ~~sulphur~~ sulphate (*m/z* 48, SO^+; 64, SO_2^+; 80, SO_3^+; 81, HSO_3^+; and 98, $H_2SO_4^+$), ammonium (*m/z* 15, NH^+; 16, NH_2^+; and 17, NH_3^+), and chloride~~s~~ (*m/z* 35, Cl^+ and 36, HCl^+). Error matrices were calculated by PIKA based on uncertainty in ion counts, background signal, air beam correction, and electronic noise (Sueper, 2014). Atomic O/C and H/C ratios were calculated based on established methods (Aiken et al., 2007; Aiken et al., 2008; Canagaratna et al., 2015). Where needed for comparison with the PTR_{CHARON}, mass concentrations of PAHs were estimated from fragments as described previously (Herring et al., 2015), and levoglucosan was estimated as detailed in **Section S4**.

Species with *m/z* 12–120 were retained for PMF in this study, excluding important PAHs detected up to *m/z* 252; such PAHs were used as external tracers for factor identification. All PAHs were included in total OA quantification and associated comparisons. This exclusion is expected to cause underestimation below the 2% ~~(by <2%)~~ of the mass of some factors, particularly HOA (hydrocarbon-like organic aerosol) and BBOA (biomass-burning organic aerosol). ~~After removing empty rows and columns,~~Final matrices from AMS_{org} and $AMS_{org+inorg}$ analyses had the following dimensions: 193 × 24,762 and 205 × 24,762, respectively.

2.3 Source apportionment: Positive matrix factorisation

Source apportionment was performed using a PMF implemented in the multilinear engine (ME-2) (Paatero, 1997a, 1999). The PMF was configured and analysed using the SoFi (Source Finder) Pro interface (Canonaco et al., 2013) (version 8.4.1.9.1; Igor 8.04). PMF is a descriptive mathematical algorithm that describes the input data, i.e. measurements of several variables collected over time (here, *m/z* × sampling time points), as a linear combination of factors that have constant mass spectra associated with temporally varying concentrations of the spectral constituents (Paatero, 1997b; Paatero and Tapper, 1994)~~; each of the factors is representative of an emission source~~. The mathematical expressions and functions of the PMF algorithm have been exhaustively detailed in previous studies (e.g., refs. (Tong et al., 2021; Stefenelli et al., 2019a; Chen et al., 2022; Chazeau et al., 2022), etc.). Below we summarise the user-defined configurations applied in SoFi Pro to optimise the PMF of our datasets, PTR_{CHARON}, AMS_{org}, and $AMS_{org+inorg}$. ~~The results were compared in terms of identified sources and the mass of OA (or total NR-PM_1) apportioned to each source.~~

2.3.1. General methodology for PMF analysis

Preliminary PMF was performed without using *a priori* information ~~, i.e., the so-called unconstrained factorisation,~~ to ~~understand the data~~explore ~~the structure of the dataset, potential~~ factor variability, ~~preliminary~~ source contributions, and guide the selection of an optimal solution before applying constraints. ~~These unconstrained trials explored tested~~We considered solutions ranging from 3 ~~three~~ to 13 factors~~.~~, applying a ~~Cell-wise,~~ step-wise, cell-wise ~~down-weighting was applied~~approach~~,~~: ~~whereby~~ variables with S/N < 0.2 (“bad” variables) were down-weighted by a factor of 10, while those with ~~or~~ 0.2 < S/N < 2 (“weak” variables) were down-weighted by a factor of ~~10 and~~ 2~~, respectively~~ (Paatero and Hopke, 2003; Ulbrich et al., 2009). Upon establishing some ~~that~~ primary factors, ~~e.g.,~~ such as cooking and biomass burning, which ~~could~~ were successfully identified ~~readily be factorised~~ in unconstrained trials, we narrowed ~~explored only a subset of~~ the range of possible solutions by applying the a-value approach, which allows for ~~directing the PMF toward meaningful solutions with the *a*-value approach. For this approach, the user can~~ improve factorisation ~~results~~ by constraining the PMF with external data~~, if~~ when available (Canonaco et al., 2013; Paatero, 1999). For instance, a factor profile from a PMF trial in the same experiment, a time series from an external tracer ~~from the same campaign~~, or a well-established factor profile for a source from another experiment may be provided to the PMF as an ‘anchor/vector’ around which it can build a factor in its overall solution. The extent to which each PMF factor can diverge from the anchor is defined by the value of *a* (Tong et al., 2021), which varies from 0 to 1~~, where 0 = no divergence and 1 = up to 100% divergence~~. This anchor can be provided for one or multiple factors and has been proven to improve the quality of PMF solutions compared to unconstrained trials (Tong et al., 2021; Stefenelli et al., 2019a; Chen et al., 2022).

Currently, there are no fully objective criteria for choosing the best number of factors ~~in a solution~~, but ~~;~~some criteria have been suggested in the literature to make an appropriate selection (Chen et al., 2022; Zhang et al., 2011; Ulbrich et al., 2009; Crippa et al., 2014). The PMF solutions reported here were primarily selected based on their ~~-~~physical meaning~~interpretability~~, which was ~~in turn,~~ determined by the presence of ~~the distribution of~~ known tracer compounds in the factors, temporal correlation with co-located measurements of external tracers (e.g., NO_x, SO_2)~~., and the temporal agreement of factors determined by the two instruments~~. We selected an ~~esolved~~ eight, four, and six factors solution from PTR_{CHARON}, AMS_{org}, and $AMS_{org+inorg}$, respectively. The justification for these solutions ~~choices~~ is presented in **Table S2**. Once the most suitable solution, i.e., the base-case, was established, bootstrap analyses were performed to assess its stability, evaluate uncertainties, and conduct a sensitivity analysis on the range of *a*-values used. In an unblocked bootstrapping approach, the original matrices (both data and error) are perturbed by random resampling of the rows to create a new input of the same dimensions, resulting in some duplications and deletions throughout the input (Paatero et al., 2014). The need and application of this approach differed between the PTR_{CHARON} and the two AMS datasets as discussed in **Sections S5** and **S6**, respectively. Ancillary data on particle size distribution ~~in~~ have been associated to mass spectrometry data in an additional PMF analysis ~~each factor was generated by a fully constrained PMF or simple linear regressions of the SMPS datasets~~ (**Section S7**). Finally, the quality of solutions was gauged by the Q/Q_{exp} values and from key diagnostic plots of residuals and the statistical stability across multiple runs (**Figure S5–S7**).

3 Results and Discussion

3.1 Campaign overview

Figure 1 summarises ~~depicts a summary~~ meteorological conditions, chemical composition and particle size distribution of NR-PM_1 observed from January 20 to February 26, 2022. High aerosol loads coincided with poor atmospheric dispersion, due to low wind speeds (<2 m/s), low temperature (below - 10°C) associated with strong surface temperature inversions, as temperature differences between 23 and 3 m above sea level ranging from 3°C to 10°C. The ~~campaign~~ average valuess of BC and NR-PM_1 measured with the MAAP and AMS were **1.4 ± 1.4 µg/m^3** and **8.3 ± 9.3 µg/m^3**, respectively. ~~Intense~~ During intense pollution events ~~episodes occurred from Jan 31 to Feb 02, during which the~~ daily average concentrations of NR-PM_1 were **24–27 µg/m^3**. ~~For this polluted period, another ALPACA study~~ During the same sampling period at NCore site (Fairbanks) ~~reported campaign averaged~~ $PM_{2.5}$ value of ~25 and ~29 µg/m^3 were reported ~~at NCore (a monitoring station located approximately 580 m from the CTC) using a beta attenuation mass monitor and a nearby site of Downtown using a DustTrak DRX~~

aerosol monitor (Robinson et al., 2023). In our study, the hourly PM_1 concentrations measured at the CTC site comprised up to 99% of the $PM_{2.5}$ measured with an OPC, warranting that future studies in Fairbanks must explore the distribution, dynamics, and impacts of sub-micron aerosol to gauge the need for its targeted mitigation. Ancillary OPC measurements at the CTC site showed that the hourly PM_1 mass comprised up to 99% of the $PM_{2.5}$.

Organics were the predominant component of NR-PM_1 throughout the campaign, constituting **~66 ± 11**% of its total mass, while chloride, ammonium, nitrate, and sulphursulphate-based inorganics contributed **2 ± 3, 3 ± 3**, **6 ± 4**, and **22 ± 10**%. This is in line with previous studies in Fairbanks, where OA was the largest component of $PM_{2.5}$ mass (Ward et al., 2012; Ye and Wang, 2020; Robinson et al., 2024). Specifically, according to a recent study from 2020 to 2021, ACSM analysis during the wintertime demonstrated inorganics to form less than 25% of the $PM_{2.5}$ mass only, with sulphate (~10%) and nitrate (~8%) being the predominant components (Robinson et al., 2024). Despite the different average concentrations, the fractional contributions of these non-refractory components remained almost invariable throughout the campaign (**Figure 1D**). Detailed molecular-level composition of organics with the PTR_{CHARON} reveals a large majority of organics to comprise only C, H, and/or O atoms, while only **~9 ± 4%** of the OA_{CHARON} mass measured with this instrument was attributable to heteroatomic speciesmolecules, including organonitrates and organosulphates (**Figure 4 and S8**). Generally, heteroatomic species cannot be distinguished at a resolving power of 5000 FWHM in complex environmental mixtures, such as atmospheric aerosol (Reemtsma, 2009). In this study, based on the low formula error and lack of an appropriate alternate, we gave 53 low-concentration ions (< 2% of the total signal) CHOS or CHNO identities, but due to the low confidence in their formula assignments, they were not considered for factor identification. Prominent peaks include *m/z* 217.09 ($C_{12}H_{12}N_2O_2$), 219.09 ($C_{15}H_{10}N_2$), 123.05 ($C_4H_{10}O_2S$), and 151.08 ($C_6H_{14}O_2S$).

On average, the OA mass loading recovered by PTR_{CHARON} (i.e., OA_{CHARON}) accounted for approximately 85% of the OA mass measured by the AMS (i.e., OA_{AMS}). While the two instruments showed a strong good temporal agreement (R^2 = 0.60) as depicted in **Figures 2A–B**, measurements were biased either toward the AMS_{org} or the PTR_{CHARON} (i.e., distributed away from the 1:1 line in the scatter plot of **Figure 2C**) during different periods of the campaign. These trends could be explained by the variation in relative contributions of two major emission sources identified by both instruments in this study: on-road traffictransport and biomass burning. OA_{CHARON} was comparable to OA_{AMS}, when the relative contribution of $BBOA_{AMS,org}$ was more than 50% of total OA_{AMS} and $HOA_{AMS,org}$ (i.e., traffictransport$_{CHARON}$) was less than 10% (**Figure 2D–E**). Similar trends were observed for some major constituents of BBOA, e.g., levoglucosan and a PAH ($C_{20}H_{12}$) as shown in **Figure S9**. Part of such discrepancy This relationship of instrument performance with the source can be traced back to the size

transmission of particles, where sub-100 nm urban vehicular emissions are underestimated by the PTR_{CHARON} (Guo et al., 2020; Pikridas et al., 2015; Louis et al., 2017; Kostenidou et al., 2020), and larger than 100 nm biomass burning emissions (Reid et al., 2005) are estimated well (Janhäll et al., 2010). Another pPart of the quantitative difference between the two instruments can also be explained by the detection abilities of PTR limitation in ionisation and the ionisation induced fragmentation of analyte ions. during PTR ionisation that introduces a negative biaThis Only abias has been reported to be small underestimation of for oxidised organic compounds has been reported with the PTR_{CHARON} that can be corrected using previously proposed methods (Leglise et al., 2019). Contrarily, Additional Ttests carried outconducted in our laboratory with five C_{16}–C_{26} alkanes as markers of vehicle emissions revealed that they undergo extensive fragmentation, increases dramatically and resultings in a 2–4 times underestimation of their actual concentrations. In line with this, tThe ineffective ionisation of saturated alkanes by PTR (Ellis and Mayhew, 2014) and their tendency of alkanes from vehicular exhausts to undergo dissociative PTR ionisation has also been reported previously (Gueneron et al., 2015) hashave also been reported.

3.2 Source apportionment

3.2.1. Overview of source apportionment

A four-factor solution was selected for the AMS_{org} measurements with three primary factors (i.e., HOA, COA, and BBOA) and an oxygenated or aged OA factor (i.e., OOA). The mass spectra and time series are presented in the supplement (**Figure S10**). Counterparts of these four factors were diagnosed in $AMS_{org+inorg}$ based on a high temporal correlation ($R^2 > 0.9$; Table S4), along with two additional factors: a sulphur-rich factor (labelled sulph-OA) and a nitrate-rich factor (labelled AmNi) (**Figure 3**). An eight-factor solution was selected for PTR_{CHARON} and is summarised in **Figures 4 and 5**. To differentiate between corresponding factors retrieved from the different datasets, they have been given unique subscripts, e.g. $COA_{AMS,org}$, $COA_{AMS,org+inorg}$, COA_{AMS} (i.e., referring to both AMS datasets), or COA_{CHARON}. Amongst the three datasets COA, HOA (labelled '~~traffic~~transport' in PTR_{CHARON} analyses), and OOA were common. A single BBOA factor was observed in AMS_{org} and $AMS_{org+inorg}$, while four chemically distinct, but closely co-varying counterparts were detected by PTR_{CHARON}.

3.2.2. Organic aerosol from residential heating.

Both AMS analyses indicate that biomass burning is among the major sources of PM_1 during the ALPACA campaign. On average, BBOA contributed **1.5 ± 1.9 µg/m³** (**28 ± 18%** of total OA_{AMS}) and **1.6 ± 2.2 µg/m³** NR-PM_1 (**19 ± 14%** of total NR-PM_1 mass). The mass spectra of $BBOA_{AMS}$ featured a strong peak at *m/z* 60 ($C_2H_4O_2^+$) and 73 ($C_3H_5O_2^+$) (**Figure S10A–B**). These fragments are markers of anhydrosugars in wood-forming polymers, such as cellulose(Tobler et al., 2021). Wood combustion has

previously been estimated to be the largest emitter of aerosols in Fairbanks and surrounding areas, where it may produce as much as 80% of the aerosol load (Haque et al., 2021; Ward et al., 2012; Wang and Hopke, 2014; Kotchenruther, 2016). Wood burning emissions are also the major driver of the spatial variability of $PM_{2.5}$ and BC in Fairbanks during strong atmospheric temperature inversions (Robinson et al., 2023). Other typical residential heating sources of emissions in Fairbanks include coal, gas, and fuel oil (Simpson et al., 2019).

The $BBOA_{AMS}$ factor was strongly correlated with PAHs ($R^2 \geq 0.7$) while a . In addition, a moderate correlation was observed with SO_2 ($R^2 = 0.4$) (**Table 1**). While PAHs are a major component of biomass combustion emissions, the emission of SO_2 is largely associated with coal and oil combustion (Smith et al., 2011; Dunleavy and Brune, 2019). However, the AMS was unable to distinguish between multiple combustion-related sources. As shown in the diurnal plots in **Figure 3**, the concentration of the $BBOA_{AMS}$ factor enhanced at ~1800 AKST, stayed stable through the night and then decreased in the early morning. Its lowest mass concentrations occurred during the afternoon (1300–1500 AKST). Therefore, $BBOA_{AMS}$ was could be associated with residential heating, i.e., the combustion of a variety of fuels by residents within their homes (non-commercially), such as in wood-burning stoves, furnaces, boilers, etc. for heating living space. We did not find evidence of OA or NR-PM_1 from commercial heat providers, such as power plants, likely due to their small contribution to surface-level aerosol due to smokestacks lying above the inversion layer.

PTR_{CHARON} apportioned **2.6 ± 3.4** $\mu g/m^3$ of OA_{CHARON}, on average, to four distinct residential heating-related sources expressed as ResH1–4 (**62 ± 26%** of total OA_{CHARON}). These factors closely co-varied in time and were correlated reasonably well (R^2 = 0.5–0.7; **Table S5**) with the $BBOA_{AMS}$ factor. In addition, combining all four residential heating-related factors in PTR_{CHARON} into a composite factor increased the correlation (R^2) with AMS_{org} and $AMS_{org+inorg}$ to 0.79 and 0.82, respectively, suggesting that PMF was not able to effectively separate these closely co-varying residential heating factors when their molecular signatures were weakened due to the extensive EI-induced fragmentation in AMS dataset.

The four factors from PTR_{CHARON} were identified as different sources based on the distribution of key marker species and correlation with external (e.g., trace gases, etc.) and internal (e.g., PAHs). measured with co-located instruments; particle size distribution) tracers. The lLevoglucosan signal is used here as an internal tracer of biomass burning being because it is relatively stable under typical atmospheric conditions (Fraser and Lakshmanan, 2000). A majority of the signal from pProtonated levoglucosan (*m/z* 163) and its fragments (at *m/z* 85, 127, and 145) were found appeared in ResH1, ResH4, and ResH2 with **30, 26, 14%** of the total signal respectively **(Figure S11)** in the same order), with only minor

~~association with ResH3accounted for~~ suggesting that they ~~the former three to~~ originate from biomass ~~burning – more specifically,~~ wood-burning (**Figure 4 and S11**). These three ~~wood-burning related~~ factors collectively accounted for ~~produced an average of~~ **2.1 ± 2.5 µg/m³** (~~of OA$_{CHARON}$ (~~**47 ± 20%**~~)~~ of total factorised OA$_{CHARON}$~~)~~.

ResH1 includes low temperature combustion markers: this factor is small as it contributes to only an average of **0.5 ± 0.5 µg/m³** (**14%**) of the total OA $_{CHARON}$, but it contains the highest fraction of levoglucosan (~30%). Approximately 65% of the total signal of ResH1 is due to compounds with six or fewer carbon atoms, compared to heavier species present in the other factors (**Figure S13**). The most abundant species are at *m/z* 69.03 (C_4H_4O; furan) (Palm et al., 2020; Jiang et al., 2019), m/z 87.04 ($C_4H_6O_2$; oxobutanal) (Brégonzio-Rozier et al., 2015), *m/z* 97.03 ($C_5H_4O_2$; furfural), *m/z* 109.0286 ($C_6H_4O_2$; benzoquinone) (Stefenelli et al., 2019b) and *m/z* 115.04 ($C_5H_6O_3$; methyl-dihydrofuran) (Koss et al., 2018). Consistent with these molecular formulae, the concentration-weighted average O/C of ResH1 was relatively higher (i.e., 0.42) compared to other residential heating factors (O/C = 0.2–0.3). The most abundant species observed in ResH1 can be related to depolymerisation reactions occurring during low temperature and early stages of the combustion process (Collard and Blin, 2014; Sekimoto et al., 2018). ~~***ResH1 includes mixed wood-burning OA:*** Although ResH1 had the strongest levoglucosan signal, it contributed the least OA with an average of **0.5 ± 0.5 µg/m³** and did not feature any other prominent wood-burning tracers, such as PAHs. As shown in **Figure S13**, ~65% of the total signal of ResH1 came from compounds with six or fewer carbon atoms, compared to heavier species in other factors. Many species with the greatest concentrations in ResH1, relative to other factors, have been reported as oxidation products of BBOA ageing in previous studies, such as *m/z* 69.03 (C_4H_4O; furan) (Palm et al., 2020; Jiang et al., 2019), *m/z* 87.04 ($C_4H_6O_2$; oxobutanal) (Brégonzio-Rozier et al., 2015), *m/z* 97.03 ($C_5H_4O_2$; furfural), and *m/z* 109.0286 ($C_6H_4O_2$; benzoquinone)(Stefenelli et al., 2019b). Collectively, ResH1 comprises OA from the combustion of a variety of mixed wood-based solid fuels as evidenced by the presence of levoglucosan, but it also likely includes OA in the early stages of processing.~~

ResH2 and ResH4 include OA from hardwood and pinewood combustion, respectively: Two more factors associated with wood-burning were ResH2 and ResH4. Their average ~~OA$_{CHARON}$~~ concentrations were **1.1 ± 1.9** and **0.8 ± 0.9 µg/m³**, respectively, corresponding to **28** and **20%** of the OA$_{CHARON}$ (**Figure 6**). ~~As shown in **Figure 6A**,~~ The ResH2 was dominant factor in the PMF ~~of PTR$_{CHARON}$ that~~and could reach ~**37 µg/m³** ~~of OA$_{CHARON}$ alone~~ during the most severe pollution episodes. ~~Not only did these~~ Both factors ~~correspond to~~ were associated to ~~OA~~ particles ~~sizes~~ greater than 300 nm (**Figure S12**), ~~which is~~ typical of woodsmoke (Glasius et al., 2006), and ~~but they also~~ presented unique molecular signatures of different wood types ~~as shown in (~~**Figure S11**~~) and discussed next~~. Generally, the specific nature of

wood cannot be inferred unambiguously because the emissions of known marker species, such as levoglucosan or methoxy phenols, vary not just with fuel used and its quality, but also with the type of heating appliance, operational conditions, appliance efficiency, and stage in the combustion cycle (Fine et al., 2002; Alves et al., 2017). Regardless, several studies (Fine et al., 2002; Schauer and Cass, 2000; Kawamoto, 2017) have distinguished between softwood from hardwood by investigating the presence of marker compounds that were observed in our study as well, such as substituted phenols and resin acids **(Figure S11)**.

ResH2 featured an abundance of ~~of prominent~~ methoxy phenols, including $C_7H_8O_2$ (guaiacol), $C_8H_{10}O_3$ (syringol), $C_{10}H_{10}O_3$ (coniferaldehyde), $C_6H_6O_2$ (benzenediol ~~(catechol)~~ or methylfurfural), and $C_8H_{10}O_2$ (creosol), that ~~where they~~ collectively accounted for ~9% of the total signal, compared to 1, 2, and 2% in ResH1, ResH3, and ResH4, respectively. These compounds are important products of lignin pyrolysis in birch, aspen, and spruce and are usually ~~found~~ detected in the gas phase at mild ambient temperatures (Kong et al., 2021). Guaiacol and syringol are depolymerisation products of guaiacyl and syringyl units of lignin at 200–400°C, and they rapidly transition to catechols, cresols, and phenols during secondary pyrolysis reactions at 400–450°C~~, eventually leading to enhanced PAH formation at >700°C~~ (Kawamoto, 2017). While guaiacols are emitted ~~to some extent~~ by ~~the burning of~~ both hardwood and softwood, semi- or low-volatility substituted syringols ~~that primarily exist in the condensed phase~~ are emitted in ~~much~~ higher amounts by hardwood combustion (Kawamoto, 2017; Fine et al., 2002, 2001; Schauer and Cass, 2000). In this study, derivatives of guaiacols, including $C_{10}H_{12}O_2$ (eugenol), $C_{10}H_{14}O_2$ (4-propyl guaiacol), and $C_{10}H_{10}O_3$ (coniferaldehyde) presented ~~much~~ higher "relative concentration" ~~concentrations~~ (**Equation S4**) of 0.56–1.41 for ResH2 and ResH4 compared to ~~< 0 for~~ ResH1 (<0). Other compounds, such as $C_8H_8O_3$ (vanillin), $C_9H_{10}O_3$ (acetovanillone), $C_{10}H_{12}O_3$ (propiovanillone), and $C_{10}H_{12}O_4$ (methyl homovanillate) were predominantly found in ResH2. Similarly, substituted syringols, i.e., $C_{11}H_{14}O_3$ (methoxy eugenol), $C_{10}H_{12}O_4$ (acetosyringone), and $C_{11}H_{14}O_4$ (syringyl acetone, propionyl syringol, or sinapyl alcohol) were almost entirely associated with ResH2 as well. These compounds have been reported as markers of hardwood burning (Fine et al., 2001), implying a ~~potentially~~ greater contribution of hardwood emissions ~~smoke~~ to the ResH2 factor. In Alaska, relevant hardwood species include deciduous leafy trees, i.e., paper birch, balsam poplar, quaking aspen, etc (Adec, 2023).

~~For~~ The ResH4~~, in addition to the levoglucosan marker ions, a predominance of large~~presented a unique fingerprint characterised by~~,~~ ~~oxygenated molecules ~~with more~~bearing more than 13 carbon atoms ~~was observed~~ (**Figure S13**), such as $C_{16}H_{30}O_6$ (*m/z* 319.21), $C_{20}H_{28}O_2$ (*m/z* 301.21), ~~$C_{22}H_{18}O$ (*m/z* 299.14),~~ $C_{20}H_{18}O_4$ (*m/z* 323.12), ~~and~~ $C_{20}H_{30}O_2$ (*m/z* 303.24) and $C_{22}H_{18}O$ (*m/z* 299.14), in addition to the levoglucosan marker ions (26% of the total signal). ~~Amongst these, more than 60% of the~~The intense

signals from *m/z* 301 ($C_{20}H_{28}O_2$) and *m/z* 303 ($C_{20}H_{30}O_2$) was associated with ResH4 (**Figure S11**). These species are likely related to resin acids, dehydroabietic acid and abietic acid, respectively, which are almost exclusively emitted from the thermal alteration of resins in coniferous species, and thus, are indicative of softwood burning (Simoneit, 2002, 1999). Owing Due to the presence of these compounds, ResH4 was identified interpreted as an OA factor influenced by softwood combustion. Softwood species in Alaska include trees with needles and cones, e.g. hemlock, cedar, and spruce (Adec, 2023).

ResH3 includes OA from heating oil combustion: this factor A factor, labelled ResH3, contributed to **16 ± 9%** of the total OA_{CHARON} (**0.6 ± 0.6 µg/m³**) and showed the characteristic diurnal pattern of residential heating as it . It correlated quite well (R^2 = 0.56) with $BBOA_{AMS,org.}$ However, its chemical composition was very different from the other residential heating factors. Notably, levoglucosan contributed to a smaller fraction of the total signal of ResH3 (i.e., 9%) compared to other residential heating factors (1314–2930%; **Figure S11**), but while PAHs represented a much larger fraction of its total signal (for instance, 30, 31, and 29% of $C_{16}H_{10}$ (*m/z* 203.09), $C_{18}H_{12}$ (*m/z* 229.10), and $C_{20}H_{12}$ (*m/z* 253.10); **Figure S13**). These PAHs could be fluoranthene (or pyrene), naphthacene (or benzo[*x*]anthracene, chrysene), and benzo(*x*)pyrene (or benzo(*x*)fluoranthene)), which have been reported in emissions of light oil combustion (Bari et al., 2009). Additionally, ResH3 was strongly correlated with SO_2 (R_2 = 0.61) during the campaign, compared to a moderate lower correlation (R^2 of ≤ 0.47) with the other the remaining residential heating factors. Residential combustion of heating oil is an important source of SO_2 in Fairbanks, compared to wood and coal, due to ~2/3rd of the households using oil-fired space heaters and the high sulphur content of > 1600 ppm in fuel oils commonly consumed here (e.g., #1 and #2 fuel oil and waste motor oil are relevant in Fairbanks)(Dunleavy and Brune, 2019). Consistent with the possibility of the ResH3 factor denoting being associated with fuel oil emissions, the factor is characterised by particles smaller than 100 nm (**Figure S12**) and due to the CHARON inlet's cut-off, its mass concentration was possibly fuel oil emissions, a fully constrained PMF on SMPS measurements matched it with particles smaller than 100 nm (Figure S12). Due to the small particle size, it is possible that mass concentrations of OA_{CHARON} were under apportioned toestimated. ResH3; this possibility is discussed in detail for the on-road traffic factor in the next section.

3.2.3. Hydrocarbon-like and cooking organic aerosol

The HOA_{AMS} factors were characterised by notable peaks at *m/z* 43 ($C_3H_7^+$), 57 ($C_4H_9^+$), 71 ($C_5H_{11}^+$), 85 ($C_6H_{13}^+$), and 99 ($C_7H_{15}^+$), belonging to $[C_nH_{2n+1}]^+$ series, that are typical of *n*- and branched alkanes. There were also Additional peaks at *m/z* 55 ($C_4H_7^+$), 69 ($C_5H_9^+$), 81 ($C_6H_9^+$), 83 ($C_6H_{11}^+$), 95 ($C_7H_{11}^+$), 97 ($C_7H_{13}^+$), 107 ($C_8H_{11}^+$), 109 ($C_8H_{13}^+$), and 111 ($C_8H_{15}^+$) that belong to represented $[C_nH_{2n-1}]^+$ and

$[C_nH_{2n-3}]^+$ series, related to ~~which are typical indicative of~~ cycloalkanes (McLafferty et al. 1993). These ~~are key~~ ions are associated with engine-lubricating oils, vehicular exhaust, and diesel fuel (Canagaratna et al., 2004). The $HOA_{AMS,org}$ ~~and $HOA_{AMS,org+inorg}$~~ factors contributed **38 ± 20%** ~~(of the OA_{AMS})~~ and **21 ± 14%** ~~(~~of the OA_{AMS} and ~~total~~ NR-PM_1~~)~~ mass, respectively (**Figures 6 and S14**).

~~HOA is generally associated with linked to vehicular emissions but from on-road traffic, it which were~~ The unconstrained PTR_{CHARON} analysis was not able to apportion a road transport-related factor, ~~was not observed in the unconstrained PMF of PTR_{CHARON}. H~~however, ~~an~~ ~~factor for on-road traffic factor was 'artificially' diagnosed in the PTR_{CHARON} analysis~~ by constraining the ~~its~~ factorisation with the time series of a mobile gasoline factor, identified in the gas-phase PTR-ToF MS analyses of ALPACA campaign (Temime Roussel et al., 2022), a small road transport-associated factor was identified. ~~This approach was effective, revealing success of constraining this factor was evident in characteristics typical of on-road traffic. , such as~~ For instance, this latter ~~it~~ was strongly correlat~~ion~~ed with black carbon and NO_x (R^2 of 0.58 and 0.66; **Table 1**) and featured high contributions of C_8H_{10} (xylene; ethylbenzene~~; 2%~~), C_7H_8 (toluene~~; 4%~~), and C_6H_6 (benzene~~; 0.5%~~) ~~to its total mass concentrations~~ (**Figures 4 and S11**). Despite exhibiting some reasonable diurnal trend peaking at ~~In addition~~Notably, ~~peaks in the daily average mass concentrations of the traffic$_{CHARON}$ factor coincided with~~ the morning (0900 AKST) and evening (1700–1600 AKST) rush hours (**Figure 5**)~~.~~ ~~However, the traffic$_{CHARON}$~~ the factor ~~had~~ accounted for negligible concentrations (< 1 µg/m^3) and presented some ~~it contained implausible~~unlikely species, such as *m/z* 315.22 ($C_{21}H_{30}O_2$; possibly cannabidiol) ~~that would otherwise (e.g., in~~absent in the unconstrained PMF. ~~trials) appear as PMF residuals, making its environmental representativeness suspicious. large discrepancy between the OA apportioned to HOA by PTR_{CHARON} and AMS_{org}.~~ For instance, on average, **2.1 ± 3.0 µg/m^3** of OA was associated with $HOA_{AMS,org}$ ~~during the campaign~~, compared to only **0.1 ± 0.1 µg/m^3** for the road ~~traffic~~ransport$_{CHARON}$ factor (**Figure 6**). ~~We speculate that the~~ These discrepancies ~~shortcomings seen in OA mass measuredments by the from PTR_{CHARON} relative compared to the AMS_{org} were~~are largely instrumental, ~~particularly~~ partly due~~due~~ to ~~such as~~ the poor transmission ~~low sensitivities~~ of the ~~PTR_{CHARON} for~~ small particles (<100 nm) by the CHARON inlet and the limited sensitivity towards hydrocarbons by PTR, but other possible biases can be due to heating oil OA signal interfering with the HOA_{AMS}, as discussed in **S8**. ~~Previous studies using the PTR_{CHARON} in Innsbruck, Austria, successfully observed a traffic factor, but did not detect no cooking emissions despite sampling operating at in an urban locality area (MüLler et al., 2017). A vVarietyous of environmental and user biases could also may be involved, such as the contribution of non-vehicular sources to the HOA_{AMS} factors and the choiceuse of suboptimal conversion coefficients (e.g., RIE) in the AMS analyses (see **Sections S8** and **S9** for details). These are important considerations are critical for ambient air analysis in employing the with PTR_{CHARON}, as obtaining for ambient air analyses because a full picture of the sources involved, especially in urban regions influenced by~~

~~primary OA emissions of smaller particle sizes, may not be possible without necessitate complementary measurements.~~

3.2.4. Cooking organic aerosol

Another primary factor identified in Fairbanks was cooking, likely arising ~~which could either be~~ from residential or commercial activities around the CTC. ~~Both~~ The COA_{AMS} factor~~s~~ featured a high abundance of $C_xH_y^+$ ions, along with prominent O_1 fragments at *m/z* 55 ($C_3H_3O^+$), 84 ($C_5H_8O^+$), and 98 ($C_6H_{10}O^+$) ~~, which~~ originating from organic acids (Mohr et al., 2009) and ~~. These fragments have been reported serve~~ used as diagnostic ~~spectral~~ markers of COA in urban settings (Sun et al., 2011). The *f*55/*f*57 value (i.e., the ratio of fractions of $C_4H_7^+$ to $C_4H_9^+$) was ~3.00 for COA_{AMS}, compared to ~1.04 ~~in~~ for HOA_{AMS} (**Figure S10D**). ~~Although A a~~As a reliable tracer for COA remains unidentified in the AMS spectrum, a ~~high~~ *f*55/*f*57 ratio ~~of~~ >1 is considered a characteristic feature ~~of COA~~ (Katz et al., 2021; Sun et al., 2011) ~~because a reliable external tracer for it is yet to be identified~~. The PMF analysis of PTR_{CHARON} also ~~contained~~ revealed a distinct COA factor dominated by long-chain fatty acids, $C_{18}H_{32}O_2$, $C_{18}H_{34}O_2$, and $C_{18}H_{36}O_2$, identified ~~here~~ as linoleic, oleic, and stearic acids contributing to~~,~~ ~~that which contributed~~ 11, 16, and 4% to the total COA_{CHARON} mass (**Figure 4 and S11**). These fatty acids are commonly found ~~markers of~~ in OA from cooking oil and meat (Katz et al., 2021; Mohr et al., 2009). ~~Throughout Across the whole campaign,~~ The COA_{CHARON} ~~made peaked its highest contributions of at~~ contributed to a maximum of ~9% ~~to~~ of the total OA_{CHARON} mass and exhibited a unique diurnal pattern visualised in **Figure 5** with a minor maximum~~un~~ in the afternoon (lunchtime) and a second maximum in the evening (dinnertime). ~~, creating resulting in the a unique diurnal pattern visualised in **Figure 5**. Similarly to the HOA and traffic$_{CHARON}$ factors~~The average~~everage~~ absolute concentrations of $COA_{AMS,org}$ ~~and COA_{CHARON} were quite disparate between the two instruments~~ were ~~(~~**0.6 ± 0.8** for the AMS and **0.1 ± 0.2 µg/m^3** for the CHARON, such a discrepancy can be explained by the same reason discussed above and detailed ~~), respectively for reason discussed above~~in the section ~~as well as in **Sections S8** and **S9**. **(Figure 6).**~~

3.2.45. Oxygenated organic aerosol

~~It is common in P~~In the past source apportionment studies have reported ~~, it has been common to report~~ multiple OOA factors differing ~~that differ~~ in volatilities or oxygenation levels (e.g., Stefenelli et al., 2019a; Kumar et al., 2022; Cash et al., 2020). Here~~,~~ ~~, but~~ we diagnosed only a single OOA factor in either AMS or PTR_{CHARON} measurements. Specifically, t~~T~~he OOA_{AMS} factors ~~in AMS analyses was~~ were identified based on a prominent peak at *m/z* 43 ($C_2H_3O^+$) ~~which is a tracer of less oxygenated OA, –~~and *m/z* 29 (CHO^+; **Figure S10A**) and ~~. This factor It correlated~~ showed a strong correlation (R^2 0.74)

with OOA_{CHARON} ~~, with an R^2 of 0.74,~~ . The~~whe~~ average absolute concentrations of OOA_{CHARON} and $OOA_{AMS,org}$ were **0.4 ± 0.6** and **1.0 ± 2.1 µg/m^3**, respectively.~~:~~ ~~–~~Notably, ~~ts~~~~Some of t~~he most intense ions in the mass ~~spectra~~ spectrum of OOA_{CHARON} ~~, relative to other factors,~~ have been tentatively assigned to~~included~~ *m/z* 73.03 ($C_3H_5O_2$, e.g., methylglyoxal), *m/z* 99.~~01~~ 04 (~~$C_4H_2O_3$~~$C_5H_6O_2$, e.g., ~~maleic anhydride~~oxo-pentanal), *m/z* 113.06 ($C_6H_8O_2$, e.g.,methyl-oxo-pentanal), *m/z* 127.08 ($C_7H_{10}O_2$; e.g., heptadienoic acid), *m/z* 137.06 ($C_8H_8O_2$; e.g., methoxy-benzaldehyde), *m/z* 167.10 ($C_{10}H_{14}O_2$), *m/z* 171.07 ($C_8H_{10}O_4$) and *m/z* 185.10 ($C_{13}H_{12}O$; e.g., benzyl phenol). Among these compounds some have previously been associated with atmospheric oxidation or photolysis of BBOA (Montoya-Aguilera et al., 2017; Lignell et al., 2013; Smith et al., 2020), other could be due to oxidation aromatic VOCs detected originating from road transport (Temime-Roussel et al., 2022). Few ~~Several , as well as some~~ other species ~~that~~ overlapped with the residential heating ~~factors~~tracers, notably *m/z* 163.06 ($C_6H_{10}O_5$; e.g., levoglucosan), *m/z* 179.08 ($C_{10}H_{10}O_3$; e.g., coniferaldehyde), and *m/z* 301.21 ($C_{20}H_{28}O_2$; e.g., dehydroabietic acid). ~~Some of these species~~ compounds ~~(e.g., $C_4H_2O_3$, $C_{10}H_{14}O_2$, $C_7H_{10}O_2$) have previously been associated with atmospheric oxidation or photolysis of BBOA (Montoya-Aguilera et al., 2017; Lignell et al., 2013; Smith et al., 2020).~~ But ~~G~~given the prominence of wood-burning as ~~the~~ a major primary emissions ~~in ALPACA~~, the OOA is likely linked to BBOA. A recent study in Fairbanks identified wintertime OOA as a mixture of BBOA and SOA formed from non-photochemical processing using an ACSM (Robinson et al., 2024). The examination of *f*44 versus *f*60 in the AMS_{org} dataset plot (**Figure S10C)** is consistence with aged OOA derived by biomass burning, as previously demonstrated by Xu et al., (2023). Another recent source apportionment ~~of NR-PM_1~~study ~~measured~~ with the HR-ToF AMS at a site close to the CTC did not ~~reveal~~ identified an OOA factor ~~at all~~, while BBOA, HOA, and a mixed primary factor (HOA, COA, etc.) comprised 45, 25, and 31% of total OA~~, on average, during the campaign~~ (Yang et al., 2024). ~~Minimal processing, and thus, l~~LA limited OOA formation is plausible due to reduced ~~short~~ solar light exposure ~~periods and pollution residence~~ in this period of the year ~~in Fairbanks~~ (Cesler-Maloney et al., 2024), however,~~, but a~~ the ~~complete disappearance~~ absence of OOA is more likely a result ~~to be a consequence~~ of ~~it remaining~~ an unresolved organic fraction~~under the factorisation method used~~. ~~Another recent study in Fairbanks using the ACSM identified wintertime OOA as a mixture of real BBOA and SOA formed from non-photochemical processing (Robinson et al., 2024). This aspect was investigated via an *f*44 versus *f*60 plot for AMS_{org} that supports some influence of biomass burning at all levels of oxidation of OA (**Figure S10C**). The placement of $OOA_{AMS,org}$ toward the left edge of the *f*44 versus *f*60 plot is consistent with aged OA from wood burning (Xu et al., 2023), but an urban influence cannot be ruled out in field settings (Cubison et al., 2011), especially when *m/z* 60 and 73 are only 0.2 and 0.4% of the total $OOA_{AMS,org}$ signal (**Figure S10B).**~~

Sulphate and OOA. ~~Much more~~ An intriguing insight ~~interesting information~~ about ~~regarding the~~the OOA factor emerged ~~was gleaned~~ from the $AMS_{org+inorg}$ measurements, ~~which revealed it to be rich~~

indicating a significant content of sulphur ~~in sulphur~~containing compounds (**Figure S15**). The AMS does not ~~quantitatively~~ distinguish among the different sulphur-containing species, but ~~such as hydroxymethane sulphonate (HMS; $CH_2(OH)SO^{-3}$), SO_3^{2-} (sulphite), HSO_3^- (bisulphite), and SO_4^{2-} (sulphate), or between organic and inorganic sulphur, but we have tried to use~~ following guidelines from previous works (Chen et al., 2019; Schueneman et al., 2021) we could explored ~~t~~the ratio of sulphur fragments to investigate ~~speculate on~~ the presence of different species ~~forms of sulphur present~~ such as hydroxymethane sulphonate (HMS; $CH_2(OH)SO^{-3}$), HSO_4^- (bisulphite), SO_4^{2-} (sulphate) and (H2SO4) sulphuric acid. ~~In light of previous studies on sulphur source apportionment with the AMS and source differentiation based on fragmentation patterns, (Chen et al., 2019; Schueneman et al., 2021).~~An organosulphate content of ~ **0.8 ± 1.3 µg/m^3** (~**20 ± 16%**) was then derived using the ratios of SO^+ and SO_2^+ ions against SO_3^+, HSO_3^+, and $H_2SO_4^+$ ions as detailed by Song et al., (2019). This value is in good agreement with previous reports from the same field campaign (Campbell et al., 2022; Robinson et al., 2024). Additionally, to mimic potential matrix effects of wood burning OA on sulphate fragmentation patterns, ~~we performed calibrations on the~~ AMS spectra from a solution of ~~with pure~~ $(NH_4)_2SO_4$ mixed with various amounts of levoglucosan (i.e., 0–80% in mass)~~. This mixture was used to assess the matrix effect that can potentially impact sulphur fragmentation patterns in an environment affected by wood smoke as previously demonstrated with other organic matrices. We~~ were compared to ambient data and PMF factors as shown ~~compared the fractions of HSO_3^+ to $H_2SO_4^+$ fragments normalised to the fractions $H_2SO_4^+$ and HSO_3^+ for pure $(NH_4)_2SO_4$ as suggested by Chen et al., (2019). Results are shown~~ in **Figure S16A**. ~~Results~~ Among the sulphate-rich factors the ~~are shown in **Figure S16A** where the~~ $OOA_{AMS,org+inorg}$ ~~factor~~ exhibited ~~much~~ lower HSO_3^+ to $H_2SO_4^+$ intensities suggesting ~~which is indicative of an influence of~~ an higher fraction of organosulphate ~~compounds, as it is also~~ evidenced in~~influence~~ **Figure S16D–E** by the strong correlation between derived organo-sulp~~a~~hur fraction and sulphate-ions in the $OOA_{AMS,org+inorg}$ factor (R^2 = 0.85, slope = 0.57)~~. (**Figure S16D–E**)~~. ~~The average total concentration of sulphur~~sulphate ~~related fragments in $OOA_{AMS,org+inorg}$ was **0.9 ± 1.8 µg/m^3**, on average, and which accounted for **26 ± 23%** of the total sulphur~~ sulphate ~~measured with the AMS. This finding is consistent, which agrees with the theoretical estimations of organosulphur content (Song et al., 2019).~~

Further information on chemical composition was gathered by comparing ~~this factor~~AMS results with IC measurements from $PM_{0.7}$ filters sample~~ds~~ ~~analysed~~ as part of another ALPACA study (Dingilian et al., 2024). Despite the good correlations between the two datasets, shown in **Figure 7A,** the AMS results underestimated ~~. Although there is a notable underestimation Both methods (IC and AMS) correlated well, despite a negative bias against in the AMS analysis, that underestimated the sums of approximately~~ by 30%, 26%, and 35% ~~lower sulphur~~sulphate, ammonium, and nitrate~~ related fragments~~, respectively (see **Section 2.2.2** ~~for fragments included~~). ~~the correlation between the two~~

methods remains strong by ~ 31, 26%, and 35% compared to the IC analyses (**Figure 7A**). Both the total estimated organosulphur fraction and the $OOA_{AMS,org+inorg}$ factor presented very strongrobust correlations ($R^2 > 0.90$) with the $S_{(IV)}$ and HMS ions from filter analysis(**Figures 7B and S16F–I**), and a somewhat with a relatively weaker , but still strong correlation ($R^2 > 0.61–0.68$), with the SO_4^{2-} ion (**Figures 7 and S16F–I**). In additionAdditionally, theThe $OOA_{AMS,org+inorg}$ this factor was also very strongly correlated with total ammonium (AMS data $R^2 = 0.8695$, **Table 1**; filter IC $R^2 = 0.77$, **Figure S16D–E7B**), potentially promoting the formation of $S_{(IV)}$ species under favourable meteorological conditions and aerosol composition (Campbell et al., 2024). This author also reported that $S_{(IV)}$ species, including HMS, have been represented the observed the major secondary organosulphur component of $PM_{2.5}$ in Fairbanks during wintertime, with average concentrations of 0.29 and 0.34 μg/m^3 recorded with IC in 2020 and 2021, respectively, and contributing to 26–41% of total sulphate (Campbell et al., 2022). Recently,co-varying HMS and $S_{(IV)}$ species, were distinguished in Fairbanks, and identifying the non-HMS $S_{(IV)}$ were reported to be as aldehyde-$S_{(IV)}$ compounds (Dingilian et al., 2024). In addition, this factor was very strongly correlated with total ammonium (R^2 = 0.95, **Table 1**; **Figure S16D–E**) which could raise aerosol pH, favouring the formation of $S_{(IV)}$ species under appropriate meteorological conditions and aerosol composition (Campbell et al., 2024). Therefore, the presence of HMS and other organic $S_{(IV)}$ species in the $AMS_{org+inorg}$ factor is well substantiated. Overall, the molecular level composition of OOA from PTR_{CHARON} and the inorganic chemical information from $AMS_{org+inorg}$, as well as diurnal patters with indicating enhanced peak concentrations in the afternoon (**Figure 3**), are that is indicative of chemical daytime processing that the wintertime OOA in Fairbanks is not solely comprised of HMS; . Instead, it is instead a complex mixture of secondary non-heteroatomic organic matter and organosulphur compounds, which underscoring the need for further exploration of the hints toward its formation from complex atmospheric processing pathways involvedthat needs further exploration.

3.2.56. Additional insights from combined analysis of organic and inorganic in AMS data measurements

Two additional factors, sulph-OA (i.e., sulphur-rich OA) and AmNi (i.e., ammonium nitrate), were observed from the PMF of $AMS_{org+inorg}$ (**Figure 3**). Approximately 40–60% of these factors' masses comprised sulphur and nitrogen species (**Figure S15**).

Sulphur-rich organic aerosol: Sulph-OA is composed by sulphate 60%, organics 30%, ammonium 6% and nitrate 4%. Like the $OOA_{AMS,org+inorg}$ factor, sulph-OA was also sulphur-rich. Its The chemical composition was further explored via the $fHSO_3/fH_2SO_4$ analysis detailed in **Section 3.2.4** and as shown in This factor lay in the upper-right quadrant of **Figure S16A**, the factor is positioned between pure

H_2SO_4 and~~and/or~~ $(NH_4)_2SO_4$. The measured $[NH_4]/[SO_4]$ ratio ~~for sulph-OA~~ was 0.07, ~~which is much~~ considerably lower than the theoretical mass ratio of 0.38 and 0.18 ~~for~~ of $(NH_4)_2SO_4$ and NH_4HSO_4, respectively, indicating ~~. Therefore, this factor is inferred to have~~ an acidic nature of Sulph-OA (Chen et al. 2019). The ~~sulph-OA~~ factor was well ~~strongly~~ correlated with SO_2 (R^2 = 0.6)~~, which is majorly a primary product of residential heating oil (Dunleavy and Brune, 2020)~~ and moderately correlated with the ResH3 factor (R^2 of 0.33). The factor was also associated with ~~. Therefore, it is likely that sulph-OA comprises primary~~ ultrafine particles ~~emissions~~ in the 50–80 nm range ~~from heating oil combustion~~ (**Figure S12D**). ~~Surprisingly, sulph-OA was only moderately correlated with the ResH3 factor (R^2 of 0.33), which was identified as heating oil OA in the PTR_{CHARON} analysis.~~ Regardless of the low correlation, we speculate that ResH3 and sulph-OA ~~represent~~ originated from the same source, i.e., residential heating ~~fuel~~ oil combustion, and their temporal disagreement may result from instrumental biases of the CHARON inlet in quantifying particles smaller than 100 nm (**Figures S12B and D**). For instance, as shown in **Figures S12E–F**, the organic ~~only~~ ResH3 supersedes sulph-OA concentrations~~,~~ when larger particles are abundant, and it has lower concentrations for smaller particles.

This factor contained **0.6 ± 0.5 µg/m^3** ~~of sulphur. Despite the low concentrations, sulph-OA made up~~ (~~~~**58 ± 26%**) of total ~~sulphur~~ sulphate measured with the AMS and ~~because~~ it dominated during the low-pollution periods, which were more frequent and lasted longer than the high-pollution ~~periods~~ events (**Figure 1**). Other primary factors, $HOA_{AMS,org+inorg}$, $COA_{AMS,org+inorg}$, and $BBOA_{AMS,org+inorg}$, contained an additional 11 ± 9% of the ~~sulphur~~ sulphate (**0.2 ± 0.2 µg/m^3**), so collectively, ~~. P~~primary ~~sulphur~~ factors ~~collectively~~ made up **69 ± 24%** (**0.7 ± 0.6 µg/m^3**) of total ~~sulphur~~sulphate. This value is in close agreement with a previous ALPACA study that reported ~62 ± 12% of total SO_4^{2-} mass to be of primary origin ~~and associated with particles of smaller than 700 nm (2.1 ± 1.4 µg/m^3 in $PM_{0.7}$)~~ (Moon et al., 2023).

AmNi factor ~~***includes atmospherically processed vehicular emissions.***~~ ~~:~~ The second inorganic factor was composed of 35% nitrate~~s~~, 14% ammonium, and 43% organics ~~. It accounted~~ accounting for 71 ± 23% of the total nitrate measured by the AMS ~~in NR-PM1~~ (R^2 = 0.98). The average concentration~~s~~ of this factor and the nitrate species in it were **1.1 ± 1.6** µg/m^3 and **0.4 ± 0.5** µg/m^3. The factor was more abundant when NOx concentrations were high (above 130 ppbv)(**Figure S17B**), its diurnal trend peaked around 1400 **AKST** (Figure 3), roughly 3-4 hours after the morning peak of HOA_{AMS} and was associated with relatively small particles of 110 nm (**Figure S12D**). A high contribution of aliphatic moieties characterised the organic fraction, and according to the difference in mass concentrations of $HOA_{AMS,org}$ and $HOA_{AMS,org+inorg}$ of 13% (**Figure S17A**), we speculate that some organic components of $HOA_{AMS,org}$

were transferred to the AmNi factor (**Figure 6**). All these elements suggest a probable contribution from the vehicular emissions to this factor. The presence of inorganic compounds provided more variables to the PMF, and thus, improved the resolution of factors into distinct AmNi and $HOA_{AMS,org+inorg}$ factors. ~~It presented a distinct peak from ~1200–1800 hrs and then stable, low concentrations throughout the night (Figure 3). This peak followed 3–4 hours after the peak in the mass concentrations of HOAAMS (or trafficCHARON) during the morning, implying its probable origin from vehicular NOx, which was supported by the highest contributions of this factor coinciding with peaks in NOx concentrations (Figure S17B). Generally, during the ALPACA campaign, the AmNi factor had much lower concentrations than HOAAMS,org+inorg; however, they were both associated with the highest recorded ambient temperatures (5 to -10°C) and solar radiations (as per jNO2 values)(Figure S17C–D). According to atmospheric modelling studies in Fairbanks (Joyce et al., 2014), the formation of NO3 from NOx via the nocturnal reactions slows at temperatures below -15°C, causing them to have higher concentrations during warmer periods. Interestingly, according to the difference in mass concentrations of HOAAMS,org and HOAAMS,org+inorg and its correlation with the AmNi factor (Figure S17A), we speculate that some portion of the organic components of of the AmNi factor were apportioned to HOAAMS,org causing it to have higher contributions than HOAAMS,org+inorg (Figure 6). The inclusion of inorganics provided more variables to the PMF, and thus, improved the resolution of factors into distinct AmNi and HOAAMS,org+inorg factors.~~

4. Local environmental implications ~~and conclusive remarks~~

~~For instance~~During the period of the campaign, ~~during this study,~~ 12–48-hour-long ADEC advisories for wood-burning restrictions were implemented seven times. Variation in the relative contributions of ResH1–4 during these advisories is depicted in **Figures 8** and **S18–21**. For all advisory events, ResH2 and ResH4, i.e., woodsmoke, were the predominant contributors *before* and *after* the advisories were in place. ~~ResH2 (i.e., hardwood-related fuels) remained a prominent contributor to OA_{CHARON} *during* the 3rd (Stage 2), 4th (Stage 1), and 5th (Stage 1) advisories.~~ A notable increase was observed in ResH3 contribution, i.e., heating oil, ~~at least once~~ *during* the 2nd (Stage 1), 5th (Stage 1), 6th (Stage 1), and 7th advisory events. While ~~,~~ ResH2 (i.e., hardwood-related fuels) remained a prominent contributor to OA_{CHARON} *during* the 3rd (Stage 2), 4th (Stage 1), and 5th (Stage 1) advisories. Most households in Fairbanks use heating oil (~72% of residents), followed by wood (~22% of residents) (Dunleavy and Brune, 2019), which was not reflected ~~here~~ in the relative contributions ~~of~~ apportioned to ResH3. ~~-~~This can be linked to a higher PM_1 release from wood combustion per given volume of fuel compared to ~~other commonly used sources, including~~ heating oil and/or an ~~especially under less than optimal combustion conditions (e.g., moist wood) or with inefficient appliances. There is also the possibility~~

~~that due to the typical particle size of ResH3 emissions~~underestimation of ResH3 by PTR_{CHARON} being associated with smaller than 100 nm (**Figure S12**).

~~All seven ADEC advisories coincided with the coldest periods of the campaign (**Figure 1**). Therefore, the response of Fairbanks' residents to ADEC advisories cannot be assessed independently from their response to increased need for heating or the dynamics of OA under the unique meteorology (i.e., low temperatures/low solar radiations/strong inversions) during sampling. In our study~~As expected, the absolute average concentrations of all factors were inversely related to ambient temperature, but the percent change differed considerably across factors. Specifically, as temperatures decreased from -10°C to below -25°C, the average absolute concentrations for ~~traffic~~transport$_{CHARON}$, COA_{CHARON}, OOA_{CHARON}, ResH1–4 increased 0.25×, 0.75×, 9.0×, 1.4×, 25.1×, 3.0×, and 2.9×, respectively (**Figure S22**). The steep increase in the relative contribution of ResH2, ~~was~~ associated with hardwood-tracers, contrasts with previous reports~~based fuels. In contrast~~, based on surveys (Dunleavy and Brune, 2019) and ~~ratios of~~ organic tracers ~~in ambient air samples~~ (Haque et al., 2021), ~~previous studies reported~~ indicating birch and spruce ~~whichare widely found in Alaskan boreal forests,~~ as the most popular firewood in Fairbanks. Laboratory studies have shown that the burning of softwood pellets of Douglas Fir or eastern white pine emits less PM than hardwood pellets of the same volume, and this response varies based on the moisture content of the wood and the heating appliance used (Morin et al., 2022). ~~High PM emission per volume burned could also be the reason behind hardwood burning being the dominant contributor of PM in our analysis.~~ Also ResH2 comprises a broader spectrum of volatile and semi-volatile substituted phenolic species, and thus, it is likely to undergo efficient gas-to-particle partitioning at low temperatures toward increasing OA loads (Ijaz et al., 2025). ~~Overall, investigating the variation in the emission patterns, especially in response to regulations, such as the ADEC burn restrictions, is a complex issue that requires appropriately acknowledging the influence of meteorology, the physicochemical nature of the emissions, and change in emissions at the source. Based on the observations in this study, it cannot be conclusively inferred that either hardwood- or softwood-based solid fuels are more popularly consumed wood types in Fairbanks, but they are certainly among the largest contributors to sub-micron OA emissions. These findings are critical to addressing air pollution in Fairbanks, which has been a persistent issue for a long time, by guiding policies and citizen action~~

5. Conclusion

A CHARON inlet coupled with PTR-ToF MS and HE-ToF-AMS were deployed during the Alaskan Layered Pollution and Chemical Analysis (ALPACA) campaign. The PMF analysis of AMS data revealed three primary factors: biomass burning, hydrocarbon-like and cooking factors accounting for

28, 38 and 11 % of the total OA, respectively. A combined organic and inorganic PMF analysis provided additional insights and revealed the presence of an organo-sulphate compounds mostly associated to the OOA factor and of another sulphate-rich factor of acidic nature. A nitrate factor, associated with hydrocarbon-like OA and high NOx levels, was interpreted as aged road transport emissions. The PTR_{CHARON} PMF analysis could differentiate four residential heating sources—one oil combustion and three wood combustion types, associated with low temperature, softwood, and hardwood combustion. Such factorisation was achieved with the support of specific tracers that CHARON could successfully identify, as furans, aromatic alcohols (resorcinol, guaiacol, eugenol, syringiol), aldehydes (furfural, coniferaldehyde), acids (benzoic, dehydroabietic, abietic, linoleic, oleic, and stearic) and various PAHs. Collectively all residential heating factors accounting for 79% of the total OA_{CHARON}. Cooking and road transport were also recognised as primary sources by PTR_{CHARON}. All PMF analyses could apportion a single secondary organic fraction accounting for 11-19% of the total OA. This work evidence the complementarity of the two instruments and their ability in describing the complex chemical composition of PM_1 and the related sources. The enhanced deconvolution of closely co-varying sources of ambient pollution epitomises the novelty of our study and demonstrates the capability of PTR_{CHARON} to deliver detailed qualitative and quantitative insights, thus enabling a comprehensive understanding of organic aerosol sources. These advances can assist environmental regulators and citizen efforts to improve air quality in Fairbanks and the fast-urbanising regional sub-Arctic areas.

Data availability

Supporting text, figures, and tables are available in the Supplementary Material.

Author contributions

The manuscript was written with the contributions of all authors. BT-R and BDA set up, ran, and maintained the instrumentation during the campaign in Fairbanks. SA, NB, and ED aided during the campaign. MC-S collected and contributed meteorological and trace gas data. BA, RJW, KD, and AM provided data on ion chromatography analysis of offline filter samples. BT-R and AI processed and analysed the data with help from BC. WS and KS coordinated the ALPACA and CASPA projects. KL, BDA, BB, SB, JF, JM, and JS contributed to funding acquisition for the CASPA project. BDA supervised the project reported here.

Competing interests

The authors declare that they have no conflict of interest.

Acknowledgements

We thank the ALPACA team of researchers and all others involved in designing the project and providing the necessary logistical support to carry it out. We thank Dr Anna Tobler (Datalystica Ltd, Switzerland) for providing technical support for SoFi analysis. This work was funded by the CASPA (Climate-relevant Aerosol Sources and Processes in the Arctic) project of the Agence Nationale de la Recherche (grant no. ANR-21-CE01-0017) and the IPEV (French Polar Institute Paul-Émile Victor). KD and RJW were supported by the National Science Foundation's (NSF) Atmospheric Geoscience Program (grant no. AGS-2029730) and the NSF Navigating the New Arctic Program (grant no. NNA-1927778). SRA acknowledges support from the UK Natural Environment Research Council (grant ref: NE/W00609X/1). We thank the MASSALYA instrumental platform (Aix-Marseille Université, Laboratory of Chemistry and Environment, lce.univ-amu.fr) for the measurements used in this publication. AI is grateful to Subuktageen Qitta, Nastaran Mahmud, Laal Boo'on-Wali, and Minuit Mahmud for the many useful discussions that helped compile this report.

References

Aiken, A. C., DeCarlo, P. F., and Jimenez, J. L.: Elemental analysis of organic species with electron ionization high-resolution mass spectrometry, Analytical chemistry, 79, 8350-8358, 2007.

Aiken, A. C., Decarlo, P. F., Kroll, J. H., Worsnop, D. R., Huffman, J. A., Docherty, K. S., Ulbrich, I. M., Mohr, C., Kimmel, J. R., and Sueper, D.: O/C and OM/OC ratios of primary, secondary, and ambient organic aerosols with high-resolution time-of-flight aerosol mass spectrometry, Environmental science & technology, 42, 4478-4485, 2008.

Alaska Department of Environmental Conservation, Know Your Wood: https://dec.alaska.gov/air/burnwise/know-your-wood

Alves, C. A., Vicente, E. D., Rocha, S., and Vicente, A. M.: Organic tracers in aerosols from the residential combustion of pellets and agro-fuels, Air Quality, Atmosphere & Health, 10, 37-45, 2017.

Bari, M. A., Baumbach, G., Kuch, B., and Scheffknecht, G.: Wood smoke as a source of particle-phase organic compounds in residential areas, Atmospheric Environment, 43, 4722–4732, 2009.

Brégonzio-Rozier, L., Siekmann, F., Giorio, C., Pangui, E., Morales, S., Temime-Roussel, B., Gratien, A., Michoud, V., Ravier, S., and Cazaunau, M.: Gaseous products and secondary organic aerosol formation during long term oxidation of isoprene and methacrolein, Atmospheric Chemistry and Physics, 15, 2953-2968, 2015.

Campbell, J. R., Battaglia Jr, M., Dingilian, K., Cesler-Maloney, M., St Clair, J. M., Hanisco, T. F., Robinson, E., DeCarlo, P., Simpson, W., and Nenes, A.: Source and Chemistry of Hydroxymethanesulfonate (HMS) in Fairbanks, Alaska, Environmental Science & Technology, 2022.

Campbell, J. R., Battaglia Jr, M., Dingilian, K. K., Cesler-Maloney, M., Simpson, W. R., Robinson, E. S., DeCarlo, P. F., Temime-Roussel, B., D'Anna, B., and Holen, A. L.: Enhanced aqueous formation and neutralization of fine atmospheric particles driven by extreme cold, Science Advances, 10, eado4373, 2024.

Canagaratna, M., Jayne, J., Jimenez, J., Allan, J., Alfarra, M., Zhang, Q., Onasch, T., Drewnick, F., Coe, H., and Middlebrook, A.: Chemical and microphysical characterization of ambient aerosols with the aerodyne aerosol mass spectrometer, Mass spectrometry reviews, 26, 185-222, 2007.

Canagaratna, M., Jimenez, J., Kroll, J., Chen, Q., Kessler, S., Massoli, P., Hildebrandt Ruiz, L., Fortner, E., Williams, L., and Wilson, K.: Elemental ratio measurements of organic compounds using aerosol mass spectrometry: characterization, improved calibration, and implications, Atmospheric Chemistry and Physics, 15, 253-272, 2015.

Canagaratna, M. R., Jayne, J. T., Ghertner, D. A., Herndon, S., Shi, Q., Jimenez, J. L., Silva, P. J., Williams, P., Lanni, T., and Drewnick, F.: Chase studies of particulate emissions from in-use New York City vehicles, Aerosol Science and Technology, 38, 555-573, 2004.

Canonaco, F., Crippa, M., Slowik, J. G., Baltensperger, U., and Prévôt, A. S.: SoFi, an IGOR-based interface for the efficient use of the generalized multilinear engine (ME-2) for the source apportionment: ME-2 application to aerosol mass spectrometer data, Atmospheric Measurement Techniques, 6, 3649-3661, 2013.

Cash, J. M., Langford, B., Di Marco, C., Mullinger, N., Allan, J., Reyes-Villegas, E., Joshi, R., Heal, M. R., Acton, W. J. F., and Hewitt, N.: Seasonal analysis of submicron aerosol in Old Delhi using high resolution aerosol mass spectrometry: Chemical characterisation, source apportionment and new marker identification, Atmospheric Chemistry and Physics Discussions, 2020, 1-42, 2020.

Cesler-Maloney, M., Simpson, W., Kuhn, J., Stutz, J., Thomas, J., Roberts, T., Huff, D., and Cooperdock, S.: Shallow boundary layer heights controlled by the surface-based temperature inversion strength are responsible for trapping home heating emissions near the ground level in Fairbanks, Alaska, EGUsphere, 2024, 1-51, 2024.

Cesler-Maloney, M., Simpson, W. R., Miles, T., Mao, J., Law, K. S., and Roberts, T. J.: Differences in Ozone and Particulate Matter Between Ground Level and 20 m Aloft are Frequent During Wintertime Surface-Based Temperature Inversions in Fairbanks, Alaska, Journal of Geophysical Research: Atmospheres, 127, e2021JD036215, 2022.

Chazeau, B., El Haddad, I., Canonaco, F., Temime-Roussel, B., d'Anna, B., Gille, G., Mesbah, B., Prévôt, A. S., Wortham, H., and Marchand, N.: Organic aerosol source apportionment by using rolling positive matrix factorization: Application to a Mediterranean coastal city, Atmospheric environment: X, 14, 100176, 2022.

Chen, G., Canonaco, F., Tobler, A., Aas, W., Alastuey, A., Allan, J., Atabakhsh, S., Aurela, M., Baltensperger, U., and Bougiatioti, A.: European aerosol phenomenology− 8: Harmonised source apportionment of organic aerosol using 22 Year-long ACSM/AMS datasets, Environment international, 166, 107325, 2022.

Chen, G., Li, S., Zhang, Y., Zhang, W., Li, D., Wei, X., He, Y., Bell, M. L., Williams, G., and Marks, G. B.: Effects of ambient PM1 air pollution on daily emergency hospital visits in China: an epidemiological study, The Lancet Planetary Health, 1, e221-e229, 2017.

Chen, Y., Xu, L., Humphry, T., Hettiyadura, A. P., Ovadnevaite, J., Huang, S., Poulain, L., Schroder, J. C., Campuzano-Jost, P., and Jimenez, J. L.: Response of the aerodyne aerosol mass spectrometer to inorganic sulfates and organosulfur compounds: Applications in field and laboratory measurements, Environmental science & technology, 53, 5176-5186, 2019.

Collard, F.-X. and Blin, J.: A review on pyrolysis of biomass constituents: Mechanisms and composition of the products obtained from the conversion of cellulose, hemicelluloses and lignin, Renew. Sustain. Energy Rev., 38, 594–608, https://doi.org/10.1016/j.rser.2014.06.013, 2014.

Crippa, M., Canonaco, F., Lanz, V., Äijälä, M., Allan, J., Carbone, S., Capes, G., Ceburnis, D., Dall'Osto, M., and Day, D.: Organic aerosol components derived from 25 AMS data sets across Europe using a consistent ME-2 based source apportionment approach, Atmospheric chemistry and physics, 14, 6159-6176, 2014.

Cubison, M., Ortega, A., Hayes, P., Farmer, D., Day, D., Lechner, M., Brune, W., Apel, E., Diskin, G., and Fisher, J.: Effects of aging on organic aerosol from open biomass burning smoke in aircraft and laboratory studies, Atmospheric Chemistry and Physics, 11, 12049-12064, 2011.

Czarnecki, N.: Local Air Quality Regulations: How to Participate and Comply, Clear the Air Home Heating Forum and Expo,

DeCarlo, P. F., Kimmel, J. R., Trimborn, A., Northway, M. J., Jayne, J. T., Aiken, A. C., Gonin, M., Fuhrer, K., Horvath, T., and Docherty, K. S.: Field-deployable, high-resolution, time-of-flight aerosol mass spectrometer, Analytical chemistry, 78, 8281-8289, 2006.

Dingilian, K., Hebert, E., Battaglia Jr, M., Campbell, J. R., Cesler-Maloney, M., Simpson, W., St. Clair, J. M., Dibb, J., Temime-Roussel, B., and D'anna, B.: Hydroxymethanesulfonate and Sulfur (IV) in Fairbanks Winter During the ALPACA Study, ACS ES&T Air, 2024.

Dunleavy, M. and Brune, J. W.: Amendments to: State Air Quality Control Plan. Vol. III: Appendix III.D.7.06, 2019.

Dunleavy, M. J. and Brune, J. W.: Amendments to State Air Quality Control Plan: Vol. III: Appendix III.D.7.7, Alaska Department of Environmental Conservation, 2020.

Eichler, P., Müller, M., D'anna, B., and Wisthaler, A.: A novel inlet system for online chemical analysis of semi-volatile submicron particulate matter, Atmospheric Measurement Techniques, 8, 1353-1360, 2015.

Eichler, P., Müller, M., Rohmann, C., Stengel, B., Orasche, J. r., Zimmermann, R., and Wisthaler, A.: Lubricating oil as a major constituent of ship exhaust particles, Environmental Science & Technology Letters, 4, 54-58, 2017.

Ellis, A. and Mayhew, C.: Chemical Ionization: Chemistry, Thermodynamics and Kinetics, Proton Transfer Reaction Mass Spectrometry, 25-48, 2014.

Fairbanks Air Quality Plan: https://www.epa.gov/ak/fairbanks-air-quality-plan, last access: May 07, 2024.

Fine, P. M., Cass, G. R., and Simoneit, B. R.: Chemical characterization of fine particle emissions from fireplace combustion of woods grown in the northeastern United States, Environmental Science & Technology, 35, 2665-2675, 2001.

Fine, P. M., Cass, G. R., and Simoneit, B. R.: Organic compounds in biomass smoke from residential wood combustion: Emissions characterization at a continental scale, Journal of Geophysical Research: Atmospheres, 107, ICC 11-11-ICC 11-19, 2002.

Fraser, M. P. and Lakshmanan, K.: Using levoglucosan as a molecular marker for the long-range transport of biomass combustion aerosols, Environmental Science & Technology, 34, 4560-4564, 2000.

Fye, M., Havel, B., Havel, H., and Putnam, J.: Opportunities for Air Quality Improvement in the Fairbanks North Star Borough, 2009.

Gkatzelis, G. I., Hohaus, T., Tillmann, R., Gensch, I., Müller, M., Eichler, P., Xu, K.-M., Schlag, P., Schmitt, S. H., and Yu, Z.: Gas-to-particle partitioning of major biogenic oxidation products: a study on freshly formed and aged biogenic SOA, Atmospheric chemistry and physics, 18, 12969-12989, 2018.

Glasius, M., Ketzel, M., Wåhlin, P., Jensen, B., Mønster, J., Berkowicz, R., and Palmgren, F.: Impact of wood combustion on particle levels in a residential area in Denmark, Atmospheric Environment, 40, 7115-7124, 2006.

Gueneron, M., Erickson, M. H., VanderSchelden, G. S., and Jobson, B. T.: PTR-MS fragmentation patterns of gasoline hydrocarbons, International Journal of Mass Spectrometry, 379, 97-109, 2015.

Guo, S., Hu, M., Peng, J., Wu, Z., Zamora, M. L., Shang, D., Du, Z., Zheng, J., Fang, X., and Tang, R.: Remarkable nucleation and growth of ultrafine particles from vehicular exhaust, Proceedings of the National Academy of Sciences, 117, 3427-3432, 2020.

Haque, M. M., Kawamura, K., Deshmukh, D. K., Kunwar, B., and Kim, Y.: Biomass burning is an important source of organic aerosols in interior Alaska, Journal of Geophysical Research: Atmospheres, 126, e2021JD034586, 2021.

Herring, C. L., Faiola, C. L., Massoli, P., Sueper, D., Erickson, M. H., McDonald, J. D., Simpson, C. D., Yost, M. G., Jobson, B. T., and VanReken, T. M.: New methodology for quantifying polycyclic aromatic hydrocarbons (PAHs) using high-resolution aerosol mass spectrometry, Aerosol Science and Technology, 49, 1131-1148, 2015.

Ijaz, A., Temime Roussel, B., Kammer, J., Mao, J., Simpson, W., Law, K., and D'Anna, B.: In situ measurements of gas-particle partitioning of organic compounds in Fairbanks, Faraday Discussions - In Prep, 2025.

Janhäll, S., Andreae, M. O., and Pöschl, U.: Biomass burning aerosol emissions from vegetation fires: particle number and mass emission factors and size distributions, Atmospheric chemistry and physics, 10, 1427-1439, 2010.

Jentgen, M.: Technical support document for Alaska Department of Environmental Conservation's (ADEC) control measure analysis, under 40 CFR 1010(a) and (c), US EPA, Region 10, Air and Radiation Division, 2022.

Jiang, X., Tsona, N. T., Jia, L., Liu, S., Zhang, H., Xu, Y., and Du, L.: Secondary organic aerosol formation from photooxidation of furan: effects of NO x and humidity, Atmospheric chemistry and physics, 19, 13591-13609, 2019.

Joyce, P., Von Glasow, R., and Simpson, W.: The fate of NO x emissions due to nocturnal oxidation at high latitudes: 1-D simulations and sensitivity experiments, Atmospheric Chemistry and Physics, 14, 7601-7616, 2014.

Katz, E. F., Guo, H., Campuzano-Jost, P., Day, D. A., Brown, W. L., Boedicker, E., Pothier, M., Lunderberg, D. M., Patel, S., and Patel, K.: Quantification of cooking organic aerosol in the indoor environment using aerodyne aerosol mass spectrometers, Aerosol Science and Technology, 55, 1099-1114, 2021.

Kawamoto, H.: Lignin pyrolysis reactions, Journal of Wood Science, 63, 117-132, 2017.

Kong, X., Salvador, C. M., Carlsson, S., Pathak, R., Davidsson, K. O., Le Breton, M., Gaita, S. M., Mitra, K., Hallquist, Å. M., and Hallquist, M.: Molecular characterization and optical properties of primary emissions from a residential wood burning boiler, Science of the Total Environment, 754, 142143, 2021.

Koss, A. R., Sekimoto, K., Gilman, J. B., Selimovic, V., Coggon, M. M., Zarzana, K. J., Yuan, B., Lerner, B. M., Brown, S. S., Jimenez, J. L., Krechmer, J., Roberts, J. M., Warneke, C., Yokelson, R. J., and De Gouw, J.: Non-methane organic gas emissions from biomass burning: identification, quantification, and emission factors from PTR-ToF during the FIREX 2016 laboratory experiment, Atmospheric Chem. Phys., 18, 3299–3319, https://doi.org/10.5194/acp-18-3299-2018, 2018.

Kostenidou, E., Marques, B., Temime-Roussel, B., Liu, Y., Vansevenant, B., Sartelet, K., and D'Anna, B.: Secondary organic aerosol formed by Euro 5 gasoline vehicle emissions: chemical composition and gas-to-particle phase partitioning, Atmospheric Chemistry and Physics, 24, 2705-2729, 2024.

Kostenidou, E., Martinez-Valiente, A., R'Mili, B., Marques, B., Temime-Roussel, B., André, M., Liu, Y., Louis, C., Vansevenant, B., and Ferry, D.: Emission factors, chemical composition and morphology of particles emitted from Euro 5 diesel and gasoline light duty vehicles during transient cycles, Atmospheric Chemistry and Physics Discussions, 2020, 1-33, 2020.

Kotchenruther, R. A.: Source apportionment of PM2. 5 at multiple Northwest US sites: Assessing regional winter wood smoke impacts from residential wood combustion, Atmospheric Environment, 142, 210-219, 2016.

Kumar, V., Giannoukos, S., Haslett, S. L., Tong, Y., Singh, A., Bertrand, A., Lee, C. P., Wang, D. S., Bhattu, D., and Stefenelli, G.: Highly time-resolved chemical speciation and source apportionment of organic aerosol components in Delhi, India, using extractive electrospray ionization mass spectrometry, Atmospheric Chemistry and Physics, 22, 7739-7761, 2022.

Lannuque, V., d'Anna, B., Kostenidou, E., Couvidat, F., Martinez-Valiente, A., Eichler, P., Wisthaler, A., Müller, M., Temime-Roussel, B., and Valorso, R.: Gas–particle partitioning of toluene oxidation products: an experimental and modeling study, Atmospheric Chemistry and Physics, 23, 15537-15560, 2023.

Leglise, J., Müller, M., Piel, F., Otto, T., and Wisthaler, A.: Bulk Organic Aerosol Analysis by Proton-Transfer-Reaction Mass Spectrometry: An Improved Methodology for the Determination of Total Organic Mass, O: C and H: C Elemental Ratios, and the Average Molecular Formula, Analytical chemistry, 91, 12619-12624, 2019.

Lignell, H., Epstein, S. A., Marvin, M. R., Shemesh, D., Gerber, B., and Nizkorodov, S.: Experimental and theoretical study of aqueous cis-pinonic acid photolysis, The Journal of Physical Chemistry A, 117, 12930-12945, 2013.

Liu, L., Breitner, S., Schneider, A., Cyrys, J., Brüske, I., Franck, U., Schlink, U., Leitte, A. M., Herbarth, O., and Wiedensohler, A.: Size-fractioned particulate air pollution and cardiovascular emergency room visits in Beijing, China, Environmental research, 121, 52-63, 2013.

Lopez-Hilfiker, F., Mohr, C., Ehn, M., Rubach, F., Kleist, E., Wildt, J., Mentel, T. F., Lutz, A., Hallquist, M., and Worsnop, D.: A novel method for online analysis of gas and particle composition: description and evaluation of a Filter Inlet for Gases and AEROsols (FIGAERO), Atmospheric Measurement Techniques, 7, 983-1001, 2014.

Louis, C., Liu, Y., Martinet, S., D'Anna, B., Valiente, A. M., Boreave, A., R'Mili, B., Tassel, P., Perret, P., and Andre, M.: Dilution effects on ultrafine particle emissions from Euro 5 and Euro 6 diesel and gasoline vehicles, Atmospheric environment, 169, 80-88, 2017.

Mainka, A. and Zajusz-Zubek, E.: PM1 in ambient and indoor air—urban and rural areas in the Upper Silesian Region, Poland, Atmosphere, 10, 662, 2019.

Mayfield, J. A. and Fochesatto, G. J.: The layered structure of the winter atmospheric boundary layer in the interior of Alaska, Journal of Applied Meteorology and Climatology, 52, 953-973, 2013.

McLafferty, F. W. and Tureˇcek, F.: Interpretation of mass spectra, Mill Valley (Calif.) : University Science Books, 4th ed. edn., ISBN 0935702253, 1993.

Meng, X., Ma, Y., Chen, R., Zhou, Z., Chen, B., and Kan, H.: Size-fractionated particle number concentrations and daily mortality in a Chinese city, Environmental health perspectives, 121, 1174-1178, 2013.

Middlebrook, A. M., Bahreini, R., Jimenez, J. L., and Canagaratna, M. R.: Evaluation of composition-dependent collection efficiencies for the aerodyne aerosol mass spectrometer using field data, Aerosol Science and Technology, 46, 258-271, 2012.

Mohr, C., Huffman, J. A., Cubison, M. J., Aiken, A. C., Docherty, K. S., Kimmel, J. R., Ulbrich, I. M., Hannigan, M., and Jimenez, J. L.: Characterization of primary organic aerosol emissions from meat cooking, trash burning, and motor vehicles with high-resolution aerosol mass spectrometry and comparison with ambient and chamber observations, Environmental Science & Technology, 43, 2443-2449, 2009.

Montoya-Aguilera, J., Horne, J. R., Hinks, M. L., Fleming, L. T., Perraud, V., Lin, P., Laskin, A., Laskin, J., Dabdub, D., and Nizkorodov, S. A.: Secondary organic aerosol from atmospheric photooxidation of indole, Atmospheric Chemistry and Physics, 17, 11605-11621, 2017.

Moon, A., Jongebloed, U., Dingilian, K. K., Schauer, A. J., Chan, Y.-C., Cesler-Maloney, M., Simpson, W. R., Weber, R. J., Tsiang, L., and Yazbeck, F.: Primary Sulfate Is the Dominant Source of Particulate Sulfate during Winter in Fairbanks, Alaska, ACS ES&T Air, 2023.

Morin, B., Allen, G., Marin, A., Rector, L., and Ahmadi, M.: Impacts of wood species and moisture content on emissions from residential wood heaters, Journal of the Air & Waste Management Association, 72, 647-661, 2022.

Müller, M., Leglise, J., Piel, F., and Wisthaler, A.: A CHARON PTR-ToF-MS study on the volatility of freshly formed biogenic SOA, Geophysical Research Abstracts,

Müller, M., Eichler, P., D'Anna, B., Tan, W., and Wisthaler, A.: Direct sampling and analysis of atmospheric particulate organic matter by proton-transfer-reaction mass spectrometry, Analytical chemistry, 89, 10889-10897, 2017.

Paatero, P.: Least squares formulation of robust non-negative factor analysis, Chemometrics and intelligent laboratory systems, 37, 23-35, 1997a.

Paatero, P.: A weighted non-negative least squares algorithm for three-way 'PARAFAC'factor analysis, Chemometrics and Intelligent Laboratory Systems, 38, 223-242, 1997b.

Paatero, P.: The multilinear engine—a table-driven, least squares program for solving multilinear problems, including the n-way parallel factor analysis model, Journal of Computational and Graphical Statistics, 8, 854-888, 1999.

Paatero, P. and Hopke, P. K.: Discarding or downweighting high-noise variables in factor analytic models, Analytica Chimica Acta, 490, 277-289, 2003.

Paatero, P. and Tapper, U.: Positive matrix factorization: A non-negative factor model with optimal utilization of error estimates of data values, Environmetrics, 5, 111-126, 1994.

Paatero, P., Eberly, S., Brown, S., and Norris, G.: Methods for estimating uncertainty in factor analytic solutions, Atmospheric Measurement Techniques, 7, 781-797, 2014.

Palm, B. B., Peng, Q., Fredrickson, C. D., Lee, B. H., Garofalo, L. A., Pothier, M. A., Kreidenweis, S. M., Farmer, D. K., Pokhrel, R. P., and Shen, Y.: Quantification of organic aerosol and brown carbon evolution in fresh wildfire plumes, Proceedings of the National Academy of Sciences, 117, 29469-29477, 2020.

Peng, Y., Wang, H., Gao, Y., Jing, S., Zhu, S., Huang, D., Hao, P., Lou, S., Cheng, T., and Huang, C.: Real-time measurement of phase partitioning of organic compounds using a proton-transfer-reaction time-of-flight mass spectrometer coupled to a CHARON inlet, Atmospheric Measurement Techniques, 16, 15-28, 2023.

Piel, F., Müller, M., Mikoviny, T., Pusede, S. E., and Wisthaler, A.: Airborne measurements of particulate organic matter by proton-transfer-reaction mass spectrometry (PTR-MS): a pilot study, Atmospheric Measurement Techniques, 12, 5947-5958, 2019.

Piel, F., Müller, M., Winkler, K., Skytte af Sätra, J., and Wisthaler, A.: Introducing the extended volatility range proton-transfer-reaction mass spectrometer (EVR PTR-MS), Atmospheric Meas. Tech., 14, 1355–1363, 2021.

Pikridas, M., Sciare, J., Freutel, F., Crumeyrolle, S., Von Der Weiden-Reinmüller, S., Borbon, A., Schwarzenboeck, A., Merkel, M., Crippa, M., and Kostenidou, E.: In situ formation and spatial variability of particle number concentration in a European megacity, Atmospheric Chemistry and Physics, 15, 10219-10237, 2015.

Qi, L., Chen, M., Stefenelli, G., Pospisilova, V., Tong, Y., Bertrand, A., Hueglin, C., Ge, X., Baltensperger, U., and Prévôt, A. S.: Organic aerosol source apportionment in Zurich using an extractive electrospray ionization time-of-flight mass spectrometer (EESI-TOF-MS)–Part 2: Biomass burning influences in winter, Atmospheric Chemistry and Physics, 19, 8037-8062, 2019.

Reemtsma, T.: Determination of molecular formulas of natural organic matter molecules by (ultra-) high-resolution mass spectrometry: status and needs, Journal of chromatography A, 1216, 3687-3701, 2009.

Reid, J., Koppmann, R., Eck, T., and Eleuterio, D.: A review of biomass burning emissions part II: intensive physical properties of biomass burning particles, Atmospheric chemistry and physics, 5, 799-825, 2005.

Robinson, E. S., Cesler-Maloney, M., Tan, X., Mao, J., Simpson, W., and DeCarlo, P. F.: Wintertime spatial patterns of particulate matter in Fairbanks, AK during ALPACA 2022, Environmental Science: Atmospheres, 3, 568-580, 2023.

Robinson, E. S., Battaglia Jr, M., Campbell, J. R., Cesler-Maloney, M., Simpson, W., Mao, J., Weber, R. J., and DeCarlo, P. F.: Multi-year, high-time resolution aerosol chemical composition and mass measurements from Fairbanks, Alaska, Environmental Science: Atmospheres, 2024.

Schauer, J. J. and Cass, G. R.: Source apportionment of wintertime gas-phase and particle-phase air pollutants using organic compounds as tracers, Environmental science & technology, 34, 1821-1832, 2000.

Schueneman, M. K., Nault, B. A., Campuzano-Jost, P., Jo, D. S., Day, D. A., Schroder, J. C., Palm, B. B., Hodzic, A., Dibb, J. E., and Jimenez, J. L.: Aerosol pH indicator and organosulfate detectability from aerosol mass spectrometry measurements, Atmospheric Measurement Techniques, 14, 2237-2260, 2021.

Simoneit, B. R.: A review of biomarker compounds as source indicators and tracers for air pollution, Environmental Science and Pollution Research, 6, 159-169, 1999.

Simoneit, B. R.: Biomass burning—a review of organic tracers for smoke from incomplete combustion, Applied Geochemistry, 17, 129-162, 2002.

Simpson, W., Law, K., Schmale, J., Pratt, K., Arnold, S., Mao, J., Alexander, B., Anenberg, S., Baklanov, A., Bell, D., Brown, S., Creamean, J., Boer, G. d., DeCarlo, P., Descari, S., Elleman, R., Flynn, J., and al, e.: Alaskan Layered Pollution And Chemical Analysis (ALPACA) White Paper, 2019.

Simpson, W. R., Mao, J., Fochesatto, G. J., Law, K. S., DeCarlo, P. F., Schmale, J., Pratt, K. A., Arnold, S. R., Stutz, J., Dibb, J. E., Creamean, J. M., Weber, R. J., Williams, B. J., Alexander, B., Hu, L., Yokelson, R. J., Shiraiwa, M., Decesari, S., Anastasio, C., D'Anna, B., Gilliam, R. C., Nenes, A., St. Clair, J. M., Trost, B., Flynn, J. H., Savarino, J., Conner, L. D.,

Kettle, N., Heeringa, K. M., Albertin, S., Baccarini, A., Barret, B., Battaglia, M. A., Bekki, S., Brado, T. J., Brett, N., Brus, D., Campbell, J. R., Cesler-Maloney, M., Cooperdock, S., Cysneiros De Carvalho, K., Delbarre, H., DeMott, P. J., Dennehy, C. J. S., Dieudonné, E., Dingilian, K. K., Donateo, A., Doulgeris, K. M., Edwards, K. C., Fahey, K., Fang, T., Guo, F., Heinlein, L. M. D., Holen, A. L., Huff, D., Ijaz, A., Johnson, S., Kapur, S., Ketcherside, D. T., Levin, E., Lill, E., Moon, A. R., Onishi, T., Pappaccogli, G., Perkins, R., Pohorsky, R., Raut, J.-C., Ravetta, F., Roberts, T., Robinson, E. S., Scoto, F., Selimovic, V., Sunday, M. O., Temime-Roussel, B., Tian, X., Wu, J., and Yang, Y.: Overview of the Alaskan Layered Pollution and Chemical Analysis (ALPACA) Field Experiment, ACS EST Air, 1, 200–222, https://doi.org/10.1021/acsestair.3c00076, 2024.

Smith, D. M., Cui, T., Fiddler, M. N., Pokhrel, R. P., Surratt, J. D., and Bililign, S.: Laboratory studies of fresh and aged biomass burning aerosol emitted from east African biomass fuels–Part 2: Chemical properties and characterization, Atmospheric Chemistry and Physics, 20, 10169-10191, 2020.

Smith, S. J., van Aardenne, J., Klimont, Z., Andres, R. J., Volke, A., and Delgado Arias, S.: Anthropogenic sulfur dioxide emissions: 1850–2005, Atmospheric Chemistry and Physics, 11, 1101-1116, 2011.

Song, S., Gao, M., Xu, W., Sun, Y., Worsnop, D. R., Jayne, J. T., Zhang, Y., Zhu, L., Li, M., Zhou, Z., Cheng, C., Lv, Y., Wang, Y., Peng, W., Xu, X., Lin, N., Wang, Y., Wang, S., Munger, J. W., Jacob, D. J., and McElroy, M. B.: Possible heterogeneous chemistry of hydroxymethanesulfonate (HMS) in northern China winter haze, Atmos. Chem. Phys., 19, 1357-1371, 10.5194/acp-19-1357-2019, 2019.

Stefenelli, G., Pospisilova, V., Lopez-Hilfiker, F. D., Daellenbach, K. R., Hüglin, C., Tong, Y., Baltensperger, U., Prévôt, A. S., and Slowik, J. G.: Organic aerosol source apportionment in Zurich using an extractive electrospray ionization time-of-flight mass spectrometer (EESI-TOF-MS)–Part 1: Biogenic influences and day–night chemistry in summer, Atmospheric Chemistry and Physics, 19, 14825-14848, 2019a.

Stefenelli, G., Jiang, J., Bertrand, A., Bruns, E. A., Pieber, S. M., Baltensperger, U., Marchand, N., Aksoyoglu, S., Prévôt, A. S., and Slowik, J. G.: Secondary organic aerosol formation from smoldering and flaming combustion of biomass: a box model parametrization based on volatility basis set, Atmospheric Chemistry and Physics, 19, 11461-11484, 2019b.

Sueper, D.: Squirrel and Pika Error Estimates, 2014.

Sun, Y.-L., Zhang, Q., Schwab, J., Demerjian, K., Chen, W.-N., Bae, M.-S., Hung, H.-M., Hogrefe, O., Frank, B., and Rattigan, O.: Characterization of the sources and processes of organic and inorganic aerosols in New York city with a high-resolution time-of-flight aerosol mass apectrometer, Atmospheric Chemistry and Physics, 11, 1581-1602, 2011.

Temime Roussel, B., Cesler-Maloney, M., Chazeau, B., Ijaz, A., Brett, N., Law, K., Bekki, S., Mao, J., Ketcherside, D., Selimovic, V., Hu, L., Simpson, W. R., and D'Anna, B.: Concentrations and Sources of VOCs during wintertime urban pollution at Fairbanks, Alaska, December 01, 20222022: https://agu.confex.com/agu/fm22/meetingapp.cgi/Paper/1072876

Tobler, A. K., Skiba, A., Canonaco, F., Močnik, G., Rai, P., Chen, G., Bartyzel, J., Zimnoch, M., Styszko, K., and Nęcki, J.: Characterization of non-refractory (NR) PM 1 and source apportionment of organic aerosol in Kraków, Poland, Atmospheric chemistry and physics, 21, 14893-14906, 2021.

Tong, Y., Pospisilova, V., Qi, L., Duan, J., Gu, Y., Kumar, V., Rai, P., Stefenelli, G., Wang, L., and Wang, Y.: Quantification of solid fuel combustion and aqueous chemistry contributions to secondary organic aerosol during wintertime haze events in Beijing, Atmospheric Chemistry and Physics, 21, 9859-9886, 2021.

Tran, H. N. and Mölders, N.: Investigations on meteorological conditions for elevated PM2. 5 in Fairbanks, Alaska, Atmospheric Research, 99, 39-49, 2011.

Ulbrich, I., Canagaratna, M., Zhang, Q., Worsnop, D., and Jimenez, J.: Interpretation of organic components from Positive Matrix Factorization of aerosol mass spectrometric data, Atmospheric Chemistry and Physics, 9, 2891-2918, 2009.

Wang, Y. and Hopke, P. K.: Is Alaska truly the great escape from air pollution?-long term source apportionment of fine particulate matter in Fairbanks, Alaska, Aerosol and Air Quality Research, 14, 1875-1882, 2014.

Wang, Y., Zhang, X., Sun, J., Zhang, X., Che, H., and Li, Y.: Spatial and temporal variations of the concentrations of PM 10, PM 2.5 and PM 1 in China, Atmospheric Chemistry and Physics, 15, 13585-13598, 2015.

Ward, T., Trost, B., Conner, J., Flanagan, J., and Jayanty, R.: Source apportionment of PM2. 5 in a subarctic airshed-fairbanks, Alaska, Aerosol and Air Quality Research, 12, 536-543, 2012.

Williams, B. J., Goldstein, A. H., Kreisberg, N. M., and Hering, S. V.: An in-situ instrument for speciated organic composition of atmospheric aerosols: T hermal desorption a erosol GC/MS-FID (TAG), Aerosol Science and Technology, 40, 627-638, 2006.

Xu, W., Li, Z., Zhang, Z., Li, J., Karnezi, E., Lambe, A. T., Zhou, W., Sun, J., Du, A., and Li, Y.: Changes in physicochemical properties of organic aerosol during photochemical aging of cooking and burning emissions, Journal of Geophysical Research: Atmospheres, 128, e2022JD037911, 2023.

Yang, Y., Battaglia, M. A., Mohan, M. K., Robinson, E. S., DeCarlo, P. F., Edwards, K. C., Fang, T., Kapur, S., Shiraiwa, M., and Cesler-Maloney, M.: Assessing the Oxidative Potential of Outdoor PM2. 5 in Wintertime Fairbanks, Alaska, ACS ES&T Air, 2024.

Ye, L. and Wang, Y.: Long-term air quality study in Fairbanks, Alaska: Air pollutant temporal variations, correlations, and PM2. 5 source apportionment, Atmosphere, 11, 1203, 2020.

Zhang, Q., Jimenez, J. L., Canagaratna, M. R., Ulbrich, I. M., Ng, N. L., Worsnop, D. R., and Sun, Y.: Understanding atmospheric organic aerosols via factor analysis of aerosol mass spectrometry: a review, Analytical and bioanalytical chemistry, 401, 3045-3067, 2011.

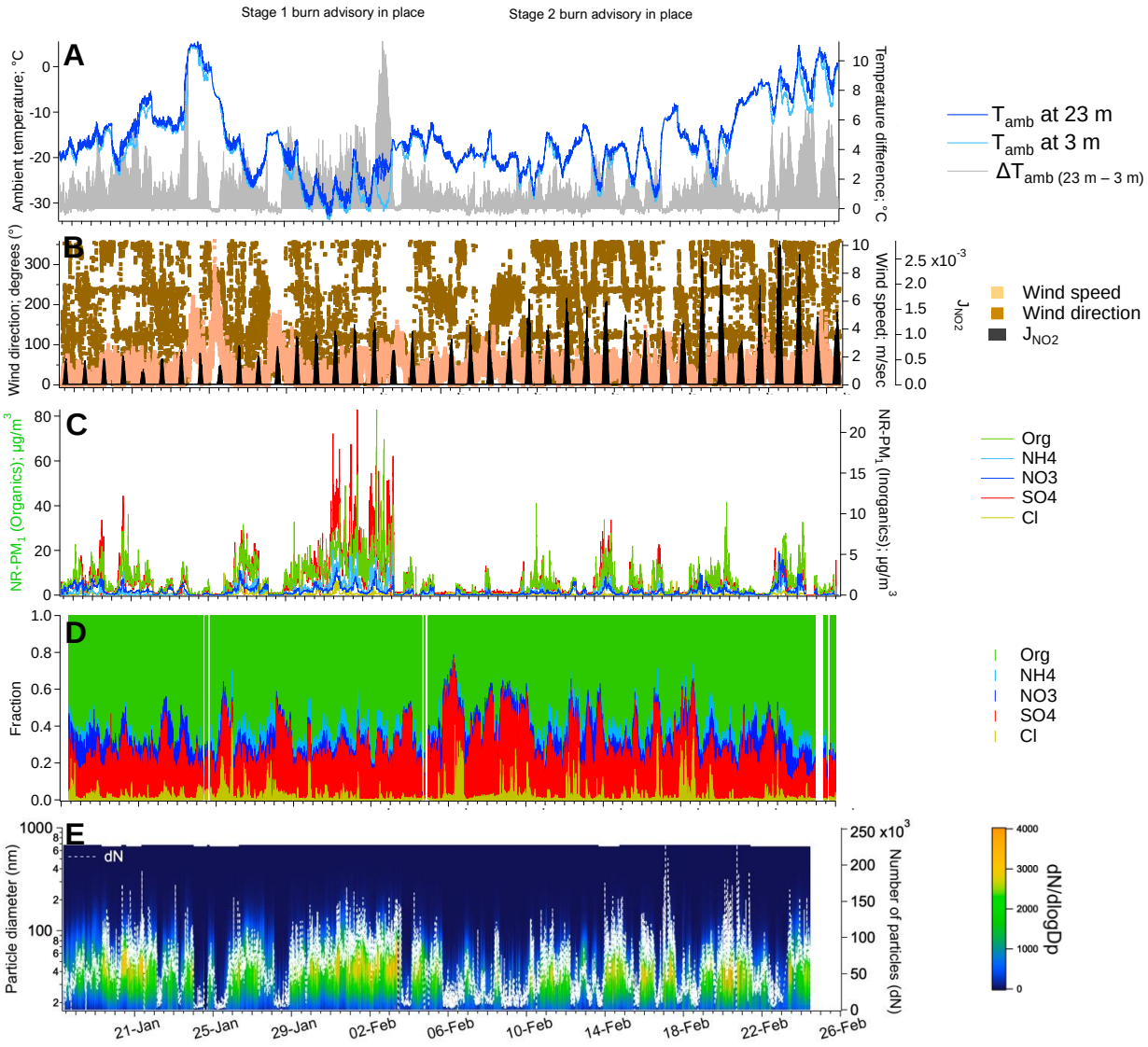

Figure 1. Overview of meteorological parameters and aerosol properties. The shaded areas show the periods, when Stage 1 (red) and 2 (black) advisories ("burn bans") from the Alaska Department of Environmental Conservation, were in place in Fairbanks. (**A**) Ambient temperature at 3 and 23 m and difference of temperature between the two heights; (**B**) wind speed and direction with the daily sunlight in terms of the NO_2 photolysis rate coefficient (J_{NO2}) (Simpson et al., 2024) (**C**–**D**) absolute and fractional compositions of composition of non-refractory fine particulate matter (NR-PM_1) from the AMS; and (**E**) size distribution of PM_1 from the SMPS.

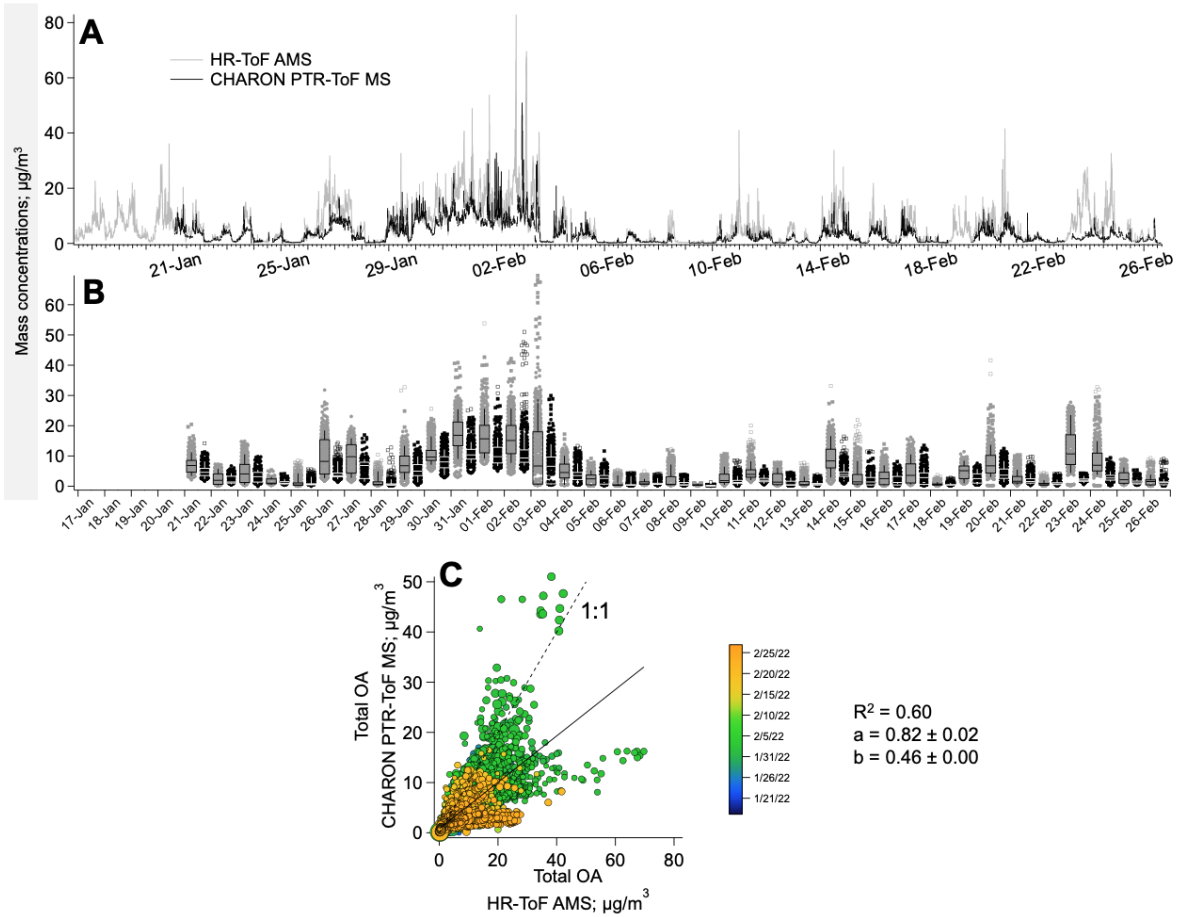

Figure 2. Comparison of total OA measured with the PTR_{CHARON} and the AMS. (**A**) Absolute concentrations of OA measured with the AMS and OA_{corr} (fragmentation-corrected OA) from PTR_{CHARON}; (**B**) Daily average concentrations of OA; and (**C**) Scatter plot of total OA measured with the AMS and the PTR_{CHARON}. Data points are coloured by the dates and the legend is written as MM/DD/YY. Data points are sized by the geometric mean mass of the dM/dlogDp from SMPS (50–500 nm). The dashed line denotes the 1:1 relationship. Coefficients, *a* and *b*, denote the slope and the intercept for the linear regression ($p \leq 0.05$; solid line) and are written with ± one standard deviation.

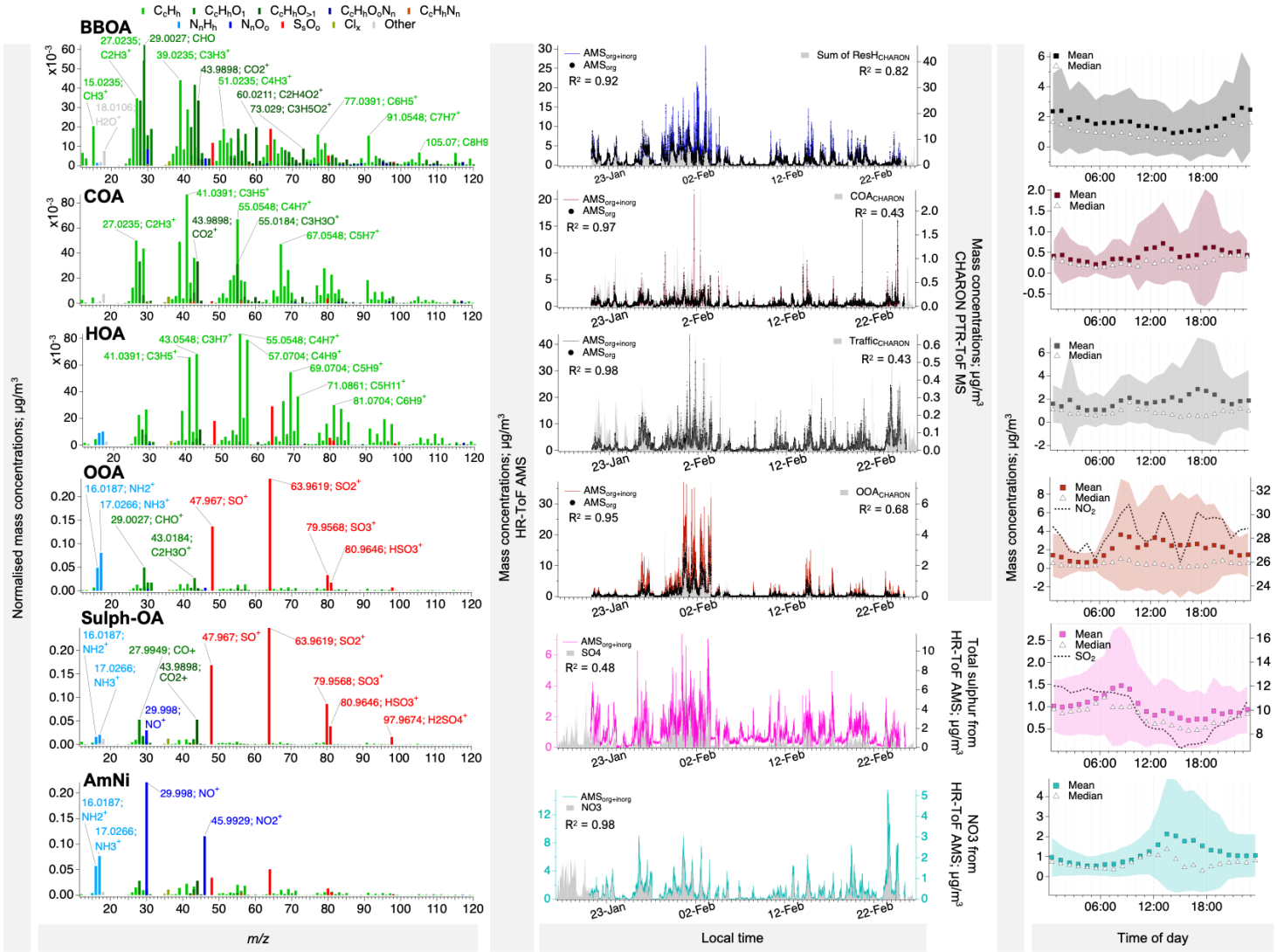

Figure 3. Overview of the positive matrix factorisation output for NR-PM$_1$ measurements with the AMS$_{org+inorg}$. Mass concentrations were normalised to the sum of the concentrations of all ions. Time series are overlaid with those of the corresponding factor (if available) in AMS$_{org}$ and PTR$_{CHARON}$ analysis or an external tracer. Correlation coefficients (R^2; $p \leq 0.05$) are also provided and slopes can be found in **Table S5** or **Table 1**.

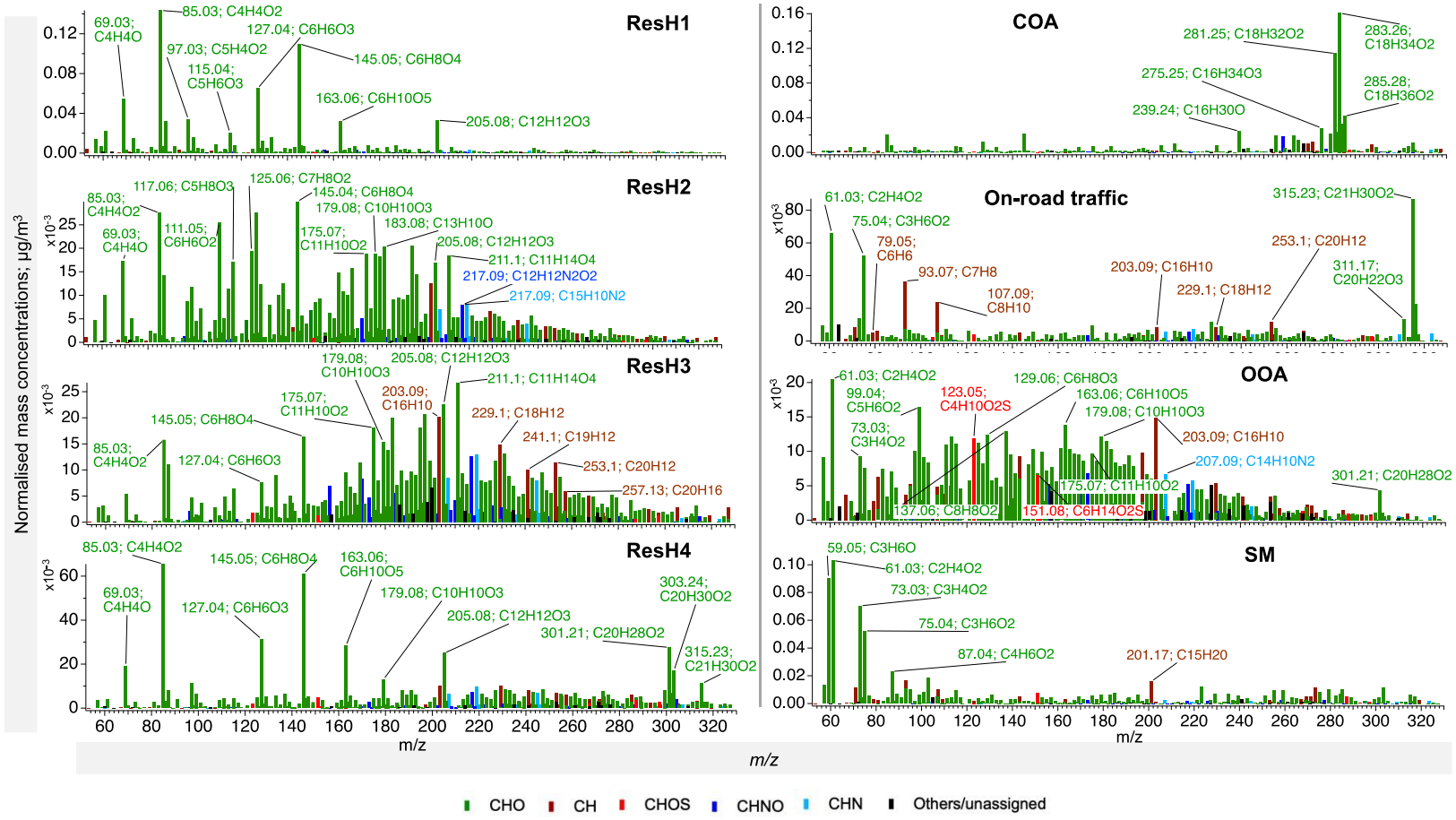

Figure 4. Normalised mass spectra of factors from the PMF of PTR_{CHARON} measurements. Mass concentrations are normalised to the sum of concentrations of all ions. Peaks are coloured by the molecular group (CHO, CHNO, CHOS, CH, CHN) of the formula assigned. Unassigned species are shown in black. Further information, such as tentative identities and formula errors, can be found in **Supplementary Dataset 1**.

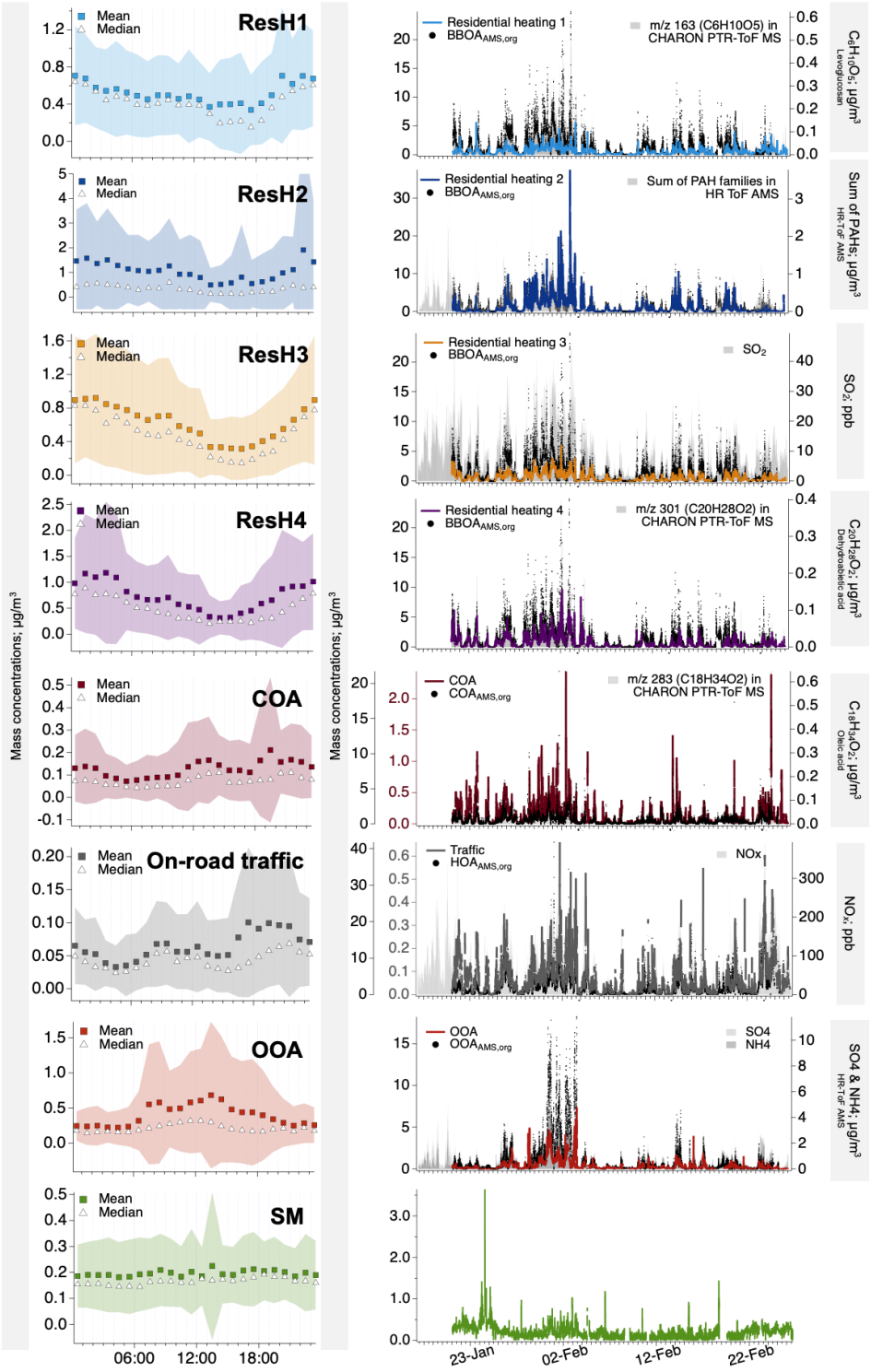

Figure 5. Diurnal profiles and complete time series of factors from the positive matrix factorisation of PTR_{CHARON} measurements. In the second column, time series are overlaid on those of the corresponding factor in AMS_{org} and an external tracer or marker ion. Correlation coefficients (R^2; $p \leq 0.05$) are also provided and slopes can be found in **Table S4** or **Table 1**.

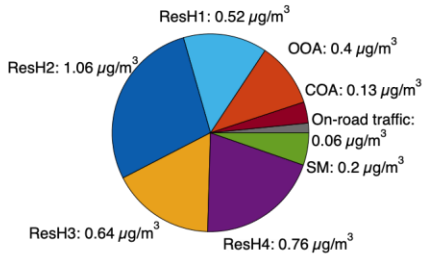

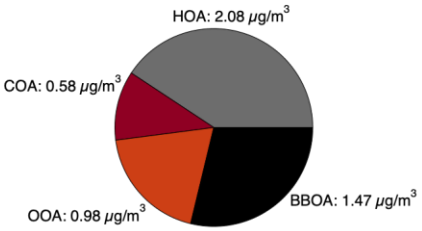

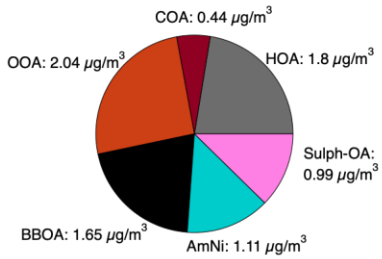

A	Mean mass concentration; μg/m³	Standard deviation	Maximum mass concentration; μg/m³
Total measured	3.41	3.84	51.04
Total modelled	3.35	3.77	48.01
Residential heating 1 (ResH1)	0.52	0.49	5.69
Residential heating 2 (ResH2)	1.06	1.88	37.56
Residential heating 3 (ResH3)	0.64	0.64	6.07
Residential heating 4 (ResH4)	0.76	0.90	9.73
Cooking (COA)	0.13	0.16	2.44
On-road traffic	0.06	0.07	0.66
Oxygenated OA (OOA)	0.40	0.60	7.43
Small molecules (SM)	0.20	0.14	3.64

B	Mean mass concentration; μg/m³	Standard deviation	Maximum mass concentration; μg/m³
Total measured	5.68	6.39	82.94
Total modelled	4.98	5.74	51.65
Biomass burning OA (BBOA)	1.47	1.93	24.85
Cooking (COA)	0.58	0.81	21.73
Hydrocarbon-like OA (HOA)	2.08	2.98	41.81
Oxygenated OA (OOA)	0.98	2.05	18.24

C	Mean mass concentration; μg/m³	Standard deviation	Maximum mass concentration; μg/m³
Total measured	8.31	9.29	92.66
Total modelled	7.57	8.74	67.66
Biomass burning OA (BBOA)	1.64	2.21	30.94
Cooking (COA)	0.44	0.72	21.05
Hydrocarbon-like OA (HOA)	1.80	2.71	43.85
Oxygenated OA (OOA)	2.04	4.14	37.18
Sulphate-rich (Sulph-OA)	0.99	0.83	7.39
Ammonium nitrate (AmNi)	1.12	1.59	15.63

Figure 6. Campaign-averages of mass concentrations apportioned to each factor in (**A**) PTR_{CHARON}, (**B**) AMS_{org}, and (**C**) $AMS_{org+inorg}$ analyses. Slices of pies are equivalent to the average absolute concentrations. A complete time series of fractional contributions can be found in **Figure S14**.

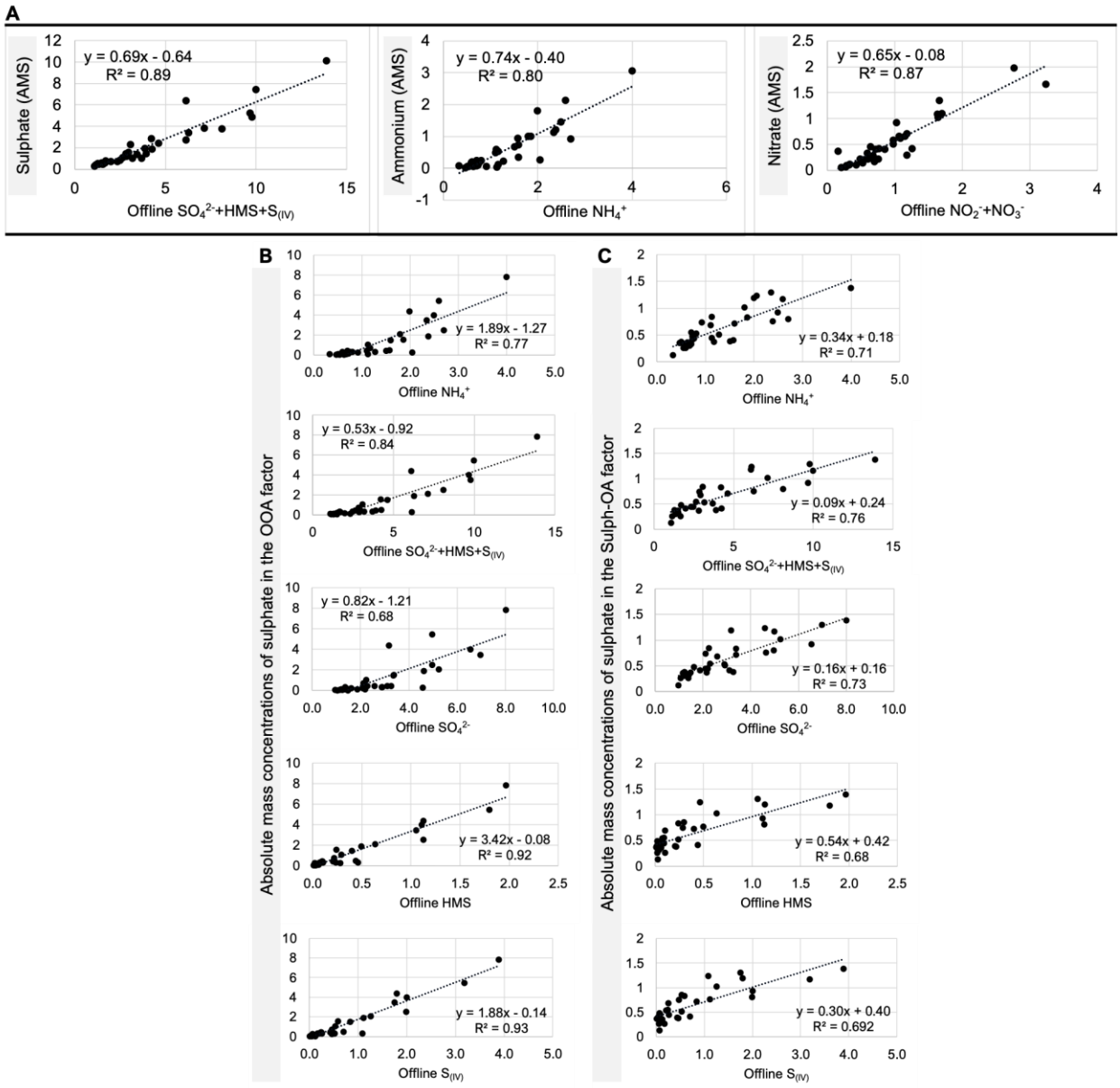

Figure 7. Scatter plots showing the correlation (R^2; $p \leq 0.05$) between inorganic species measured with the AMS and offline ion chromatography of chemical species in $PM_{0.7}$ collected on filters. Comparison of (**A**) total mass concentrations of sulphur and nitrogen-containing species; (B) $OOA_{AMS,org+inorg}$ factor with different species from IC analysis; and (**C**) Sulph-OA factor with different species from IC analysis.

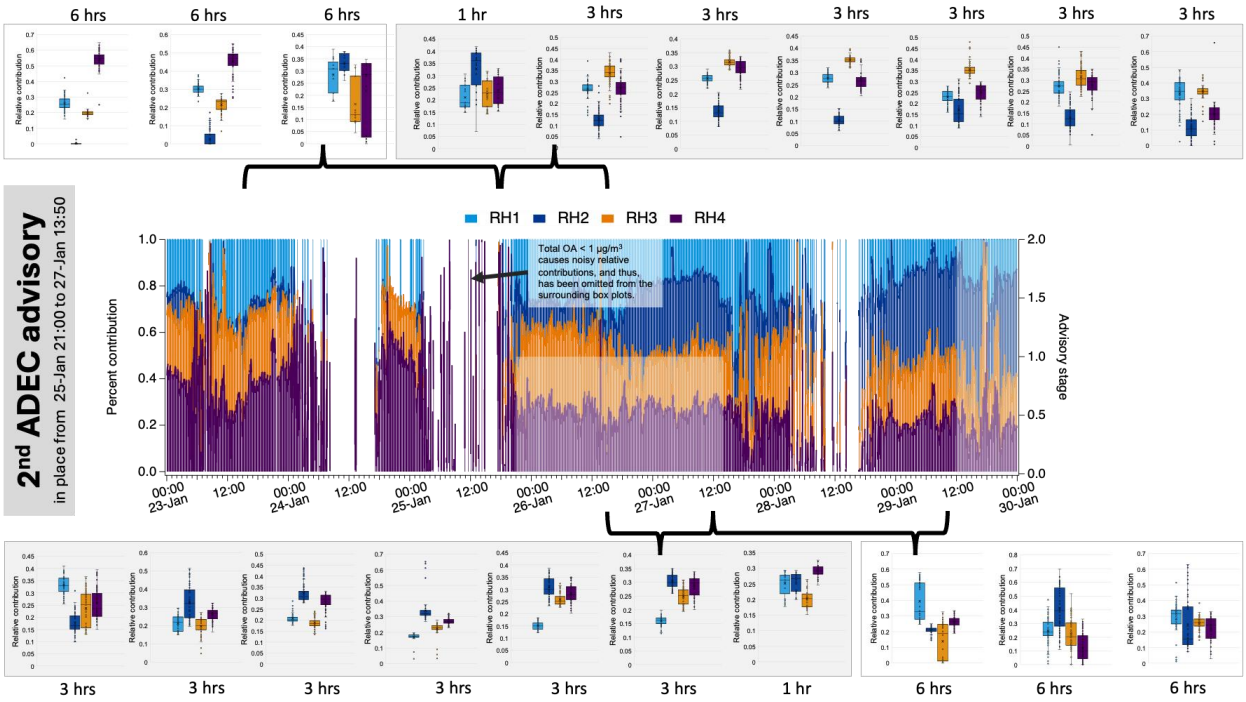

Figure 8. Variation in the relative contributions of residential heating factors to total biomass-burning OA concentrations. For simplicity, only the 2nd ADEC advisory implemented during the campaign is shown. Contributions are also shown for approximately 2 days before and after the advisory for comparison, along with their 6-hour averages as box plots (white panels), when suitable data was available (e.g., periods with noisy data were omitted and the adjacent period is shown instead). For better visualisation of variation in contributions, when the advisory was in place, 3-hour averages are shown (grey panels). To account for a lag in the appearance of variations in emission sources, 1-hour averages are shown for the beginning and end of the advisory event.

Table 1. Linear regression (R^2; $p \leq 0.05$) between the time series of factors derived from (**A**) PTR_{CHARON}, (**B**) AMS_{org}, and (**C**) $AMS_{org+inorg}$ measurements with external tracers and chemical species (S and N-containing species and PAHs) measured with the AMS.

A

	Traffic	COA	OOA	ResH1	ResH2	ResH3	ResH4	SM
Amb. Temp.	0.01	0.02	0.22	0.14	0.27	0.27	0.20	0.16
Black carbon	0.58	0.27	0.22	0.37	0.16	0.27	0.22	0.04
Trace gases								
NO_2	0.46	0.19	0.26	0.37	0.15	0.27	0.16	0.01
NO	0.65	0.24	0.22	0.32	0.10	0.16	0.13	0.06
NO_x	0.66	0.25	0.25	0.36	0.12	0.20	0.15	0.05
CO_2	0.67	0.38	0.31	0.51	0.24	0.39	0.30	0.02
CO	0.61	0.18	0.08	0.14	0.02	0.04	0.03	0.08
SO_2	0.27	0.20	0.19	0.46	0.34	0.61	0.47	0.01
O_3	0.34	0.19	0.13	0.39	0.12	0.31	0.20	0.00
Chemical species measured with the HR-ToF AMS								
Sulphur	0.43	0.22	0.71	0.35	0.22	0.23	0.13	0.04
NO_3	0.31	0.16	0.25	0.17	0.02	0.04	0.01	0.02
NH_4	0.43	0.20	0.64	0.30	0.15	0.14	0.06	0.05
Cl	0.10	0.05	0.12	0.06	0.01	0.03	0.01	0.01
UnSub PAH	0.30	0.25	0.34	0.50	0.59	0.55	0.58	0.01
M-PAH	0.33	0.27	0.33	0.52	0.60	0.53	0.60	0.01
O-PAH	0.27	0.22	0.36	0.56	0.70	0.61	0.64	0.01
N-PAH	0.28	0.23	0.26	0.54	0.62	0.61	0.68	0.01
A-PAH	0.28	0.24	0.19	0.48	0.50	0.55	0.61	0.04

B

	HOA	COA	OOA	BBOA
Amb. Temp.	0.02	0.02	0.19	0.22
Black carbon	0.49	0.27	0.29	0.25
Trace gases				
NO_2	0.42	0.25	0.25	0.25
NO	0.61	0.26	0.33	0.16
NO_x	0.62	0.28	0.34	0.20
CO_2	0.49	0.30	0.41	0.35
CO	0.38	0.19	0.19	0.06
SO_2	0.18	0.14	0.25	0.44
O_3	0.26	0.20	0.12	0.27
Chemical species measured with the HR-ToF AMS				
Sulphur	0.37	0.27	0.89	0.19
NO_3	0.49	0.27	0.23	0.06
NH_4	0.48	0.29	0.79	0.13
Cl	0.12	0.06	0.13	0.03
UnSub PAH	0.31	0.26	0.39	0.71
M-PAH	0.36	0.30	0.39	0.76
O-PAH	0.23	0.23	0.43	0.79
N-PAH	0.24	0.22	0.33	0.78
A-PAH	0.23	0.20	0.26	0.69

Very strong	≥0.75
Strong	≥0.5 and <0.75
Moderate	≥0.3 and <0.5
Weak	≥0.1 and <0.3
None	<0.1

C

	HOA	COA	OOA	BBOA	AmNi	Sulph-OA
Amb. Temp.	0.01	0.03	0.19	0.26	0.00	0.24
Black carbon	0.43	0.21	0.32	0.30	0.30	0.30
Trace gases						
NO_2	0.37	0.18	0.27	0.28	0.31	0.40
NO	0.55	0.19	0.36	0.22	0.35	0.32
NO_x	0.56	0.21	0.37	0.26	0.38	0.37
CO_2	0.41	0.24	0.47	0.41	0.28	0.48
CO	0.35	0.17	0.21	0.08	0.25	0.11
SO_2	0.14	0.11	0.27	0.45	0.07	0.61
O_3	0.23	0.14	0.12	0.25	0.23	0.34
Chemical species measured with the HR-ToF AMS						
Sulphur	0.26	0.24	0.95	0.34	0.23	0.48
NO_3	0.38	0.18	0.24	0.09	0.98	0.12
NH_4	0.34	0.25	0.86	0.25	0.44	0.33
Cl	0.09	0.05	0.15	0.04	0.16	0.04
UnSub PAH	0.26	0.25	0.40	0.77	0.15	0.31
M-PAH	0.31	0.28	0.40	0.82	0.17	0.32
O-PAH	0.18	0.23	0.41	0.87	0.11	0.33
N-PAH	0.20	0.20	0.33	0.82	0.11	0.30
A-PAH	0.20	0.18	0.26	0.70	0.11	0.25

Supplementary information *for* 'Complementary aerosol mass spectrometry elucidates sources of wintertime sub-micron particle pollution in Fairbanks, Alaska, during ALPACA 2022'

A. Ijaz[1,2], B. Temime-Roussel[1], B. Chazeau[1], S. Albertin[3], S. R. Arnold[4], B. Barret[5], S. Bekki[6], N. Brett[6], M. Cesler-Maloney[7], E. Dieudonne[8], K. K. Dingilian[9], G. J. Fochesatto[10], J. Mao[7], A. Moon[11], Joel Savarino[3], W. Simpson[7], R. J. Weber[9], K.S. Law[6], B. D'Anna[1]

[1]Aix-Marseille Université, CNRS, LCE, Marseille, France
[2]Present Address: Atmospheric, Climate, & Earth Sciences Division, Pacific Northwest National Laboratory, Richland, Washington 99354, United States
[3]University of Grenoble Alpes, CNRS, IRD, Grenoble INP, INRAE, IGE, F-38000 Grenoble, France
[4]School of Earth and Environment, University of Leeds, Leeds, LS2 9JT, United Kingdom
[5]Laboratoire d'Aérologie, Université Toulouse III-Paul Sabatier, CNRS, Toulouse, France
[6]Sorbonne Université, UVSQ, CNRS, LATMOS-IPSL, Paris, France
[7]Department of Chemistry and Biochemistry and Geophysical Institute, University of Alaska, Fairbanks, AK, United States
[8]Laboratory of Physics and Chemistry of the Atmosphere, University of Littoral and Opal Coast, Dunkerque, France
[9]School of Earth and Atmospheric Sciences, Georgia Institute of Technology, Atlanta, Georgia 30332, United States
[10]Department of Atmospheric Sciences, University of Alaska, Fairbanks, AK, United States
[11]Department of Atmospheric Sciences, University of Washington, Seattle, Washington 98195, United States

Correspondence to: Barbara D'Anna (barbara.danna@univ-amu.fr) and Amna Ijaz (amna.ijaz@pnnl.gov)

The dataset comprising the ions detected and identified in this study is available with the DOI 10.5281/zenodo.14254283.

S1. Conversion from mixing ratios to mass concentrations

The mixing ratios in ppbV were calculated using **Equation S1**.

$$R = \frac{RH^+}{H_3O^+} \times \frac{Tr_{H3O^+}}{Tr_{RH^+}} \times \frac{U_{drift} \times T_{drift}^2}{k \times p_{drift}^2} \text{.....Equation S1}$$

Where the RH^+ and H_3O^+ are the signal intensity in counts per second (cps) of the analyte and the reagent ions corrected according to their respective relative transmissions (Tr). U_{drift}, T_{drift}, and p_{drift} denote the voltage, temperature, and pressure (in mbar) in the drift tube, and *k* is the reaction rate coefficient (cm^3/s) between the reagent ion and a given volatilised analyte.

The Tr in the range of 21–135 amu was determined experimentally with a calibration gas mixture (12-component mix at ppmV level each from Apel Riemer Environmental Inc, Miami, USA) after 10-fold dilution with pure nitrogen at the beginning and at the end of the measurement campaign. The composition of the calibration gas mixture and the experimental sensitivity measured in the field are summarised in **Table S1**.

The value of *k* in **Equation S1** for the proton-transfer reaction between an analyte ion and $[H_3O]^+$ can be estimated theoretically. The Langevin−Gioumousis−Stevenson and the Su and Chesnavich theories are applied to pure hydrocarbons (Langevin, 1903) and oxygenated compounds (Su and Chesnavich, 1982), respectively. Both use the molecular weight (MW) and dipole moment (μ_D), while the former also includes polarizability (α) to predict ion-molecule reaction rates (Ellis and Mayhew, 2014). The values of *k* for organic compounds cover a wide range typically from 1.7–2.5×10^{-9} cm^3/sec (Zhao and Zhang, 2004), while high values, up to 5.48×10^{-9} cm^3/sec (norpionaldehyde; $C_9H_{14}O_2$)(Cappellin et al., 2012) have been reported for oxygenated organic compounds. For quantification purposes, the standard protonation *k* of 2×10^{-9} cm^3/sec has been widely used (Holzinger et al., 2010; Capozzi et al., 2016; Pieber et al., 2018). This is expected to introduce a substantive error in quantifying most organic compounds, and thus, various estimation approaches have been proposed (Cappellin et al., 2012; Cappellin et al., 2010).

In this study, α was calculated using an elemental composition-based parameterisation for heteroatom-containing compounds following Sekimoto et al., (2017). For all other species with known elemental compositions, the parameterisation of Bosque and Sales (Bosque and Sales, 2002) was applied. For unknown species (no formula assigned), another parameterisation based solely on MW was used (Sekimoto et al., 2017). The range of α varied from 3.25×10^{-30} (for HNO_3) – 5.435×10^{-29} (for $C_{30}H_{48}O$). For heteroatom-containing species, μ_D were predicted based on elemental composition and/or MW (Sekimoto et al., 2017). For unknown species, a constant μ_D of 2.75 was used considering a predominance of oxygenated hydrocarbons (Müller et al., 2017). The final range thus obtained was 1.30–2.75 D. In a previous study, a constant μ_D of 2.75 and polarizabilities based on elemental composition were associated with quantification uncertainty of ±40% in the mass concentrations (Müller et al., 2017). MW and heteroatomic classes reduce uncertainties in the calculated *k* values (Sekimoto et al., 2017), and thus, were used to improve quantification accuracy. The *k* values calculated here for hydrocarbons were in close agreement with rates reported in the literature (**Figure S1**). In other cases, they were poorly aligned with previously reported protonation *k*-rates, due to the presence of different polarisable functional groups in species with the same empirical formula. For instance, proton-transfer *k* of 3.58×10^{-9}, 2.69×10^{-9}, 2.51×10^{-9}, and 3.32×10^{-9} cm^3/sec have been reported for acetone, oxetane, 2-propen-1-ol, and propanal (Cappellin et al., 2012), respectively, despite the same empirical formula (i.e., C_3H_6O). Such isomers cannot be differentiated in high-resolution mass spectrometry, and thus, only the general elemental composition is used to estimate the values of *k*. When the formula assignment is unambiguous, the relative uncertainty regarding the concentration derived from the propagation of the relative uncertainties on the transmission and the *k* is estimated to be within ±30% (Ellis and Mayhew, 2014). Due to the higher *k* values, the mixing ratios and mass concentrations measured here are expected to be underestimated. Specifically, mixing ratios and mass concentrations were 38.79 and 42.06% lower than those calculated with the standard value of *k* = 2×10^{-9} cm^3/sec.

Mass concentrations associated with individual ions were calculated by using the standard method (Seinfeld and Pandis, 2016) expressed in **Equation S2**.

$$\text{Mass concentration } (\mu g/m^3) = \left(\frac{P \times \left(\frac{m}{z}\right) - 1.0072765}{8.314 \times T}\right) \times mixing\ ratio\ (ppm) \quad \text{.....Equation S2}$$

Where P, *m/z*, and T denote ambient pressure (in Pascals), the measured mass-to-charge of the ion, and ambient temperature (in Kelvin). 1.0072765 and 8.314 are the mass of a proton (in kg) and the molar gas constant (J/K/mol).

S2. Assignment of molecular formulae

Molecular formulae were assigned to accurate *m/z* measured with the PTR_{CHARON} (*m/z* 50–425) using the following constraints: $C_cH_hO_oN_{0\text{-}3}S_{0\text{-}1}$ (number of C, H, and O were unrestricted), $-13 \leq$ DBE-O ≤ 20 (integer DBE values only); $0 \leq$ O/C ≤ 2.0; and $0.1 \leq$ H/C ≤ 3. Species assigned ^{13}C were retained for quantification and factorisation. Elemental composition was obtained with an average formula error of **1.23 ± 23.54 ppm** (ranging between -63.26 and 146.52 ppm). Relatively broad *m/z* accuracy and a mass resolution ($\Delta m/m$) of ~5000 inevitably returned multiple prospective formulae for every ion. Both the selected formula and the second likely candidate are presented in the supplementary information, where the former was chosen based on the following priorities: lower number of heteroatoms > lower formula error > relevance to atmospheric emission sources identified here. Among the 1118 ions resolved, 336 were retained above the S/N, and 318 could be chemically identified in this way. Associated parameters (e.g., concentration-weighted O/C, H/C, etc.) were derived for total OA as described previously (Müller et al., 2017).

S3. Concentration-weighted average enrichment factor (EF)

The EF of particles sampled by the CHARON inlet is dependent on their size as demonstrated in **Figure S2**. Particles larger than 150 nm have been reported to undergo enrichment of ~25 (Eichler et al., 2015b) or ~44-fold (Müller et al., 2017) in the aerodynamic lens. The EF reduces steeply for particles of <60–150 nm (Eichler et al., 2015b). Here, the distribution of mass concentrations across particles of 15–661 nm was calculated from particle number and density measured with a scanning mobility particle sizer (SMPS). **Figure S3** indicates that particles of 100–250 nm are predominant during the ALPACA campaign. In the dataset obtained from PTR_{CHARON} measurements, it is not possible to connect individual ions detected at any specific sampling time with a unique particle size or range of sizes. Therefore, we calculated the concentration-weighted average EF for $k = 1{:}n$ measurements using **Equation S3**. The time series for EF thus obtained is shown in **Figure S3**. The detected concentrations were then converted to sampled concentrations by dividing them with the corresponding EF value.

$$EF_{weighted} = \frac{\sum_{k=1}^{k=n} EF_k \cdot Conc_k}{\sum Conc} \quad \text{.....Equation S3}$$

Equation used to calculate the relative importance of a variable in a factor

$$RI_{i,f} = \frac{C_{i,f}^{norm} - C_i^{norm}}{\sigma_i^{norm}} \qquad \textbf{Equation S3}$$

Where,

$RI_{i,f.}$ = the relative importance of variable *i* in factor *f*

$C_{i,f}^{norm}$ = normalised concentration of variable *i* in factor *f*

C_i^{norm} = mean normalised concentration of variable *i* across all factors

σ_i^{norm} = standard deviation of the normalised concentration of variable *i* across all factors

S4. Commentary on levoglucosan fragmentation and total OA quantification

Where required for the sake of discussion, uncorrected and corrected total OA (using a previously described method (Leglise et al., 2019)) from PTR_{CHARON} are denoted as OA_{uncorr} and OA_{corr}, respectively. Although PTR is a soft ionisation mechanism, when it is applied to large and heavily functionalised molecules, such as levoglucosan, fragmentation is inevitable (Müller et al., 2017; Leglise et al., 2019). Fragment and precursor ions cannot be distinguished in mass spectra generated for ambient air due to the molecular complexity. However, in our study, owing to the strong influence of biomass burning as a major source of emissions, *m/z* 163.06 was a dominant ion and was attributed to $C_6H_{10}O_5$ (levoglucosan and anhydrous monosaccharide isomers). It could unambiguously be associated with its known fragments at *m/z* 85 ($C_4H_4O_2$), 127 ($C_6H_6O_3$), and 145 ($C_6H_8O_4$) due to high correlation coefficients between the precursor and fragments ($R^2 > 0.95$; **Figure S4**). It must be noted that the possibility of isomers on the *m/z* values associated with levoglucosan fragments cannot be fully ruled out. Like a previously reported PTR_{CHARON} analysis of pure levoglucosan (Müller et al., 2017), these fragment ions were more intense than the molecular ion, $[M+H]^+$.

Strong fragmentation of oxygenated compounds, such as levoglucosan and *cis*-pinonic acid, in ambient aerosol causes an underestimation in the total mass concentrations by 32–33%. Here, correcting for the fragmentation of levoglucosan only (i.e., by adding the mixing ratios calculated for the fragments to those of the precursor ion before conversion to mass concentrations with **Equation S2**) improved OA_{uncorr} by 5%; the total OA concentrations thus obtained are referred to as OA_{corr_levo}. A greater increase of 17% was observed in OA_{uncorr} upon fragmentation correction with the method of Leglise et al. (Leglise et al., 2019) as compared to correction for levoglucosan fragmentation only. This indicated that levoglucosan was not the only molecule prone to fragmentation based on molecular composition, and a more holistic approach to fragmentation correction is preferable. Therefore, the results presented herein report OA_{corr}, rather than OA_{corr_levo}. However, where required for the quantification of levoglucosan alone (such as the results in **Figure S9A**), OA_{corr_levo} was used.

In the case of the AMS, calibrations conducted during the ALPACA campaign with pure levoglucosan indicated *m/z* 60, i.e., $C_2H_4O_2$, to constitute 12% of the overall signal for levoglucosan. This quantitative relationship was used to estimate levoglucosan in ambient OA and is expected to be an upper bound of the estimation, considering that other compounds can contribute to the signal at *m/z* 60 as well.

S5. Specifics of the factorisation of PTR_{CHARON} measurements

A preliminary unconstrained factorisation of the PTR_{CHARON} (mixing ratios used at this stage of analysis) did not delineate on-road traffic as a source unless the number of factors was allowed to be unreasonably high (e.g., >19 factors). However, a factor identified as ' road transport gasoline' constituted a major fraction of total VOCs in gas-phase PTR-ToF MS measurements during the ALPACA campaign (Temime Roussel et al., 2022). We used the time series of this gas-phase mobile gasoline factor to constrain the PMF of PTR_{CHARON} measurements, which helped isolate a reasonable on-road transport factor, albeit with very low concentrations of OA in it.

A cooking (COA) factor was observed in the unconstrained PMF trial, but it suffered from mixing with the transport and oxygenated OA (OOA) factors. To optimise it, we used the time series of a clean-looking COA factor from an unconstrained solution as an anchor and configured subsequent PMF runs to isolate this factor first. Once an eight-factor solution was established as the base-case (**Table S2**), 125 bootstrapping replicates were run, where COA and on-road transport factors were constrained with random *a*-values between 0 and 0.3 with a step-size of 0.05. This range of *a*-values was chosen to allow reasonable divergence of the factor from the anchor (i.e., up to 30%) while maintaining a strong correlation (at least 70%) with it.

We chose to leave the remaining factors unconstrained to take full advantage of the factor speciation possible with the molecular-level data from PTR_{CHARON}. The criteria used to select reasonable bootstrapped runs are listed in **Table S3**. Seventy-four runs (52.9%) passed the evaluation criteria for further analysis and were satisfactorily classified as distinct and unmixed (Stefenelli et al., 2019). The source apportionment results presented throughout the text (for AMS datasets as well) are an average of these selected runs. The mixing ratios apportioned to each factor were converted to mass concentrations and corrected for fragmentation with excellent agreement between the measured and factorised OA concentrations (**Figure S5**).

The factorisation of PTR_{CHARON} produced a unique factor that comprised largely of very small ions of *m/z* < 65, labelled as the small molecules (SM) factor. This factor could not be given an environmentally relevant identity based on a lack of correlations with the external tracers, and thus, it has not been discussed in the main text. Its major constituents were small species, such as *m/z* 59.05 (C_3H_6O), 61.03 ($C_2H_4O_2$), 73.03 ($C_3H_4O_2$), 75.04 ($C_3H_6O_2$), etc., that are expected to be in the gaseous phase, rather than the condensed phase. Its average concentration swas ~~remained below 4 µg/m^3 (average =~~ **0.2 ± 0.1 µg/m^3** ~~) over the campaign~~ with large relative contributions to total OA (>80%) during short and clean periods of the campaign, when ambient OA_{CHARON} was below 1 µg/m^3. We speculate that the SM factor is an artefact produced by instrumental chemical background and possible remnants of VOC species on the denuder as we switched from collecting gas-phase samples to particle sampling through the CHARON inlet.

S6. Specifics of the factorisation of AMS measurements

In both (organics only and organics + inorganics) the AMS analyses, O^+ (*m/z* 16), OH^+ (*m/z* 17), H_2O^+ (*m/z* 18), and CO^+ (*m/z* 43) were calculated as constant fractions of CO_2^+ (*m/z* 44), rather than being measured. They were thus excluded from PMF to avoid giving extra weight to CO_2^+ and reinserted into the profiles

after factorisation (Xu et al., 2016; Datalystica, 2022). Unconstrained factorisation of AMS (measurements not corrected for CDCE or RIE at this stage) did not delineate an optimal unmixed COA factor in either AMS_{org} or $AMS_{org+inorg}$ datasets until six or more factors were allowed; this caused splitting and mixing of the hydrocarbon-like (HOA) or the biomass-burning OA (BBOA) factors. Primary factors, other than BBOA, were thus constrained using profiles obtained from suitable unconstrained runs. BBOA was left unconstrained with the same intention as in PTR_{CHARON}, i.e., to leave room for the separation of multiple biomass-based fuels. Four and six-factor solutions were chosen as the most reasonable choices for AMS_{org} and $AMS_{org+inorg}$, where only HOA and COA factors were constrained (**Tables S3**).

250 bootstrapping replicates each were run for the two datasets with random *a*-values between 0 and 0.3 with a step-size of 0.05. The evaluation criteria for selecting reasonable runs are listed in **Table S3**, which led to the selection of 200 (80%) and 249 (99.6%) distinct and unmixed runs (Stefenelli et al., 2019), respectively. After PMF analysis, matrices of factors from AMS_{org} and $AMS_{org+inorg}$ measurements were corrected for CDCE and RIE as described in a previous study (Zografou et al., 2022) using the CDCE and RIE values stated in **Section 2.2.2**.

Section S7. Positive matrix factorisation of size distributions from SMPS

PMF inputs need an error matrix, which was prepared by using the method of (Rivas et al., 2020) on both the number and mass concentrations; only results from mass concentration analysis have been discussed in this study. Briefly, the final uncertainty at each sampling point was measured as **α × (measured concentration + average concentration of a given size bin) + (C_3 × measured concentrations)**. Recommended α and C_3 range from 0.005–0.04 and 0.05–0.15 and were found to be optimum at 0.0175 and 0.1 for our matrix of mass concentrations. The optimisation was achieved based on the least scaled residuals. To remove noisy data, size bins with average concentrations lower than 10% of the entire matrix's average were removed leaving behind 96 size bins from 21.7 to 661 nm.

To find sizes corresponding to the PTR_{CHARON} or $AMS_{org+inorg}$ factors, fully constrained PMF trials with eight and six factors were run on SoFi with 10 calls in each. The time series of the factors of interest were used as anchors with an exact *a*-value of 0.1 (i.e., 10% divergence). Results of all calls were averaged. Bootstrapping was redundant due to the fully constrained nature and tight *a*-values used in these PMF trails.

S8. Discrepancies in mass concentrations of HOA/on-road transport emissions from PTR_{CHARON} and AMS analysis

A significant quantitative discrepancy is observed between the OA contributions measured for the on-road transport-related factors with PTR_{CHARON} and the AMS_{org}. On average, **2.1 ± 3.0 µg/m^3** of OA was associated with $HOA_{AMS,org}$, compared to only **0.1 ± 0.1 µg/m^3** for the $transport_{CHARON}$ factor (**Figure 6**). The slope of the scatter ~~plot in Figure 5~~ comparing $HOA_{AMS,org}$ and road $transport_{CHARON}$ suggests that the OA mass apportioned to the latter was only ~2% of that apportioned to the former (Table S4). This discrepancy could have several reasons. First, instrumental biases, i.e., the tendency of alkanes from gasoline to undergo dissociative PTR ionisation (Gueneron et al., 2015) and the limited ability of PTR_{CHARON} to analyse particles smaller than 150 nm (Eichler et al., 2015a; Eichler et al., 2015b) are

important considerations. Indeed, the laboratory quantification of standard compounds by the PTR_{CHARON}, including alkanes (hexadecane, octadecane, eicosane, docosane, hexacosane, etc.), fatty acids (palmitic, oleic, stearic acid, etc.), and biomass burning markers (levoglucosan, vanillic, acid, coniferaldehyde, acetosyringone, etc.) revealed that alkanes are underestimated by 2–4 times their actual concentrations while the O-containing species remained unaffected. Furthermore, a fully constrained PMF of SMPS matrices (see **Section S7**) is shown in **Figure S12**, where peaks in road $transport_{CHARON}$ concentrations coincide with peaks in the contribution of particles sized 50–100 nm.

Lastly, an analysis of the relative variation in $HOA_{AMS,org}$ and NO_x based on a previous approach (Zhang et al., 2019) provided evidence that non-vehicular emissions (specifically, heating oil combustion) contribute to $HOA_{AMS,org}$ as well, rendering its concentrations different from road $transport_{CHARON}$. The HOA/NO_x ratio in the ALPACA campaign was up to 5× higher during the evening than during the morning (data not shown); considering that NO_x is majorly emitted from vehicles in Fairbanks, this ratio should remain consistent through the day if HOA were also released from vehicles only. The diurnal patterns provide insight into the additional source: while tracers of vehicular emissions, NO_x and BC, decreased continuously from 18:00 hrs onwards, $HOA_{AMS,org}$ and HOA/NO_x ratio decreased from 18:00 hrs and then increased again from 20:00 hrs onwards, which coincides with residential heating emissions. Collectively, these aspects provide plausible reasons for the important quantitative differences in the $transport_{CHARON}$ and $HOA_{AMS,org}$ factor.

S9. Discrepancies in mass concentrations of the cooking factor from PTR_{CHARON} and AMS analysis

Similar to $HOA_{AMS,org}$ and $transport_{CHARON}$, the OA mass concentrations apportioned to COA exhibited some difference between the two instruments ($COA_{AMS,org}$ = **0.6 ± 0.8 µg/m³**; COA_{CHARON} = **0.1 ± 0.2 µg/m³**; **Figure 6**) with a temporal correlation (R^2) of 0.47 (**Table S4**). ~~and a steep slope of 0.13 (**Figure** ~~ Like HOA, these differences ~~were~~ are partly attributable to the particle size as greater ~~relative~~ contribution~~s~~ of cooking emissions to OA are for particles centered around ~~could be traced back to increased mass concentrations of much smaller particles of~~ ~100 nm (**Figure S12 plot A**)~~., which could be a potential reason for lower OA apportioned to this source in PTR_{CHARON} analyses~~. Another potential explanation ~~is~~ could be related to ~~also the~~an overestimation of COA with the AMS~~. In both AMS datasets~~, as standard RIE ~~was used for organics, i.e.~~ of 1.4 was used for organics;~~.~~ r~~R~~ecent studies have reported an overestimation of COA ~~with~~ by the AMS ~~analyses~~ compared to co-located instruments, such as the chemical ionisation mass spectrometer and SMPS, and suggested a ~~higher~~ RIE varying from ~~of~~ 1.5~~6~~ up to ~~–~~3.1~~06~~ (Reyes-Villegas et al., 2018) ~~or~~ and 4.3~~26~~ ~~–~~6.5~~0~~ (Katz et al., 2021). However, these studies focused on fresh indoor or laboratory-generated cooking emissions~~. , which may induce a different response factor in the AMS than ambient COA.~~ For instance, i~~COA has a high response factor in the AMS (Katz et al., 2021). I~~n our study, the COA factor presented low O/C of ~~<~~0.17, 0.11, and 0.09 with the PTR_{CHARON}, AMS_{org}, and $AMS_{org+inorg}$ respectively, indicating fresh emissions, which ~~could be~~ due to the proximity of CTC, UAF to restaurants and urban areas.

Supplementary figures

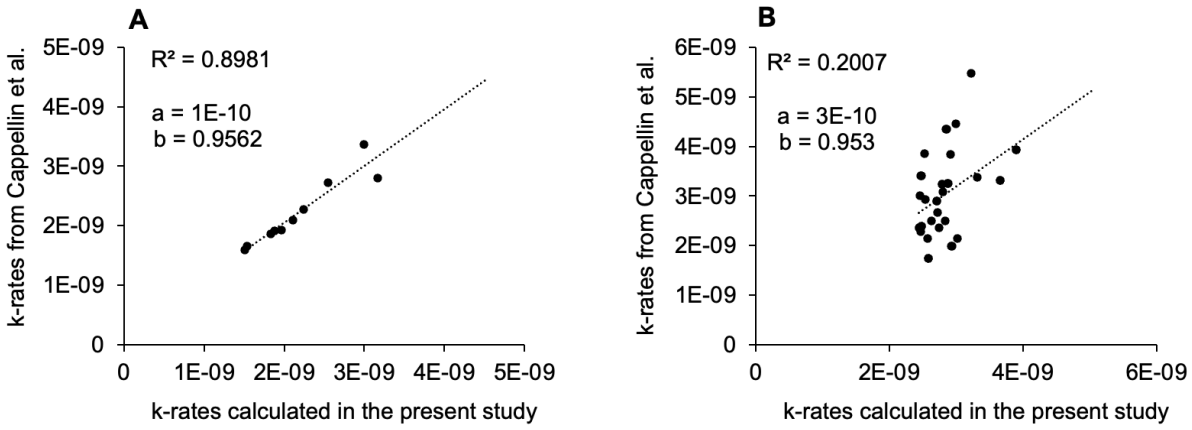

Figure S1. Assessing the agreement between protonation rate coefficients (*k*-rates) predicted in this study and those estimated by (Cappellin et al., 2012) for (**A**) hydrocarbons and (**B**) heteroatom-containing species.

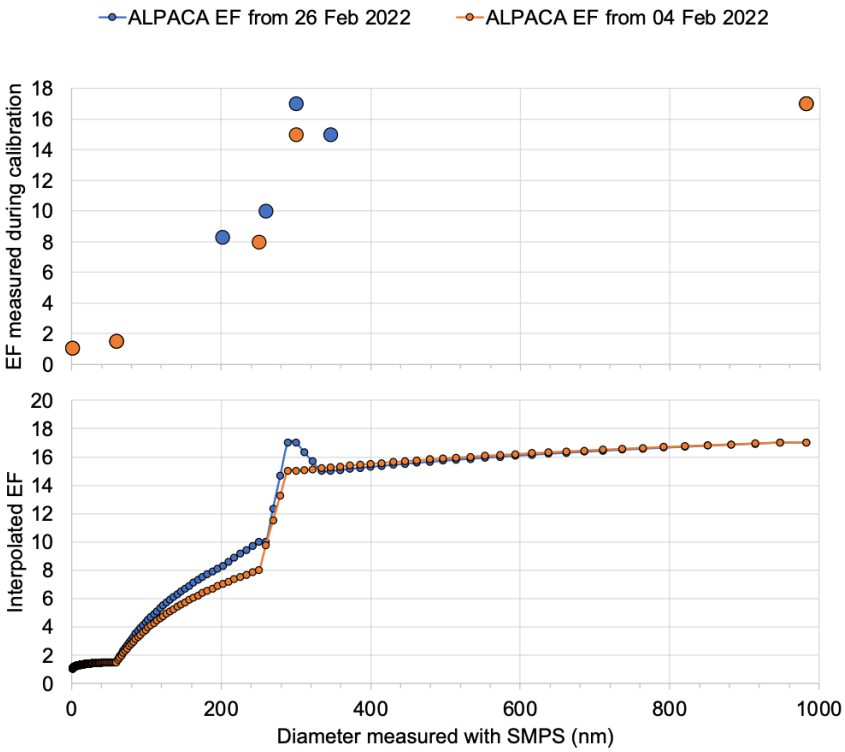

Figure S2. Overview of enrichment factors (EF) used in this study. (**A**) EF measured from calibrations with pure levoglucosan during the ALPACA campaign for particles of specific sizes; and (**B**) interpolation of EF across the complete range of particle sizes from 15–1000 nm.

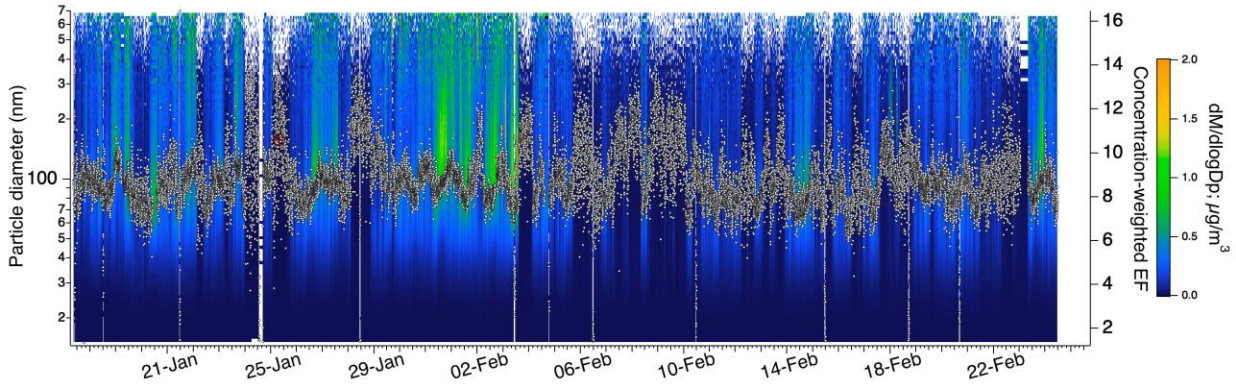

Figure S3. Particle size distribution from an SMPS. Gray data points represent the average enrichment factor (EF) weighted to these mass concentrations. This time series was generated using the calibration curve from Feb 26, 2022 (shown in Figure S2).

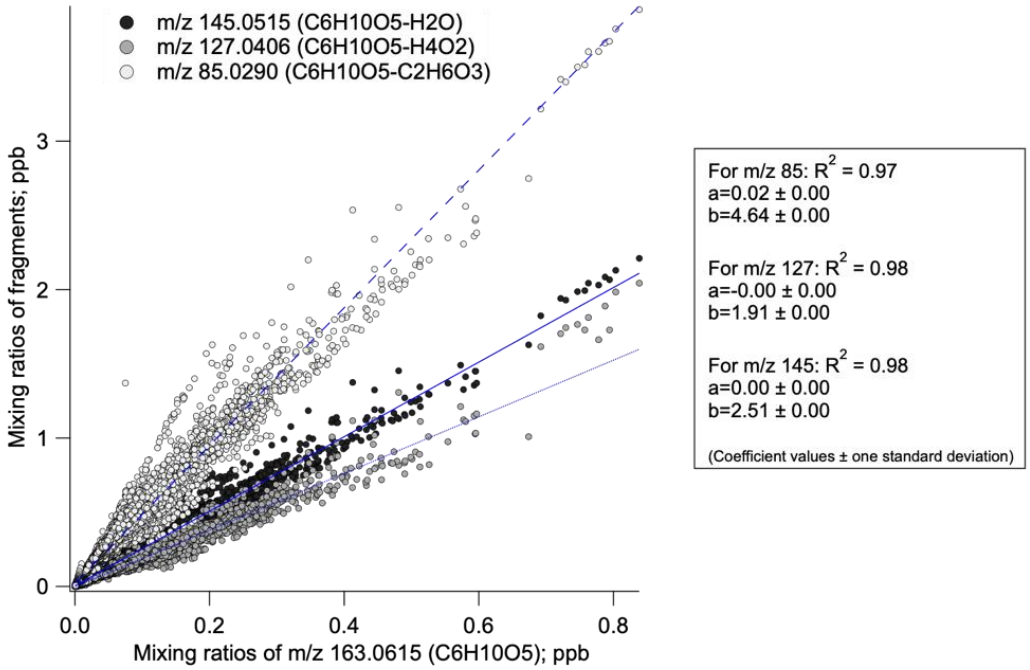

Figure S4. Scatter plot to show the correlation ($p \leq 0.05$) between the mixing ratios of levoglucosan (*m/z* 163) and its expected fragments at *m/z* 85, 127, and 145.

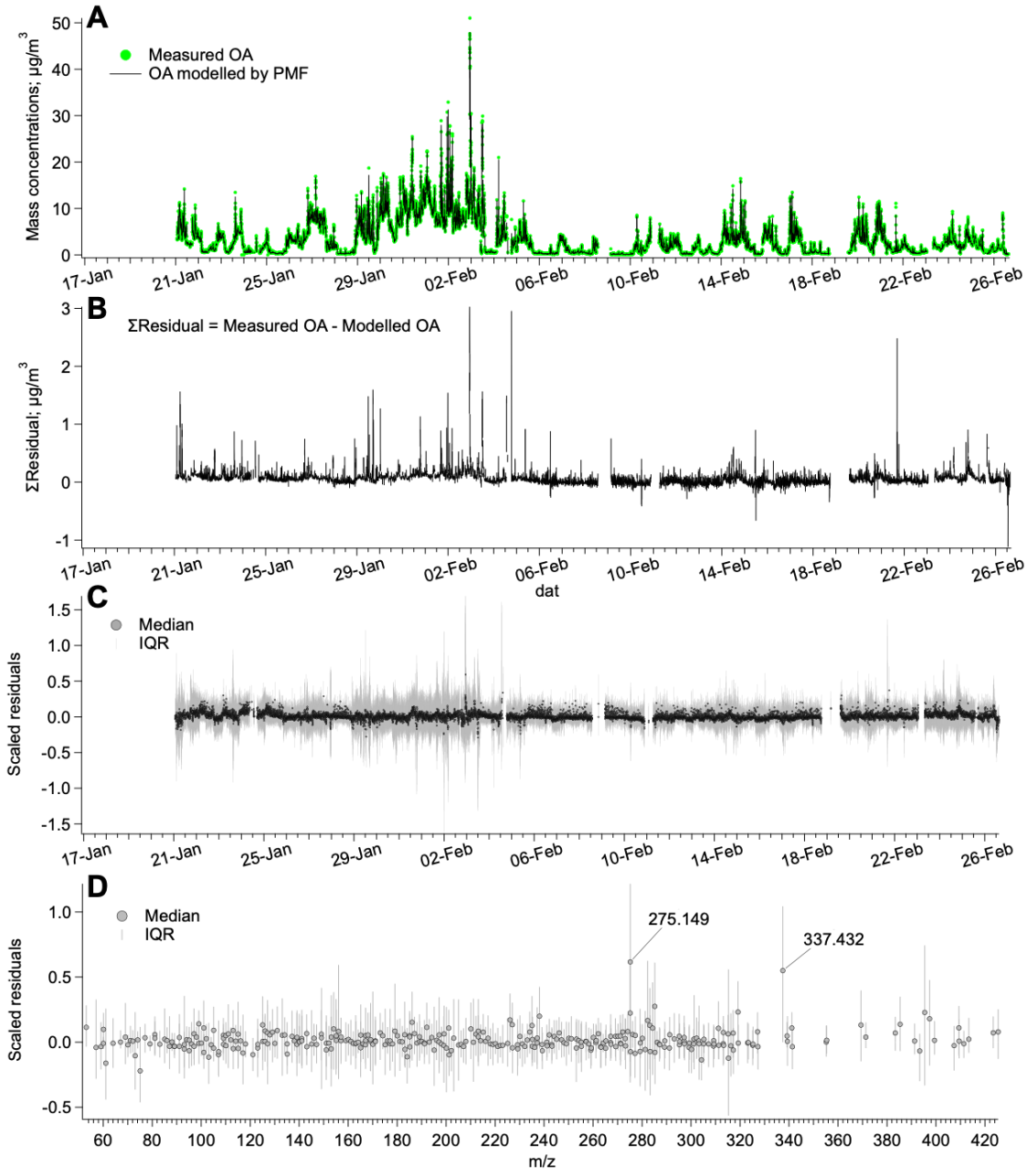

Figure S5. Diagnostics for the positive matrix factorisation of PTR_{CHARON} measurements. (**A**) Total measured OA and the sum of OA apportioned to all eight factors, i.e., the so-called *modelled* OA; (**B**) Sum of residuals; (**C**) Scaled residuals in the time series; and (**D**) Scaled residuals in the mass spectra. The median and interquartile range (IQR) of the scaled residuals for 75 runs (total runs = 125) selected after bootstrapping are shown. *Note: Scaled residuals indicate how well the PMF model fits the measurements and how much of the variability in the input data remains unexplained (Juntto and Paatero, 1994); it should ideally be ± 2.*

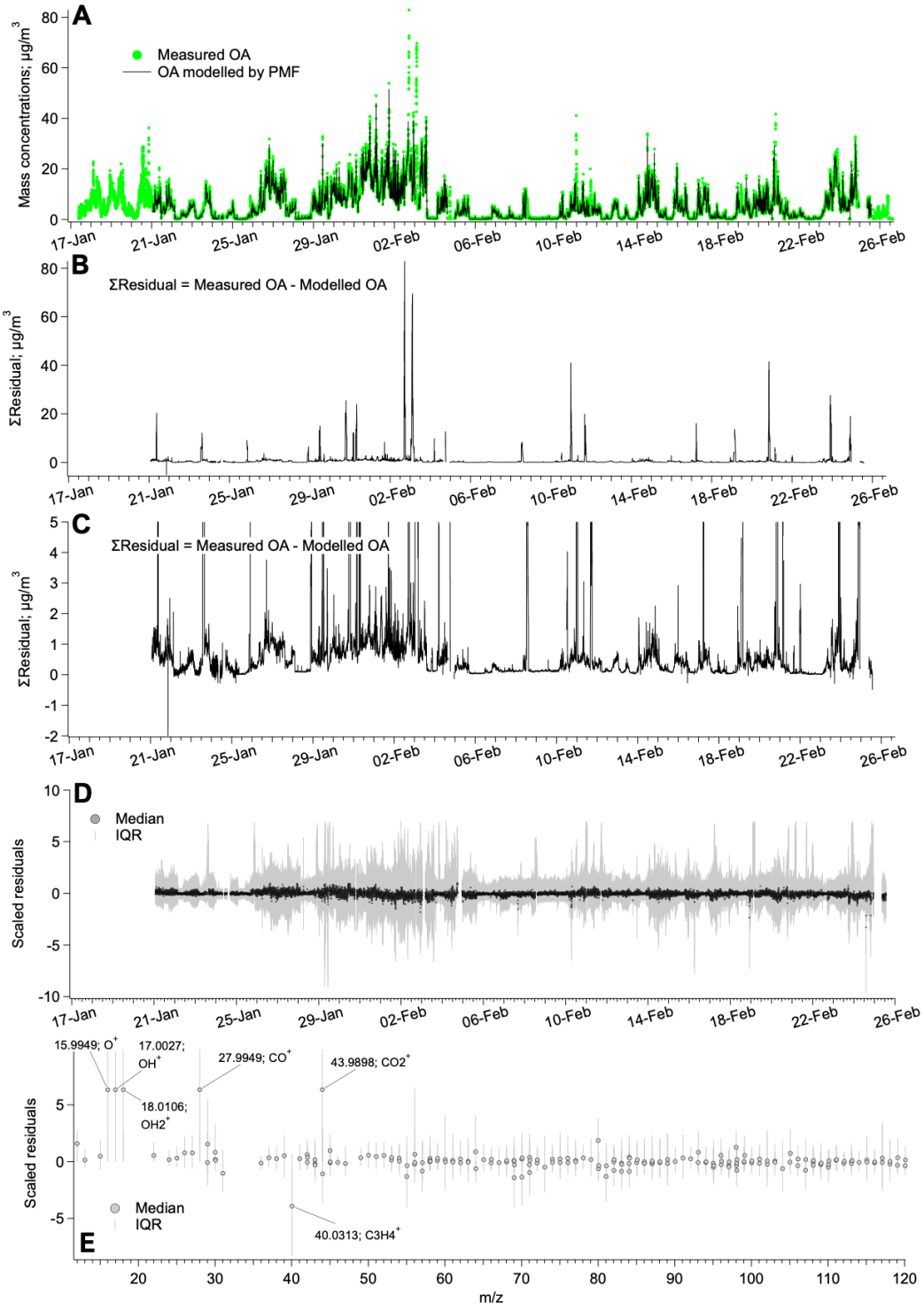

Figure S6. Diagnostics for the positive matrix factorisation of AMS_{org} measurements. (**A**) Total measured OA and the sum of OA apportioned to all four factors, i.e., the so-called *modelled* OA; (**B–C**) Sum of residuals, where C is zoomed-in at low concentrations; (**D**) Scaled residuals in the time series; and (**E**) Scaled residuals in the mass spectra. The median and interquartile range (IQR) of the scaled residuals for the 200 runs (total runs = 250) selected after bootstrapping are shown. *Note: Please see **Figure S5** for the definition of scaled residuals*

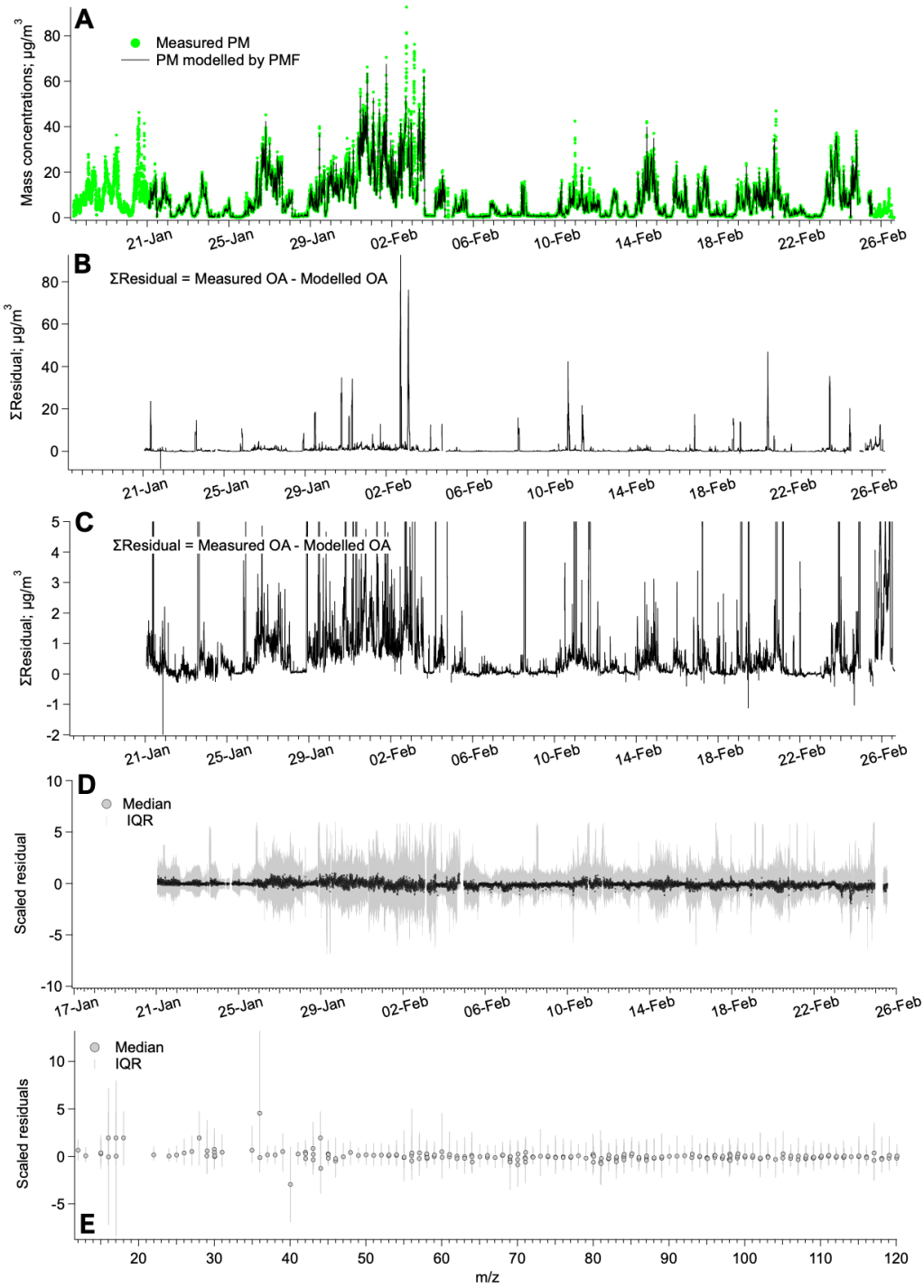

Figure S7. Diagnostics for the positive matrix factorisation of $AMS_{org+inorg}$ measurements. (**A**) Total measured NR-PM_1 and the sum of NR-PM_1 apportioned to all six factors, i.e., the so-called *modelled* NR-PM_1, (**B–C**) Sum of residuals, where (C) is zoomed-in at low concentrations, (D) Scaled residuals in the time series, and (E) Scaled residuals in the mass spectra. The median and interquartile range (IQR) of the scaled residuals for the 249 runs (total runs = 250) selected after bootstrapping are shown. *Note: Please see* ***Figure S5*** *for the definition of scaled residuals.*

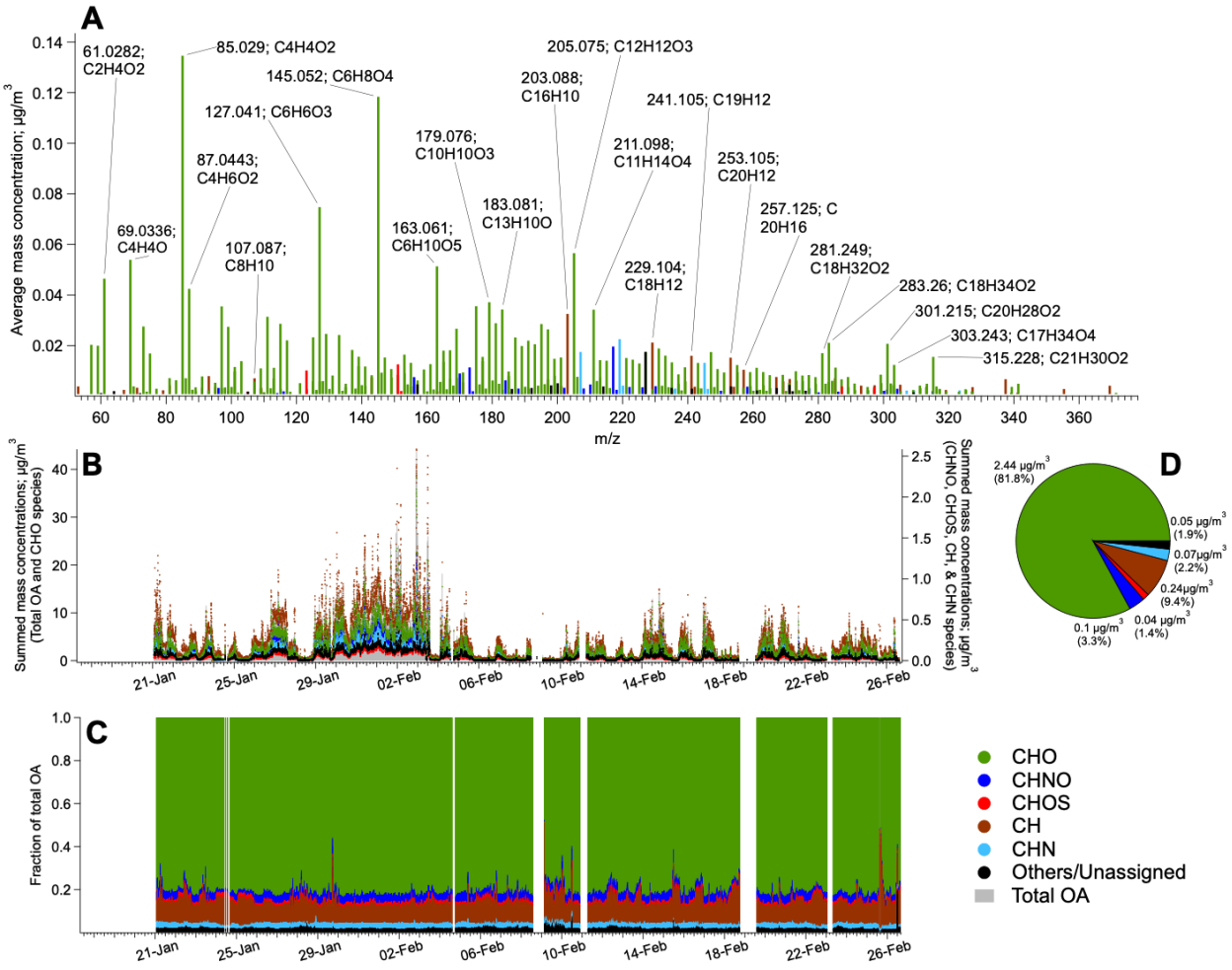

Figure S8. Molecular composition of ambient OA from PTR_{CHARON}. (**A**) Mass spectra of ion concentrations averaged over the campaign; (**B**) Time series of species belonging to the five molecular groups: CHO, CHNO, CHOS, CH, and CHN. Species that could not be assigned a formula are shown as the black; and (**C**) fractions of the aforementioned molecular groups in the total OA_{CHARON} mass.

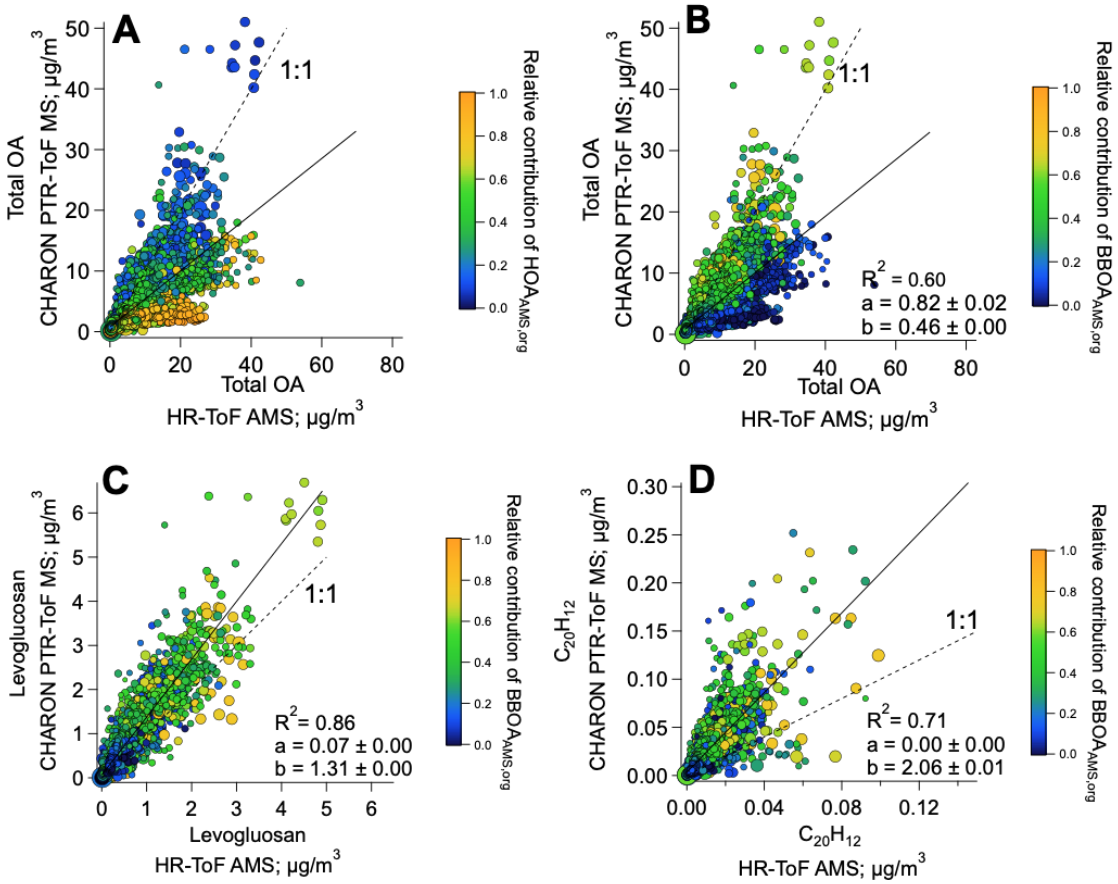

Figure S9. Scatter plots showing the linear regression ($p \leq 0.05$) of (**A**–**B**) total OA measured with the AMS and the PTR_{CHARON} coloured by the relative contribution of biomass burning OA and hydrocarbon-like OA factors diagnosed in AMS analysis, (**C**) levoglucosan and (**D**) $C_{20}H_{12}$ (assumed to be a PAH that was estimated using the method of (Herring et al., 2015)) measured with the AMS and PTR_{CHARON}. In (**C**) and (**D**) data points are coloured by the relative contributions of the BBOA factor diagnosed in AMS measurements. Data points are sized by the geometric mean mass of the dM/dlogDp calculated from the SMPS (50 to 500 nm). The dashed line denotes the 1:1 relationship. Coefficients, *a* and *b*, denote the slope and the intercept for the linear regression ($p \leq 0.05$; solid line) and are written with ± one standard deviation.

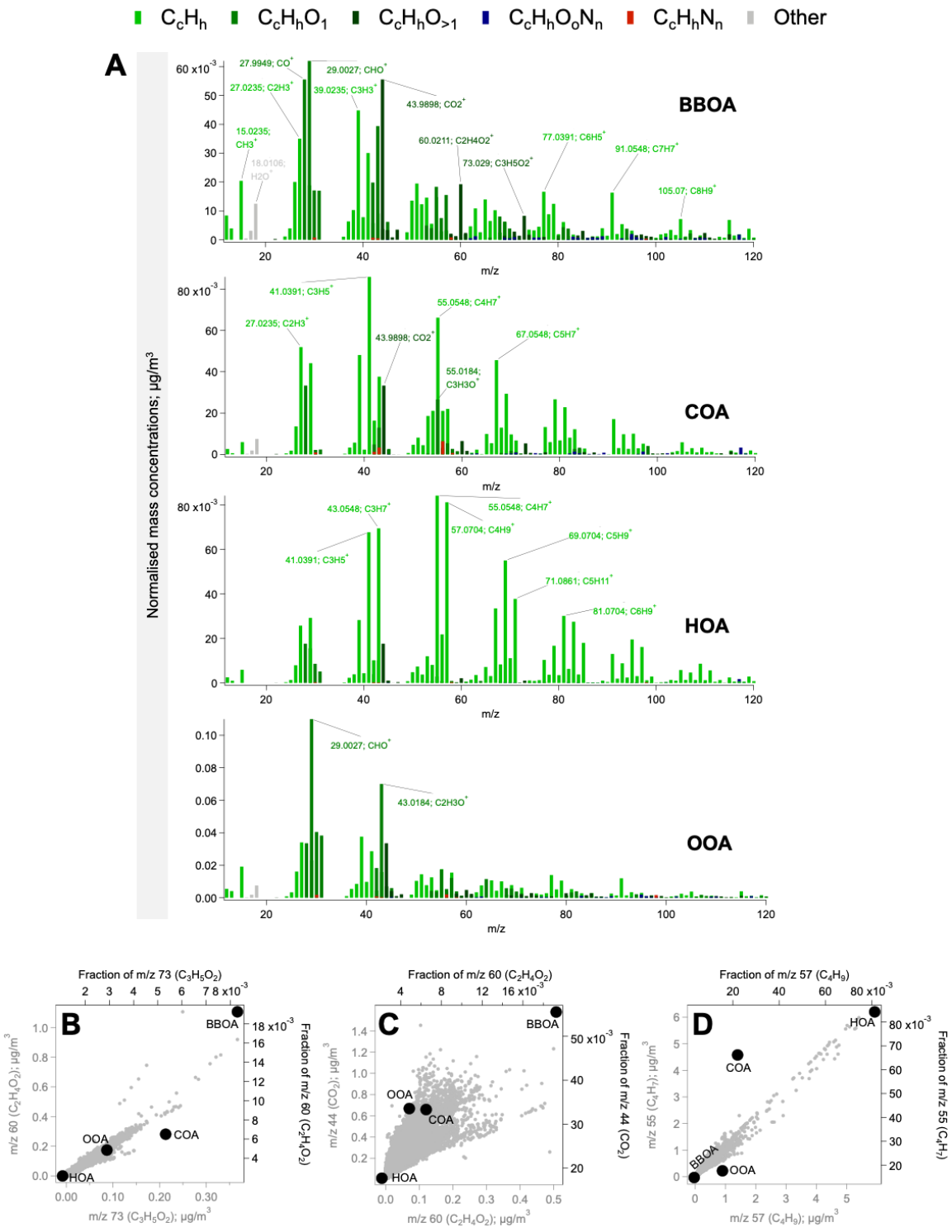

Figure S10. Overview of the factorisation output for AMS_{org} measurements. **(A)** Normalised mass spectra of factors coloured by the elemental composition of the fragments. Mass concentrations are normalised to the sum of the concentrations of all ions. Comparison of the absolute concentrations in ambient OA (grey data points; bottom and left axes) and fractional contribution in each factor (black data points; top and right axes) of (**B**) *m/z* 60 versus *m/z* 73; (**C**) *m/z* 44 versus *m/z* 60; and (**D**) *m/z* 55 versus *m/z* 57.

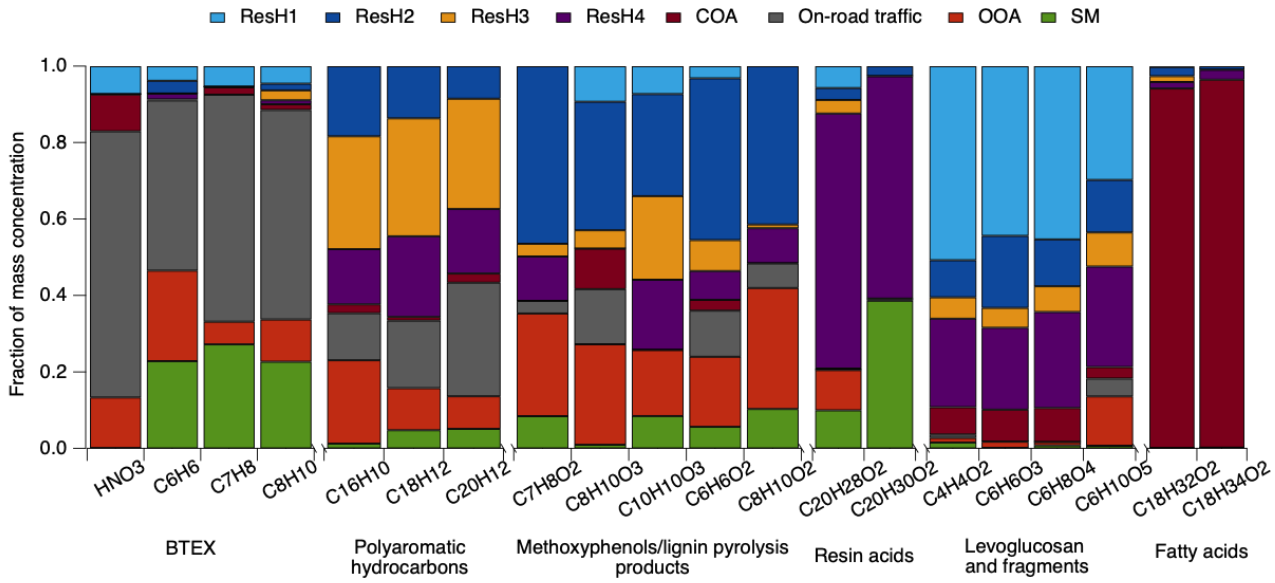

Figure S11. Fraction distribution of key markers species in the eight factors diagnosed for OA measured with the PTR_{CHARON}.

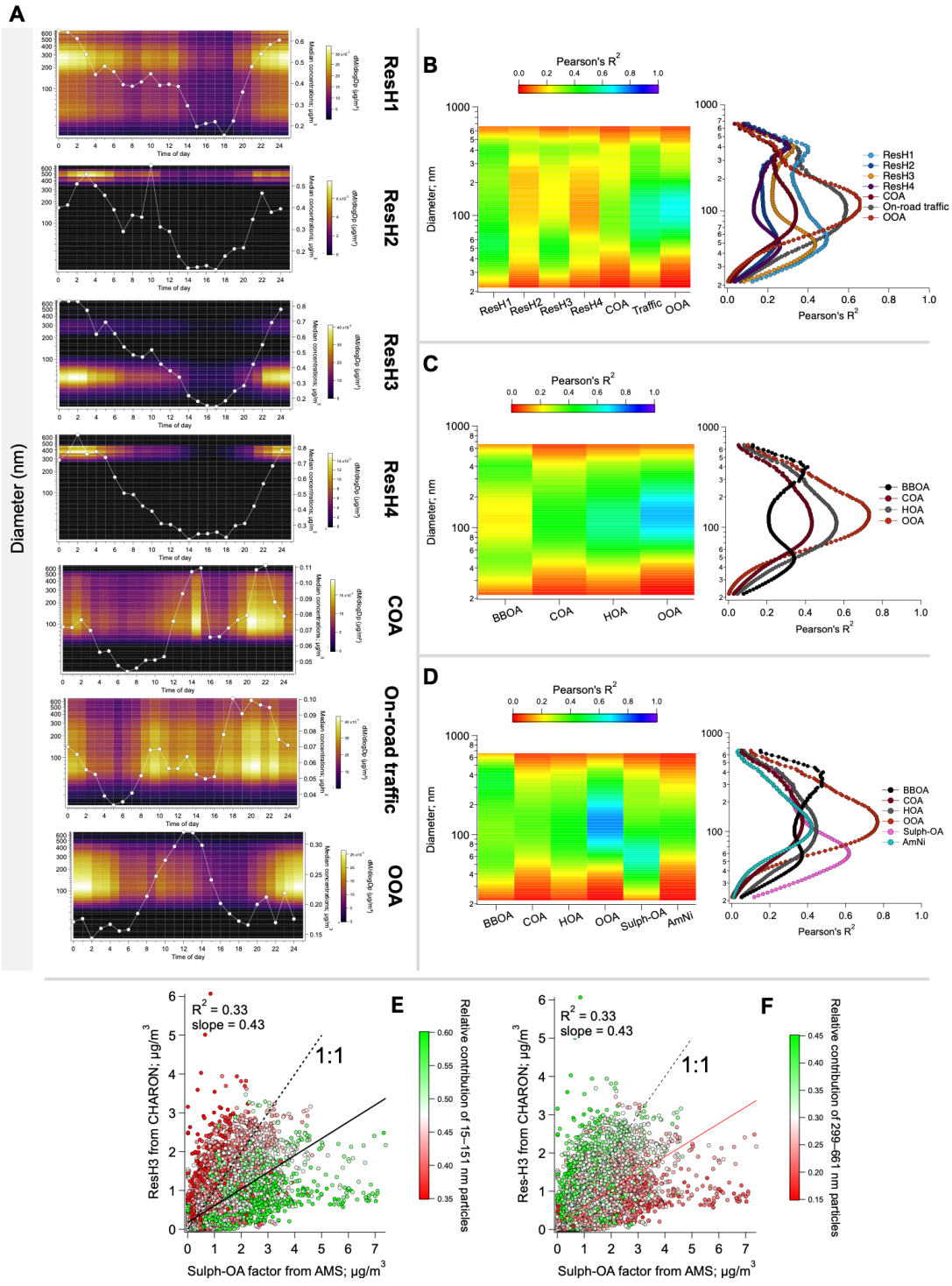

Figure S12. Particle mass size distributions from SMPS for all factors identified in this study. (**A**) Diurnal trends for PTR_{CHARON} factors and their corresponding particle sizes; (**B-D**) Linear regression ($p < 0.05$) over time between the particle size bins and factors in PTR_{CHARON}, AMS_{org}, and $AMS_{org+inorg}$ analysis, respectively. Please see **Section S7** for the methodology of SMPS analysis; (**E-F**) scatter plot of sulph-OA and ResH3 factor from PTR_{CHARON} analysis coloured by the relative contributions of smaller (15–151 nm) and larger (299–661 nm) aerosol particles.

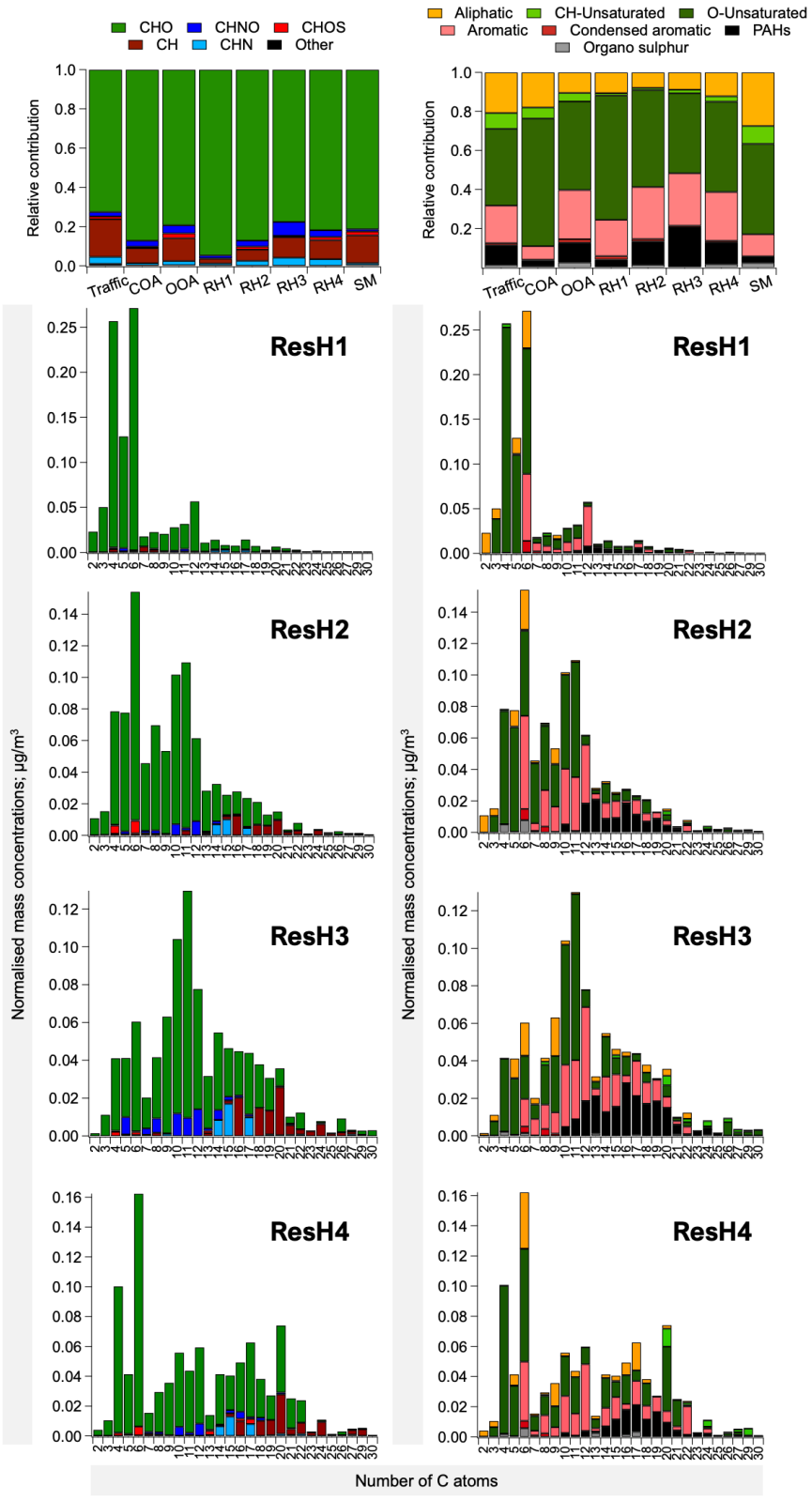

Figure S13. Overview of the distributions of chemical composition and estimated aromaticity of the residential heating factors as a function of the number of C atoms in the species identified and signal contributed by them to each of the factors.

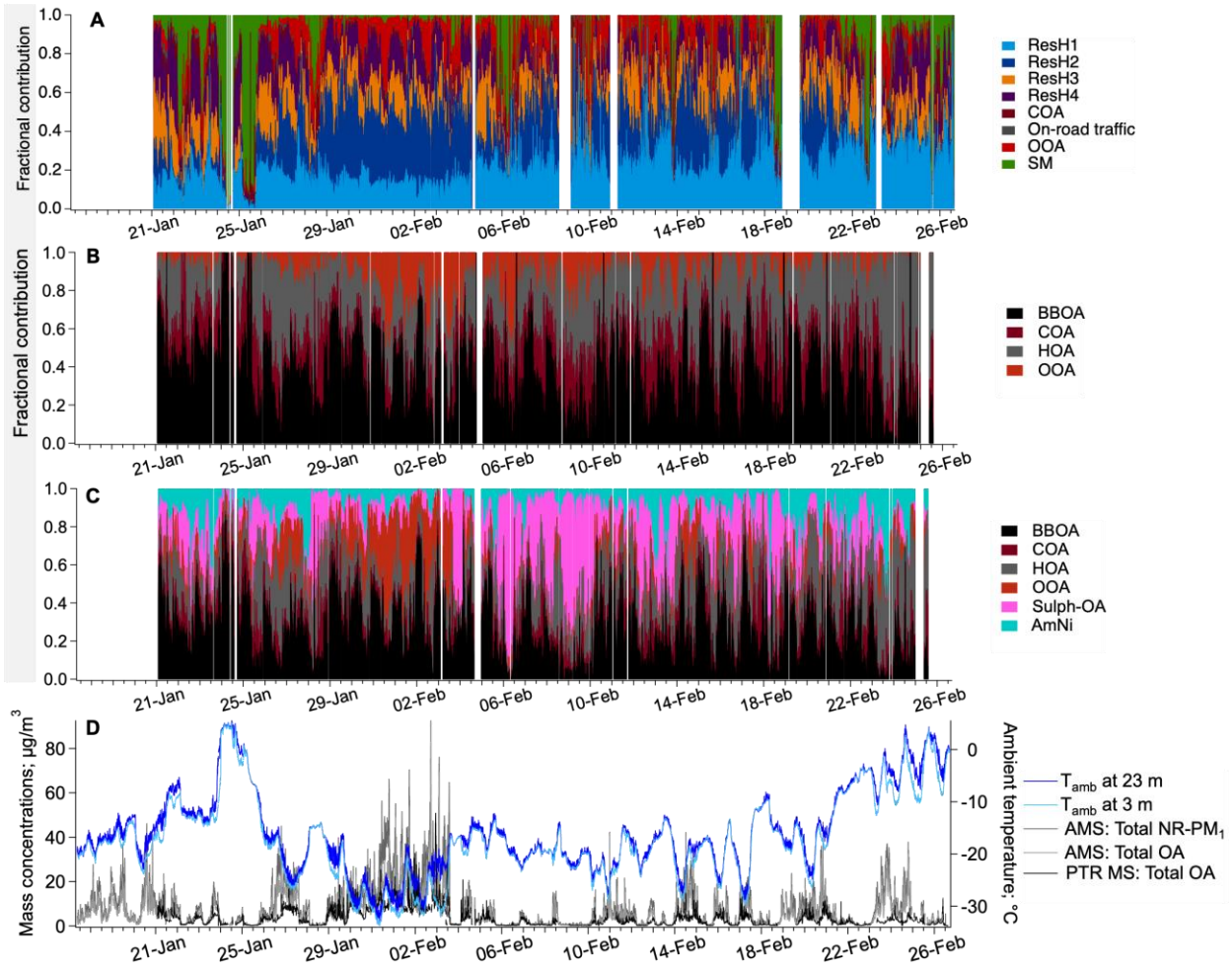

Figure S14. Fractional contributions of the factors identified for the different datasets. (**A**) OA with the PTR_{CHARON}; (**B**) OA with the AMS; and (**C**) NR-PM_1 with the AMS. Corresponding campaign-averages are given in **Figure 6**; (**D**) Ambient air temperature and absolute mass concentrations of NR-PM_1 and OA to indicate periods of relatively more importance due to high aerosol loads.

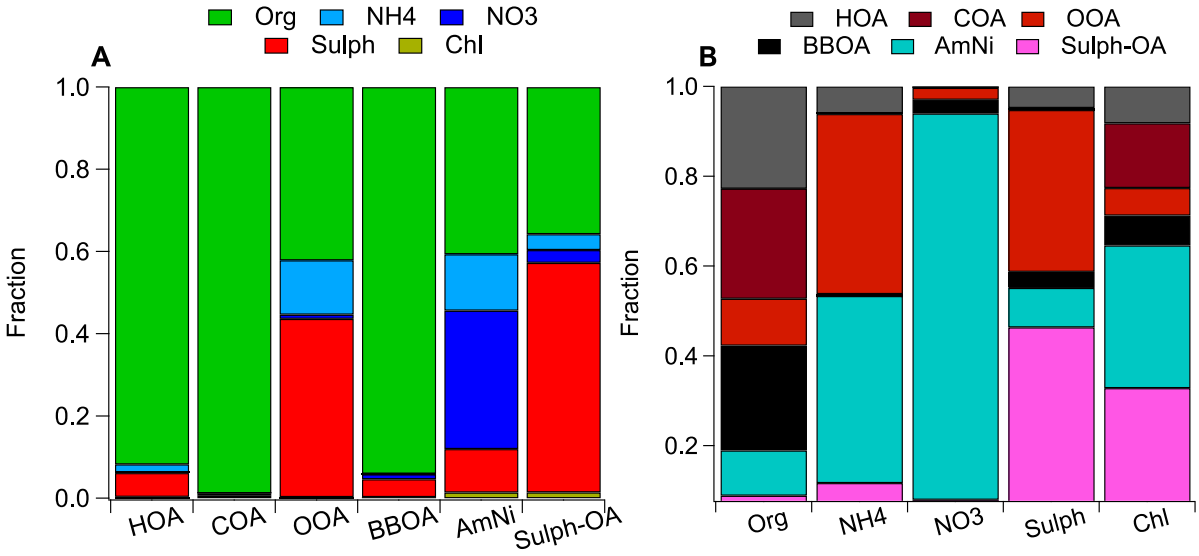

Figure S15. Distribution of organic and inorganic constituents across the six factors identified in $AMS_{org+inorg}$ analysis.

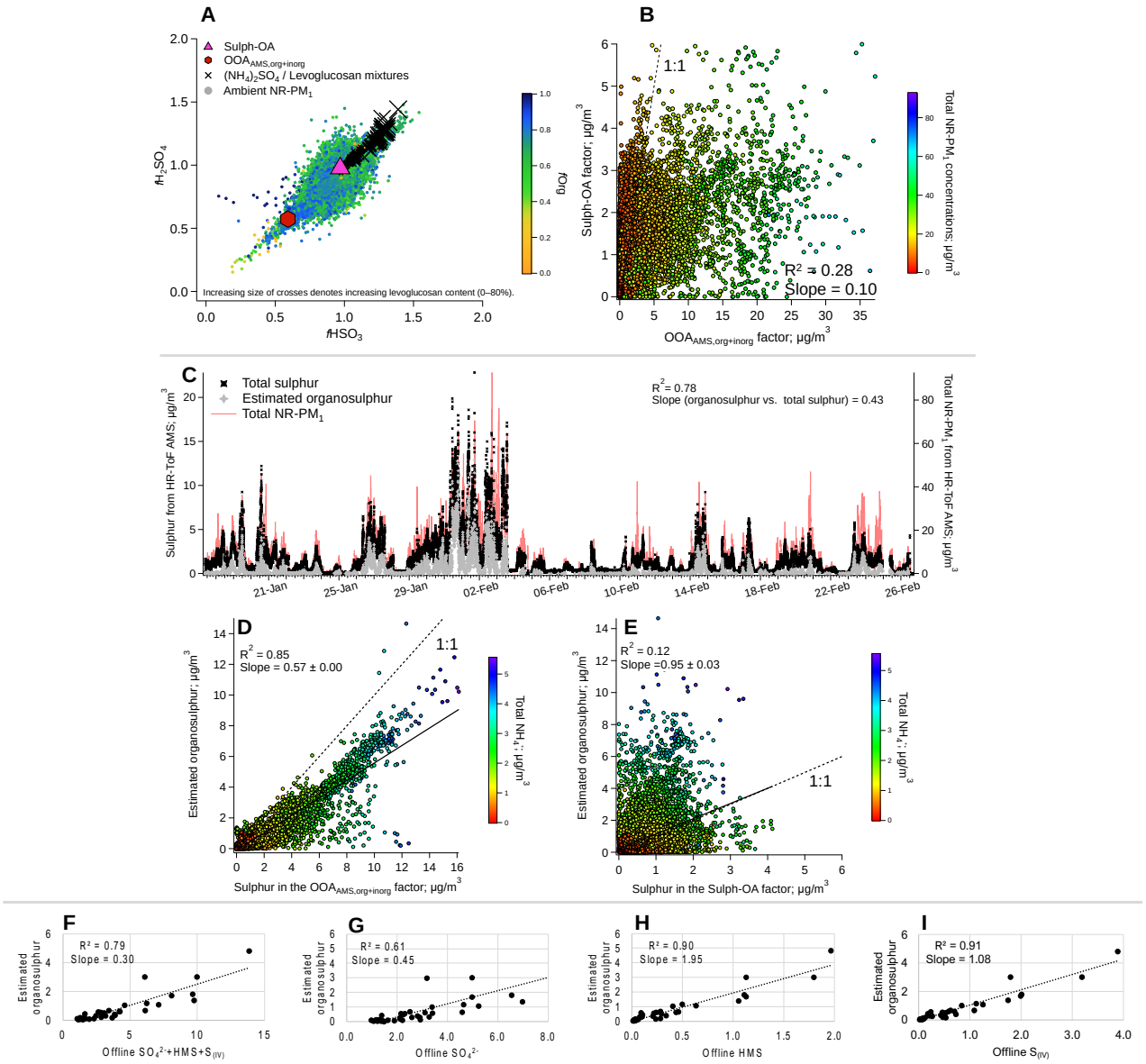

Figure S16. Differentiating between the two sulphur-rich factors in this study, i.e., $OOA_{AMS,org+inorg}$ and sulph-OA. (**A**) Scatter plot of normalised fractions of HSO_3^+ to $H_2SO_4^+$ fragments for the ambient aerosol, $OOA_{AMS,org+inorg}$, sulph-OA, and standard mixtures of pure ammonium sulphate with 0–80% by mass of levoglucosan (inspired by (Chen et al., 2019)); (**B**) scatter plot of the absolute concentrations of $OOA_{AMS,org+inorg}$ and sulph-OA coloured by total NR-PM_1 concentrations; (**C**) Times series of estimated concentrations of organosulphur using the method of (Song et al., 2019), along with total sulphur and NR-PM_1 from the AMS; (**D–E**) scatter plot showing linear regression ($p < 0.05$) between estimated organosulphur and factors, $OOA_{AMS,org+inorg}$ and sulph-OA. Data points are coloured by total NH_4^+ measured with the AMS; and (**F–I**) Scatter plots showing the correlation (R^2; $p \leq 0.05$) between estimated organosulphur from the AMS and offline ion chromatography of sulphur-containing chemical species in $PM_{0.7}$ collected on filters as part of a separate study (Dingilian et al., 2024).

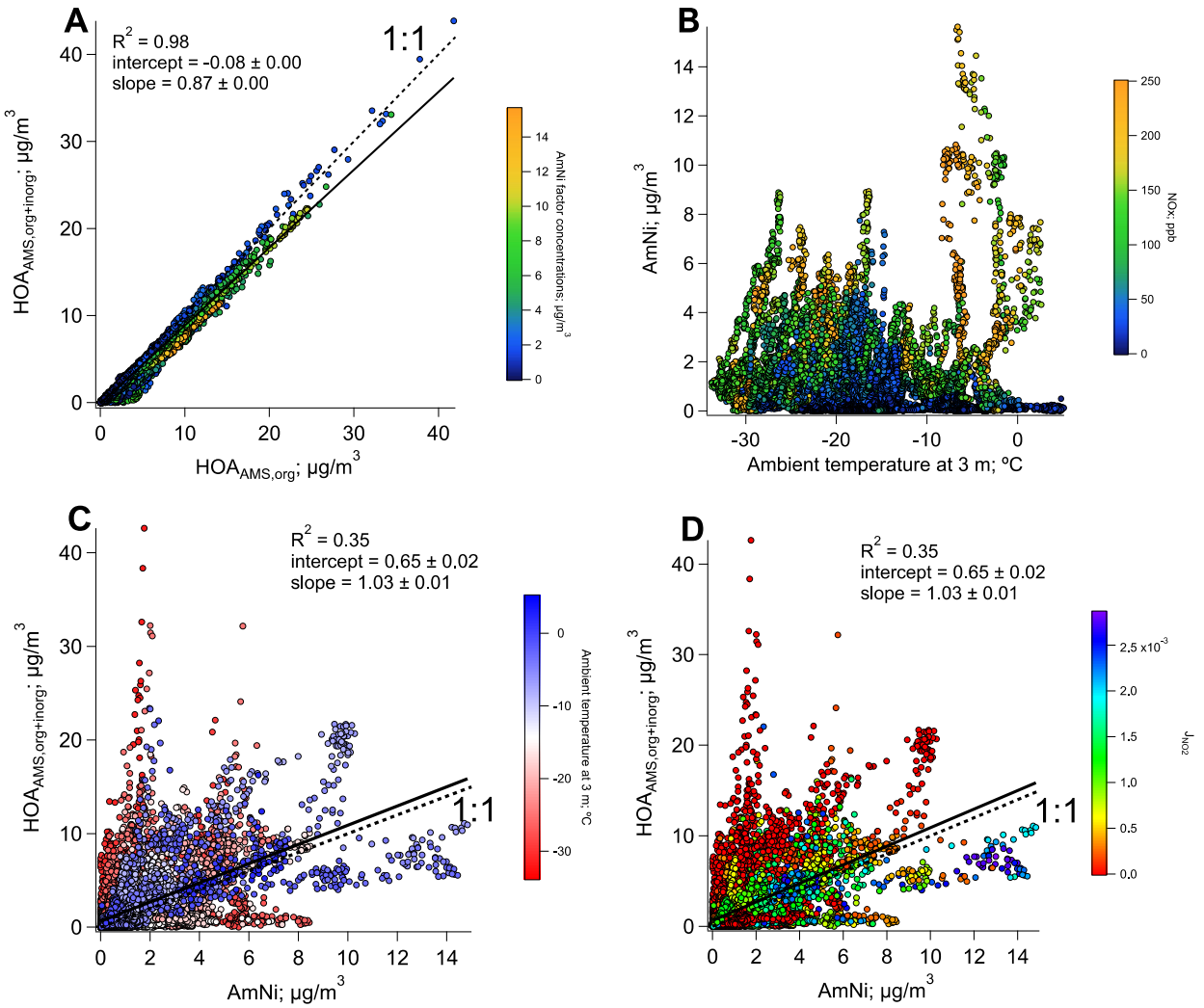

Figure S17. Possible origin and trends of distribution of the AmNi factor during the campaign. (**A**) A scatter plot of the hydrocarbon-like OA (HOA) factor with and without organics shows two "arms" of data points. Data points with higher-than-expected concentrations of the $HOA_{AMS,org}$ coincide with higher AmNi concentrations; (**B**) Distribution of AmNi factor as a function of temperature. Highest concentrations are recorded at > -10ºC and coincide with high NO_x concentrations; (**C–D**) Scatter plot of $HOA_{AMS,org+inorg}$ with AmNi shows comparable concentrations at temperatures above > 10ºC and non-zero J_{NO2} values > 0.5×10^{-3} indicating some sunlight.

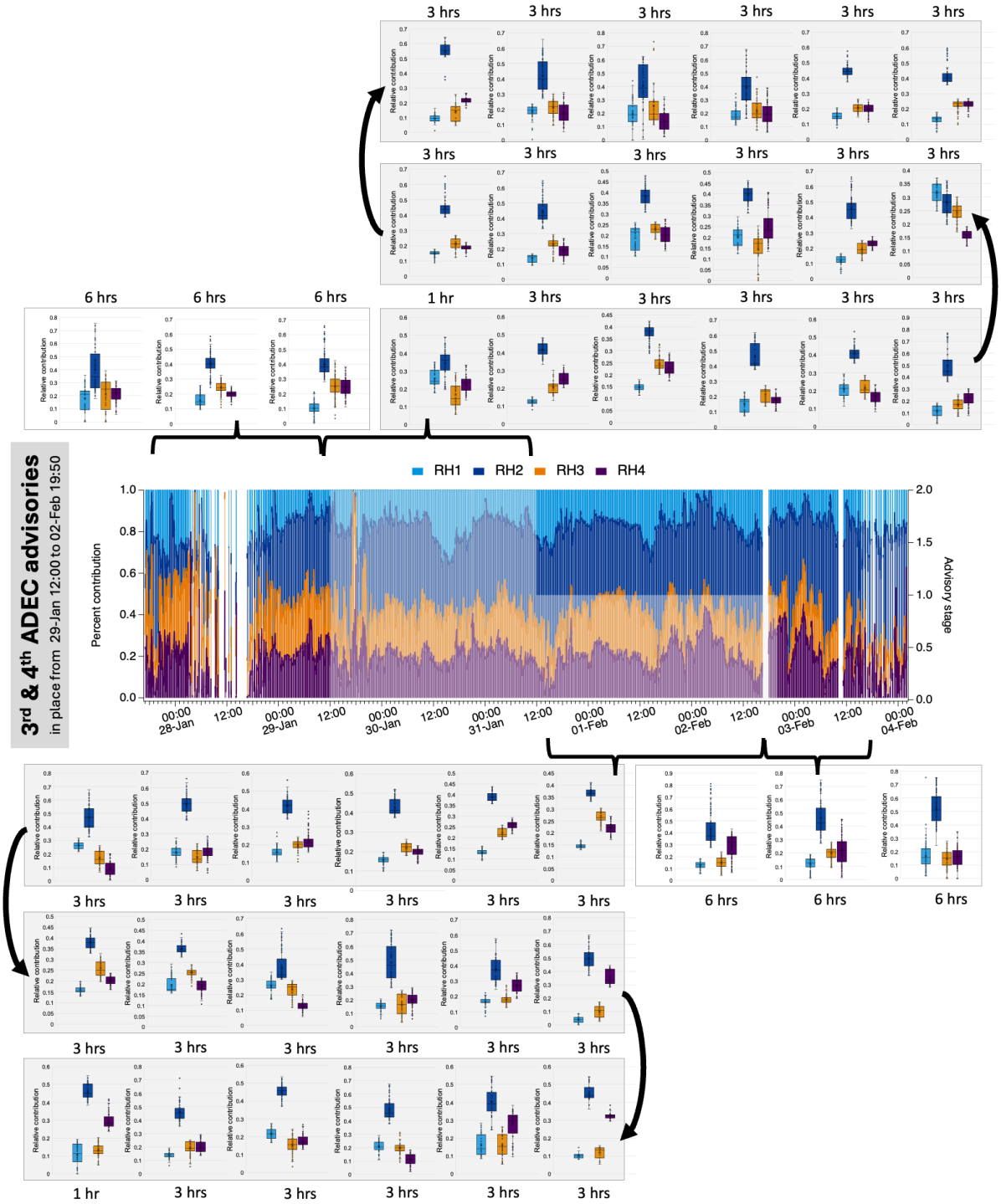

Figure S18. Variation in the relative contributions of residential heating factors to biomass-burning OA concentrations during the 3rd and 4th ADEC advisories. Contributions are also shown for approximately a day before and after the advisory for comparison, along with 6-hour averages as box plots (white panels),

when suitable data was available (e.g., periods with noisy data were omitted and the adjacent period is shown instead). For better visualisation of variation in contributions, when the advisory was in place, 3-hour averages are shown (grey panels). To account for a lag in the appearance of variations in emission sources, 1-hour averages are shown for the beginning and end of the advisory event. ~~Total OA < 1 μg/m^3 causes noisy relative contributions, and thus, has been omitted from the surrounding box plots.~~

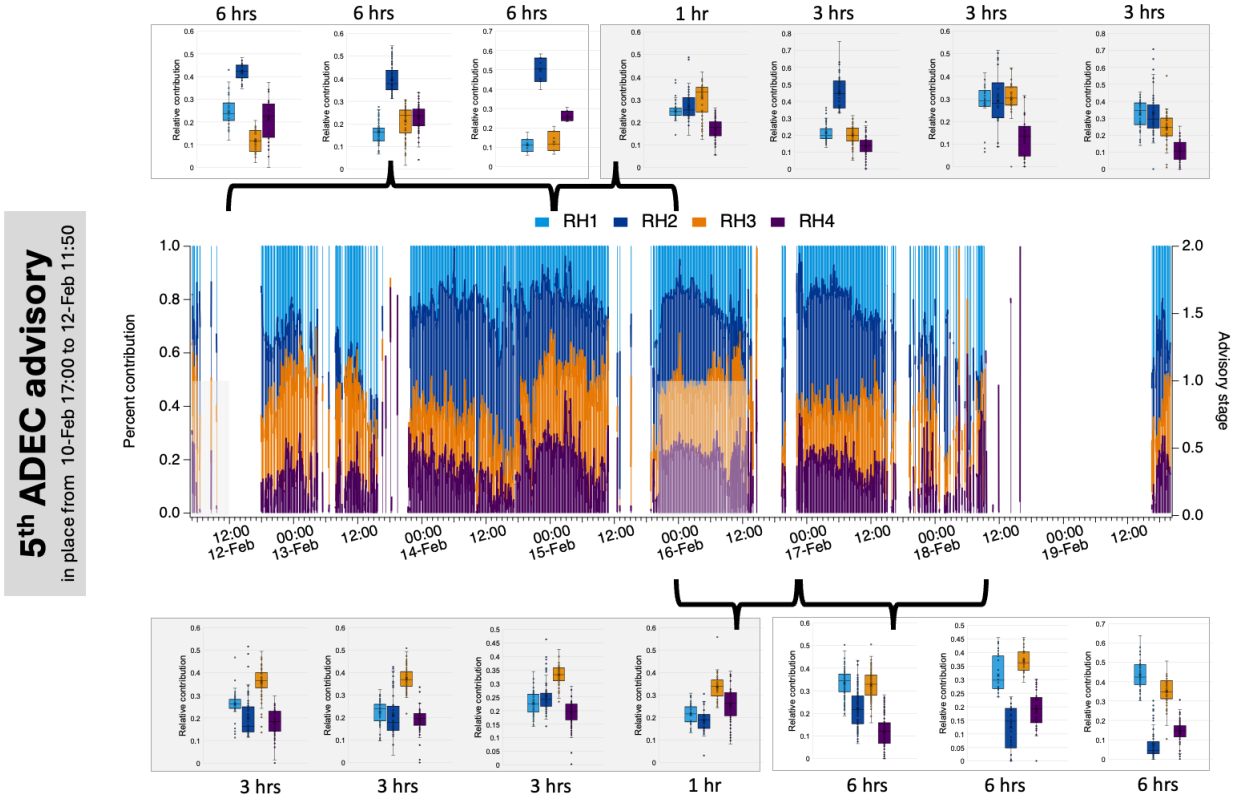

Figure S19. Variation in the relative contributions of residential heating factors to biomass-burning OA concentrations during the 5th ADEC advisory. Contributions are also shown for approximately 2 days before and after the advisory for comparison, along with 6-hour averages as box plots (white panels), when suitable data was available (e.g., periods with noisy data were omitted and the adjacent period is shown instead). For better visualisation of variation in contributions, when the advisory was in place, 3-hour averages are shown (grey panels). To account for a lag in the appearance of variations in emission sources, 1-hour averages are shown for the beginning and end of the advisory event. ~~Total OA < 1 μg/m^3 causes noisy relative contribution, and thus, has been omitted from the surrounding box plots.~~

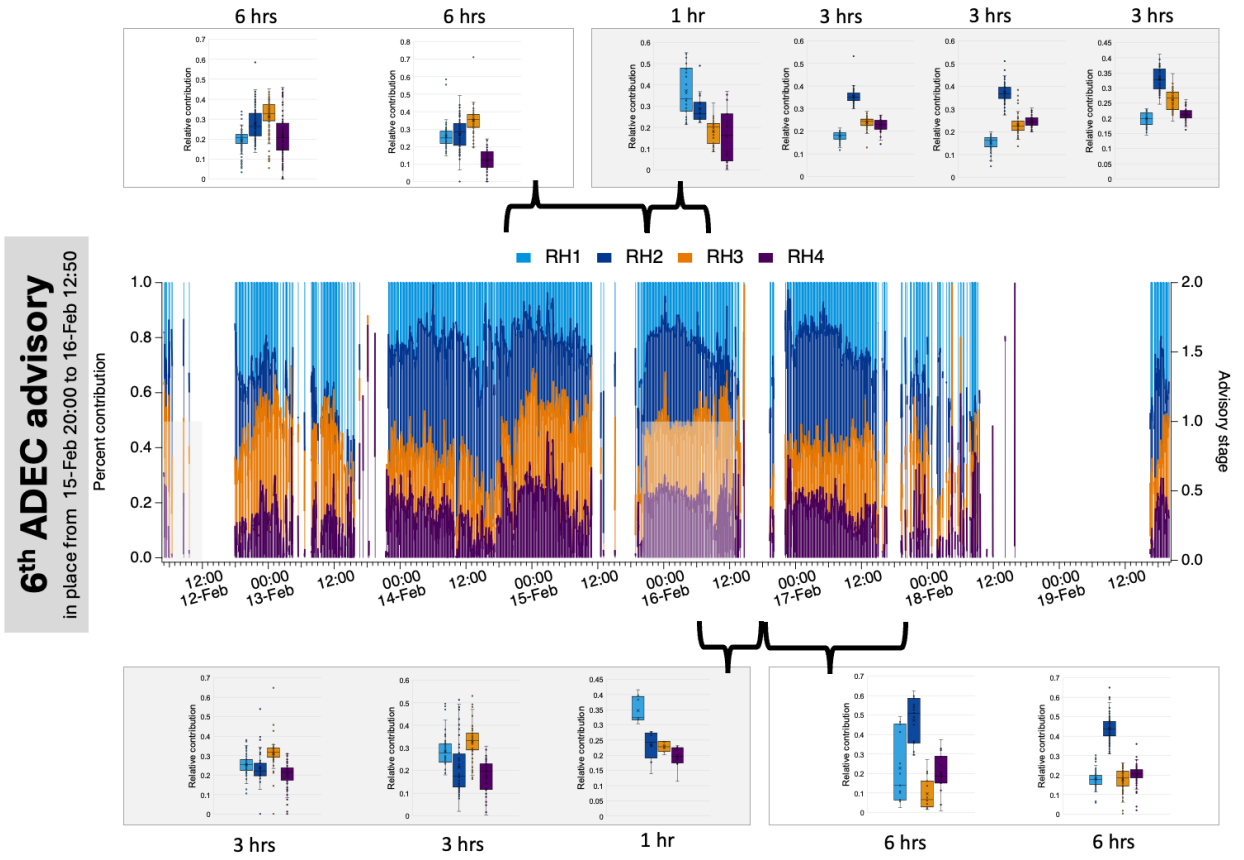

Figure S20. Variation in the relative contributions of residential heating factors to biomass-burning OA concentrations during the 6th ADEC advisory. Contributions are also shown for approximately 2 days before and after the advisory for comparison, along with 6-hour averages as box plots (white panels), when suitable data was available (e.g., periods with noisy data were omitted and the adjacent period is shown instead). For better visualisation of variation in contributions, when the advisory was in place, 3-hour averages are shown (grey panels). To account for a lag in the appearance of variations in emission sources, 1-hour averages are shown for the beginning and end of the advisory event. ~~Total OA < 1 μg/m^3 causes noisy relative contributions, and thus, has been omitted from the surrounding box plots.~~

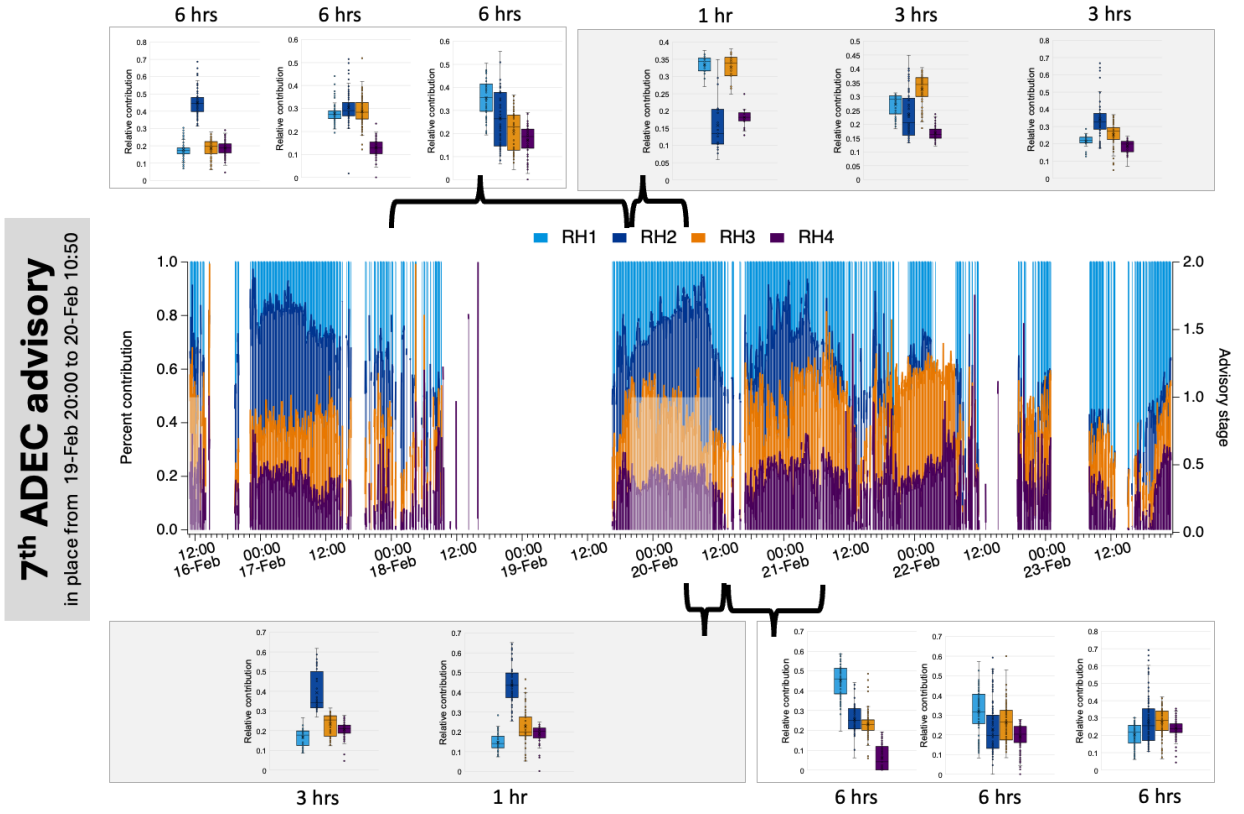

Figure S21. Variation in the relative contributions of residential heating factors to biomass-burning OA concentrations during the 7th ADEC advisory. Contributions are also shown for approximately 2 days before and after the advisory for comparison, along with 6-hour averages as box plots (white panels), when suitable data was available (e.g., periods with noisy data were omitted and the adjacent period is shown instead). For better visualisation of variation in contributions, when the advisory was in place, 3-hour averages are shown (grey panels). To account for a lag in the appearance of variations in emission sources, 1-hour averages are shown for the beginning and end of the advisory event. ~~Total OA < 1 μg/m^3 causes noisy relative contributions, and thus, has been omitted from the surrounding box plots.~~

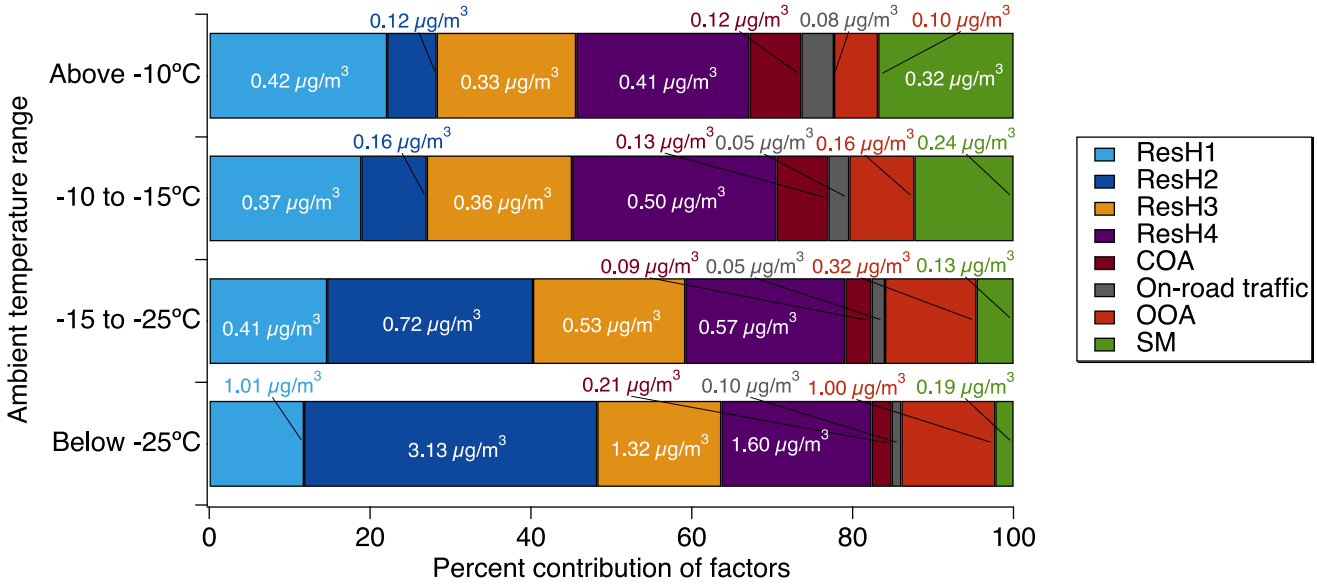

Figure S22. Variation in the absolute mass concentrations and relative contributions of the PTR_{CHARON} factors with temperature.

Supplementary tables

Table S1 Composition of the calibration gas mixture and the experimental sensitivity obtained in the field.

Compound	***m/z***	***k*-rate (10^{-9} cm^3/sec)**	**Sensitivity$_{start}$ (ncps/ppb)**	**Sensitivity$_{end}$ (ncps/ppb)**
Methanol	33.033	2.36	77	72
Acetonitrile	42.033	4.45	211	194
Acetaldehyde	45.033	3.40	289	207
Acetone	59.049	3.58	317	286
Isoprene	69.069	1.96	151	134
Benzene	79.054	1.93	196	173
Toluene	93.069	2.09	279	247
m-Xylene	107.087	2.27	366	324
1,3,5 Trimethylbenzene	121.101	2.4	462	405
1,2,4,5 Tetramethylbenzene	135.116	2.5	600	521

Table S2 A summary of factors observed in all runs of the constrained analyses to justify the selection of the base-cases (green highlight), other than the environmental explainability of source apportionment (e.g., Q/Q_{exp}, residuals, etc.)

Number of factors	**PTR$_{CHARON}$**	**AMS$_{org}$**	**AMS$_{org+inorg}$**
3	No COA or OOA observed, unless constrained	COA not observed, unless it was constrained	COA not observed, unless it was constrained
4	COA observed without constraining; OOA mixed with ResH	**Distinct HOA, COA, OOA, BBOA, even without constraining**	BBOA and OOA factors mixed; COA and HOA mixed
5	Additional distinct ResH; OOA mixed with ResH	HOA split into two very similar factors	COA and HOA mixed
6	OOA was separated but the 3 ResH factors presented some mixing based on inter-factor and with-tracer temporal correlations	HOA split into very similar factors; additional factors with no reasonable physical explanation	**Distinct AmNi, sulph-OA, HOA, COA, OOA, and BBOA factors even without constraining**
7	The SM factor appeared; 3 distinct Res-H factors and one that was mixed with OOA	Factor splitting; additional factor with no reasonable physical explanation	An additional sulphur-rich factor with no reasonable physical explanation
8	**Distinct OOA, COA; 4 distinct ResH factors; no evidence of mixing among the factors**	Factor splitting; additional factor with no physical explanation	Factor splitting; additional factor with no physical explanation
9	An additional factor that was a mix of OOA and ResH	Factor splitting; additional factor with no physical explanation	Factor splitting; additional factor with no physical explanation
10	Evidence of factor splitting along with a factor with OOA and ResH mixed	Factor splitting; additional factor with no physical explanation	Factor splitting; additional factor with no physical explanation

Table S3 Evaluation criteria for the selection of reasonable runs after bootstrapping. Each evaluation criterion is applied by SoFi to extract the factors (in all runs) that satisfy it(Datalystica, 2022). Those factors are then not considered for any other evaluation criteria. Therefore, the sequence in which the different criteria are evaluated in SoFi is critical to avoid mixing and association with the wrong criteria, especially in cases where the same criteria could apply to multiple factors. The position of each criterion in our analyses is given in brackets.

Factor (number of bootstrapped runs, *n*)	**PTR_{CHARON} (*n* = 125)**	**AMS_{org} (*n* = 250)**	**$AMS_{org+inorg}$ (*n* = 250)**
ResH1/BBOA	No evaluation criteria applied	R^2 with *m/z* 60 ≥ 0.70 (**2nd**)	R^2 with *m/z* 60 ≥ 0.70 (**2nd**)
ResH2	R^2 with *m/z* 60.0831 (C_3H_9N; trimethylamine) ≥ 0.70 (**4th**)	--	--
ResH3	R^2 with SO_2 ≥ 0.60 (**6th**)	--	--
ResH4	R^2 with *m/z* 303.2428 ($C_{20}H_{30}O_2$; abietic acid) ≥ 0.80 (**3rd**)	--	--
COA	R^2 with *m/z* 281.2486 ($C_{18}H_{32}O_2$; linoleic acid) ≥ 0.80 (**0th**)	Ratio between the lunch peak (1400 hrs) to morning hours (i.e., average of 0600 and 0700 hrs) (**0th**)	Ratio between the lunch peak (1400 hrs) to morning hours (i.e., average of 0600 and 0700 hrs) (**0th**)
On-road traffic/HOA	R^2 with NO_x ≥ 0.65 (**1st**)	R^2 with NO_x ≥ 0.65 (**1st**)	R^2 with NO_x ≥ 0.65 (**1st**)
OOA	R^2 with *m/z* 97.0653 (C_6H_8O) ≥ 0.80 (**2nd**)	R^2 with NH_4 ≥ 0.75 (**3rd**)	R^2 with NH_4 ≥ 0.85 (**4th**)
SM	R^2 with *m/z* 59.0491 (C_3H_6O; acetone) ≥ 0.60 (**5th**)	--	--
Sulph-OA	--	--	No evaluation criteria applied
AmNi	--	--	R^2 with NO_3 ≥ 0.85 (**3rd**)

Table S4 Linear regression correlations (R^2; $p \leq 0.05$) among the time series of factors derived from different methods. (**A**) PTR_{CHARON} versus AMS_{org}, (B) PTR_{CHARON} versus $AMS_{org+inorg}$, and (C) AMS_{org} versus $AMS_{org+inorg}$. Slopes are given in brackets, for which columns and rows were treated as dependent and independent variables, respectively.

A

	Traffic	COA	OOA	ResH1	ResH2	ResH3	ResH4	SM
HOA	0.48 (0.02)	0.18 (0.02)	0.19 (0.09)	0.22 (0.07)	0.06 (0.15)	0.07 (0.05)	0.04 (0.06)	0.02 (0.01)
COA	0.27 (0.04)	0.47 (0.13)	0.24 (0.36)	0.17 (0.23)	0.06 (0.59)	0.06 (0.18)	0.05 (0.23)	0.03 (0.03)
OOA	0.33 (0.02)	0.17 (0.03)	0.74 (0.24)	0.26 (0.11)	0.23 (0.41)	0.14 (0.11)	0.09 (0.12)	0.09 (0.02)
BBOA	0.12 (0.01)	0.14 (0.03)	0.12 (0.11)	0.51 (0.17)	0.65 (0.76)	0.56 (0.24)	0.66 (0.35)	0.00 (0.00)

B

	Traffic	COA	OOA	ResH1	ResH2	ResH3	ResH4	SM
HOA	0.43 (0.02)	0.15 (0.02)	0.12 (0.08)	0.18 (0.07)	0.05 (0.14)	0.06 (0.05)	0.04 (0.06)	0.01 (0.01)
COA	0.22 (0.04)	0.43 (0.14)	0.23 (0.40)	0.14 (0.24)	0.08 (0.73)	0.05 (0.19)	0.06 (0.27)	0.03 (0.03)
OOA	0.36 (0.01)	0.17 (0.02)	0.68 (0.12)	0.25 (0.06)	0.18 (0.19)	0.13 (0.05)	0.08 (0.05)	0.09 (0.01)
BBOA	0.18 (0.01)	0.15 (0.03)	0.26 (0.14)	0.53 (0.15)	0.72 (0.70)	0.52 (0.20)	0.62 (0.30)	0.02 (0.01)
AmNi	0.26 (0.02)	0.13 (0.03)	0.17 (0.15)	0.11 (0.10)	0.00 (0.05)	0.01 (0.04)	0.00 (0.00)	0.02 (0.01)
Sulph-OA	0.22 (0.04)	0.11 (0.06)	0.31 (0.41)	0.28 (0.30)	0.16 (0.82)	0.33 (0.43)	0.14 (0.38)	0.00 (0.01)

C

	HOA	COA	OOA	BBOA
HOA	0.98 (1.09)	0.18 (0.13)	0.13 (0.30)	0.08 (0.21)
COA	0.17 (1.54)	0.97 (1.11)	0.25 (1.54)	0.15 (1.03)
OOA	0.26 (0.37)	0.20 (0.09)	0.95 (0.51)	0.11 (0.16)
BBOA	0.12 (0.43)	0.18 (0.16)	0.32 (0.53)	0.92 (0.84)
AmNi	0.45 (1.25)	0.24 (0.25)	0.14 (0.49)	0.03 (0.21)
Sulph-OA	0.14 (1.34)	0.11 (0.32)	0.27 (1.28)	0.21 (1.04)

Very strong	≥0.75
Strong	≥0.5 and <0.75
Moderate	≥0.3 and <0.5
Weak	≥0.1 and <0.3
None	<0.1

Table S5 Inter-factor similarity for each instrument. Correlations (R^2; $p \leq 0.05$) among the time series of factors derived from (**A**) PTR_{CHARON}, (B) AMS_{org}, and (C) $AMS_{org+inorg}$ with all other factors from the same method. Slopes are given in brackets, for which columns and rows were treated as dependent and independent variables, respectively.

A

	Traffic	COA	OOA	RH1	RH2	RH3	RH4	SM
Traffic	1.00							
COA	0.29 (0.24)	1.00						
OOA	0.17 (0.05)	0.11 (0.09)	1.00					
RH1	0.27 (0.08)	0.19 (0.15)	0.18 (0.54)	1.00				
RH2	0.07 (0.01)	0.08 (0.02)	0.15 (0.13)	0.36 (0.16)	1.00			
RH3	0.10 (0.04)	0.12 (0.09)	0.12 (0.34)	0.52 (0.56)	0.41 (1.90)	1.00		
RH4	0.08 (0.02)	0.11 (0.06)	0.06 (0.17)	0.35 (0.32)	0.50 (1.54)	0.55 (0.52)	1.00	
SM	0.06 (0.12)	0.05 (0.28)	0.02 (0.64)	0.00 (0.07)	0.01 (1.54)	0.00 (0.00)	0.01 (0.51)	1.00

B

	HOA	COA	OOA	BBOA
HOA	1.00			
COA	0.21 (1.66)	1.00		
OOA	0.22 (0.64)	0.24 (0.18)	1.00	
BBOA	0.09 (0.43)	0.14 (0.16)	0.13 (0.38)	1.00

C

	HOA	COA	OOA	BBOA	AmNi	Sulph-OA
HOA	1.00					
COA	0.14 (1.27)	1.00				
OOA	0.16 (0.26)	0.21 (0.08)	1.00			
BBOA	0.09 (0.34)	0.20 (0.15)	0.26 (0.94)	1.00		
AmNi	0.35 (1.00)	0.14 (0.18)	0.15 (0.98)	0.04 (0.29)	1.00	
Sulph-OA	0.11 (1.04)	0.07 (0.23)	0.28 (2.57)	0.24 (1.24)	0.06 (0.48)	1.00

Very strong	≥0.75
Strong	≥0.5 and <0.75
Moderate	≥0.3 and <0.5
Weak	≥0.1 and <0.3
None	<0.1

References

Bosque, R. and Sales, J.: Polarizabilities of solvents from the chemical composition, Journal of chemical information and computer sciences, 42, 1154-1163, 2002.

Capozzi, V., Makhoul, S., Aprea, E., Romano, A., Cappellin, L., Sanchez Jimena, A., Spano, G., Gasperi, F., Scampicchio, M., and Biasioli, F.: PTR-MS characterization of VOCs associated with commercial aromatic bakery yeasts of wine and beer origin, Molecules, 21, 483, 2016.

Cappellin, L., Probst, M., Limtrakul, J., Biasioli, F., Schuhfried, E., Soukoulis, C., Märk, T. D., and Gasperi, F.: Proton transfer reaction rate coefficients between H3O+ and some sulphur compounds, International Journal of Mass Spectrometry, 295, 43-48, 2010.

Cappellin, L., Karl, T., Probst, M., Ismailova, O., Winkler, P. M., Soukoulis, C., Aprea, E., Märk, T. D., Gasperi, F., and Biasioli, F.: On quantitative determination of volatile organic compound concentrations using proton transfer reaction time-of-flight mass spectrometry, Environmental science & technology, 46, 2283-2290, 2012.

Chen, Y., Xu, L., Humphry, T., Hettiyadura, A. P., Ovadnevaite, J., Huang, S., Poulain, L., Schroder, J. C., Campuzano-Jost, P., and Jimenez, J. L.: Response of the aerodyne aerosol mass spectrometer to inorganic sulfates and organosulfur compounds: Applications in field and laboratory measurements, Environmental science & technology, 53, 5176-5186, 2019.

Datalystica: Source Finder (SoFi) 8.2 Manual for the software package SoFi (Pro) in IGOR Wavemetrics Inc., 2022.

Dingilian, K., Hebert, E., Battaglia Jr, M., Campbell, J. R., Cesler-Maloney, M., Simpson, W., St. Clair, J. M., Dibb, J., Temime-Roussel, B., and D'anna, B.: Hydroxymethanesulfonate and Sulfur (IV) in Fairbanks Winter During the ALPACA Study, ACS ES&T Air, 2024.

Eichler, P., Müller, M., D'anna, B., and Wisthaler, A.: A novel inlet system for online chemical analysis of semi-volatile submicron particulate matter, Atmospheric Measurement Techniques, 8, 1353-1360, 2015a.

Eichler, P., Müller, M., Klinger, A., Jordan, A., and Wisthaler, A.: CHARON PTR-ToF-MS: a new method for real-time measurement and molecular-level characterization of submicron organic aerosol, 2015b.

Ellis, A. and Mayhew, C.: Chemical Ionization: Chemistry, Thermodynamics and Kinetics, Proton Transfer Reaction Mass Spectrometry, 25-48, 2014.

Gueneron, M., Erickson, M. H., VanderSchelden, G. S., and Jobson, B. T.: PTR-MS fragmentation patterns of gasoline hydrocarbons, International Journal of Mass Spectrometry, 379, 97-109, 2015.

Herring, C. L., Faiola, C. L., Massoli, P., Sueper, D., Erickson, M. H., McDonald, J. D., Simpson, C. D., Yost, M. G., Jobson, B. T., and VanReken, T. M.: New methodology for quantifying polycyclic aromatic hydrocarbons (PAHs) using high-resolution aerosol mass spectrometry, Aerosol Science and Technology, 49, 1131-1148, 2015.

Holzinger, R., Williams, J., Herrmann, F., Lelieveld, J., Donahue, N., and Röckmann, T.: Aerosol analysis using a Thermal-Desorption Proton-Transfer-Reaction Mass Spectrometer (TD-PTR-MS): a new approach to study processing of organic aerosols, Atmospheric chemistry and physics, 10, 2257-2267, 2010.

Juntto, S. and Paatero, P.: Analysis of daily precipitation data by positive matrix factorization, Environmetrics, 5, 127-144, 1994.

Katz, E. F., Guo, H., Campuzano-Jost, P., Day, D. A., Brown, W. L., Boedicker, E., Pothier, M., Lunderberg, D. M., Patel, S., and Patel, K.: Quantification of cooking organic aerosol in the indoor environment using aerodyne aerosol mass spectrometers, Aerosol Science and Technology, 55, 1099-1114, 2021.

Langevin, P.: Sur la loi de recombination des ions, Ann. Chim. Phys, 28, 433-530, 1903.

Leglise, J., Müller, M., Piel, F., Otto, T., and Wisthaler, A.: Bulk Organic Aerosol Analysis by Proton-Transfer-Reaction Mass Spectrometry: An Improved Methodology for the Determination of Total Organic Mass, O: C and H: C Elemental Ratios, and the Average Molecular Formula, Analytical chemistry, 91, 12619-12624, 2019.

Müller, M., Eichler, P., D'Anna, B., Tan, W., and Wisthaler, A.: Direct sampling and analysis of atmospheric particulate organic matter by proton-transfer-reaction mass spectrometry, Analytical chemistry, 89, 10889-10897, 2017.

Pieber, S. M., Kumar, N. K., Klein, F., Comte, P., Bhattu, D., Dommen, J., Bruns, E. A., Kılıç, D., El Haddad, I., and Keller, A.: Gas-phase composition and secondary organic aerosol formation from standard and particle filter-retrofitted gasoline direct injection vehicles investigated in a batch and flow reactor, Atmospheric Chemistry and Physics, 18, 9929-9954, 2018.

Reyes-Villegas, E., Bannan, T., Le Breton, M., Mehra, A., Priestley, M., Percival, C., Coe, H., and Allan, J. D.: Online chemical characterization of food-cooking organic aerosols: Implications for source apportionment, Environmental science & technology, 52, 5308-5318, 2018.

Rivas, I., Beddows, D. C., Amato, F., Green, D. C., Järvi, L., Hueglin, C., Reche, C., Timonen, H., Fuller, G. W., and Niemi, J. V.: Source apportionment of particle number size distribution in urban background and transport stations in four European cities, Environment international, 135, 105345, 2020.

Seinfeld, J. H. and Pandis, S. N.: Atmospheric chemistry and physics: from air pollution to climate change, 3rd, John Wiley & Sons2016.

Sekimoto, K., Li, S.-M., Yuan, B., Koss, A., Coggon, M., Warneke, C., and de Gouw, J.: Calculation of the sensitivity of proton-transfer-reaction mass spectrometry (PTR-MS) for organic trace gases using molecular properties, International Journal of Mass Spectrometry, 421, 71-94, 2017.

Song, S., Gao, M., Xu, W., Sun, Y., Worsnop, D. R., Jayne, J. T., Zhang, Y., Zhu, L., Li, M., Zhou, Z., Cheng, C., Lv, Y., Wang, Y., Peng, W., Xu, X., Lin, N., Wang, Y., Wang, S., Munger, J. W., Jacob, D. J., and McElroy, M. B.: Possible heterogeneous

chemistry of hydroxymethanesulfonate (HMS) in northern China winter haze, Atmos. Chem. Phys., 19, 1357-1371, 10.5194/acp-19-1357-2019, 2019.

Stefenelli, G., Pospisilova, V., Lopez-Hilfiker, F. D., Daellenbach, K. R., Hüglin, C., Tong, Y., Baltensperger, U., Prévôt, A. S., and Slowik, J. G.: Organic aerosol source apportionment in Zurich using an extractive electrospray ionization time-of-flight mass spectrometer (EESI-TOF-MS)–Part 1: Biogenic influences and day–night chemistry in summer, Atmospheric Chemistry and Physics, 19, 14825-14848, 2019.

Su, T. and Chesnavich, W. J.: Parametrization of the ion–polar molecule collision rate constant by trajectory calculations, The Journal of Chemical Physics, 76, 5183-5185, 1982.

Temime Roussel, B., Cesler-Maloney, M., Chazeau, B., Ijaz, A., Brett, N., Law, K., Bekki, S., Mao, J., Ketcherside, D., Selimovic, V., Hu, L., Simpson, W. R., and D'Anna, B.: Concentrations and Sources of VOCs during wintertime urban pollution at Fairbanks, Alaska, December 01, 20222022.

Xu, L., Williams, L., Young, D., Allan, J., Coe, H., Massoli, P., Fortner, E., Chhabra, P., Herndon, S., and Brooks, W.: Wintertime aerosol chemical composition, volatility, and spatial variability in the greater London area, Atmospheric Chemistry and Physics, 16, 1139-1160, 2016.

Zhang, Y., Favez, O., Petit, J.-E., Canonaco, F., Truong, F., Bonnaire, N., Crenn, V., Amodeo, T., Prévôt, A. S., and Sciare, J.: Six-year source apportionment of submicron organic aerosols from near-continuous highly time-resolved measurements at SIRTA (Paris area, France), Atmospheric Chemistry and Physics, 19, 14755-14776, 2019.

Zhao, J. and Zhang, R.: Proton transfer reaction rate constants between hydronium ion (H3O+) and volatile organic compounds, Atmospheric Environment, 38, 2177-2185, 2004.

Zografou, O., Gini, M., Manousakas, M. I., Chen, G., Kalogridis, A. C., Diapouli, E., Pappa, A., and Eleftheriadis, K.: Combined organic and inorganic source apportionment on yearlong ToF-ACSM dataset at a suburban station in Athens, Atmospheric Measurement Techniques, 15, 4675-4692, 2022.

Response to **Reviewer 1**

This manuscript reports and discusses the source apportionment of organic and inorganic aerosols in Fairbanks, Alaska during winter, as measured by HR-ToF-AMS and CHARON-PTR-ToF-MS. Fairbanks is of particular interest as during winter, it frequently has poor air quality due to enhanced biomass burning emissions (residential heating) combined with poor air dispersion caused by temperature inversions. The focus of the paper is on comparison of the source apportionment results from the AMS and CHARON-PTR data, emphasizing their complementary nature. While AMS data have been extensively used for source apportionment, that is not the case for CHARON-PTR or even PTR-MS. To my knowledge, there is only one (very recent) source apportionment study that uses both CHARON-PTR and AMS data. The paper by Ijaz et al provides a very detailed source apportionment study and it will serve as a useful resource for future source apportionment studies using both CHARON-PTR and AMS data. It also demonstrates the ability of CHARON-PTR, due to its molecular level characterisation of OA, to distinguish additional residential heating sources. This is something that would not be possible to identify based only on the AMS data. Based on the arguments outlined above I recommend this paper for publication in the ACP.

→ Thank you for your thoughtful review and valuable feedback! We appreciate your acknowledgment of the complementary roles of AMS and CHARON PTR-ToF MS datasets in source apportionment. We look forward to incorporating your suggestions to enhance our manuscript and are grateful for your recommendation for publication in *ACP*. For your information, due to the request from reviewer 2, we did revise and reformulate some parts of the article (abstract, results, and conclusion).

Below are my specific comments (most of which I would describe as minor).

Line 120: I suggest "molecular level information" instead of "good molecular resolution"

→ We have revised the manuscript to incorporate "molecular level information" instead of "good molecular resolution" to enhance clarity.

Line 134 Please use sulfate instead of sulfur.

→ The revised manuscript reflects the change from sulphur to sulphate, where appropriate, as requested (**multiple lines along the document**).

Line 174: what was *m/z* range?

→ The *m/z* range applied was *m/z* 50–425. This has now been specified as follows:

"Among the resolved 1118 ions spanning the range of m/z 50–425, only 336 were retained above the S/N, and 318 ions could be given a molecular formula based on the criteria described in Section S2." (section 2.2.1 now line 193)

Line 188: no need for "PeTeR version 6.0…" as it has already been mentioned

→ We have removed the redundant mention in the revised manuscript.

Line 195: As AMS' come with either capture or standard vaporiser, it is worth mentioning which one you had.

→ The HR-ToF-AMS used in this study is equipped with a standard vapouriser. We have modified the sentence as follows: ***"Briefly, ambient particles are sampled through a critical orifice, focused into a narrow beam by an aerodynamic lens, accelerated toward a standard vapouriser heated at 600°C, and then ionised by electron impact (70 eV at 10^{-7} torr)."***

Line 199: ..nitrate, ammonium, sulfate, chloride.

→ The revised manuscript reflects the change from sulphur to sulphate throughout the document.

Line 208-9: nitrate, sulfate, chloride (please use singular for these ions).

→ These species have now been written in singular forms (**section 2.2.2)**.

Line 2016: why max m/z was only 120; why were PAHs excluded?

→ Our initial analysis incorporated all PAHs in the AMS analysis, and the resulting factorisation was the same as what we presented in the paper, achieving the primary aim. Another possible concern regarding the removal of PAHs is the potential underestimation of the mass concentration attributed to the factors. However, ~98% of AMS signal was present in fragments with *m/z* <120. Still, this limitation was acknowledged in the original manuscript as follows: *"**This exclusion is expected to cause underestimation (by <2%) of the mass of some factors, particularly HOA (hydrocarbon-like organic aerosol) and BBOA (biomass-burning organic aerosol)".***

→ First we extracted PAHs from AMS measurements to be utilized as external tracers for PTR_{CHARON} analysis, where they are not quantified as clearly, and were necessary for a better understanding of the factors. Specifically, we used them to differentiate factors like BBOA and HOA from other factors. Since the external tracers used for measuring external correlations of factors from PTR_{CHARON} and AMS analysis were kept consistent for the sake of data comparability, it was redundant to include PAHs in the PMF analysis of the AMS measurements.

Furthermore, many PMF analyses restrict the high-resolution organic mass spectra to *m/z* 120 (e.g., Aiken et al, https://doi.org/10.5194/acp-9-6633-2009; Young et al, https://doi.org/10.5194/acp-16-5427-2016, Duan et al, https://doi.org/10.5194/acp-22-10139-2022; Qi et al., https://doi.org/10.1016/j.scitotenv.2021.151800, among many others).

This approach is warranted because most of the signal from OA and inorganic species is produced within this mass range, largely due to extensive fragmentation resulting from electronic impact ionization of larger molecules. So finally, we extracted PAHs from AMS measurements to utilise them as external tracers (Figure 5). Specifically, we used them to differentiate factors like BBOA and HOA from other factors.

Line 220: not needed to mention that empty rows and columns were removed (same for line 188).

→ We agree that the phrase was redundant. It has now been removed from the revised manuscript.

Line 271: have you tried to look at the correlation between aerosol loadings and WS for the periods with strong temperature inversion? This would be a nice visual confirmation of your statement.

→ Yes, Figure 1 depicts the wind speed, as well as wind direction and temperature inversion, and their correlation with aerosol loading and particle number concentration throughout the campaign. This figure and accompanying text are emphasized in section 3.1. Figure 1 description:

"Figure 1 depicts meteorological conditions, chemical composition and particle size distribution of NR-PM_1 observed from January 20 to February 26, 2022. Intense aerosol loads coincided with poor atmospheric dispersion, associated with low wind speeds (<2 m/s), low temperature (below - 10°C) associated with strong surface temperature inversions, with temperature differences between 23 and 3 m above sea level ranging from 3°C to 10°C)."

Line 272: low instead of slow

→ Thank you for pointing out the error. We have corrected (see sentence above).

Line 276: daily average instead of campaign-averaged?

→ The term, campaign-average, is used because it means something else than daily average. We also have mentioned daily averages specifically for the pollution episodes. It is important to mention both to clearly illustrate how the pollution episodes differed from the overall campaign average.

Line 284: sulfate instead of sulfur. I am assuming the authors chose to use sulfur as species other than SO_4^{2-} can result in fragments that are used to calculate the overall SO_4^{2-} mass loadings (e.g. organosulfates). The choice of naming should be either explained in the Exp section, or use sulfate and discuss the contribution of organosulfates to SO_4^{-2} later in the text (page 15). Note that Fig 1 has SO4, not S.

→ We agree with the reviewer. Our reasoning behind using "sulphur," rather than "sulphate" was indeed the possibility of the contribution from non-SO_4^{2-} species. However, considering the traditional use of "sulphate" in the AMS community, we have corrected in the revised manuscript (multiple lines).

Line 318: fragmentation increases dramatically when?

→ Thank you for pointing out this phrase. This was an improperly phrased sentence. We have now rephrased it to "***Tests conducted in our laboratory with five C_{16}–C_{26} alkanes as markers of vehicle emissions revealed that they undergo extensive fragmentation, resulting in 2–4 times underestimation of their actual concentrations. In line with this finding, the ineffective***

***ionisation of saturated alkanes by PTR (Ellis and Mayhew, 2014) and their tendency to undergo dissociative ionisation (Gueneron et al., 2015) has also been reported previously.* "**

Line 359: Considering that ResH1_4 "closely co-varied in time", how strongly do they correlate with each other? Could they all, or some of them be a part of the same factor (i.e. be a result of factor splitting)?

→ We understand the reviewer's concerns about the complexity of the 8-factor solution and the potential for co-varying factors. However, we would like to assert that we have thoroughly evaluated the PMF results and molecular compositions to separate residential heating sources accurately. Table S2 presents a summary of PMF results from 3 to 10 factors. In the PTR_{CHARON} a splitting is observed for more than 8 factors, while below 8 factors, we could see mixing of ResH4 (hardwood) and ResH3 (heating oil), which are different sources based on their molecular compositions and correlation with SO_2.

Also the time correlation of the 4 residential factors is not as good as we could suppose for split factors (R^2 from 0.35 to 0.55) as can be observed in the table below.

A	Traffic							
Traffic	1.00	COA						
COA	**0.29** a=0.04 ± 0.00 b=1.20 ± 0.01	1.00	OOA					
OOA	**0.17** a=0.17 ± 0.00 b=3.42 ± 0.06	**0.11** a=0.25 ± 0.00 b=1.24 ± 0.03	1.00	RH1				
RH1	**0.27** a=0.29 ± 0.00 b=3.55 ± 0.04	**0.19** a=0.38 ± 0.00 b=1.33 ± 0.02	**0.18** a=0.40 ± 0.00 b=0.34 ± 0.00	1.00	RH2			
RH2	**0.07** a=0.58 ± 0.02 b=6.87 ± 0.20	**0.08** a=0.67 ± 0.02 b=3.22 ± 0.09	**0.15** a=0.57 ± 0.02 b=1.16 ± 0.02	**0.36** a=-0.23 ± 0.02 b=2.30 ± 0.02	1.00	RH3		
RH3	**0.10** a=0.44 ± 0.01 b=2.81 ± 0.06	**0.12** a=0.48 ± 0.01 b=1.28 ± 0.03	**0.12** a=0.49 ± 0.01 b=0.36 ± 0.01	**0.52** a=0.1 ± 0.00 b=0.94 ± 0.01	**0.41** a=0.43 ± 0.00 b=0.21 ± 0.00	1.00	RH4	
RH4	**0.08** a=0.50 ± 0.01 b=3.48 ± 0.10	**0.11** a=0.52 ± 0.01 b=1.74 ± 0.04	**0.06** a=0.61 ± 0.01 b=0.34 ± 0.01	**0.35** a=0.09 ± 0.01 b=1.08 ± 0.01	**0.50** a=0.39 ± 0.01 b=0.32 ± 0.00	**0.55** a=0.03 ± 0.01 b=1.05 ± 0.01	1.00	SM
SM	**0.06** a=0.16 ± 0.00 b=0.47 ± 0.01	**0.05** a=0.29 ± 0.00 b=3.55 ± 0.04	**0.02** a=0.18 ± 0.00 b=0.03 ± 0.00	**0.00** a=0.19 ± 0.00 b=0.00 ± 0.00	**0.01** a=0.18 ± 0.00 b=0.01 ± 0.00	**0.00** a=0.19 ± 0.00 b=-0.00 ± 0.00	**0.01** a=0.66 ± 0.01 b=0.51 ± 0.06	1.00

Correlations with AMS BBOA factor are shown in **Table S4 (R^2 = 0.5–0.7).** These temporal correlations are expected, as different types of residential heating are likely to be synchronised in time due to similar public needs for heating during the wintertime, despite potential differences in fuel usage.

Furthermore, when combining OA PMF-charon with size distribution data, we see that the factors are associated with particles having distinct size distributions (notably ReshH3 is associated with smaller particles than the other wood combustion factors, **see Figure S12 plot A**). This supports our choice of an 8-factor solution as the most stable representation of the data.

Line 369: what is in the same order? I assume peak intensity?

→ Yes, correct. The signal (or peak intensity!) of levoglucosan and its fragments were distributed in ResH1, ResH4, and ResH2 in the same order as the factors listed, i.e., most signal belonged to ResH1 and the least to ResH2. However, "in the same order" appears to be confusing and unnecessary in this instance, and thus, has been removed.

Line 385: atmospheric processing. Could it be that ResH1 is related more to low-temperature combustion?

→ Yes the reviewer is right, actually in a first version of the article we discussed it and then it was removed it. But we do agree the ResH1 factors presents considerable high content of oxygenated compounds and have a relatively high value of O/C ratio (0.42), among the most abundant molecules we observe furans, furfurals etc. We therefore modified the paragraph as follows:

"ResH1 includes low temperature combustion markers: this factor is small as it contributes to only an average of 0.5 ± 0.5 µg/m³ of the total OA_{CHARON} concentration, but it contains the highest fraction of levoglucosan (~30%). Approximately 65% of the total signal of ResH1 is due to compounds with six or fewer carbon atoms, compared to heavier species present in the other factors (Figure S13) and the most abundant species are at m/z 69.03 (C_4H_4O; furan) (Palm et al., 2020; Jiang et al., 2019), m/z 87.04 ($C_4H_6O_2$; oxobutanal) (Brégonzio-Rozier et al., 2015), m/z 97.03 ($C_5H_4O_2$; furfural), m/z 109.0286 ($C_6H_4O_2$; benzoquinone) (Stefenelli et al., 2019b) and m/z 115.04 ($C_5H_6O_3$; methyldihydrofuran) (Koss et al., 2018). Consistent with these molecular formulae, the concentration-weighted average O/C of ResH1 was relatively higher (i.e., 0.42) compared to other residential heating factors (O/C = 0.2–0.3). The most abundant species observed in ResH1 can be related to depolymerisation reactions occurring during low temperature and early stages of the combustion process(Collard and Blin, 2014; Sekimoto et al., 2018)."

Line 483: CHARON can see species that can evaporate at 150ºC (I am assuming this is the thermodenuder temp.; please mention operating TD temperature in the Experimental section); there are also species that will not be efficiently ionised by proton transfer. This should also be mentioned as a potential reason for the observed discrepancy.

→ We agree with your perspective and have clarified this aspect in the Methodology section by specifying the thermodenuder operating temperature as follows: "***The thermodesorber in the CHARON inlet was operated at 150°C and 8 mbar; this combination of moderate temperature with low pressure expands the range of detection to include ELVOCs as well*** **(Piel et al., 2021)."**

To address the potential reasons for discrepancies between AMS and PTR_{CHARON}, we have revised the text as follows: **"*Part of the quantitative difference between the two instruments can also be explained by the PTR limitation in ionisation and the ionisation-induced fragmentation of analyte ions. Tests conducted in our laboratory with five C16–C26 alkanes as markers of vehicle emissions revealed that they undergo extensive fragmentation, resulting in 2–4 times underestimation of their actual concentrations. In line with this, the ineffective ionisation of saturated alkanes by PTR (Ellis and Mayhew, 2014) and their tendency to undergo dissociative PTR ionisation (Gueneron et al., 2015) has also been reported previously."***

how do overall mass loadings of AMS Org and Charon Org compare? Are there any other studies reporting concurrent measurements by CHARON and AMS? How did their mass loadings compare? And doing source apportionment? If yes, you did their factor loadings compare?

→ The difference in OA mass loadings measured by the AMS and PTR_{CHARON} have been thoroughly discussed in our paper, particularly in Section 3.1 and shown in Figures 2 and S9. Briefly, the OA mass loading from PTR_{CHARON} was ~85% of the OA mass measured by the AMS. Although both instruments displayed a strong temporal agreement ($R^2 = 0.60$) as depicted in Figures 2A–B, the measurements were skewed either toward AMS_{org} or the PTR_{CHARON} during different periods of the campaign. These different periods were characterised by varying contributions from two primary sources: either HOA or BBOA. When BBOA contributed significantly (and thus, larger particles were present), PTR_{CHARON} performed slightly better or comparably to the AMS; however, its performance declined during periods dominated by HOA emissions due to its inability to detect particles smaller than 100 nm and ineffective ionisation of long aliphatic chain molecules as explained to your previous comment.

These overall trends align with what we already know from previous studies, such as seminal papers by Muller et al, https://doi.org/10.1021/acs.analchem.7b02582), Leglise et al (https://doi.org/10.1021/acs.analchem.9b02949), and Song et al (https://doi.org/10.5194/acp-24-6699-2024). In these studies, AMS and PTR_{CHARON} were compared, revealing that similar concentration variations were noted throughout the measurement intervals. In Muller et al. and Song et al, PTR_{CHARON} detected ~88% and 62%, on average, of total OA mass measured by the AMS. Absolute concentrations were in agreement during certain times, while considerable differences were observed at other times, largely due to changes in emission characteristics and the relative abilities of the instruments to measure them.

As for the difference in mass loadings in source factors, Muller et al. and Song et al. conducted PMF on measurements from both instruments, but they did not provide direct numerical comparisons of concentrations between factors that were commonly identified in AMS and PTR_{CHARON} analyses. Their focus was instead on gaining insights into source identities provided by the two instruments.

Line 513: How well do OOA and BBOA correlate with each other?

→ In the AMS measurements, there was a very weak correlation with $R^2 = 0.13$. Upon the inclusion of inorganics, the correlation becomes $R^2 = 0.26$. For PTR_{CHARON}, the R^2 values between OOA and the four residential heating factors ranged from 0.06–0.15. These values are presented in table S3 (time evolution correlation) and table S4 (spectral correlation).

Line 524: I think it should be the other way around 0.4 and 0.2%.

→ Thank you for catching this error! I rechecked our data on signal distribution across the factors and, to be exact, these were 0.48 and 0.29%. Other than the swapped sequence, these values also needed to be properly rounded off to 0.5 and 0.3%. The revision has been made.

Line 591: remove "of"

→ Thank you for catching the error. We have made the correction.

Line 630: If the goal of this discussion and Fig 8 + S18-21 was to see which factor "responds" the most to ADEC advisories, then looking at relative contributions of ResH factors could be misleading as a decrease in absolute concentrations of only one factor will impact rel. contributions of all factors.

→ We advocate for the use of relative contributions primarily because they allow a comparison among different sources without being influenced by overall pollution levels. In Fairbanks, the total pollution levels were strongly influenced by temperature and meteorology. Using relative contributions enabled us to overcome the effects of both total pollution and meteorology to divulge the changes in heating practices.

Figure 1 B) Personally I find it hard to make a distinction between WS and WD colours on the graph. How was J(NO2) calculated? I do not think that is mentioned anywhere. E) I do not think Fig1E is discussed anywhere in the text. How is PM2.5 number concentration measured?

→ jNO2 values were measured using a filter radiometer (MetCon Gmbh) installed at the NCore site. These measurements were not a part of our study. The original study reporting them has now been cited in the caption of Figure 1 (Simpson et al., 2024, https://doi.org/10.1021/acsestair.3c00076).

As for $PM_{2.5}$ measurement, there was a miscommunication on our part. Figure 1 does not show any PM2.5. The caption has been updated accordingly.

Figure 2: if data points are sized, then size legend should be included.

→ I acknowledge the reviewer's concern for this figure. Please note that the size of the data points is a rather trivial (or even redundant) aspect of this figure, so its explanation was shifted to the caption to avoid overcrowding the figure itself with legends. Data point 'sizing' in this figure is only meant to better visualise overlaying data points, which would otherwise completely cover one another. Keeping this in mind, we prefer to maintain the figure as it is and mention both the largest and the smallest sizes in the caption for simplicity.

All mass spectra figures: considering CHARON resolution of around 5000, not more than 2 decimal places should be given for m/z.

→ Thank you for your feedback. We completely agree and have revised Figure 4 accordingly.

Figure 4 and 5: I suggest to combine these two figures to look the same as Fig 3 and put the last column in figure 5 in the supplement.

→ This is actually an excellent suggestion and something that we did consider before submission as well. However, we would like to emphasize Figure 4 needs to be presented independently to accommodate all the essential ions' labels without crowding the figure.

Figure 7A: on y-axis next to HR-ToF AMS put the ion in question

→ Thank you for pointing out this error. It was a serious oversight on my part. I have corrected Figure 7 accordingly.

Table 1: I suggest moving it in the supplement

→ We have heavily relied on the information provided in **Table 1** to justify the identification of our factors. Therefore, we would like to keep it in the main text, even if it is toward the end.

Supplementary:

S3: I am assuming the sentence " This introduces a sust the campaign, and so must the EF" is there by mistake

→ Thank you for noticing this error. The sentence did not belong there and has been removed in the revised version.

S5 and S6: Can you please briefly justify the number of bootstrap replicates for both PTR(CHARON) and AMS factorisation?

→ The goal of bootstrapping in PMF is primarily statistical, helping in assessing the stability and uncertainty of source profiles through resampling the data. Some studies have used up to 250–1000 bootstraps runs (Tobler et al: https://doi.org/10.5194/acp-21-14893-2021; Chazeau et al. https://doi.org/10.1016/j.aeaoa.2022.100176), but we chose 100 because they provided a sufficient estimate of the stability of our solutions and uncertainty without being computationally demanding, given the large dimensions of all three of our datasets. Although using a larger number of bootstraps would undoubtedly yield even greater precision (e.g., reduced scaled residuals) and enhanced stability (e.g., same factor identities and distribution), we simply lacked the CPU/GPU power to have that many bootstrap runs. Particularly, since the residuals – both with and without bootstrapping – remained minimal, and we observed little to no change in the factor types identified, therefore, using a smaller number of bootstraps is justified.

Figure S3: Why is not starting from 15nm?

→ Thank you for noticing this oddity. The actual data from SMPS begins at 15 nm and we have revised Figure S3 accordingly.

Figure S5: why should scaled residuals ideally be +/- 2?

→ Scaled residuals are a metric to quantify how well the PMF model fits the provided data. Mathematically, it is described as follows: *(Observed Value − Modeled Value)/ Uncertainty*. In PMF, it is generally recommended that scaled residuals remain within ±3 or 2, based on standard statistical principles (simply put, it is a glorified standard deviation!) for assessing model performance (EPA PMF User guide: https://www.epa.gov/sites/default/files/2015-02/documents/pmf_5.0_user_guide.pdf). Large positive scaled residual values suggest that PMF is not adequately fitting the input variables or that those variables are associated with an infrequent source. A good fit maintains a balance of accuracy and uncertainty, ensuring that most data points fall within this range without excessive outliers.

General comment: the font in most of the figures (axis numbers, labels, legend) is too small. Please consider increasing the font.

→ Thank you for the suggestion. We have enlarged the font in the axes, labels, and legends in all the figures in the main text. This has been done specifically for Figures 3, 4, 5, and 6.

Response to **Reviewer 2**

The manuscript titled "Complementary aerosol mass spectrometry elucidates sources of wintertime sub-micron particle pollution in Fairbanks, Alaska, during ALPACA 2022 " uses aerosol mass spectrometry techniques, including CHARON PTR-ToF MS and HR-AMS, to analyze non-refractory particulate matter and its sources. Positive Matrix Factorization was applied to identify and estimate the contributions of various pollution sources, with a particular focus on residential heating emissions, on-road traffic, and secondary aerosol formation. The findings highlight the significant role of residential heating, alongside secondary organic aerosol processes, notably organosulphur, on air quality.

These observations offer valuable insights into this subarctic region, which is prone to significant particulate pollution events during winter. However, I have several concerns regarding the manuscript's structure, novelty, and methodology, which I outline in the general comments. A list of specific comments follows thereafter.

→ Thank you for your thorough review of our manuscript. We value the time and effort you took to evaluate our research on wintertime sub-micron particle pollution in Fairbanks, Alaska. We appreciate your acknowledgement of the study's valuable insights into subarctic particulate pollution. Your feedback helped us improve the quality of our study.

Structure and presentation:

1. The text is at times lacking conciseness and its structure could be optimized. In some instances, a potential issue is identified, but its possible causes are only discussed several paragraphs later, making the argumentation harder to follow. For example, the relatively low CHARON_traffic mass mentioned in L.486 is its potential causes debated only a few paragraphs later in the text, on the following page.

→ We acknowledge the reviewer's concerns regarding the paper's structure and writing quality. In response, we have made significant revisions of whole article (abstract, results and conclusion). Notably, we separated the discussions on HOA and COA into two distinct sections (Sections 3.2.3 and 3.2.4). We have also simplified the explanations for the discrepancies in mass concentrations from the PTR_{CHARON} and AMS by placing them in their respective sections, rather than placing it all the way at the end of both sections as originally done. And we reduced some sections. All changes are visible (track changes) but since too many changes have been realized to facilitate the reader, we also provide a revised article (no track changes)

2. The inclusion of three PMF analyses for two instruments is not easy to follow, particularly due to the way the acronyms are introduced. The results section lacks clarity, as multiple PMF analyses are presented in a fragmented manner. Moreover, the added value of applying PMF to both AMS OA and OA+Inorganics is unclear. Upon reading, one has the feeling that PMF AMS organics could be removed from the manuscript without any meaningful loss while improving readability.

→ We recognize that discussing three datasets can complicate readability. Considering that AMS is established as a refence technique, provides additional information on the inorganic fraction, we think it is important to keep the 3 PMF in this paper. We have streamlined the text by minimising the repetitive mention of AMS_{org} and $AMS_{org+inorg}$, using just AMS where both are applicable. HOA and COA were also divided up into two sections. Additionally, we introduced some headers and specified a new section, "Contribution of Sulphate to the OOA Factor," to clarify the discussion on OOA.

3. I don't find the figures particularly suitable for publication in their current form. Their layout, font sizes and colour choices should be refined to meet article-level standards.

→ We have enlarged the font in the axes, labels, and legends in all the figures in the main text. This has been done specifically for Figures 3, 4, 5, and 6.

Novelty

4. The authors repeatedly justify in the abstract and introduction that "significant uncertainties exist about aerosol sources, formation, and chemical processes during cold winter" in Fairbanks, Alaska (e.g. L.31). However, an extensive body of literature spanning over a decade has already attributed residential heating as a major driver of air quality degradation in that region, as well studies focusing on sulphur-containing particles. The manuscript should more precisely articulate the specific knowledge gaps that remain unresolved. Conversely, care must be taken not to extrapolate its findings to other arctic regions given the localized representativeness of their findings (e.g. L.138).

→ We appreciate your point regarding the existing literature on residential heating as a significant contributor to air quality degradation in Fairbanks, Alaska. We acknowledge that previous studies have identified this factor, and we aim to build upon that foundation. **The novelty of this study is related to the added value of a novel soft-ionisation technique (CHARON PTR-ToF MS) in providing molecular-level insights together with high temporal resolution. This allows us to separate different types of biomasses burning organic aerosol (BBOA) and identify an oil heating factor, which has not been extensively characterised in prior research. We also computed a combined PMF with SMPS data in order to combine chemical factors with particle size distribution. This work enhances our understanding of the sources of organic aerosol during cold winter months in Fairbanks.**

We modified or removed some of the sentences (L31 and L138 of the main text) and we rewrote the abstract.

We recognise the importance of not extrapolating our findings to other Arctic regions without caution. Our results are indeed localised to Fairbanks, but they could be relevant for other urbanized sub-Arctic areas. So we have rephrased to "**fast-urbanising sub-arctic" and "anthropogenically-influenced regions of the sub-arctic"** to align with the reviewer's suggestion.

5a. There appears to be little "complementarity" between CHARON and HR-AMS analyses in providing new insights into wintertime PM levels. CHARON independently proposes a novel separation of residential heating sources (discussed further below), while HR-AMS produces results that are largely consistent with prior literature (traffic, residential heating, and OS as key winter

contributors). Some of these findings have already been reported in studies from related or the same field campaigns (e.g., Campbell et al., 2022; Robinson et al., 2024; Yang et al., 2024).

→ The two deployed instruments are "objectively" complementary – even without the context of our study. One ensures very good mass closure, identification/quantification of both an organic and inorganic fraction but with reduced capability for compound identification, while the other delivers significantly better source resolution for the organic fraction. Together, they enhance our understanding PM composition and sources.

The reviewer rightly cites the contributions of Campbell et al. (2022), Robinson et al. (2024), Yang et al. (2024), Edwards et al. (2024), and Campbell et al. (2024) regarding air quality dynamics during the ALPCA campaign in Fairbanks. While overlaps in findings are common in scientific research (especially during a field campaign), our paper offers additional insights, particularly in delineating PM_1 sources and moving beyond single-instrument studies.

Our focus on the chemical composition of aerosols – particularly PM_1 – addresses significant health concerns and underscores the necessity for further investigation and regulation of specific source contributions. By identifying distinct types of wood and oil burning in residential heating, we aid targeted mitigation strategies. Additionally, our examination of resident behavior in response to burn bans contributes to understanding policy effectiveness. The molecular-level information we provide is fundamental for assessing potential health impacts, including evaluating factors, such as total PAHs and their associated toxicity.

For comparison, the following table outlines other closely related studies conducted during the ALPCA campaign, including those mentioned by the reviewer:

Edwards et al., 2024: Residential Wood Burning and Vehicle Emissions as Major Sources of Environmentally Persistent Free Radicals in Fairbanks, Alaska	First study to quantify EPFRs in Fairbanks and link them to specific sources and health risks (particularly oxidative stress).
Campbell et al., 2024: Enhanced aqueous formation and neutralization of fine atmospheric particles driven by extreme cold	Investigates the unique role of low temperature in enhancing aqueous reactions and modulating secondary aerosol formation, particularly HMS, through its impact on particle pH.
Yang et al., 2024: Assessing the Oxidative Potential of Outdoor PM2.5 in Wintertime Fairbanks, Alaska	First assessment of oxidative potential (OP) in Fairbanks $PM_{2.5}$, contrasting it with other urban areas and linking OP to specific sources.
Robinson et al., 2024: Multi-year, high-time resolution aerosol chemical composition and mass measurements from Fairbanks, Alaska	Provides a unique, multi-year, high-time resolution dataset, offering a comprehensive overview of aerosol behavior in Fairbanks across different seasons and meteorological conditions using long-term ACSM data.
Campbell et al., 2022: Source and Chemistry of Hydroxymethanesulfonate (HMS) in Fairbanks, Alaska	First in situ measurements of HMS in Fairbanks, highlighting its significant contribution to $PM_{2.5}$ sulfur and exploring its relationship with meteorological parameters and other species.

Given the study's title, I expected some type of combined analysis of CHARON and HR-AMS to yield results beyond the simple sum of their individual analysis, but this expectation is not met.

The title has been modified to "***Sources of wintertime sub-micron particle pollution in Fairbanks, Alaska, during ALPACA 2022"***

→ We chose to analyze CHARON PTR-ToF MS and HR-ToF AMS datasets separately, a decision that may seem counterintuitive given the value of combined factor analysis, as reported by Tong et al. (2022) (doi: 10.5194/amt-15-7265-2022), among others. However, this choice was driven by the preliminary idea to work preferentially on the PTR_{CHARON} dataset. By applying traditional PMF to PTR_{CHARON} and using HR-ToF AMS as a validation tool, we successfully met our primary goals of identifying PM_1 sources in Fairbanks and highlighting the PTR_{CHARON} capability to help do so. We also decided to change the title of the article as indicated above.

Methodology:

6. The PMF on CHARON data is difficult to verify, notably with this complex 8-factor solution. As far as I can gather, I am not completely convinced that the four residential heating factors are well-separated. This is often an issue for co-varying factors, which is the case here where Pearson is between 0.6 and 0.75.

Furthermore, there seems to be some issues among the four residential heating factors. For example, when normalized to their OA contributions, ResH2 (attributed here to hardwood combustion) and ResH3 (attributed to heating oil combustion) have the same relative fraction of levoglucosan - a compound that is a unique tracer of cellulose pyrolysis.

→ We understand the reviewer's concerns about the complexity of the 8-factor solution and the potential for co-varying factors. However, we would like to assert that we have thoroughly evaluated the PMF results and molecular compositions to separate residential heating sources accurately. Table S2 presents a summary of PMF results from 3 to 10 factors. In the PTR_{CHARON} a splitting is observed for more than 8 factors, while below 8 factors, we could see mixing of ResH4 (hardwood) and ResH3 (heating oil), which are different sources based on their molecular compositions and correlation with SO_2. Furthermore, when combining OA PMF-charon with size distribution data, we see that the factors are associated with particles having distinct size distributions (notably ReshH3 is associated to smaller particles than the other wood combustion factors, see Figure S12 plot A). This supports our choice of an 8-factor solution as the most stable representation of the data.

Regarding the separation of the four residential factors, in the specific case of Fairbanks we rather rely on the molecular composition than on time series as the latter are expected to strongly co-vary due to the co-emissions during strong temperature inversions. Also the time correlation of the 4 residential factors is not as good as we could expect for split factors (R^2 from 0.35 to 0.55) as can be observed in the table below.

A	Traffic							
Traffic	1.00	COA						
COA	**0.29** a=0.04 ± 0.00 b=1.20 ± 0.01	1.00	OOA					
OOA	**0.17** a=0.17 ± 0.00 b=3.42 ± 0.06	**0.11** a=0.25 ± 0.00 b=1.24 ± 0.03	1.00	RH1				
RH1	**0.27** a=0.29 ± 0.00 b=3.55 ± 0.04	**0.19** a=0.38 ± 0.00 b=1.33 ± 0.02	**0.18** a=0.40 ± 0.00 b=0.34 ± 0.00	1.00	RH2			
RH2	**0.07** a=0.58 ± 0.02 b=6.87 ± 0.20	**0.08** a=0.67 ± 0.02 b=3.22 ± 0.09	**0.15** a=0.57 ± 0.02 b=1.16 ± 0.02	**0.36** a=-0.23 ± 0.02 b=2.30 ± 0.02	1.00	RH3		
RH3	**0.10** a=0.44 ± 0.01 b=2.81 ± 0.06	**0.12** a=0.48 ± 0.01 b=1.28 ± 0.03	**0.12** a=0.49 ± 0.01 b=0.36 ± 0.01	**0.52** a=0.1 ± 0.00 b=0.94 ± 0.01	**0.41** a=0.43 ± 0.00 b=0.21 ± 0.00	1.00	RH4	
RH4	**0.08** a=0.50 ± 0.01 b=3.48 ± 0.10	**0.11** a=0.52 ± 0.01 b=1.74 ± 0.04	**0.06** a=0.61 ± 0.01 b=0.34 ± 0.01	**0.35** a=0.09 ± 0.01 b=1.08 ± 0.01	**0.50** a=0.39 ± 0.01 b=0.32 ± 0.00	**0.55** a=0.03 ± 0.01 b=1.05 ± 0.01	1.00	SM
SM	**0.06** a=0.16 ± 0.00 b=0.47 ± 0.01	**0.05** a=0.29 ± 0.00 b=3.55 ± 0.04	**0.02** a=0.18 ± 0.00 b=0.03 ± 0.00	**0.00** a=0.19 ± 0.00 b=0.00 ± 0.00	**0.01** a=0.18 ± 0.00 b=0.01 ± 0.00	**0.00** a=0.19 ± 0.00 b=-0.00 ± 0.00	**0.01** a=0.66 ± 0.01 b=0.51 ± 0.06	1.00

Regarding the relative fractions of levoglucosan in ResH2 (hardwood combustion) and ResH3 (heating oil combustion), there may be some misunderstanding. Approximately 30%, 14%, 9%, and 26% of the protonated levoglucosan signal and its fragments are distributed across ResH1, ResH2, ResH3 and ResH4, respectively, indicating an uneven distribution of this tracer through the 4 factors. While PMF has inherent complexities, our results suggest clear distinctions in levoglucosan allocation across the four residential heating factors.

Furthermore, all four factors exhibit a fairly high and comparable correlation with SO_2, while ResH1 "mixed wood burning" even shows a stronger correlation with "sulphate" than heating oil combustion, discussed here and previous references to be the main source of sulphur dioxide. I'll refrain from commenting on the separation between softwood vs. hardwood emissions, i.e. factors ResH2 and ResH4, as I am not an expert on the topic, but it also seems to be at least somewhat debatable. I believe this needs to be strengthened. As I discussed above, the separation of residential heating sources is a key novelty aspect of this work.

→ We appreciate the reviewer's comment regarding the correlation between residential heating factors and SO_2. We would like to highlight that the correlation coefficients for each residential heating factor with SO_2 present some difference. Specifically, ResH1 (mixed BB), ResH2 (hardwood), and ResH4 (pinewood) show correlation coefficients of 0.46, 0.34, and 0.47, respectively, compared to 0.61 for ResH3 (heating oil combustion). While one could argue that the R^2 differences are insufficient to attribute SO_2 solely to ResH3, as mentioned above particle size distribution supports the interpretation of a combustion oil factor associate to small particles while the other factors are rather related to larger particles (Figure S12 plot A).

PMF is inherently uncertain, often relying on informed interpretations based on time series data (e.g., rush hours for traffic, week-day or week-end, ect). We provided a related disclosure in the manuscript: "***The specific nature of wood cannot be inferred unambiguously, as emissions of marker species like levoglucosan or methoxy phenols vary with the type of fuel, heating appliance, operational conditions, and combustion cycle stage (Fine et al., 2002; Alves et al., 2017). Nevertheless, several studies (Fine et al., 2002; Schauer and Cass, 2000; Kawamoto, 2017) have differentiated between softwood and hardwood by identifying marker compounds present in our study, such as substituted phenols and resin acids*".** We minimised guesswork by relying on well-established marker species from the literature. Our identification of hardwood and pinewood species is grounded in objective analysis of these marker species, detailed in Section 3.2.2. We are confident in our 8-factor solution, evidenced by clear factor

separation at higher numbers and mixing at lower numbers, as well as the identities assigned to each source. However, we are open to revising our interpretations if the reviewer could clarify/specify why the hardwood and pinewood identities should not be trusted.

7. L.216-219: It's unclear why m/z > 120 was used for OA calculation but removed from PMF analysis, notably when co-emission of PAH is expected with factors such as BBOA and HOA. Their use as "external tracers" raises some questions about the robustness of the analysis. Please provide arguments to justify this (as well as re-phrase sentence for clarity).

→ Our initial analysis incorporated all PAHs in the AMS analysis, and the resulting factorisation was the same as what we presented in the paper, achieving the primary aim. Another possible concern regarding the removal of PAHs is the potential underestimation of the mass concentration attributed to the factors. However, ~98% of AMS signal was present in fragments with *m/z* <120. Still, this limitation was acknowledged in the original manuscript as follows (line 251): *"**This exclusion is expected to cause underestimation (by <2%) of the mass of some factors, particularly HOA (hydrocarbon-like organic aerosol) and BBOA (biomass-burning organic aerosol)".***

Furthermore, it is quite common to restrict the PMF on the high-resolution organic mass spectrum to *m/z* 120 (e.g., Aiken et al, https://doi.org/10.5194/acp-9-6633-2009; Young et al, https://doi.org/10.5194/acp-16-5427-2016, Duan et al, https://doi.org/10.5194/acp-22-10139-2022; Qi et al., https://doi.org/10.1016/j.scitotenv.2021.151800; among many others). This approach is warranted because most of the signal from OA and inorganic species is produced within this mass range, largely due to extensive fragmentation resulting from electronic impact ionization of larger molecules. So finally, we extracted PAHs from AMS measurements to utilise them as external tracers (Figure 5). Specifically, we used them to differentiate factors like BBOA and HOA from other factors.

Specific comments

1. Please rework the abstract providing a more quantitative view of the results presented here, highlighting their novelty.

à We have made substantial modifications to the abstract, the updated text is as follows*:* ***"Fairbanks, Alaska, is a sub-arctic city that frequently suffers from non-attainment of national air quality standards in the wintertime due to the coincidence of weak atmospheric dispersion and increased local emissions. As part of the Alaskan Layered Pollution and Chemical Analysis (ALPACA) campaign, we deployed a Chemical Analysis of Aerosol Online (CHARON) inlet coupled with a proton transfer reaction - time of flight mass spectrometer (PTR-ToF MS) and an Aerodyne high-resolution aerosol mass spectrometer (AMS) to measure organic aerosol (OA) and NR-PM_1, respectively. Positive Matrix Factorisation (PMF) analysis was used for source identification of the NR-PM_1. The PTR_{CHARON} factorisation of the organic fraction identified four residential heating sources, with oil combustion accounting for 16 % and wood combustion contributing significantly at 47 %. The analysis could further differentiate between hardwood and softwood combustion. The AMS analysis revealed only one biomass burning-related factor contributing 28 % of total OA and assigned the largest organic fraction to a hydrocarbon-like factor related to road transport with 38 % of the OA. Additionally, two factors enriched in sulphate (including both organic and inorganic fraction) and nitrate were identified. These***

results evidence the complementarity of the two instruments and demonstrate as PTR$_{CHARON}$ provides both qualitative and quantitative information, offering a comprehensive understanding of the organic aerosol sources. Such insights into the sources of sub-micron aerosol pollution can assist environmental regulators and citizen efforts to improve air quality in Fairbanks and the fast-urbanising regional sub-Arctic areas."

2. L. 35: "Which" instead of "that".

→ we have modified the section.

3. L101: remove "in detail"

→ The phrase, 'in detail,' was an unnecessary descriptor and has been removed as you suggested.

4. L111: Do you mean "more selective"? Or just selective, since it depends on proton affinity.

→ Selectivity – less or more – was irrelevant to the intended message, so it has been omitted for brevity.

5. L.120: "Information on NR-PM1 OA" or something along those lines.

→ We have rephrased this sentence to: ***" the former features molecular level information of the OA faction but has limited ability to detect particles below 150 nm (Eichler et al., 2015); the latter covers smaller particle size range (i.e., > 60 nm) and detects inorganic components too (Decarlo et al., 2006). Together they provide an excellent combination of real-time and quantitative data on atmospheric ambient aerosol."***

6. L.127: "Not well understood".

→ The suggested change has been made: ***"The detailed composition of sub-micron aerosol in Fairbanks and other anthropogenically influenced sub-Arctic regions – is not well-understood"***

7. L134: I'd advise maintaining sulphate, or rewrite "chloride-, nitrogen- and sulphur-containing species". Albeit well known by the community (and underlying current understanding of sulphate at Fairbanks), sulphur is the element, not the species or the aerosol type.

→ We agree with the reviewer. Our reasoning behind using "sulphur," rather than "sulphate" was indeed the possibility of the contribution from non-SO_4^{2-} species. We have revised in the entire manuscript.

8. L.134: "What does "good mass resolution" mean? ToF-ACSM would be enough? V-mode? W-mode? I suggest being more accurate here, notably on the role of mass resolution in the findings of the manuscript.

→ We have revised the whole text we remove resolution the actual version is the following ***:***

" These findings highlight the synergistic benefits of combining multiple analytical techniques and emphasise how soft ionisation mass spectroscopic methods enhance molecular-level insights into particulate organic carbon. This integrated approach advances our understanding of the complex composition of particulate matter, offering valuable contributions to environmental characterisation and source apportionment studies."

9. L.150: "recorded"

→ The tense has now been corrected (now line 149).

10. L.182: What is the validity of Leglise fragmentation correction into Fairbanks OA?

→ The Leglise et al. method addresses a key limitation in PTR_{CHARON} mass spectrometry: the fragmentation of analyte ions during PTR ionization can introduce a negative bias in quantification. This correction is particularly important for comparison between PTR_{CHARON} and AMS measurements of OA. Its application does not overcome the underestimation of vehicle emissions (due to the bad detection of aliphatic compounds as alkanes, etc.) known to undergo dissociative PTR ionisation. Despite applying this correction, there remains some underestimation in PTR_{CHARON} measurements of OA. The exact uncertainty associated with this should be explored via controlled laboratory experiments on known OA mixtures in the future.

L.199: RIE for sulphate was 1.93. Is that consistent with previous characterizations of the instrument? Has estimated SO4 from HR-AMS been compared with other observations?

→ Yes, typically an RIE within the 1.8–1.9 range is obtained for sulphate using this instrument. The sulphate levels estimated with the AMS were found to be 30% lower than those obtained from IC measurements from $PM_{0.7}$ filter samples. Additionally, the nitrate and ammonium components determined with the AMS also showed almost 30% reduction compared to the IC measurements, suggesting that such systematic differences among all species could rather arise from sampling uncertainties and/or non-overlapping particle sizes.

11. L.203: Confirm that the CDCE algorithm on PIKA calculated a correction factor down to 0.35

→ The correction factor of 0.35 is the experimental CE observed when the ammonium concentration was below the threshold of 0.03 $\mu g/m^3$. This value was used as the default CE input for the CDCE algorithm.

12. L.237: please develop "to understand the data" for clarity.

→ We have now updated this sentence as follows: ***"Preliminary PMF was performed without using a priori information to explore the dataset's structure, potential factor variability, and source contributions and guide the selection of an optimal solution before applying constraints."***

13. L.239-242: Re-phrase for improved readability.

→ We have considerably shortened and simplified the language as follows :

"We considered solutions from 3 to 13 factors, applying a step-wise, cell-wise down-weighting approach: variables with S/N < 0.2 ("bad" variables) were down-weighted by a factor of 10, while those with 0.2 < S/N < 2 ("weak" variables) were down-weighted by a factor of 2 (Paatero and Hopke, 2003; Ulbrich et al., 2009). Once primary factors, such as cooking and biomass burning, were successfully identified in unconstrained trials, we narrowed the range of possible solutions by applying the a-value approach, which allows for improved factorisation by constraining the PMF with external data when available (Canonaco et al., 2013; Paatero, 1999)."

14. L.272: the correct SI notation for the second is "s" and not "sec".

→ Thank you for pointing out this error. We have converted 'sec' to 's' throughout the revised manuscript.

15. L.274: Indicate what the variability range stands for.

→ The average values of BC and NR-PM_1 measured with the MAAP and AMS were **1.4 ± 1.4 µg/m$_3$** and **8.3 ± 9.3 µg/m$_3$**, respectively (variability range stands for standard deviation over the entire field campaign).

16. L.276: remove "campaign".

→ We removed campaign average

17. L.276-L.278: Methodology section, on ancillary observations?

18. → Ancillary observations in this study included SMPS, CPC, and OPC using standard protocols. These were specified in Section 2.1 of the Methodology (now highlighted in yellow).**L.291-298: I find this paragraph somewhat unclear, albeit highly relevant. Is 9% of the CHARON mass attributed to heteroatomic ions, being roughly 7% oxygenated ions (CHO) and the rest ON and OS? Are all OS and ON removed from the source apportionment analysis? Also, it's unclear what the relevancy of those "prominent peaks" is, they don't seem to be identifiable in Figure S8.**

→ 9% of the OA mass from PTR_{CHARON} is attributed to heteroatomic species, that include organo-nitrates (ON) and organosulphates (OS). We believe there is a misunderstanding regarding the "7% of oxygenated ions (CHO)". We explicitly state that "***Detailed molecular-level composition of organics with the PTR_{CHARON} reveals a large majority of organics to comprise only C, H, and/or O atoms, while only ~9% of the OA_{CHARON} mass measured with this instrument was attributable to heteroatomic species, including organonitrates and organosulphates (Figure S8)***."

The OS and ON components were retained for source apportionment, although we did not dwell on for "factor identification". Their distribution can be seen in Figure 4. It is true that the ON and OS peaks are not discernible in Figure S8, which shows the contributions of all OS, ON, and CHO peaks combined. We have now also referred to Figure 4 in this text, which distinctly shows these peaks. Regardless, you are justified in questioning the "relevance" of these peaks in this context. They were mentioned for the benefit of interested readers – to indicate their presence, even though we did not elaborate on them extensively due to the scope of this particular work.

19. L.278-281: eBC has already been estimated at 15% of PM1, how can PM2.5 be 99% of NR-PM1? There is a quantification issue with one (or both) methods, besides other refractory PM1 species that have not been considered, and the PM1-PM2.5 fraction. The analysis seems to completely miss those basic considerations.

→ Thanks for catching this error, the sentence was confusing, we deployed an OPC at the site and comparing PM1 and PM2.5 we can say that PM1/PM2.5 is 0.99. Now this reads in the manuscript "***Ancillary measurement at the CTC site with an OPC showed that the hourly PM1 comprised up to 99% of the PM2.5"***

20. L.304: avoid "could unequivocally be identified"

→ The term, unequivocally, has been removed from the sentence.

21. Figure 2: To improve readability I suggest not to colour code against PMF factors that have not yet been presented in the manuscript but some standard tracers (whether levoglucosan from CHARON or more "usual" tracers from AMS like f60 and f55, for example). Otherwise, panes D and E can go into supplementary, where results from different sections can be combined without impacting the flow of the manuscript.

→ Figure 2 has now been updated to remove panels D and E. The latter two panels are now a part of Figure S9.

22. L.308-312: Shouldn't the size-dependent EF correct for that effect?

Yes, the size-dependent EF is meant to correct for that effect. According to the results, the correction has only a limited compensatory effect for particle below 100nm. Therefore, sources that produce ultrafine particles (≤100nm), including vehicular emissions and fuel oil, are the most affected.

23. L.316-318: Has total OA been observed to decrease during laboratory experiments in the lab or just the concentration of those particular species? Fragmentation does not necessarily induce OA mass loss, it will of course depend on the PA of the fragments.

→ Equation S2 clearly shows that OA concentrations can be biased toward molecules yielding fragments with *m/z* values that are significantly lower than their molecular weight. This was the case for alkanes C16–C26 alkanes that we tested in the laboratory which extensively fragment into C_nH_{2n+1} with the most abundant ions being *m/z* 43, *m/z* 57, *m/z* 71, and *m/z* 85. Taking hexacosane as an example, assigning the original molecular weight (i.e m/z_i = 366) to each of the fragments resulted in a mass concentration that was roughly 4 times higher than the one obtained using fragments' individual *m/z*.

24. L.335: Clarify PMF of OA and OA+inorganics. Given that OA+inorganics analysis has seen added one factor for NO3 and one for SO4, it's not unexpected that the main source of OA has remained unchanged.

→ We appreciate the reviewer's suggestion. Indeed, the distinction between the PMF of AMS_{org} and $AMS_{org+inorg}$ only lies in the additional factors, ammonium nitrate (AmNi) and sulphate-rich OA (Sulph-OA). As expected, the primary OA sources remain mostly unchanged. Nevertheless, we conducted a first separate AMS_{org} PMF for direct comparison with PMF of PTR_{CHARON}.

L.346: It's curious about the low correlation with BC for such a dominating OA source, has it been corroborated also on previous studies for this site? Is there an explanation for the complete lack of correlation with CO?

→ The lower correlation between BC and the dominant OA source (i.e., residential heating) may result from differences in the combustion conditions. Wood-burning emissions can be very variable, producing organic-rich emissions with varying BC content depending on the burn phase and type of appliance used for burning. Previous studies in Fairbanks have similarly reported weak or inconsistent correlations between BC and OA from wood combustion. For example, Ward et al. (2012) observed that while wood combustion is a significant $PM_{2.5}$ source, the BC-to-OA ratio varies greatly with the combustion conditions. Similarly, Robinson et al. (2023) reported that BC and OA from wood burning do not always correlate strongly, which could be due to differences in combustion efficiency and meteorological conditions. These studies support our observation of BC not being a reliable tracer for BBOA, especially from residential sources, in Fairbanks.

As for CO, the CTC site being located close to main roads, it is expected that the CO variations are driven by the vehicle emissions. This is confirmed by the measured diurnal cycle of CO that follows the on-road mobile sector on the sampling site, as shown by Brett et al (2024) (Figure 9A in Brett et al. 2025; https://doi.org/10.5194/acp-25-1063-2025.

25. L.374: Rephrase the analysis (also L.369), where 14% (ResH2) of LEV is considered robust and 9% (ResH3) minor.

→ We would like to assert that the comparison of levoglucosan (LEV) contributions to the different residential heating factors could have been misunderstood to some extent. While ResH2 does contain 14% of the total levoglucosan signal and is considered a major wood-burning factor, ResH3 at 9% is still a relevant source but is more strongly associated with oil combustion due to its distinct molecular signature, containing enhanced quantities of PAHs and a better correlation with gaseous SO_2. The text has been revised as follows:

"***Levoglucosan is used here as an internal tracer of biomass burning being relatively stable under atmospheric conditions (Fraser and Lakshmanan, 2000). Most of signal from protonated levoglucosan (m/z 163) and its fragments (at m/z 85, 127, and 145) were found in ResH1, ResH4, and ResH2 (13-29%, Figure S11), while ResH3 contained a smaller fraction (i.e., 9%), suggesting that at least three factors do originate from biomass burning – more specifically,***

wood-burning (Figure 4 and S11). These three wood-burning related factors collectively accounted for an average of 2.1 ± 2.5 µg/m³ of OA_{CHARON} (corresponding to 47 ± 20% of total factorised OA_{CHARON}).”

L.412: present the relative contribution in the form of an equation.

This formula has been used to calculate and has been added to supplementary section:

$$RI_{i,f} = \frac{C_{i,f}^{norm} - C_i^{norm}}{\sigma_i^{norm}}$$

Where:
$RI_{i,f.}$ = the relative importance of variable i in factor f
$C_{i,f}^{norm}$ = normalised concentration of variable i in factor f
C_i^{norm} = mean normalised concentration of variable i across all factors
σ_i^{norm} = standard deviation of the normalised concentration of variable i across all factors

26. L.460: The journal and DOI of this reference are lacking, I could not find it.

à This reference pertains to a poster from our group on this work presented at the EGU, so there is no DOI. We have provided the link to the abstract:
https://agu.confex.com/agu/fm22/meetingapp.cgi/Paper/1072876

27. L.466: Please include already here possible explanations for discrepancies on mass loadings between HOA from AMS and traffic factor from CHARON from page 14.

→ We thank you for pointing out this disorganised arrangement of text. We have now created two distinct sections for HOA and COA, separately addressing the reasons for the discrepancies in their mass concentrations from PTR_{CHARON} and AMS, rather than combining them at the end. More details are discussion in the SI section.

28. L.475-477: Rephrase “reliable tracer for it is yet to be identified” as a direct sentence.

→ Rephrased to “***Although a reliable tracer for COA remains unidentified, a high f55/f57 ratio of >1 is considered characteristic (Katz et al., 2021; Sun et al., 2011).***”

29. S3: correct “sust”

→ Thank you for catching this error. This entire phrase was mistakenly left in the supplement and has now been removed.

30. Fig. S3: Most of the EF calculated is above 7, which if I read correctly implies a volume-weighted distribution generally >200nm for submicrometric aerosols. Is that correct?

→ Yes, you have read correctly! Such an EF value implies that a considerable "concentration-weighted" portion of the PM_1 OA mass was associated with particles with diameters ≥ 200 nm. The EF values > 7 indicate a shift toward accumulation-mode aerosols, which is consistent with emissions from biomass burning and aged aerosol. This also agrees with the SMPS data that showed that ResH1, ResH2 and Resh4 factors are dominated by particles in the 200–400 nm range (Figure S12 A).

References

Campbell, J. R., Battaglia, M. J., Dingilian, K., Cesler-Maloney, M., St Clair, J. M., Hanisco, T. F., Robinson, E., DeCarlo, P., Simpson, W., Nenes, A., Weber, R. J., and Mao, J.: Source and Chemistry of Hydroxymethanesulfonate (HMS) in Fairbanks, Alaska, Environ. Sci. Technol., 56, 7657–7667, https://doi.org/10.1021/acs.est.2c00410, 2022.

Eichler, P., Müller, M., D'anna, B., and Wisthaler, A.: A novel inlet system for online chemical analysis of semi-volatile submicron particulate matter, Atmospheric Measurement Techniques, 8, 1353-1360, 2015.

Müller, M., Eichler, P., D'Anna, B., Tan, W., and Wisthaler, A.: Direct sampling and analysis of atmospheric particulate organic matter by proton-transfer-reaction mass spectrometry, Analytical chemistry, 89, 10889-10897, 2017.

Robinson, E. S., Cesler-Maloney, M., Tan, X., Mao, J., Simpson, W., and DeCarlo, P. F.: Wintertime spatial patterns of particulate matter in Fairbanks, AK during ALPACA 2022, Environmental Science: Atmospheres, 3, 568-580, 2023.

Robinson, E. S., Battaglia, Jr, M., Campbell, J. R., Cesler-Maloney, M., Simpson, W., Mao, J., Weber, R. J., and DeCarlo, P. F.: Multi-year, high-time resolution aerosol chemical composition and mass measurements from Fairbanks, Alaska, Environ. Sci. Atmos., 4, 685–698, https://doi.org/10.1039/D4EA00008K, 2024.

Ward, T., Trost, B., Conner, J., Flanagan, J., and Jayanty, R.: Source apportionment of PM2. 5 in a subarctic airshed-fairbanks, Alaska, Aerosol and Air Quality Research, 12, 536-543, 2012.

Yang, Y., Battaglia, M. A., Mohan, M. K., Robinson, E. S., DeCarlo, P. F., Edwards, K. C., Fang, T., Kapur, S., Shiraiwa, M., Cesler-Maloney, M., Simpson, W. R., Campbell, J. R., Nenes, A., Mao, J., and Weber, R. J.: Assessing the Oxidative Potential of Outdoor PM2.5 in Wintertime Fairbanks, Alaska, ACS ES\&T Air, 1, 175–187, https://doi.org/10.1021/acsestair.3c00066, 2024.

Response to **Reviewer 3**

The authors describe analysis of a mass spectrometry dataset collected in Fairbanks, Alaska, aimed at investigating sources of ambient PM_1 that contribute to local poor air quality events resulting in non-attainment of health-based air quality standards. Local meteorology, in particular temperature inversions, lead to accumulation of emissions from local activities including home heating, traffic and cooking. The novelty of this work lies in the additional insights obtained from leveraging the PTR-CHARON molecular compositional data. Most real-time organic aerosol apportionment studies rely on analysis of heavily fragmented EI mass spectra from AMS instruments. While these are useful for mass closure, and for informing air quality policy (eg traffic vs woodburning mass contributions) relatively little information on organic aerosol composition is obtained. In this work, separate, thorough analyses of the AMS organic, AMS organic+inorganic and the PTR-CHARON datasets through PMF are used to maximize the value of each technique. There are also synergistic aspects. For example, the CHARON dataset reveals multiple distinct local residential combustion source profiles featuring marker ions that can be associated with hardwood, softwood, resin and even oil combustion, whereas only a single residential combustion factor (BBOA) is extracted from the AMS data. The identification of specific marker ions (eg furfural, guiacol, eugenol, vanillin, coniferaldehyde) will undoubtedly be useful for CHARON users going forward. On the other hand, mass closure appears to be an issue for the CHARON dataset, which is limited by poor particle transmission at lower sizes and significant fragmentation of alkanes despite the soft ionization used. In the case of this work I don't believe the mass concentration underestimation of the CHARON for the various factors is too concerning because the AMS functions as a quantitative instrument for closing PM_1 OA. However, I think the conclusions would benefit from a broader discussion on where the authors feel that CHARON systems fit in to future source apportionment efforts that aim to instruct policy. Should an AMS system always be co-deployed for example, to ensure accurate OA mass loading measurements, with the emphasis on the CHARON data to speciate the AMS "factors" in more detail? Is there a potential for the CHARON data to target and reasonably accurately quantify specific air toxics that represent health risks, for example PAHs or quinones? Or does the size-dependent transmission efficiency introduce too much uncertainty in the absence of co-located SMPS measurements? This would be useful for the community. Overall, I find the manuscript to be well written and the analysis is rigorous, and I have only minor comments below.

→ Thank you for your thoughtful review of our manuscript. We appreciate your acknowledgement of the novelty in leveraging PTR-CHARON data for enhanced organic aerosol compositional insights, complementing traditional AMS analysis. We agree that mass closure is a limitation, particularly for smaller particles and fragmented alkanes. As noted, the synergistic approach with AMS ensures quantitative PM_1 OA assessment. We have carefully addressed this point, as well as other concerns and suggestions, in the itemized response below. We have modified the conclusion, adding some discussion about the use of these two instruments. Due to quite severe requests from reviewer 2 the article has been modified abstract, some results section and conclusion have been rewritten. We therefore provide two version of the revised article (one with track changes, quite difficult to read and a second one without track changes).

How often was zeroing performed for the CHARON mass spectral signals? Any humidity dependence of instrumental response?

→ We specified in the manuscript (last paragraph of section 2.1.) as follows : ***"A HEPA filter was placed upstream of the inlet for an hour at regular intervals (twice a week) to measure the instrumental background."***

Extremely low temperatures were encountered during the campaign outside the trailer. The water content estimated using temperature and relative humidity from the gauge positioned at the AMS inlet was 1.2 ± 0.8 mmol/mol, corresponding to an equivalent relative humidity at 25°C of 2.65 ± 1.75% (trailer temperature was around 5-7 °C). Humidity was quite constant throughout the campaign in the inlet, and dependence is considered negligible in this range.

For the PTR, for the species in the gas calibration mix, how well do the reported mixing ratios based on transmission efficiency and dipole moment/polarizability-derived k values agree with the expected mixing ratios?

→ The table below lists the measured vs expected mixing ratio for the calibrated compounds.

VOC	Measured/Expected
33	0.97
42	1.06
45	1.25
59	1.16
69	0.84
79	0.91
93	0.96
107	0.96
121	0.97
135	1.04

The difference between the expected and measured mixing ratio arises only from using the modeled transmission curve. The *k* values do not affect the calculation of mixing ratios: since they are used to determine relative transmission, and the conversion from cps to ppb relies on the same *k* values, their influence is canceled out.

Are the signals for BTEX observed in the constrained CHARON traffic factor from the condensed fraction of those species in OA or breakthrough of gases from the denuder?

→ The combined effect of slight gas breakthrough from the denuder and memory effect from the previous VOC measurement could explain the presence of a residual signal (2-3% of the signal found during the gas-phase measurement) for these compounds in CHARON mode.

If the residential heating factors co-vary how were they resolved by PMF? Do they have slightly different temporal dependencies? Presumably home heating emissions from all fuel types peak at the same times of day. Or is there a slightly different wind dependence that results in changes in the relative contributions to OA from these different fuel types because of different uses in different parts of the community.

→ PMF is dependent on not just temporal trends. The residential heating factors co-varied but not a hundred percent. As shown in Table S5, R^2 values ranged between 0.35 and 0.52 for the four residential heating factors. This temporal difference, along with the presence of different molecular markers from the various fuel types, allows PMF to effectively resolve them.

Figure 4: What is the SM factor? Small carboxylic acids? Is the acetone from denuder breakthrough? Does the lack of a diurnal trend mean this is background OA?

→ The SM factor was an instrumental artefact, which was discussed in the supplementary section. I have appended this paragraph below for your review:

Supplementary section. S5. Specifics of the factorisation of PTR_{CHARON} measurements

"The factorisation of PTR_{CHARON} produced a unique factor that comprised largely of very small ions of m/z < 65, labelled as the small molecules (SM) factor. This factor could not be given an environmentally relevant identity based on a lack of correlations with the external tracers, and thus, it has not been discussed in the main text. Its major constituents were small species, such as m/z 59.05 (C_3H_6O), 61.03 ($C_2H_4O_2$), 73.03 ($C_3H_4O_2$), 75.04 ($C_3H_6O_2$), etc., that are expected to be in the gaseous phase, rather than the condensed phase. Its average concentration was ***0.2 ± 0.1 µg/m^3*** *with large relative contributions to total OA (>80%) during short and clean periods of the campaign, when ambient OA_{CHARON} was below 1 µg/m^3. We speculate that the SM factor is an artefact produced by instrumental chemical background and possible remnants of VOC species on the denuder as we switched from collecting gas-phase samples to particle sampling through the CHARON inlet."*

Was there an external validation of the AMS total mass concentrations from a gravimetric/nephelometer particle mass monitor?

→ External validation of AMS total mass concentrations of PM_1 was conducted using mass concentrations from IC (PM0.7) of sulphates, nitrates, ammonium as shown in **Figure 7**.

How is the fragmentation correction performed for the CHARON data? Are smaller fragment ions quantified or is there a fraction from the MH+ signal that is assumed to be "missing"?

→ Fragmentation correction in our study does not involve direct quantification of small fragments or parent ions as we cannot differentiate between fragment and parent ions in a complex unknown aerosol mixture. Instead, we used correction factors derived in a previous study from the fragmentation patterns of 26 known oxidized organic compounds that were representative of atmospheric particulate organic matter (Leglise et al. 2019 https://doi.org/10.1021/acs.analchem.9b02949). The authors validated their correction methodology with the HR-ToF AMS measurements.

The description of the varying enrichment factors is hard to follow. How is it dependent on concentration? Isn't the EF selected for each hour based on the mass-size mode of the SMPS? Although there seems to be bimodal distributions for some of the residential factors in the SI. Are the EF values relatively low compared to other studies?

→ We are sorry that the reviewer found the EF-related discussion hard to follow. It seems there has been a misunderstanding. First, SMPS data was not collected hourly; all our data, including the concentration-weighted EF, depicted in Figure S3 has a 2-minute resolution. Second, the EF was not "selected". Rather, it was calculated at each sampling time point using the most predominant size as seen by the SMPS. How do we know which size is the *most predominant* at a given moment? - By picking the particle size

presenting the largest concentration. Hence, "concentration-weighted EF". The mathematical expression for this and associated discussion is given in Section S3 of the supplementary.

$$EF_{weighted} = \frac{\sum_{k=1}^{k=n} EF_k \cdot Conc_k}{\sum Conc} \text{.....Equation S3}$$

Yes, the EF values were much lower during the ALPACA campaign compared to those reported in other studies and the manufacturer, Ionicon, as shown in the Figure below.

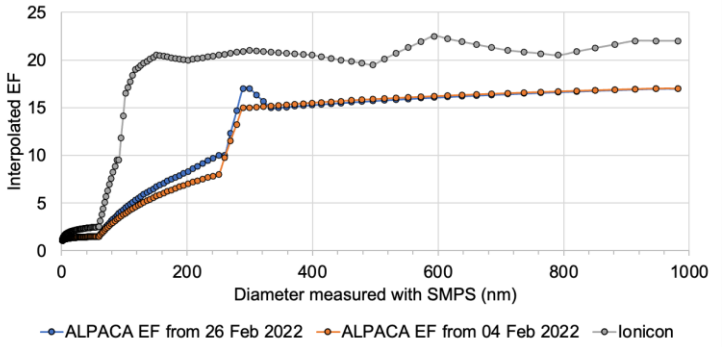

Figure 8 and the corresponding figures in the SI are very hard to follow. I think to show how the relative mass contributions of the residential factors change before, during and after an advisory period, the format in Figure 1D might be useful. If it's noisy the temporal resolution could be reduced. It's hard to track all of the box plots and in the SI versions it's hard to track the temporal order with the curved arrows.

→ Yes, we agree. These figures are rather gruesome to see. Based on your suggestion, we have now updated the percent contribution plots to be stacked as in Figure 1D. Other than that, we deemed it simpler to remove the box plots around the Figure for simplicity. We hope that the updated figure is easier to interpret.

The mass size mode information in Figure S12 is great. Confirms that there are distinct residential combustion sources.

→ Thank you! That was the goal we had in mind for this figure.

The externally derived size distributions for the different factors suggest that COA and the traffic factor have similar size distributions. Does that mean that the large difference in the slopes benchmarking against the AMS in Figure 5 (0.016 vs 0.13) is driven almost entirely by composition?

→ Yes, despite having similarly sized particles, it is likely that the difference in composition between the two factors, i.e., more fragmentation-prone alkanes in road transport, causes a much larger underestimation of HOA, compared to COA. The measurement discrepancies for these two factors have been discussed in detail in the Supplementary Sections S9 and S10. Figure 5 has been modified

accordingly to request from reviewer 2. These correlations are now moved in the supplementary section **Figure S12.**